# Innate Immune Regulation in HIV Latency

Rebecca M. Olson

A dissertation

submitted in partial fulfillment of the

requirements for the degree of

Doctor of Philosophy

University of Washington

2021

Reading Committee:

Michael Gale, Jr., Chair

Adam Geballe

Sheila Lukehart

Ram Savan

Program Authorized to Offer Degree:

Immunology

University of Washington

# ABSTRACT

Rebecca M. Olson

Innate Immune Regulation in HIV Latency

Chair of the Supervisory Committee:

Michael Gale, Jr.

Innate immunity and type 1 interferon (IFN) defenses are critical for early control of HIV-1 infection within CD4+ T cells. Despite these defenses, some acutely infected cells silence viral transcription to become latently infected and form the HIV-1 reservoir *in vivo*. Latently infected cells persist through antiretroviral therapy (ART) and are a major barrier to HIV-1 cure. Here, I evaluated innate immunity and type 1 IFN signaling in multiple CD4+ T cell models of HIV-1 latency, including established latent cell lines, Jurkat cells latently infected with a reporter virus, and a primary CD4+ T cell model of virologic suppression. I found that while latently infected T cell lines have functional RNA sensing and IFN signaling pathways, they fail to induce specific interferon-stimulated genes (ISGs) in response to innate immune activation or type 1 IFN treatment. Jurkat cells latently infected with a fluorescent reporter HIV-1 similarly demonstrate attenuated responses to type 1 IFN. Using bulk and single-cell RNA sequencing I applied a functional genomics approach to define ISG expression dynamics in latent HIV-1 infection, including HIV-infected ART-suppressed primary CD4+ T cells. My observations indicate that HIV-1 latency and viral suppression each link with cell-intrinsic defects in ISG induction, though the specific defects vary among latency models and clones. In this study I identify a set of ISGs for consideration as latency restriction factors whose expression and function could possibly mitigate establishment of latent HIV-1 infection.

# ACKNOWLEDGMENTS

I am indebted to many for the contents of this dissertation.

Science is never an individual effort, but a massive undertaking by many unique minds. First, I would like to acknowledge the scientific contributions of the many other researchers involved in this work:

The Gale lab sequencing group, for your outstanding efforts throughout my sequencing studies. Michelle Carlson, Jenny Go, Lynn Law, and Elise Smith, for your help with experiment design, library prep, and sequencing. Dan Newhouse for your seamless analysis of bulk RNA sequencing data. Especially Leanne Whitmore, for your patience over dozens of zoom meetings and for the countless hours you spent sorting through a very complicated single cell RNA sequencing data set.

Collaborators at the Hladik lab for your incredible work designing and optimizing the NanoLuc virus and primary CD4+ T cell infection protocol. Rena Astronomo, Christina Ochsenbauer, Florian Hladik, and especially Germán Gornalusse. Thank you Germán for your optimism and encouragement over many tedious hours spent infecting primary cells.

Michele Black at the Cell Analysis Facility at UW Medicine, for your aid in ImageStream analysis, flow sorting, and general troubleshooting of a multitude of flow cytometry issues.

I would also like to thank:

My PhD mentor, Michael Gale, Jr., for your endless optimism, for encouraging me to tackle big questions, and for always thinking science is cool.

My research mentors over the years, including Mark Pegram, Kevin Urdahl, and Jessica Hamerman.

My colleagues in the Gale lab, especially our lab managers Nanette Crochet and Elyse Verstelle for creating a beautiful and safe research space, fiercely handling every misplaced order or freezer crash, and generally being the safety net every graduate student needs. Bryan Turnbull and Marian Fairgrieve for daily conversations about data and life.

My fellow graduate students in the Gale lab and the Immunology PhD program, for sharing your joys and failures, as science always has both. Especially Andrey Shuvarikov, Kate Wuertz, Frank Soveg, and my 2014 cohort: Annelise Snyder, Rudy Nazitto, Kerri Thomas, and Jared Delahaye.

The Immunology Department for giving me this opportunity and supporting me along the way. Peggy McClune, Sandy Turner, Sarah Bland, and countless others who provide essential administrative support.

The STD/AIDS Research Training Fellowship Program at UW for funding a large portion of this work and offering incredible and diverse training opportunities.

My doctoral supervisory committee: Michael Gale, Jr., Adam Geballe, Sheila Lukehart, Julie McElrath, Ram Savan, and Daniel B. Stetson.

My parents Sharon and Bryan Olson, for teaching me that I could do anything I put my mind to. The Stokes family: my sister Julie, brother-in-law Graham, niece Audrey, and nephew James, for endless joy and laughter. My cousin Jessica Kocak and aunt Beth Olson for your steadfast encouragement during challenging times.

My wonderful friends in Seattle, especially Elyse and Steven Verstelle, Tori and Justin Ulrich-Lewis, Alexis Aljuni, Mikel Ruterbusch, and everyone else in our Seattle Squad. I love you all.

Lastly, I would like to acknowledge Washington's incredible mountains, for offering challenge, peace, glory, escape, healing, and breathtaking beauty.

*The world's big and I want to have a good look at it before it gets dark.*

-John Muir

# TABLE OF CONTENTS

# LIST OF FIGURES

# LIST OF TABLES

# CHAPTER 1: INTRODUCTION

## History of the HIV-1 epidemic

The human immunodeficiency virus 1 (HIV-1) has caused a terrifying and perplexing pandemic that emerged rapidly, spread to virtually every country on the globe, and killed millions of people worldwide. HIV-1 first appeared in humans sometime in the early 1900's in west central Africa through cross-species transmission of Simian immunodeficiency virus (SIV) in chimpanzees (Hahn et al. 2000). A similar cross-species transmission event created HIV-2, which is structurally similar to HIV-1 and also pathogenic in humans, though spread has been geographically limited to countries mainly in Africa (Ceccarelli et al. 2021). The research presented here focuses exclusively on HIV-1. HIV-1 spread for 50-70 years before it was recognized in an official CDC report in 1981 (Gottlieb et al. 1981) and the causative virus identified in 1983 (Barre-Sinoussi et al. 1983). By 1984, the resulting disease Acquired Immunodeficiency Syndrome (AIDS) was the leading cause of death of all Americans aged 25 to 44. Research efforts in the next two years led to molecular cloning of HIV-1 (Hahn et al. 1984), determining the viral nucleotide sequence (Wain-Hobson et al. 1985), and identifying CD4 as the main cell surface receptor (Dalgleish et al. 1984). Major therapeutic advancements began in 1987 with the first clinical trial with azidothymidine, and by the mid 1990s antiretroviral drugs were used to effectively prevent and treat HIV-1 infection. Another major leap forward came in the mid 1990s with the discovery of the HIV-1 latent reservoir (Finzi et al. 1997; Chun et al. 1995; Chun et al. 1997), which is now understood as the biggest obstacle to a functional cure for HIV-1 infection. In 2009, a single patient was functionally cured of HIV-1 through a bone marrow transplant of donor cells lacking the HIV-1 coreceptor (Hutter et al. 2009); this 'Berlin patient' remains the only individual truly cured of HIV-1. At present, over 37 million people are currently infected with HIV-1 worldwide

and no curative therapy exists (UNAIDS 2021). Despite substantial progress with antiretroviral drug development, the HIV pandemic is far from over.

### HIV-1 pathogenesis and latent infection

HIV-1 infects immune cells that express the CD4 surface receptor and a coreceptor (CCR5 or CXCR4). These are primarily CD4+ T cells, but also include CD4+ macrophages and dendritic cells. Upon receptor-mediated entry, the HIV-1 RNA genome is reverse transcribed into a double-stranded DNA provirus, which is imported into the cell nucleus, then permanently integrated into the host cell genome. While HIV-1 provirus integration tends to occur near active genes, the viral mechanism for integration site selection remains a mystery, if a selective process even exists. Following provirus integration, viral genes are transcribed by host machinery into viral RNAs that mimic host mRNA in cap structure and RNA modifications. Viral structural proteins (including tat, gag, pol) and regulatory proteins (including vif, vpr, vpu, nef) are translated, and the viral RNA genome assembled into a virion that buds from the plasma membrane to infect neighboring cells (Fig. 1).

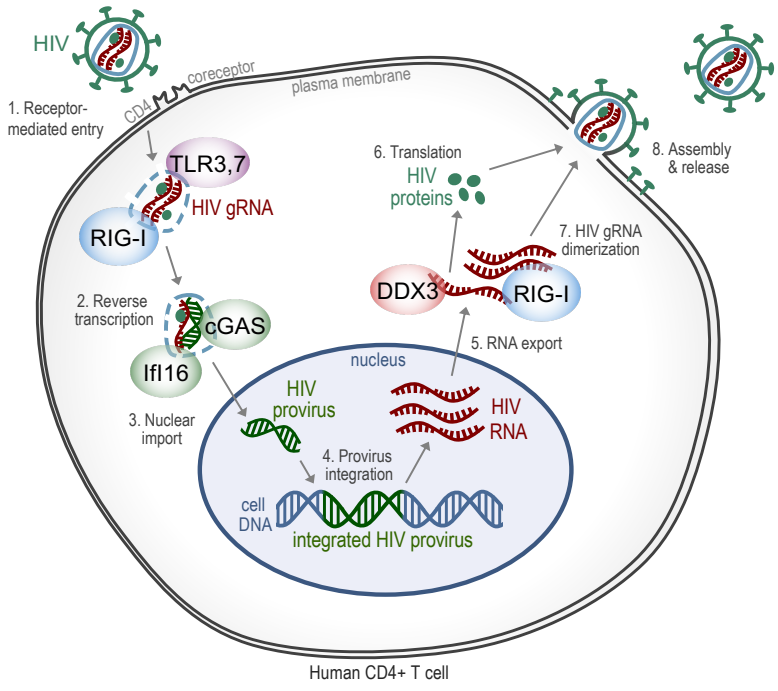


**Figure 1. HIV-1 replication and innate immune sensing.**
HIV-1 binds CD4 and a coreceptor (CCR5 or CXCR4) to enter the cell via receptor-mediated entry. The HIV-1 RNA genome is reverse transcribed into a double stranded DNA provirus, which is imported into the nucleus then permanently integrated into host DNA. HIV-1 RNA is transcribed from the integrated provirus using host machinery, then exported out of the nucleus where it is translated into HIV-1 proteins or dimerized into HIV genomic RNA. The virus particle is assembled at the plasma membrane then released from the cell. Viral DNA sensors IFI16 and cGAS have been shown to bind proviral HIV-1 DNA prior to nuclear import. The viral RNA sensors RIG-I, TLR3, and TLR7 may bind HIV-1 RNA after receptor-mediated entry, and RIG-I might also bind newly transcribed HIV RNA in the cytoplasm.

Some HIV-infected cells will silence viral transcription, cease virus production, and transition to a resting state of latency. Latently infected cells retain integrated HIV-1 provirus but otherwise mimic uninfected cells and can survive for many years until triggered to initiate viral transcription and resume virus production. The reservoir of latent cells in humans is established within the first few days after HIV-1 transmission (Whitney 2009), is responsible for virus rebound following antiretroviral therapy (ART) cessation, and is the primary barrier to curing HIV-1. Reservoir cells in HIV+ patients can be found in many anatomical sites but are most abundant in lymphoid tissues (Wong and Yukl 2016). This reservoir is a small population of cells comprised primarily of resting memory CD4+ T cells, as well as some naïve CD4+ T cells, tissue macrophages, peripheral blood monocytes, NK cells, and others (Vanhamel, Bruggemans, and Debyser 2019; Archin et al. 2014). Despite its small size, this reservoir is an incredibly heterogenous population of cells with different life spans (Buzon et al. 2014), activation levels, proliferative capacities (Lee 2014; Bui 2017), epigenetic programs, capacities to support viral replication (Vanhamel, Bruggemans, and Debyser 2019), provirus integration sites (Cohn et al. 2015), and frequency of intact proviruses (Simonetti 2015; Ho et al. 2013). Most HIV-infected cells have defective proviruses that cannot support viral replication, so only a small fraction (about 1.5%) of reservoir cells can be reactivated to produce infectious virus (Ho et al. 2013). While there is no known protein marker to reliably identify reservoir cells, reservoir size can be estimated by quantifying copies of HIV-1 proviral DNA in isolated cells. Using this method, the frequency of functional latent infection in patients on suppressive ART is predicted to be only few cells per million CD4+ T cells (Archin et al. 2012). Given the vast heterogeneity of latent cells, lack of an identifiable protein marker, and small population size, it is not surprising that decades of research have not yielded a treatment to eradicate this reservoir.

The cellular mechanisms governing HIV-1 latency are complex and incompletely understood. Latent HIV-1 infection probably arises from productively infected CD4+ T cells that have ceased viral transcription and transitioned to a resting state of stable latency. The reservoir

is comprised predominantly of resting memory CD4+ T cells, but unlike T effector precursors, memory cells are not very permissive to HIV-1 infection. It remains unclear if HIV-1 targets activated cells that later transition to a memory phenotype (Cameron et al. 2010; Shan et al. 2017), or if HIV-1 infects T cells already in a quiescent state (Saleh et al. 2007). Furthermore, the HIV-1 reservoir may be replenished through clonal expansion of latent cells (Cohn et al. 2018). Because there is no single viral transcription inhibitor, transcriptional repression of the provirus in latent cells likely results from a complex and variable combination of many cellular mechanisms (Khoury et al. 2018). These include histone modifications and chromatin structure changes, which physically block transcription factors from accessing the HIV-1 provirus (Van Lint, Bouchat, and Marcello 2013). The human positive transcription elongation factor p-TEFb becomes sequestered in an inactive small nuclear ribonucleoprotein complex (snRNP), reducing cellular transcription (Taube and Peterlin 2013). Modulation of expression levels of key transcription factors like NF-κB and IRF1 further reduce proviral transcription (Sivro et al. 2013). Reversal of these changes by various cytokines, chemicals, or other cell activating stimuli enables proviral transcription, HIV-1 protein translation, and resumed production of infectious virus.

Despite these many genetic and transcriptional changes, latent cells do not seem to express a known protein marker to distinguish them from uninfected cells. Discovery of a protein expression pattern unique to latent cells would have enormous implications for HIV-1 cure research and might enable design of therapeutics that specifically target and destroy latent cells. Considerable research has been dedicated to identifying the elusive marker of HIV-1 latency, yet no such marker has been definitively found.

**Antiviral immunity against HIV-1 infection**

Activation of intracellular innate immunity is critical for control of HIV-1 infection in CD4+ T cells and myeloid cells (Yin et al. 2020; Altfeld and Gale 2015). This response is initiated by pathogen recognition receptors (PRRs) that recognize and bind viral replication products known

as pathogen associated molecular patterns (PAMPs). In the context of productive HIV-1 infection, studies have shown that HIV-1 RNA and DNA products can be recognized as PAMPs through the actions of multiple PRRs including cGAS (Gao et al. 2013), IFI16 (Jakobsen et al. 2013), TLRs (Schlaepfer et al. 2006; Meas et al. 2020), DDX3 (Stunnenberg, Geijtenbeek, and Gringhuis 2018), and RIG-I (Berg et al. 2012; Li et al. 2016) (Fig. 1). Upon PAMP engagement, these PRRs undergo signaling activation to direct downstream actions of transcription factors including interferon regulatory factor (IRF)3 and NF-kB that mediate the expression of antiviral and immune modulatory genes, including type I interferon (IFNα/β), type III interferons (IFNλ), and inflammatory cytokines (Jensen and Thomsen 2012) (Fig. 2). Type 1 IFNs signal through their cognate receptor IFNAR1 to activate JAK/STAT signaling and induce hundreds of interferon-stimulated genes (ISGs), whose products have antiviral and immune regulatory actions to locally and systemically limit virus replication and spread (Harrison and Moseley 2020; Stark and Darnell 2012). However, this type 1 IFN response does not seem to prevent formation of the latent HIV-1 reservoir.

Many ISGs specifically function as HIV-1 restriction factors including APOBEC3G (Yang et al. 2020; Albin and Harris 2010), IFITM1 (Lu et al. 2011), IFIT1 (Nasr et al. 2017), MX2 (Goujon et al. 2013; Kane et al. 2013; Liu et al. 2013), ISG15 (Okumura et al. 2006), BST2 (tetherin) (Liberatore and Bieniasz 2011), and others (Altfeld and Gale 2015; Raftery and Stevenson 2017; Fitzgerald 2011; Nchioua et al. 2020). These restriction factors can directly or indirectly inhibit HIV-1 in the early stages of replication. This restriction is dynamic and highly regulated by the inflammatory environment, which can be modulated by HIV-1. ISG restriction of viral replication and subsequent viral escape is an important area of ongoing research, though much of this work has focused on productively infected cells with ongoing viral replication. It remains unclear how activation of these ISGs might affect the transition to or reversal from latency, or what viral mechanisms of immune escape might be employed.

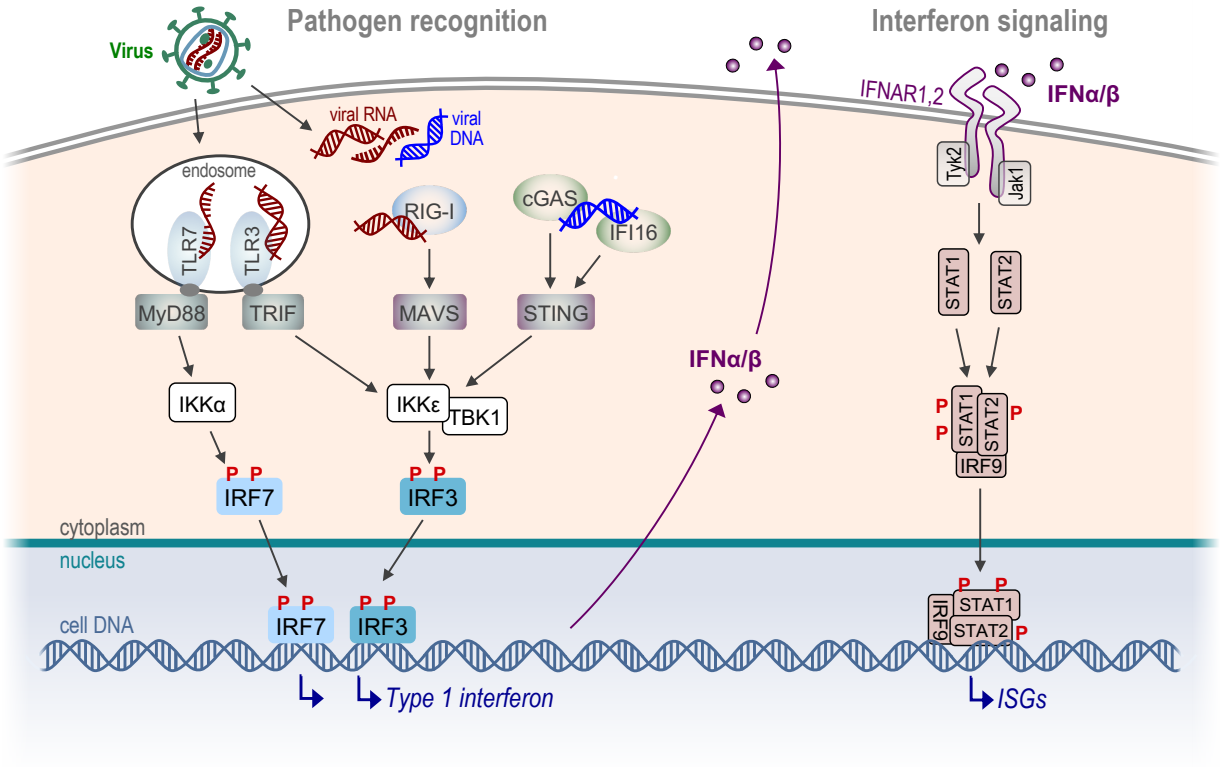


**Figure 2. Innate antiviral immune pathways.**
Upon viral entry, viral nucleic acids are available within the host cell for recognition by pathogen recognition receptors (PRRs). Cytoplasmic viral DNA can be sensed by cGAS or IFI16, and viral RNA can be sensed in the cytoplasm by RIG-I or within endosomes can be sensed by TLR7 or TLR3 within the endosome. Upon recognition of a nonself nucleic acid, each of these PRRs activate signaling adaptors that ultimately induce phosphorylation of IRF proteins, which enter the nucleus to drive transcription of type 1 interferon (IFN). IFN is secreted from the cell where it binds its cognate receptor (IFNAR1), activating a separate signaling pathway involving dimerization and phosphorylation of STAT1 & STAT2, forming the ISGF3 complex. ISGF3 enters the nucleus to drive transcription of hundreds of antiviral ISGs that can restrict viral replication and spread.

The type 1 IFN response significantly impacts the course of HIV-1 infection *in vivo*, though this response counterintuitively can be beneficial or pathogenic, with differential results based on the timing of infection. IFNα is detectable in human plasma following HIV-1 transmission (Hardy et al. 2013), leading to a type 1 IFN response that can restrict viral replication and direct cell death to limit viral spread (Altfeld and Gale 2015; Doyle, Goujon, and Malim 2015; Van der Sluis et al. 2020; Cheng, Yu, et al. 2017). IFNα from plasmacytoid DCs inhibited the establishment of latent infection in CD4+ T cells *in vitro* (Van der Sluis et al. 2020). In the SIV (simian immunodeficiency virus) model, intravenous IFNα2a administered before or shortly after infection was associated

with elevated ISGs including *MX2* and *OAS1*, as well as reduced virus transmission and slow disease progression in rhesus macaques (Sandler et al. 2014). However, continued treatment with IFNα2a led to reduced ISG expression and increased reservoir size in these animals, suggesting an IFN-desensitized state during chronic infection. In humans, therapeutic administration of IFNα during chronic HIV-1 infection failed to reduce disease progression (Bosinger and Utay 2015). Moreover, two independent studies in humanized mouse models of HIV-1 infection demonstrated a decrease in inflammation and a reduction of the latent reservoir upon blocking of IFNα signaling (Zhen et al. 2017; Cheng, Ma, et al. 2017). These studies show that type 1 IFN has dynamic effects on HIV-1 infection and the latent reservoir *in vivo*, and suggest that HIV-1 latency may be associated with reduced susceptibility to innate immune activation and/or IFN signaling.

**Antiviral escape from type 1 IFN immunity**

HIV-1 has evolved myriad mechanisms to escape innate antiviral immunity and promote viral replication within infected cells (Altfeld and Gale 2015). Viral nucleic acid structure and location are tightly regulated to hinder recognition by cellular innate immune sensors. Upon viral entry, HIV-1 nucleic acids are sequestered within a complex of viral membrane and structural proteins to shield from cytoplasmic PRRs, and HIV-1 capsid variants have evolved to escape MX2 dissociation of this viral complex (Liu et al. 2013). Following reverse transcription, excess viral cDNA is degraded by the cellular DNA exonuclease TREX1 to reduce available ligand for cGAS or IFI16 recognition (Yan et al. 2010). Because HIV-1 utilizes host cell machinery for transcription, newly transcribed viral RNA transcripts bear many features of host RNA like 2'O methylation and a 5' cap, which offer protection from nonself discrimination by RNA sensors like RIG-I (Ringeard et al. 2019).

HIV-1 infection regulates the expression and availability of host transcription factors that mediate innate immune responses. IRF3 is a critical mediator of multiple innate immune pathways

(see Fig. 2) and is targeted by several HIV proteins. HIV-1 Vif and Vpr ubiquitinate IRF3 thus marking it for proteasomal degradation (Okumura et al. 2008) and Vpu targets IRF3 for caspase-mediated inactivation and lysosomal degradation (Doehle et al. 2012; Park et al. 2014). Additionally, HIV-1 infection hijacks and sequesters transcription factors that might otherwise be involved in innate immune signaling and/or ISG expression. HIV Tat interacts with the host IRF1 transcription factor to mediate viral replication, occupying the STAT1-binding domain of IRF1 and thus inhibiting IRF1/STAT1-dependent innate immune responses (Remoli et al. 2006). Vpu blocks NF-κB activation downstream of cGAS signaling to obstruct IFNα/β and ISG transcription. HIV-1 proteins also block components of the pathogen recognition and interferon signaling pathways and can directly inhibit certain ISGs (Altfeld and Gale 2015). The HIV-1 protease sequesters RIG-I (Solis et al. 2011). Vpu drives ubiquitination of BST-2 (tetherin) thus targeting it for proteasome degradation (Dube et al. 2010). Vpr and Vif directly inhibit TBK1 phosphorylation to block production of type 1 IFN, and Vif antagonizes APOBEC3G (Sheehy, Gaddis, and Malim 2003). HIV-1 infection increases expression of the host cellular factors SOCS1 and SOCS3 to block STAT2 phosphorylation and reduce cellular IFN responses (Song and Shuai 1998).

Exposure to type 1 IFN may promote viral and cellular changes that contribute to HIV-1 immune escape. The initial type 1 IFN response to HIV-1 infection imparts selection for IFN-resistant viral variants (Iyer et al. 2017), however the role of these variants in HIV-1 latency is not known, and IFN resistance might occur as only a transient phenotype (Ashokkumar et al. 2020). Cells can become desensitized to circulating IFNα/β through internalization and degradation of IFNAR1 (Hardy 2009 Blood), potentially reducing the antiviral effects of type 1 IFN throughout chronic HIV-1 infection.

**Antilatency therapies**

The latent reservoir is the biggest obstacle to curing HIV-1 and is responsible for viral rebound following ART cessation in patients. A true sterilizing cure for HIV-1 must somehow

destroy this reservoir without obliterating a patient's immune system. HIV-1 latency eradication is a critically important and rapidly growing area of research. Considerable research efforts over the last decade have yielded a variety of therapeutic approaches for eradicating latent cells, though none has yet succeeded.

Perhaps the most popular therapeutic approach to HIV-1 latency eradication is to induce latent cell reactivation, thus increasing susceptibility to therapy-induced cell death. This "shock and kill" approach involves shocking latent cells with one or more drugs that reactivate provirus transcription and virus production, then specifically triggering death of reactivated latent cells. Numerous "shock" agents, also known as latency reversal agents (LRAs), have been discovered and shown to successfully reactivate proviral transcription *in vitro*. These include histone deacetylase (HDAC) inhibitors, PKC agonists, checkpoint blockade agents, and others. Most of these LRAs target only one of the multiple cellular mechanisms known to enforce latency, thus necessitating a treatment regimen of several combined LRAs. Many LRAs have been tested as single agents and/or combination therapies in clinical trials, such as Bryostatin (PKC agonist), Protstratin (PKC agonist), Ingenol (PKC agonist), Vorinostat (HDAC inhibitor), Romidepsin (HDAC inhibitor), Panobinostat (HDAC inhibitor), Chidamide (HDAC inhibitor), Disulfuran (AKT), Ipilumimab (CTLA4 blockade) (Bashiri et al. 2018). While most of these LRAs trigger some level of virus reactivation in patients, it is unclear if they fully reactivate all replication-competent cells of the HIV-1 reservoir, and none of these therapies has successfully eradicated the reservoir in a human patient. Far more research is needed to determine how to best reactivate and destroy latent cells.

An alternate approach has focused on innate immune pathways as targets for latency eradication (Board et al. 2021). Because RNA- and DNA-sensing innate immune pathways can restrict HIV-1 replication *in vitro*, therapeutically augmenting these pathways might arm latent cells to sense HIV-1 nucleic acids, activate innate antiviral immune pathways, and block viral rebound and spread. The innate immune sensor RIG-I can bind and become activated by HIV-1

RNA *in vitro* (Berg et al. 2012; Solis et al. 2011), so researchers thought that perhaps stimulating this pathway with a retinoic acid derivative would enable RIG-I-mediated apoptosis of reactivated, latent cells. This was reported to have been demonstrated in a variety of *in vitro* cell line and primary cell models of HIV-1 latency (Li et al. 2016), but has not been repeated by other labs or led to further preclinical research. Several clinical trials have evaluated the efficacy of other innate immune augmenting agents including PolyICLC (TLR3), GS-9620 (TLR7), MGN1703 (TLR9), ALT-803 (IL-15), PEG-IFNα2b (type 1 IFN), though none of these has resulted in latency eradication.

**Modeling the HIV-1 reservoir**

Understanding the biology of HIV-1 latent infection is hampered by the difficulty of identifying and isolating viable latent cells from an infected individual, and by the lack of *in vitro* models that capture the heterogeneity of the HIV-1 reservoir. Many *in vitro* models have been developed that represent one or more aspects of the HIV-1 latent reservoir, but each has important limitations (Han et al. 2007). At present there is no known protein marker that reliably distinguishes latent from uninfected cells, so latent cells must be identified by other means. This issue is avoided by using established latent cell lines, such as the JLat and ACH2 cells used in this study (Folks et al. 1985; Jordan, Bisgrove, and Verdin 2003). Latent cell lines are clonal populations of latently infected cells that were expanded from single cells, proliferate readily, and pass integrated provirus to daughter cells upon cell division. These represent latent cells that might arise from clonal expansion *in vivo*, but each cell line represents only one unique clone with a single integrated provirus, making it difficult to draw conclusions about the entire diverse reservoir.

An alternate method for producing and identifying latent cells *in vitro* is infection with a reporter HIV-1 strain, such as the RGH virus used in this study (Dahabieh et al. 2013) or the similar R7GEmC two-color virus described elsewhere (Calvanese et al. 2013). These reporter

viruses have been modified to include fluorophore or luciferase genes that are conditionally expressed to indicate different (negative, latent, or productive) infection states. Cells latently infected with a reporter virus have unique and distinct provirus integrations, overcoming a major limitation of established latent cell lines. However, virus-driven transcriptional repression may reduce or silence fluorophore expression, impacting the accuracy of identification of latent cells.

Primary cells derived from healthy humans offer many advantages over cell lines, including increased biological diversity among individual cells and inclusion of cells in a resting state. Commonly used primary cells include CD4+ T cells isolated from healthy human PBMC, lymphoid tissue, or tonsillar explants. However, because primary cells are not very permissive to HIV-1 infection and the rate of latency *in vivo* is low (<1% of infected cells), cytokine treatments are often used to increase cell permissivenes. In the present study, primary CD4+ T cell permissiveness was increased by treatment with IL-2, IL-7, and IL-15, and HIV-1 replication was suppressed by ART. Other studies have demonstrated augmented rates of latent infection by culturing infected cells over long periods of time with suppressive cytokines or by coculture with activated DCs. Because the biological factors for triggering latency are not completely understood, controversy still exists over the best *in vitro* model. Ideally, latently infected cells would be isolated directly from a human HIV-1+ patient, but without a known latency marker, at present latent cells can only be identified after reactivation.

**Objectives of this study**

Several studies have examined innate immune and/or interferon responses in latent cells providing valuable insight into HIV-driven immune escape (Ranganath et al. 2016), but each study has focused on one or two *in vitro* latency models. The objective of the present study is to conduct a thorough analysis of innate immune and interferon responses across a variety of distinct *in vitro* models of HIV-1 latency. I examined RIG-I pathway activation, interferon responses, and ISG expression in latent cells using an integrated study design that includes established T cell line

models of HIV-1 latency, Jurkat T cells latently infected with a fluorescent reporter virus, and a primary CD4+ T cell model of HIV-1 suppression. I evaluated IFNβ induction of a panel of antiviral ISGs in each of these models, and assessed activation of key components of innate immune and type 1 IFN signaling pathways. Using a functional genomics approach including bulk mRNA sequencing and single cell RNA sequencing, I defined differences in innate immune activation and type 1 IFN signaling among uninfected cells and cells with latent or suppressed HIV-1 infection. My observations support the hypothesis that latent HIV-1 infection involves viral selection or modification of target cells to an innate immune suppressed phenotype that supports the viral reservoir.

# CHAPTER 2

*INTRODUCTION*

CD4+ T cells infected with HIV-1 can activate intracellular innate immune responses that block viral replication/spread and drive apoptosis of the infected cell (Altfeld and Gale 2015; Pitha 2011). Regardless, a reservoir of latently infected cells persists long-term in a human patient. While the exact origin of latent cells is still disputed, these cells probably arise from infected T cells that downregulate viral transcription and transition to a resting state, suggesting they have somehow survived innate immune defenses. Recent studies have shown that viral RNA sensing and type 1 interferon response pathways may be disrupted in latently infected cell lines (Li et al. 2016; Ranganath et al. 2016), while DNA sensing pathways are not perturbed. I hypothesized that latently infected cell lines would be less sensitive to innate immune and interferon agonists than uninfected cells. To address this hypothesis I conducted a study using two different types of latency models: 1) established latent cell lines, and 2) Jurkat cells acutely infected with a latency

reporter virus. I evaluated innate immune and type 1 IFN responses in these latent cell lines compared to the control, uninfected cell lines from which they were derived.

**Latency models**

Three established cell lines were used in this study. These include two different Jurkat CD4+ T cell latency models, JLat9.2 and JLat11.1, and the CEM CD4+ T cell ACH2 latency model, each harboring silent HIV-1 provirus (Jordan, Bisgrove, and Verdin 2003; Folks et al. 1989). These well-characterized latent cell lines can be compared to the uninfected, parent cells from which they were derived, and serve as a useful tool for identifying pathways to then screen in physiologically relevant models.

JLat9.2 and JLat11.1 cells were created by transducing Jurkat cells with a GFP-expressing lentivirus reporter that is replication-incompetent due to a mutation in the *Env* gene. Transduced cells were then selected for GFP induction by flow cytometry, then single cell clones cultured and expanded into a latently infected population that expresses low levels of residual HIV-1 RNA but no detectable HIV-1 proteins (Jordan, Bisgrove, and Verdin 2003). In contrast, ACH2 cells were derived by infecting A301 CEM cells with a replication-competent HIV-1 then rescuing latent cells and expanding them into a clonal population. ACH2 cells constitutively express low levels of HIV-1 RNA, proteins, and infectious virus (Folks et al. 1985). JLat9.2,

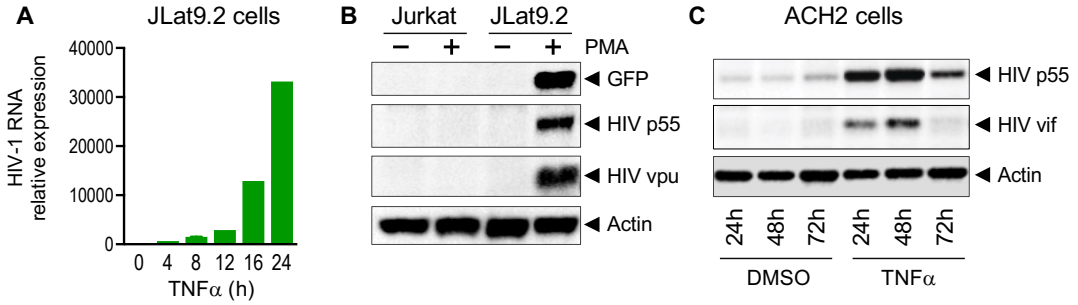


**Figure 3. Reactivation of HIV-1 latent cell lines.**

**A** qRT-PCR analysis of HIV-1 RNA expression in latent JLat9.2 cells reactivated with 10ng/ml TNFα for indicated times. **B, C** Immunoblot analysis of HIV-1 protein expression in Jurkat control cells and JLat9.2 latent cells treated with 16nM PMA for 24h, or ACH2 latent cells treated with 10ng/ml TNFα (or DMSO as negative control) for indicated times. Data in this figure are from one representative experiment.

JLat11.1, and ACH2 cells each harbor one transcriptionally silent provirus that can be reactivated with various cytokines or chemicals to transcribe viral RNA and translate viral proteins (Fig. 3). These latent cell lines can also be compared to the parent, uninfected cells from which they were originally derived (Jurkat or A301 cells) to investigate factors that might be associated with HIV-1 latent infection.

I also utilized the Red-Green-HIV-1 (RGH) dual-color reporter virus, which enables distinction of latent and productively infected cells by flow cytometry (Dahabieh et al. 2013). Infection with the RGH virus provides a platform model of populations of latently and productively-infected cells with distinct provirus integration sites, overcoming a major limitation of clonal latent cell line models. RGH-infected cells constitutively express mCherry via the cytomegalovirus (CMV) immediate-early promoter, indicating provirus integration, while expression of green fluorescence protein (GFP) under control of the viral long terminal repeat (LTR) element marks cells undergoing HIV-1 transcription. Therefore, dual color fluorescence marks cells with integrated provirus undergoing active viral gene expression (Fig. 4A). The RGH virus has a mutation in the *Env* gene preventing production of infectious virus (Dahabieh et al. 2013), and in this study was pseudotyped with VSV glycoprotein to facilitate infection. Jurkat CD4+ T cells were mock-infected (conditioned media) or were infected with a ΔINT control virus (integrase mutation prevents provirus integration) or RGH at MOI 0.2. Because this virus is replication incompetent and a low MOI was used (0.2), any infected cells are likely to have only one integrated provirus. After infection cells were cultured for five days to allow establishment of latency, then sorted by flow cytometry into distinct infection groups (negative, latent, or productive) for further phenotypic analysis as depicted in Fig. 4B. The flow cytometry gating strategies used to exclude dead cells by DAPI staining then sort live cells based on mCherry and GFP expression are shown in Figs. 4C & 4D.

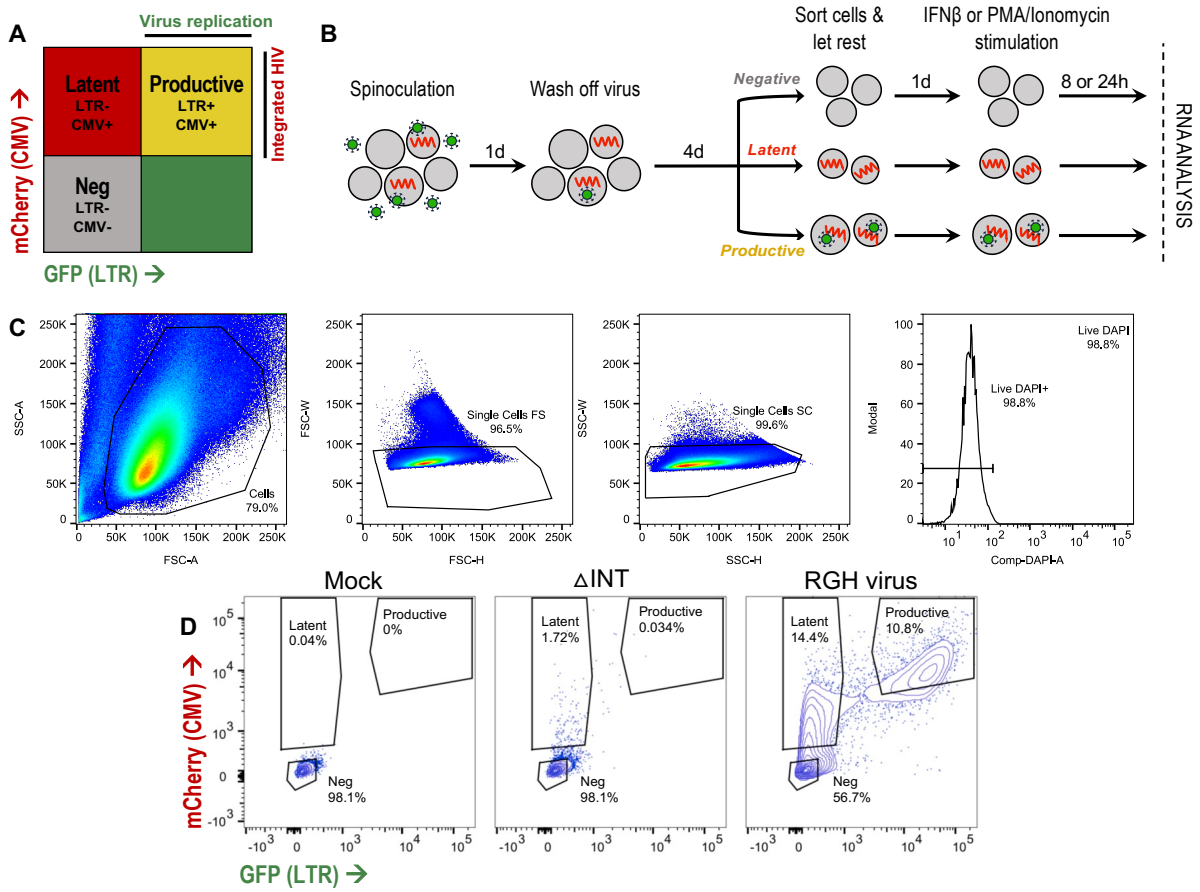


**Figure 4. Flow separation of RGH-infected Jurkat cells.**

**A** Diagram of fluorophore expression distinguishing Red-Green-HIV-1 (RGH) virus integration vs. replication. mCherry is stably expressed by the CMV promoter, and GFP is conditionally expressed by the HIV-1 LTR promoter upon HIV-1 replication. Productive infection: mCherry+GFP+; latent infection: mCherry+GFP-; no infection: mCherry-GFP-. **B** Schematic of RGH infection and sort protocol. Jurkat cells were mock-infected (conditioned media) or were spinoculated with a ΔINT control virus (no provirus integration) or RGH at MOI 0.2. After 5d cells were sorted by flow cytometry using the gating scheme shown, rested 24h in culture, then stimulated and analyzed. **C** Flow cytometry gating scheme used to exclude dead cells by DAPI staining. **D** Flow cytometry gates used to sort live (DAPI neg) Jurkat cells 5d after mock-, ΔINT-, or RGH-infection.

## *RESULTS*

### Reactivation of latent cell lines

The viral RNA sensing receptor RIG-I can be activated by HIV-1 RNA to mount an antiviral, interferon response within infected cells (Berg et al. 2012; Li et al. 2016; Solis et al. 2011). Upon reactivation, latently infected cells express HIV-1 RNA transcripts that are available for sensing by RIG-I or other viral RNA sensors. Successful RIG-I activation by HIV-1 RNA might lead to an

intracellular innate immune response that could block viral replication and spread, and drive apoptosis of the infected cell. I treated latent cell lines with media as negative control (no treatment), various reactivating agents (10 ng/ml TNFα or 16 nM PMA), or Sendai virus as positive control (100 HAU/ml) for 24h, then analyzed gene expression by qRT-PCR (Fig. 5A). As expected, TNFα and PMA treatment each induced HIV-1 RNA transcription in JLat9.2 cells indicating reactivation from latency. However, increased HIV-1 RNA expression in TNFα- or PMA-treated JLat9.2 cells was not associated with an increase in the antiviral ISGs *MX1, IFIT1*, or *IFIT2*, suggesting that newly transcribed HIV-1 RNA does not activate innate immune signaling in this model. Immunoblot analysis of PMA-treated JLat9.2 cells similarly showed expression of GFP (indicating HIV reactivation) after 12h and 24h without a corresponding increase in the ISGs *IFITM1* and *RIG-I* (Fig. 5B).

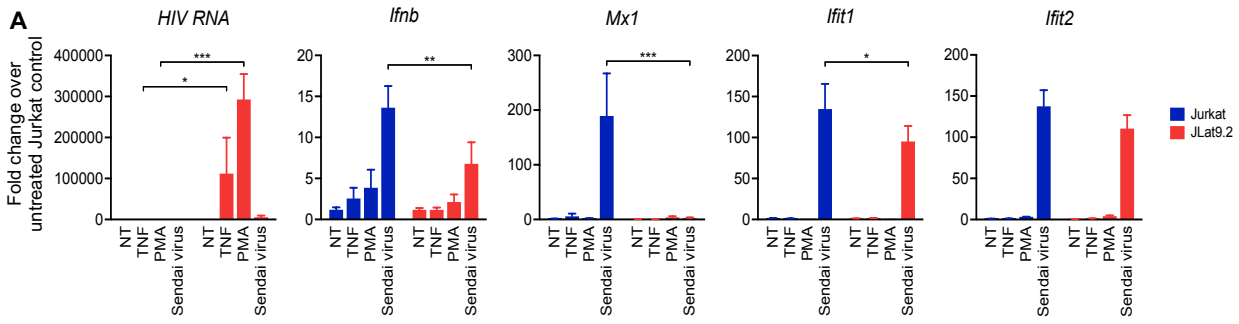


**Figure 5. ISG expression in reactivated latent cell lines.**
**A** Uninfected Jurkat (blue bars) or latent JLat9.2 cells (red bars) were left untreated (NT) or were reactivated with 10ng/ml TNFα or 16nM PMA for 24h. Sendai virus infection (100 HAU/ml, 24h) was included as a positive control for innate immune activation. Gene expression was analyzed by qRT-PCR and fold change (FC) calculated relative to untreated Jurkat cells and *RPL13a* (ΔΔCt method). Bars represent mean FC + SD from three independent experiments. Statistics: two-tailed t-test comparing similarly treated Jurkat and JLat9.2 cells. *p<0.05, **p<0.01, ***p<0.001. **B** Immunoblot analysis of protein expression in JLat9.2 cells reactivated with 16nM PMA for indicated times. GFP indicates HIV-1 reactivation. SupT1 T cells infected with Sendai virus (SeV, 100 HAU/ml, 24h) were included as positive control.

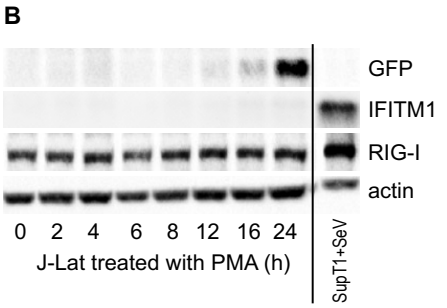


Interestingly, Sendai virus infection triggered transcription of *IFNβ* and some ISGs in both Jurkat and JLat9.2 cells, though the magnitude of expression differed between cell lines. JLat9.2 cells induced lower levels of *IFNβ* and *IFIT1* than Jurkat cells, and failed to activate *MX1*

transcription entirely (Fig. 5A), suggesting these latent cells may have limited capacity to mount an innate antiviral immune response.

JLat9.2 cells express GFP upon activation of the HIV-1 promoter. PMA treatment (16nM for 24h) causes approximately 8% of cells to reactivate high levels of HIV-1 transcription (Fig. 6A); thus, most cells in the PMA-treated population remain latent, potentially obscuring meaningful phenotypes of reactivated cells. To overcome this, I reactivated Jurkat and JLat9.2 cells with PMA for 24h then used flow cytometry to separate GFP+ and GFP- populations (Fig. 6A), before analysis of each group by qRT-PCR. As expected, PMA-treated GFP+ (reactivated) JLat9.2 cells expressed much higher levels of HIV-1 RNA than PMA-treated GFP- (latent) JLat9.2 cells, though neither population increased expression of innate immune genes (*IFNβ, MX1*) (Fig. 6B). Sendai virus treatment resulted in a type 1 IFN response in both Jurkat and JLat9.2 cells (*IFNβ* transcription; Fig. 6B), though the magnitude of response was diminished in JLat9.2 cells, similar to observations in previous experiments (see Fig. 5).

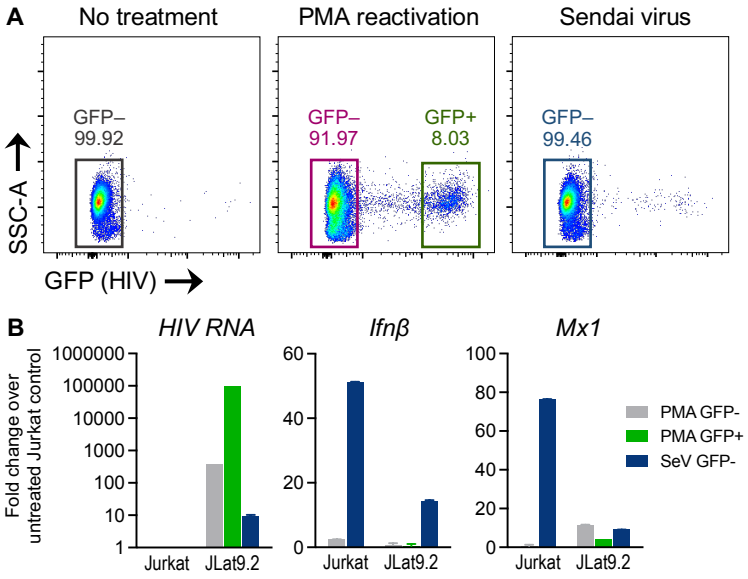


**Figure 6. ISG expression analysis in reactivated, sorted JLat9.2 cells.**
**A** Uninfected Jurkat or latent JLat9.2 cells were left untreated (NT), reactivated with 16nM PMA, or treated with 100 HAU/ml Sendai virus (SeV) for 24h, then sorted into GFP- (no HIV transcription) or GFP+ (expresses HIV RNA) groups using the gates shown. Dot plots show data from JLat9.2 cells. **B** qRT-PCR analysis of gene expression in Jurkat or JLat9.2 cells treated as described above and sorted based on GFP expression. Fold change was calculated relative to untreated (NT) Jurkat cells and *RPL13a* (ΔΔCt method). Data are shown from a single experiment.

**RIG-I pathway analysis**

Latent cell lines reactivated production of HIV-1 RNA without initiating an innate immune response (see Figs. 5 & 6). This might occur because RIG-I fails to recognize and bind HIV-1 RNA in these cells, or because RIG-I recognition of viral RNA does not activate an innate immune response. Several studies have demonstrated RIG-I recognition of HIV-1 RNA in various *in vitro* model systems (Berg et al. 2012; Solis et al. 2011), suggesting RIG-I might similarly recognize HIV-1 RNA in reactivated latent cells. Some latent cells (including JLat9.2 and ACH2) transcribe low levels of detectable HIV-1 RNA without reactivating virus production, so it's possible these cells might need to obstruct the RIG-I pathway to survive long-term without triggering innate immune defenses. To evaluate viral RNA sensing and innate immune activation throughout latent infection, I infected the latent cell lines JLat9.2 and ACH2 or control uninfected cell lines Jurkat and A301 with Sendai virus (SeV), a model RNA virus that drives robust IRF3 activation through multiple innate immune pathways including RIG-I (Doehle et al. 2009). Twelve or 24h after infection, cellular RNA was collected and evaluated by qRT-PCR for activation of a panel of ISGs. SeV-infected Jurkat and A3.01 control cells transcribed *IFNβ* and upregulated high levels of multiple ISGs (*MX1, IFIT1, IFIT2, OAS1*), indicating a robust innate immune response to SeV (Fig. 7A, B). Latent JLat9.2 and ACH2 cells also activated ISGs after SeV infection, though the magnitude of gene induction was significantly lower for most ISGs, with *MX1* induction almost completely blocked in both latent cell lines. Because SeV activates multiple innate immune pathways, I next evaluated latent cell responses to an agonist that specifically triggers only the RIG-I pathway. I transfected Jurkat and JLat9.2 cells with PAMP RNA, a synthetic RNA derived from the Hepatitis C virus (HCV) genome that directly binds and activates RIG-I (Saito et al. 2008). As a negative control, cells were transfected with a synthetic nonsignaling xRNA derived from a nonstimulatory region of the HCV genome. PAMP RNA but not xRNA induced IFNβ expression in both cell lines 24h after treatment, and induced expression of a panel of ISGs in Jurkat cells;

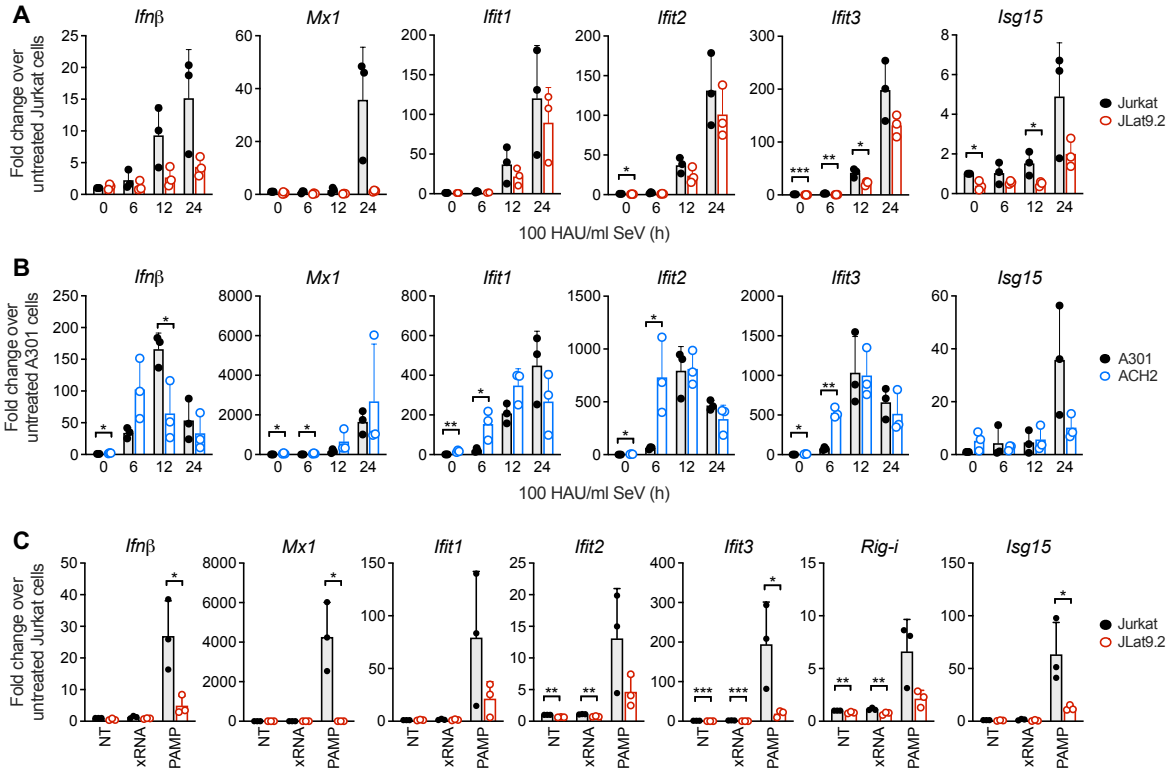


**Figure 7. HIV latent cell lines have impaired responses to RIG-I agonists.**

**A-B** qRT-PCR analysis of Jurkat vs. JLat9.2 cells or A301 vs. ACH2 cells after Sendai virus (SeV) infection (100 HAU/ml). **C** qRT-PCR analysis of Jurkat vs. JLat9.2 cell lines left untreated (NT), or transfected with nonstimulatory xRNA or RIG-I stimulatory PAMP RNA for 24h. For all qRT-PCR analyses, data points represent mean FC ± SD relative to untreated cells and RPL13a (ΔΔCt method), from three independent experiments. Statistical significance of latent (JLat9.2 or ACH2) relative to control (Jurkat or A301) cells was determined by two-tailed t-test with multiple comparisons (Holm-Sidak). *p<0.05, **p<0.01, ***p<0.001.

however, ISG expression was suppressed in JLat9.2 cells (Fig. 7C). Thus, latent but not HIV-uninfected cells demonstrate attenuated responses to the RIG-I agonists SeV and PAMP RNA, suggesting that RIG-I and/or type 1 interferon pathways are disrupted during HIV-1 latency.

The innate immune actions of RIG-I are mediated by the transcription factor IRF3. Upon activation, IRF3 gets phosphorylated then translocates to the cell nucleus to initiate *IFNα/β* transcription, ultimately leading to type 1 IFN signaling and ISG activation (see Fig. 2). Productive HIV-1 infection has been shown to drive PRR signaling but suppress IRF3 activation (Doehle et al. 2012; Okumura et al. 2008). To gain insight into how latent cells escape RIG-I-mediated immunity, I evaluated IRF3 activation in latent or control cell lines after treatment with SeV. IRF3

was present in a resting state, expressed at similar levels in Jurkat and JLat9.2 cells, and phosphorylated at serine 386 (pIRF3 S386) in both cell lines upon SeV infection (Fig. 8A, B). ImageStream analysis revealed that SeV infection triggered similar levels of IRF3 nuclear translocation in Jurkat and JLat9.2 cells (Fig. 8C-E). Together these results reveal that HIV-1 latent cells are not generally impaired in RIG-I signaling or IRF3 activation, but instead appear to exhibit suppressed IFNα/β production and/or IFN-induced ISG expression.

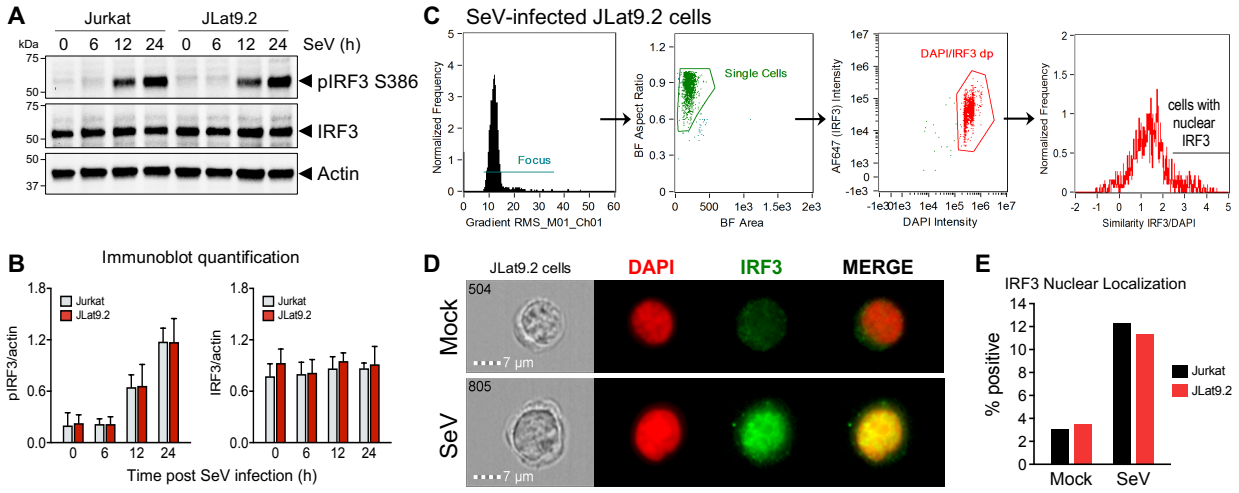


**Figure 8. Latent HIV infection disrupts type 1 IFN responses downstream of PRR signaling.**
**A-B** Immunoblot analyses of total and phosphorylated IRF3 (pIRF3) in Jurkat or JLat9.2 cells after SeV infection (100 HAU/ml). One representative image is shown in Panel A; quantified data from three independent experiments are shown in Panel B. Target protein abundance relative to actin was quantified with ImageJ. Statistical significance between Jurkat and JLat9.2 cells was determined by two-way ANOVA with multiple comparisons (Holm-Sidak). *p<0.05, **p<0.01, ***p<0.001. **C** ImageStream analysis of nuclear IRF3 in mock-treated or SeV-infected (100 HAU/ml, 24h) Jurkat or JLat9.2 cells. Nuclear IRF3 was determined by IRF3/DAPI similarity over an arbitrary cutoff of 2.3. **D** Representative images of mock-treated or SeV-infected JLat9.2 cells: brightfield, red (DAPI-stained nuclei), green (IRF3), and red/green merged images. **E** Frequency of cells with nuclear IRF3; data are shown from a single experiment.

### Type 1 IFN response in latent cell lines

RIG-I agonists (PAMP RNA and SeV) triggered lower ISG induction in latent compared to uninfected cells, but IRF3 activation was comparable among cell lines. This suggests that latent infection is associated with a defect in RIG-I mediated immunity, which occurs downstream of IRF3 (see Fig. 2). Possible mechanisms include reduced transcription/production of IFNα/β;

reduced expression of, or binding to, the IFNα/β receptor 1 (IFNAR1); disrupted JAK/STAT signaling; altered baseline expression of ISGs; dysregulated transcription of ISGs upon IFNα/β stimulation; instability of transcribed ISG mRNA; or disrupted translation of ISG proteins. I first examined cell surface IFNAR1 expression in resting latent and uninfected cell lines by flow cytometry. Interestingly, all latent lines tested express similar surface levels of the IFNAR1 receptor compared to corresponding controls (Fig. 9A-C).

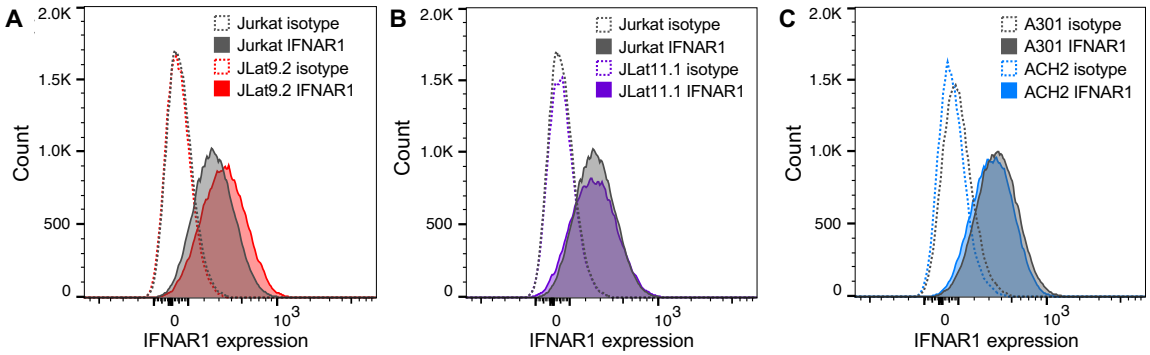


**Figure 9. Analysis of IFNα/β receptor (IFNAR1) expression in resting latent cell lines.**
FACS analysis of IFNAR1 cell surface expression compared to isotype control. **A** Uninfected Jurkat vs latent JLat9.2 cells; **B** uninfected Jurkat vs latent JLat11.1 cells; **C** uninfected A301 vs latent ACH2 cells.

I next examined expression of ISG mRNA in latent and uninfected cell lines at rest ("baseline," no IFNβ treatment) and found that Jurkat-derived latent cells (JLat9.2 and JLat11.1) tend to have similar or lower ISG expression than controls (Fig. 10A, B). A few ISGs were expressed differentially between latent JLat and uninfected Jurkat cells; JLat9.2 cells expressed lower levels of *IFITM1, IFIT3*, and *ISG15* mRNA, and JLat11.1 cells expressed elevated *IFITM1* but reduced *IFIT1* mRNA. Unlike JLat cells, which harbor a replication incompetent provirus, ACH2 cells constitutively produce low levels of infectious HIV-1 at rest and were found to express higher baseline levels of many ISGs than A301 controls (*IFNβ, MX1, IFITM1, IFIT1, IFIT2, IFIT3*, *RIG-I*) (Fig. 10C). Persistent, low-level virus production in ACH2 cells may trigger ongoing innate immune activation leading to upregulated ISGs.

To investigate responsiveness to type 1 IFN, I treated latent JLat9.2, JLat11.1, and ACH2 cells and control Jurkat and A3.01 cells with 100 IU/ml of IFNβ and harvested over a 12h time

course for expression analysis of a panel of ISGs. IFNβ-induced ISG mRNA expression was overall significantly lower in each JLat latent cell line relative to uninfected Jurkat control cells (Fig. 10D, E). Numerous ISGs were poorly induced by IFNβ in JLat9.2 cells, and MX1 was particularly poorly induced in both JLat9.2 and JLat11.1 cells. Because baseline ISG levels in these cell lines were typically expressed at similarly low levels (Fig. 10A, B), altered baseline expression alone likely does not account for differences in ISG induction between these cells. Similar results were seen in an immunoblot analysis of ISG protein expression following IFNβ treatment of Jurkat and JLat9.2 cells. IFNβ treatment results in elevated expression of ISG proteins (*MX2, IFIT1, OAS1, IFITM1*) in both Jurkat and JLat9.2 cells at 12h and 24h (Fig. 10G). However, the magnitude of expression of these proteins is lower in IFNβ-treated JLat9.2 cells than IFNβ-treated Jurkat cells. MX1 protein expression is induced by IFNβ in Jurkat cells at 12h and 24h, but is completely absent in JLat9.2 cells at any time point (Fig. 10G). Thus, JLat latency models exhibit suppressed IFNβ-induction of ISGs.

The results of IFNβ stimulation were more complicated in the ACH2 latency model. IFNβ stimulation activated ISG expression in both uninfected A301 and latent ACH2 cells. Eight to twelve hours after IFNβ stimulation, A301 and ACH2 cells expressed similarly high levels of *MX1*, *IFIT1*, and *IFIT2* (Fig. 10F). However compared to A301 cells, ACH2 cells induced lower levels of *IFITM1* but higher levels of *IFIT3* and *RIG-I*. These data represent ISG expression level in IFNβ-stimulated A301 or ACH2 cells calculated relative to an untreated mock control (resting A301 cells), and therefore do not account for initial differences in ISG expression. Because resting ACH2 cells express such high levels of ISG mRNA than A301 cells (Fig. 10C), one would expect IFNβ-treated ACH2 cells to also express higher levels of ISGs than IFNβ-treated A301 cells. Surprisingly, ISG levels post IFNβ treatment were similar between cell lines, which may indicate that IFNβ-induced ISG transcription is somewhat restricted in latent ACH2 cells.

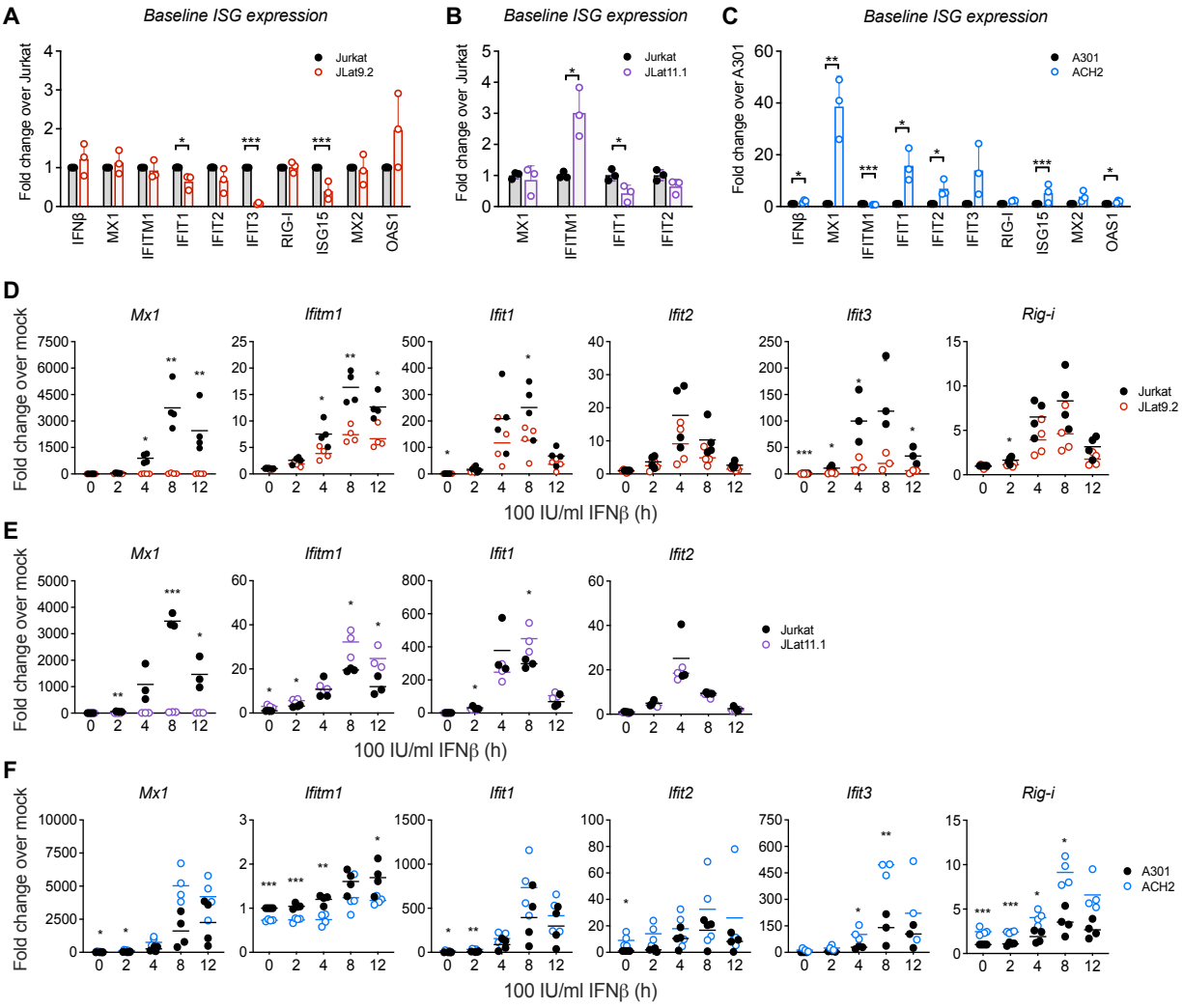


**Figure 10. Analysis of type 1 IFN responses in HIV-1 latent cell lines.**

**A-C** qRT-PCR analysis of resting (baseline) ISG mRNA in latent JLat9.2, JLat11.1, or ACH2 cells compared to corresponding control uninfected Jurkat or A301 cells. **D-F** qRT-PCR analysis of ISG mRNA induction following IFNβ stimulation (100 IU/ml, 8h) in latent or uninfected cell lines. For all qRT-PCR analyses, fold change (FC) was calculated relative to untreated control (Jurkat or A301) cells and housekeeping gene *RPL13a* (ΔΔCt method). Data points represent mean FC from multiple independent experiments (A, C, D, F) or FC of separate replicates in one experiment (B, E). At each time point, statistical significance in latent cells relative to corresponding uninfected control (Jurkat or A301) cells was determined by Student's two-tailed t-test. *p<0.05, **p<0.01, ***p<0.001. **G-H** Immunoblot analysis of Jurkat or JLat9.2 cells stimulated with 100 IU/ml IFNβ for indicated times. Representative images from one of three independent experiments are shown.

I next evaluated expression of type 1 IFN signaling proteins and found that when stimulated with IFNβ, latent JLat9.2 and uninfected Jurkat cells increased abundance of phosphorylated STAT1 and STAT2 (Fig. 10H), suggesting that in this model, HIV-1 latency does not block type 1 IFN signaling of JAK/STAT pathway activation. Interestingly, JLat9.2 cells express higher baseline levels of the inactive and phosphorylated forms of JAK1, STAT2, and STAT3 proteins than uninfected cells (Fig. 10H). Taken together, these data show that HIV-1 latent infection is associated with basal activation and aberrant regulation of type 1 IFN signaling in these latent cell line models, though this phenotype is variable between models. Aberrant regulation of type 1 IFN signaling may compromise the ability of latently infected cells to fully activate an IFN-dependent antiviral response.

**Transcriptomic analysis of latent cell lines**

To better define the extent of dysregulated ISG expression in latent HIV-1 infection, I performed a bulk RNA sequencing (RNAseq) transcriptomic analysis on JLat9.2 and Jurkat cells as models of HIV-1 latency and uninfected control cells, respectively. Jurkat and JLat9.2 cells were left untreated (mock) or were stimulated with 100 IU/ml IFNβ or IFNγ for 4, 8, or 12h, and then analyzed by RNAseq. Three biological replicates were included for each experimental condition. A principal component analysis of mock and IFNβ-treated samples is shown in Fig. 11A, validating the similarity of biological replicates and revealing the distinct transcriptomic response of each cell line to IFNβ treatment. I first determined the differentially expressed (DE) genes between resting (mock-treated) Jurkat and JLat9.2 cells, and grouped these genes into functional categories using Gene Ontology (GO) analyses (Fig. 11B). In Jurkat cells these DE genes clustered into GO categories that typically span ISG functions, including innate immune activation, inflammatory response, cytokine production, and immune regulation (Green, Ireton, and Gale 2018; Schoggins and Rice 2011). In contrast, GO categories significantly enriched in JLat9.2 cells included development and differentiation programs but lacked innate immune,

antiviral, or immune activation functions. These observations indicate that uninfected Jurkat cells could be more effective at activating and regulating an IFNβ-induced antiviral response than JLat9.2 cells which harbor HIV-1 provirus.

I next identified genes that were induced by IFNβ (ISGs) in Jurkat or JLat9.2 cells. These ISGs were defined as genes whose expression was significantly changed following 4, 8, or 12h of IFNβ treatment compared to mock-treated cells. I identified 503 DE ISGs in IFNβ-treated Jurkat and/or JLat9.2 cells within the treatment time course, shown in the heat map in Fig. 12A and listed in Table 5. While IFNβ induced transcriptional changes in both cell lines, the IFNβ response signature of Jurkat cells included significant upregulation of many innate immune and known antiviral ISGs that were lacking in expression in JLat9.2 cells.

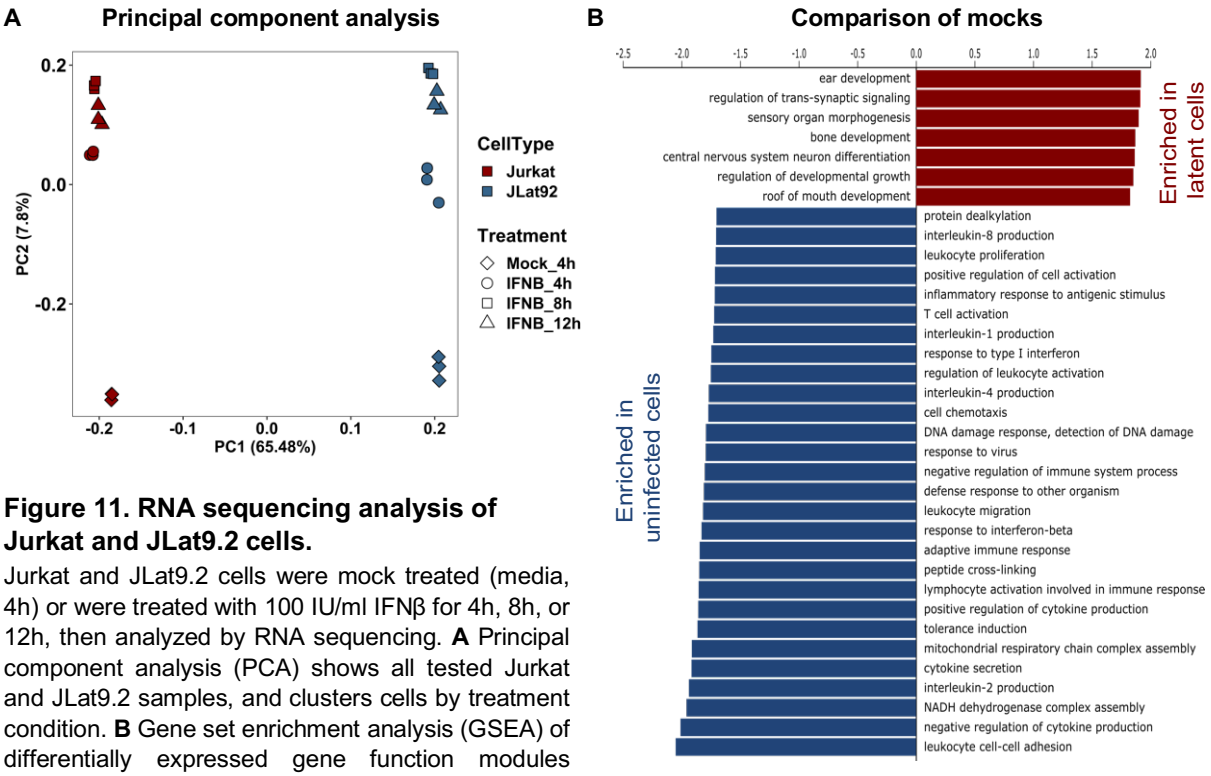


**Figure 11. RNA sequencing analysis of Jurkat and JLat9.2 cells.**

Jurkat and JLat9.2 cells were mock treated (media, 4h) or were treated with 100 IU/ml IFNβ for 4h, 8h, or 12h, then analyzed by RNA sequencing. **A** Principal component analysis (PCA) shows all tested Jurkat and JLat9.2 samples, and clusters cells by treatment condition. **B** Gene set enrichment analysis (GSEA) of differentially expressed gene function modules between untreated (mock) Jurkat and JLat9.2 cells. Genes were ranked using a t statistic.

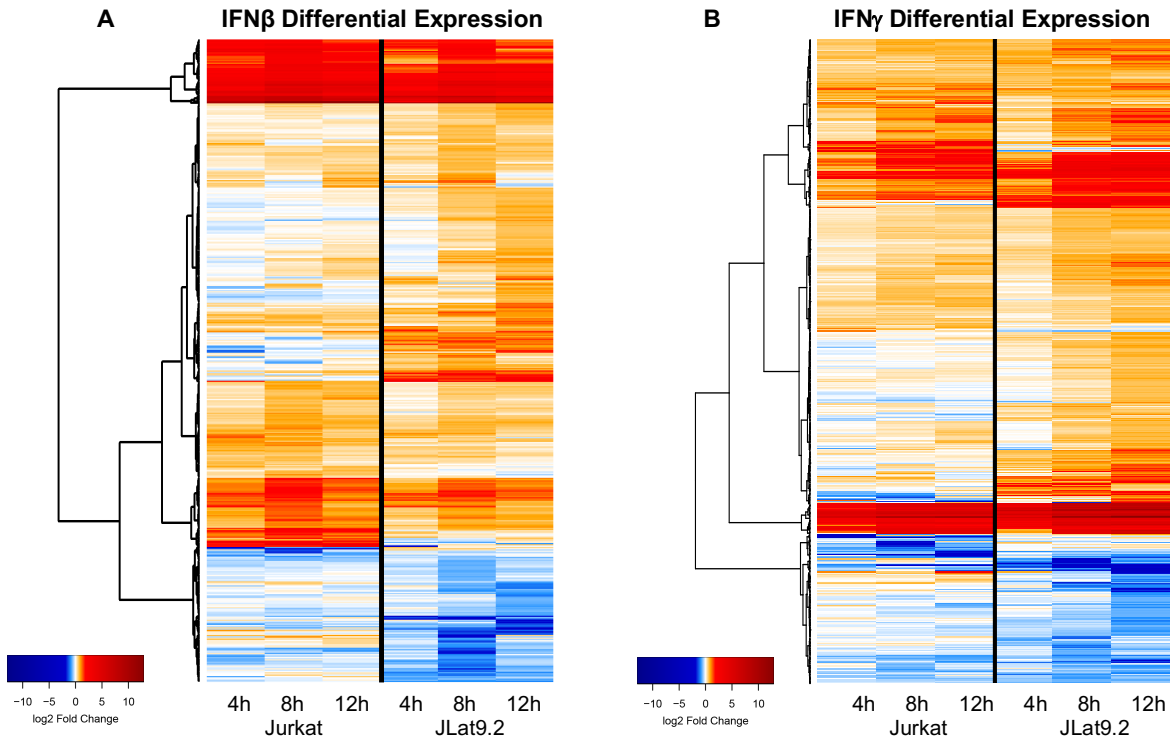


**Figure 12. RNA seq analysis of differentially expressed ISGs in Jurkat and JLat9.2 cells.**
Jurkat or JLat9.2 cells were mock-treated (media) for 4h, or were treated with type 1 IFN (100 IU/ml IFNβ) or type 2 IFN (100 IU/ml IFNγ) for 4, 8, or 12h; then analyzed by RNA sequencing. **A** Heat map shows differentially expressed (DE) genes in IFNβ-treated relative to mock-treated Jurkat or JLat9.2 cells. **B** Heat map shows DE genes in IFNγ-treated relative to mock-treated Jurkat or JLat9.2 cells. For each DE analysis, genes were determined significant if induced in any IFNβ-treated or IFNγ-treated sample relative to mock control. Three biological replicates were included for each treatment condition. FC > 1.5, $p < 0.05$. See Tables 5 & 6 for LogFC gene expression values.

A similar analysis was performed to identify genes induced by type 2 IFN (IFNγ) compared to mock-treated Jurkat or JLat9.2 cells; these DE genes are shown in the heat map in Fig. 12B and are listed in Table 6. Many genes were induced by IFNγ in both Jurkat and JLat9.2 cells. Transcriptomic differences between Jurkat and JLat9.2 cell lines were more pronounced with IFNβ treatment than with IFNγ, suggesting that HIV-1 latency may obstruct the type 1 IFN response without significantly disrupting the type 2 IFN response.

To determine how IFNβ response signatures diverge between these latent and uninfected cell models, I identified IFNβ-responsive genes which were induced differentially between JLat9.2 and Jurkat cells. This "differential of differential expression" ("DDE") analysis reveals the IFN-responsive gene correlates of HIV-1 latency. I identified 106 DDE genes (Fig. 13A; Table 7).

Remarkably, many canonical antiviral ISGs exhibited greater induction in Jurkat cells compared to JLat9.2 cells (66 genes), for example *MX1, OAS1, IFI27, STAT1, MX2, RSAD2*, and *IFITM3*, as well as additional ISGs that regulate cell proliferation/survival, such as MT2A (Ling et al. 2016). Network analyses link these genes to STAT regulatory nodes (Fig. 13B).

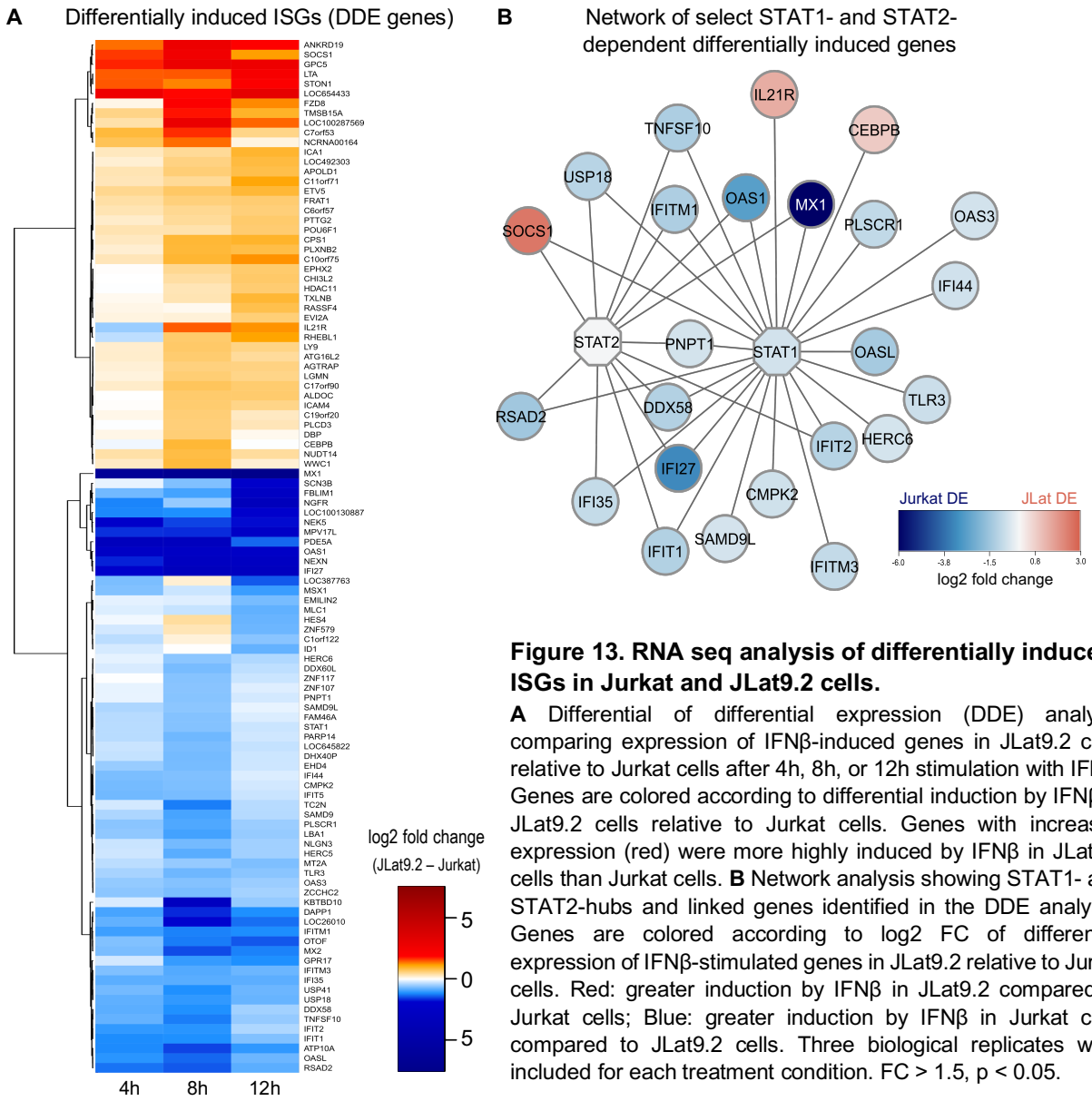


**Figure 13. RNA seq analysis of differentially induced ISGs in Jurkat and JLat9.2 cells.**

**A** Differential of differential expression (DDE) analysis comparing expression of IFNβ-induced genes in JLat9.2 cells relative to Jurkat cells after 4h, 8h, or 12h stimulation with IFNβ. Genes are colored according to differential induction by IFNβ in JLat9.2 cells relative to Jurkat cells. Genes with increased expression (red) were more highly induced by IFNβ in JLat9.2 cells than Jurkat cells. **B** Network analysis showing STAT1- and STAT2-hubs and linked genes identified in the DDE analysis. Genes are colored according to log2 FC of differential expression of IFNβ-stimulated genes in JLat9.2 relative to Jurkat cells. Red: greater induction by IFNβ in JLat9.2 compared to Jurkat cells; Blue: greater induction by IFNβ in Jurkat cells compared to JLat9.2 cells. Three biological replicates were included for each treatment condition. FC > 1.5, $p < 0.05$.

I also found that several innate immune regulatory genes were upregulated by IFNβ in JLat9.2 but not Jurkat cells, such as *SOCS1*, a known suppressor of STAT1 signaling that can block *OAS1* and *MX1* expression (Kile and Alexander 2001; Raftery and Stevenson 2017). On the other hand, IFNβ-treated Jurkat cells expressed higher levels of several immune activating genes that likely enhance the antiviral actions of IFN over JLat cells. These include *HERC5*, which encodes a major E3 ligase that supports the antiviral actions of ISG15 (Kim et al. 2016), and *PLSCR1*, a transcription co-factor of ISGs (Dong et al. 2004). Overall, these data show that compared to Jurkat cells, JLat9.2 cells induce lower levels of many antiviral ISGs and have altered expression of type 1 IFN control genes.

**Type 1 interferon response in latent vs productive infection**

To assess ISG expression across infected cells in the RGH model, Jurkat cells were mock-infected (conditioned media) or were infected with the RGH virus or an RGH-integrase mutant virus (ΔINT control) at MOI 0.2 for 5 days. Cells were then sorted into negative, latent, or productive infection groups based on mCherry and GFP expression. Dead cells were identified by DAPI staining and excluded from sorted populations. Sorted cells were then placed in culture and treated with media alone (untreated control), reactivated with PMA and ionomycin, or stimulated with IFNβ, then gene expression analyzed by qRT-PCR (see Fig. 4 above).

I first investigated if sorted, latent cells could initiate virus transcription upon reactivation with PMA, a potent stimulator of HIV-1 transcription. I treated RGH-infected, sorted Jurkat cells with PMA/ionomycin and measured gene expression by qRT-PCR relative to mock-infected control. PMA/ionomycin yielded much higher HIV-1 RNA expression in latent than other sorted populations, suggesting that latent cells reactivate virus transcription and that this model recapitulates post-integration latency (Fig. 14A). PMA/ionomycin treatment also increased HIV-1 RNA in productively infected cells, probably because these treatments are potent T cell activators

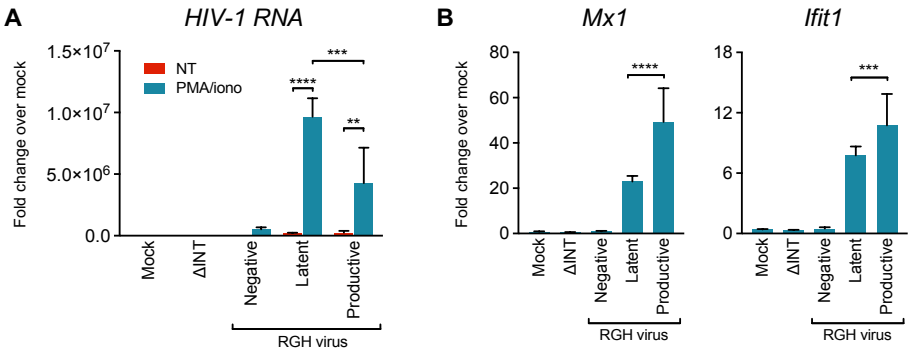


**Figure 14. Reactivation of HIV-1 RNA in Jurkat cells latently infected with RGH.**

**A,B** Jurkat cells were mock-infected (conditioned media) or were infected with ΔINT or RGH (MOI 0.2) for 5 days, sorted into subgroups (negative, latent, or productive infection), and then reactivated with 16nM PMA and 1μM ionomycin for 24h as depicted in Fig. 4, and analyzed by qRT-PCR. Red bars: untreated cells (NT); Teal bars: cells reactivated with PMA and ionomycin (PMA/iono) for 24h. Only PMA/iono-treated cells are shown in Graph B. For all qRT-PCR analyses in this figure, bars represent mean fold change + SD of three replicates from a single experiment. Fold change was calculated relative to housekeeping gene *RPL13a* and normalized to a single untreated, mock control (ΔΔCt method). Statistical significance relative to similarly treated, mock-infected cells was determined by two-way ANOVA with multiple comparisons (Dunnet). *p<0.05, **p<0.01, ***p<0.001.

that trigger many intracellular signaling pathways, and induce chromatin changes that enhance HIV-1 transcription (El Kharroubi et al. 1998).

Interestingly, PMA/ionomycin treatment was also associated with an increase in *MX1* and *IFIT1* mRNA in both latent and productively infected cells (Fig. 14B). Notably, however, the magnitude of induction of these ISGs was significantly reduced in latent relative to productively infected cells, despite the reactivated latent cells high expression of HIV-1 RNA. These data support a model in which ISG induction is restricted in latent cells.

I next assessed ISG expression levels in each sorted population before and after IFNβ treatment. At baseline (no treatment), ISG expression was generally similar between mock, ΔINT-infected, sorted negative, and sorted latent cells, though *IFITM1* and *IFIT2* levels were elevated in productively infected (dual fluorescent) cells (Fig. 15A). After treatment with 100 IU/ml IFNβ for 8h, HIV-1 RNA expression was overall unaffected (Fig. 15B). I measured fold induction of ISG mRNA in IFNβ-treated cell populations compared to IFNβ-untreated, mock-infected control cells, and found that IFNβ induced similar levels of canonical ISGs in mock- and ΔINT-infected cells, suggesting that mere virus exposure does not alter ISG activation (Fig. 15C). In contrast, ISG

induction was considerably elevated in productively infected (dual fluorescent) cells. Interestingly, IFNβ induction of select ISGs (*IFITM1* and *OAS1*) was disrupted in latent cells but not mock-infected control cells. Thus, in the RGH infection model, HIV-1 latency associates with reduced ISG induction in response to IFNβ treatment or virus reactivation. This finding of select ISG suppression is consistent with our observations in latent HIV-1 infected cell lines (see Fig. 10), though the specific genes suppressed varies between latency models.

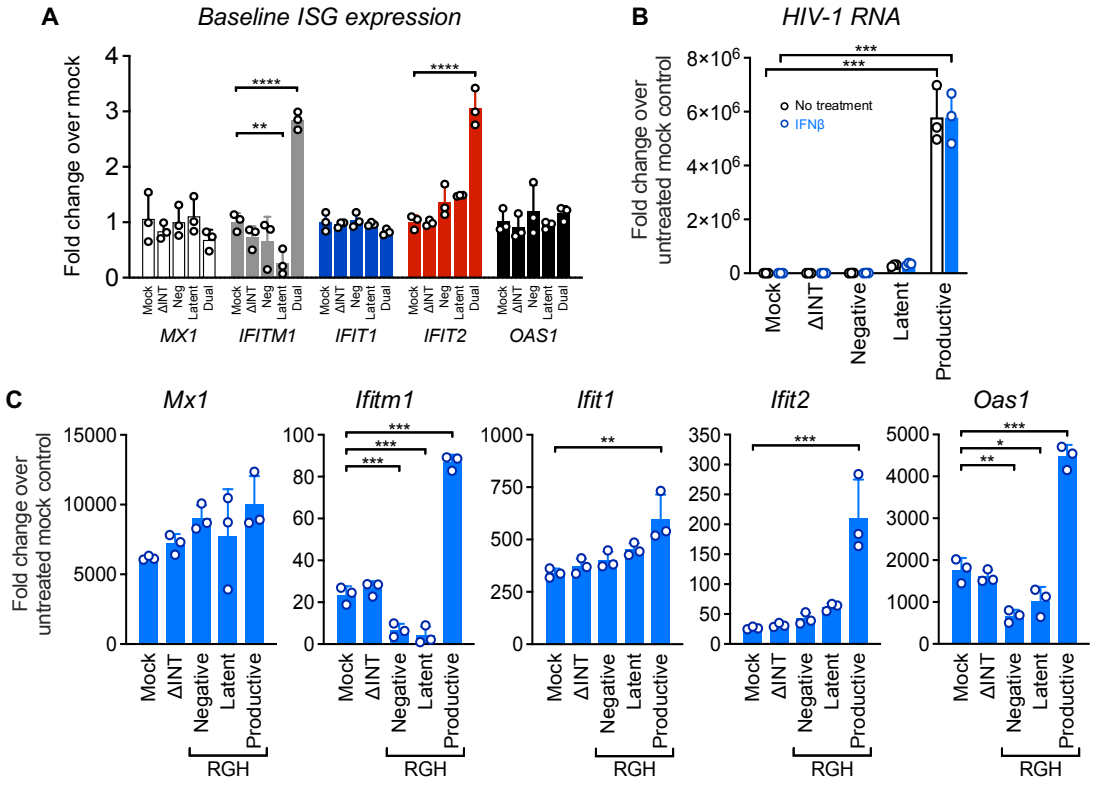


**Figure 15. Type 1 IFN response analysis in RGH-infected, sorted Jurkat cells.**
**A** qRT-PCR analysis of baseline ISG expression in Jurkat cells that were mock-infected, or were infected with ΔINT or RGH (MOI 0.2) for 5d, then sorted into subgroups (negative, latent, or productive) (see Fig. 4). **B** qRT-PCR analysis of HIV-1 RNA in infected Jurkat cells that were sorted, then stimulated with 100 IU/ml IFNβ for 8h (blue bars) or left untreated (white bars). **C** qRT-PCR analysis of ISG expression in sorted Jurkat cells following IFNβ stimulation (100 IU/ml, 8h). For all qRT-PCR analyses, bars represent mean fold change (FC) + SD of three replicates from one experiment. Mean FC was calculated relative to untreated, mock-infected cells and to *RPL13a* (ΔΔCt method). Statistics: Two-way ANOVA (Dunnet). *p<0.05, **p<0.01, ***p<0.001, ****p<0.0001.

*SUMMARY OF RESULTS*

In this study I examined innate immune and interferon responses in various cell line models of latency. JLat9.2 and ACH2 latent cells demonstrated weaker responses to RIG-I agonists Sendai virus (SeV) or RIG-I stimulatory PAMP RNA compared to control Jurkat or A3.01 cells. This suggests that in these cell lines models, latency is associated with an attenuated RIG-I-mediated innate immune response. However, because IRF3 resting expression level and SeV-induced activation was similar between Jurkat and JLat9.2 cells, any defect in this response likely occurs downstream of the RIG-I signaling pathway. Three latent cell lines (JLat9.2, JLat11.1, ACH2) also demonstrated weaker ISG upregulation after IFNβ stimulation than corresponding control cells, affirming that these latent cell lines have dysregulated type 1 IFN responses. Jurkat and JLat9.2 cells demonstrated similar levels of IFNAR1 surface expression and IFNβ-induced STAT1/2 phosphorylation, so type 1 IFN response dysregulation in JLat cells is probably not due to JAK/STAT pathway disruption.

Transcriptomic analysis of resting and IFNβ-stimulated JLat9.2 and Jurkat cells revealed significant transcriptional differences in hundreds of ISGs. At baseline (no IFNβ), JLat9.2 cells had reduced expression of many innate immune, antiviral, and type 1 IFN regulatory genes, suggesting they may be less effective than Jurkat control cells at mounting an antiviral innate immune response. Differential expression (DE) analysis revealed that Jurkat and JLat9.2 cells activate distinct transcriptional programs in response to IFNβ stimulation. Differential of differential expression (DDE) analysis of IFNβ-stimulated cells further revealed that JLat9.2 cells had poor induction of many canonical antiviral ISGs than Jurkat cells.

Jurkat cells productively infected with the RGH virus had elevated baseline expression of ISG mRNA, suggesting a virus-induced innate response. These ISGs were further upregulated upon IFNβ treatment. Interestingly, sorted latent cells from the same infected population had attenuated IFNβ responses for select ISGs, suggesting an immune escape mechanism may link with HIV-1 latency in this model.

# CHAPTER 3

*INTRODUCTION*

Suppressive antiretroviral therapy (ART) blocks viral replication but fails to eradicate reservoir cells, necessitating the design of therapies that can destroy latently infected cells in HIV+ patients taking ART. Furthermore, there is some evidence that ART influences the innate immune landscape in human patients (Nittayananta et al. 2016). I hypothesized that HIV-1-infected cells suppressed by ART would be less responsive to innate immune activation and/or IFNβ stimulation. To address this hypothesis, I examined ISG expression and IFNβ responses in a primary human CD4+ T cell model of HIV-1 suppression.

**Primary CD4+ T cell model of HIV suppression**

This primary CD4+ T cell model of ART-mediated HIV-1 suppression was established by the Hladik lab (Gornalusse et al. 2021) and is similar to models from other laboratories (Lassen et al. 2012; Saleh et al. 2007; Cameron et al. 2010; Bosque and Planelles 2009). This model allows analysis of HIV-1-infected cells, in the context of low or no detectable HIV-1 RNA expression, as a proxy for HIV-1 latency seen in patients undergoing ART. CD4+ T cells were isolated by negative selection from healthy human PBMC from three different donors, then were cultured with homeostatic cytokines (IL-2, IL-7, and IL-15) for 5 days to increase cell permissiveness. Cells were maintained in these cytokines throughout the duration of all

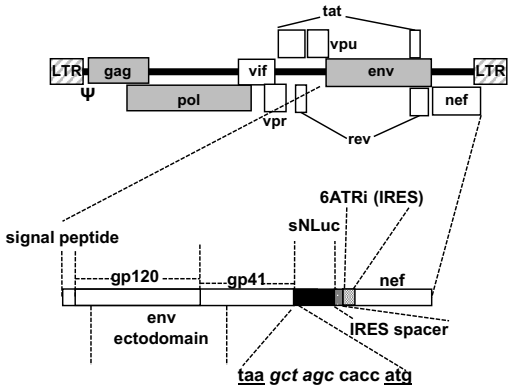


**Figure 16. NanoLuc HIV-1 genome.**
NanoLuc HIV-1 provirus contains a modified EMCV 6ATR internal ribosome element (6ATRi), which enables physiological Nef expression and function. The secreted nanoluciferase (sNluc) ORF was inserted upstream of 6ATRi, enabling expression and secretion of the sNLuc reporter upon viral replication.

experiments using this model. After 5 days of cytokine treatment, cells were infected by spinoculation with a replication competent, NanoLuc reporter HIV-1 that expresses luciferase upon HIV-1 LTR transcription as an indicator of HIV-1 replication (Fig. 16). In parallel, cells were mock treated with media containing cytokines as an infection-negative control. One day following infection, mock and HIV-infected cells were treated with ART (10μM Raltegravir and 1μM Efavirenz) for 7 days to inhibit HIV-1 reverse transcription and integration. After 7 days of ART, cells were subject to various experiments including type 1 IFN stimulation, HIV-1 reactivation with PMA/ionomycin, and single cell RNA sequencing (scRNA-seq). This infection and suppression protocol is depicted below in Fig. 17, and was consistently used for all experiments with this model.

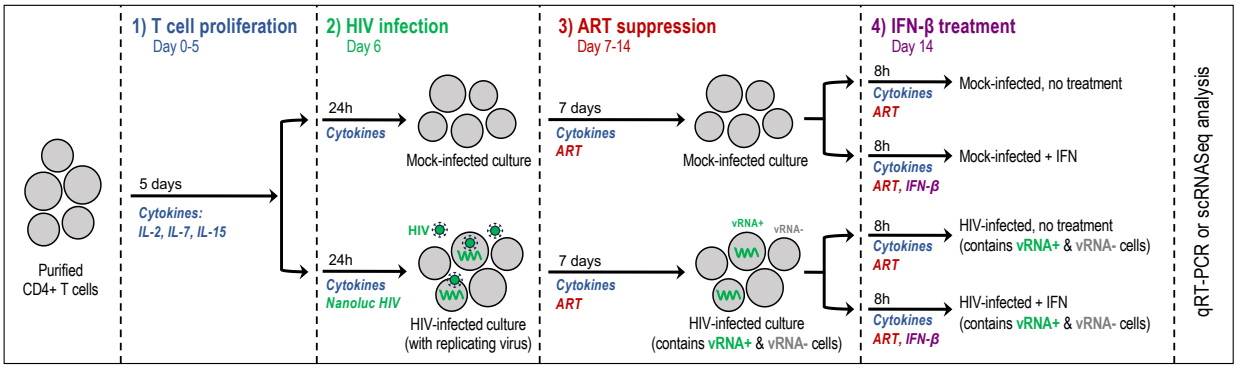


**Figure 17. Schematic of the NanoLuc HIV-1 infection and ART suppression protocol.**
Primary CD4+ T cells isolated from healthy human PBMC were cultured for 5 days in the homeostatic cytokines IL-2 (20 U/ml), IL-7 (10 ng/ml), and IL-15 (50 ng/ml). Cells were mock-infected (media) or infected with NanoLuc HIV-1 at MOI 2.0 (Donors 1 & 2) or MOI 1.0 (Donor 3). 24h following infection cells were treated with ART (10 μm Raltegravir and 1 μm Efavirenz) for 7 days to suppress HIV replication. After 7 days (day 8 post infection), cells were stimulated for 8h with IFNβ (100 IU/ml) in the presence of cytokines and ART, or were left untreated (cytokines and ART, no IFNβ), then RNA harvested for analysis by qRT-PCR or scRNA-seq.

## *RESULTS*

### Analysis of HIV suppression and reactivation in primary CD4+ T cells

Primary CD4+ T cells were treated with homeostatic cytokines, infected with NanoLuc HIV-1, then suppressed by ART for 7 days as described above (Fig. 17). At 24h following infection (prior to ART treatment), NanoLuc HIV-1-infected cells transcribed HIV-1 RNA and secreted

luciferase, indicating HIV replication (Fig. 18A). Supernatant was collected periodically from CD4+ T cell cultures and analyzed for secreted luciferase, an indicator of HIV-1 transcription in this model. Luciferase was detectable in HIV-infected cultures 24h post infection, peaked at 4 days after infection, then declined similar to mock levels at day 8, indicating suppression of viral replication (Fig. 18B). Droplet digital PCR (ddPCR) analysis showed that after 7 days of ART, approximately 3.1% of cells were positive for HIV-1 DNA (average of 3 donors). Measurements of HIV-1 infection in each donor are summarized in Table 1.

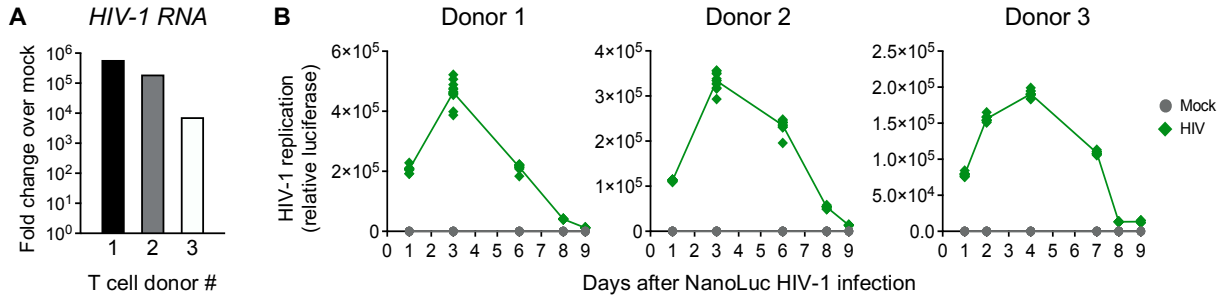


**Figure 18. HIV-1 replication and ART suppression in primary CD4+ T cells.**
**A** qRT-PCR analysis of HIV-1 RNA in primary CD4+ T cells 24h after infection with NanoLuc HIV-1 (Donors 1&2, MOI 2.0; Donor 3, MOI 1.0), prior to ART (see Fig. 17 for detailed infection protocol). No HIV-1 RNA was detected in mock-infected samples. Bars represent HIV-1 RNA expression relative to an arbitrary Ct value of 40 from one representative experiment. **B** Luciferase expression analysis of supernatant from mock-infected or NanoLuc HIV-1-infected primary CD4+ T cells. ART (Efavirenz and Raltegravir) was added one day post infection to suppress HIV-1 replication. Data points represent 12 technical replicates collected from each sample in one representative experiment.

**Table 1. HIV-1 expression in primary CD4+ T cells**

| | | % HIV DNA+ (ddPCR) | | % HIV RNA+ |
|---|---|---|---|---|
| | | 24 hpi | 8 dpi | (sc seq) 8.5 dpi |
| **Donor 1** | Mock | 0.002 | 0.002 | 0 |
| | Mock + IFN | X | X | 0 |
| | HIV infected | 29.81 | 2.47 | 9.84 |
| | HIV infected + IFN | X | X | 9.52 |
| **Donor 2** | Mock | 0.008 | 0.003 | 0 |
| | Mock + IFN | X | X | 0 |
| | HIV infected | 24.37 | 1.54 | 4.39 |
| | HIV infected + IFN | X | X | 3.91 |
| **Donor 3** | Mock | 0.24 | 0.01 | X |
| | Mock + IFN | X | X | X |
| | HIV infected | 63.64 | 5.24 | X |
| | HIV infected + IFN | X | X | X |

*X = not tested*

To validate our model of viral suppression, we removed ART from culture after 7 days and rested cells for 24h before measuring secreted luciferase. Removal of ART resulted in elevated luciferase in HIV-infected cells, indicating virus rebound and validating that ART actively suppresses HIV-1 replication in this model (Fig. 19). Reactivation with PMA and ionomycin at this time point further increased luciferase expression indicating the presence of cells with reactivatable proviruses. Thus, viral suppression and reactivation of HIV-1 is faithfully captured in this primary cell model, wherein ART-suppressed HIV-1 infection associates with reduced response to IFNβ, mirroring my observations in cell line models of HIV-1 latency (see Figs. 10 & 15).

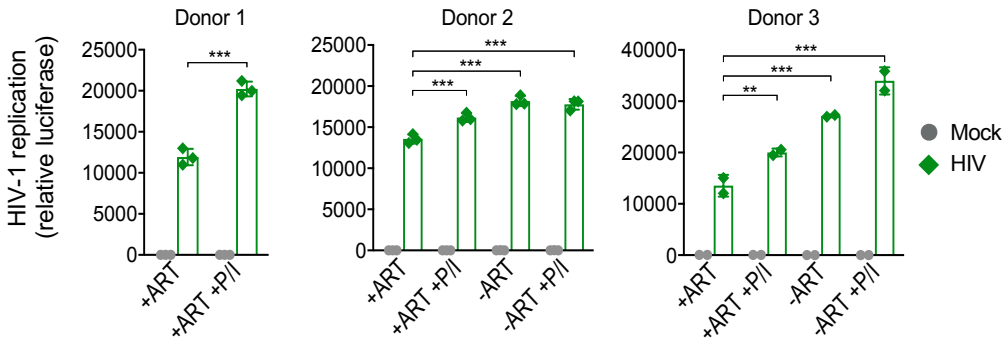


**Figure 19. Luciferase expression analysis of HIV-1 reactivation in CD4+ T cells.**
Mock-infected or NanoLuc HIV-1-infected T cells were suppressed with ART for 7 days, then cultured +/- ART and +/- PMA/ionomycin (P/I, 16nM/1μM) for 24h and supernatant luciferase measured to determine HIV-1 replication. Statistical significance relative to indicated HIV-infected control was calculated by two-way ANOVA with multiple comparisons (Holm-Sidak). Multiple independent experiments were performed; data are shown from one representative experiment with three biological replicates per treatment condition. *p<0.05, **p<0.01, ***p<0.001.

### ISG expression analysis in a primary CD4+ T cell model of HIV-1 suppression

I first examined baseline ISG mRNA levels in mock-infected and NanoLuc HIV-1-infected cells from each donor after 7 days of ART (see infection and suppression protocol in Fig. 17). qRT-PCR analysis showed that HIV-infected cells trended to slightly elevated baseline ISG RNA levels compared to mock-infected cells, though these differences were generally not statistically significant (Fig. 20). These data suggest that after a week of ART suppression, HIV infection was not persistently activating innate immune signaling programs in this model.

To assess the type 1 IFN response in suppressed cells after 7 days of ART, mock and HIV-infected cells were resuspended in media containing ART and homeostatic cytokines, then stimulated for 8h with IFNβ (20 or 100 IU/ml) or left untreated (ART and homeostatic cytokines alone). ISG mRNA expression was analyzed by qRT-PCR and fold mRNA induction was quantified relative to untreated cells. Compared to untreated cells, both mock and HIV-infected cells upregulate ISGs in response to IFNβ, though the magnitude of induction was diminished in HIV-infected cells in all three donors (Fig. 21A-C). Notably, select ISGs were significantly suppressed in each donor, with OAS1 induction impaired in HIV-infected cells from all three donors. These findings are not likely due to altered baseline expression of ISG mRNA, which was generally similar between mock and HIV-infected cells for each donor (see Fig. 20). Because the overall rate of HIV infection is low in this model (approximately 3.1%), any significant phenotypic differences in the HIV-infected cell population are probably driven at least in part from uninfected cells. This could be due to a paracrine effect of cytokines secreted from nearby infected cells.

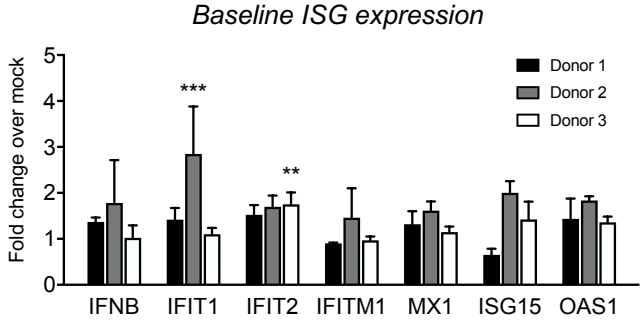


**Figure 20. Baseline ISG mRNA expression in HIV-suppressed CD4+ T cells.**

qRT-PCR analysis of ISGs in mock-infected or NanoLuc HIV-infected samples after 7d of ART suppression. Data are shown from one representative experiment with three biological replicates per treatment condition. Statistical significance of HIV-infected relative to mock for each donor was calculated by two-way ANOVA with multiple comparisons (Holm-Sidak). *p<0.05, **p<0.01, ***p<0.001.

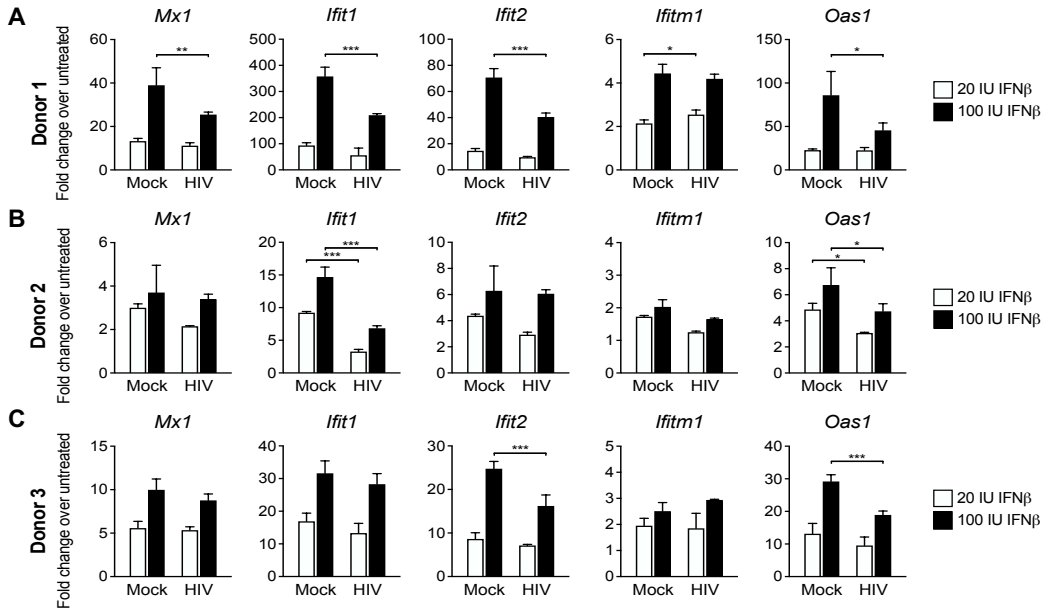


**Figure 21. ISG expression after IFNβ stimulation in NanoLuc HIV-infected primary CD4+ T cells.**
**A-C** qRT-PCR analyses of mock- or NanoLuc HIV-1-infected CD4+ T cells that were suppressed with ART for 7d, then stimulated for 8h with IFNβ (0, 20, or 100 IU/ml) (see Fig. 17). Bars represent mean FC + SD of IFNβ-stimulated relative to untreated cells for each infection group (mock or HIV). Three independent experiments were performed; data are shown from one representative experiment with three biological replicates per treatment condition. Statistical significance between mock-infected and HIV-infected cells was determined by two-way ANOVA with multiple comparisons (Holm-Sidak). *p<0.05, **p<0.01, ***p<0.001.

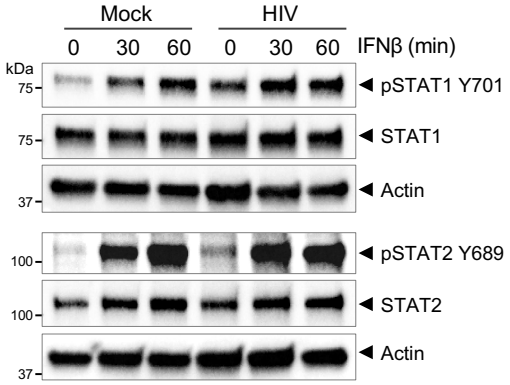


**Figure 22. STAT1/2 phosphorylation in virally suppressed CD4+ T cells.**
Immunoblot analyses of mock-infected or NanoLuc HIV-1-infected CD4+ T cells (Donor #1) that were suppressed with ART for 7d, then stimulated with 100 IU/ml IFNβ for 30 or 60 min.

I assessed JAK/STAT signaling by performing a short course IFNβ treatment on suppressed cells from one donor and found that compared to mock, HIV-infected cells had elevated levels of phosphorylated STAT1 and STAT2 both at baseline and after 30 min of IFNβ treatment (Fig. 22). Though at 60 min, phosphorylated STAT1 and STAT2 levels were similar between cell lines. These findings might be explained by HIV-1-driven priming of innate

immune pathways. I also measured secreted luciferase in IFNβ-treated, virally suppressed cells to determine whether IFNβ influences ART suppression of HIV-1 replication in our model. Luciferase expression was similar in HIV-suppressed cells before and after IFNβ treatment (Fig. 23), indicating that IFNβ did not alter HIV-1 replication in this model.

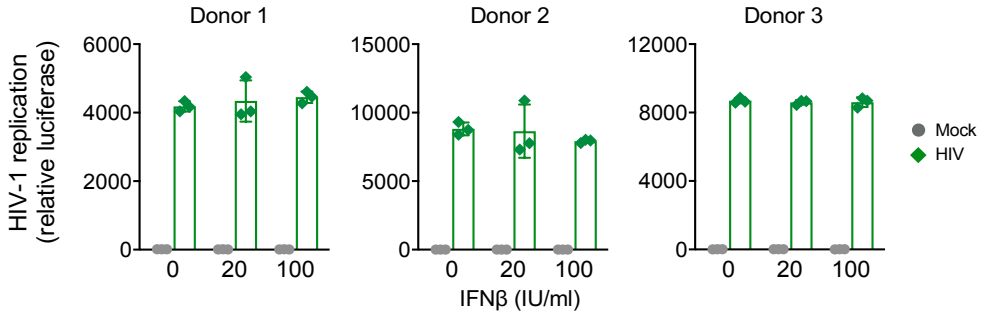


**Figure 23. HIV-1 replication in virally suppressed CD4+ T cells after IFNβ treatment.**
Luciferase analysis of supernatant from mock-infected or NanoLuc HIV-1-infected CD4+ T cells that were suppressed with ART for 7d then stimulated with IFNβ for 8h (0, 20, or 100 IU/ml). Data points represent individual replicates from a single experiment. Statistical significance of IFNβ-treated relative to untreated cells was calculated by two-way ANOVA with multiple comparisons (Holm-Sidak) ($p<0.05$).

### scRNA-seq analysis of HIV-1 expression in primary CD4+ T cells

To define the relationship between a suppressed HIV-1 provirus and innate immune defenses within primary cells on a single cell level, we examined our model of HIV-1 suppressed primary CD4+ T cells, noting that while these cells have suppressed viral replication, they typically retain low levels of detectable HIV-1 RNA. These properties of our culture model enable identification of infected cells through single cell RNA sequencing (scRNA-seq). CD4+ T cells from two healthy human PBMC donors were cultured in homeostatic cytokines (IL-2, IL-7, and IL-15) for 5 days, then mock-treated or infected with NanoLuc HIV (MOI 2.0) for 24h, suppressed for 7 days with 1μM Efavirenz and 10μM Raltegravir, then were left untreated or were treated with IFNβ (100 IU/ml) for 8h. As in our previous experiments, we chose a short course of IFNβ treatment, which neither affects HIV-1 transcription nor replication in this model (see Fig. 23). The cultures were then subjected to scRNA-seq analysis (see protocol schematic in Fig. 17). Cells

identified to contain at least one read mapping to the HIV-1 genome (one UMI count) were classified as viral RNA positive (vRNA+). Because I analyzed 40,000 reads per cell rather than the entire cellular RNA content, HIV RNA read counts per cell do not necessarily represent the total cellular expression of HIV-1 RNA. However, this method does reasonably enable distinction of vRNA+ and vRNA- cells. HIV-infected samples contained 3.9-9.8% of vRNA+ cells (see Table 1).

vRNA+ and vRNA- cells from the entire scRNA-seq data set were displayed in a uniform manifold approximation and projection (UMAP) reduction (Fig. 24A). vRNA+ cells tend to cluster near each other in the UMAP suggesting a similar transcriptome profile. A second UMAP plot demonstrates differential HIV-1 RNA expression level within these cells and suggests that vRNA+ cells tend to cluster near others with similar HIV-1 RNA abundance (Fig. 24B). Given the wide range of HIV-1 RNA expression and the sensitivity of our scRNA-seq method (detects a single viral transcript), I further classified vRNA+ cells into high- and low-viral RNA expressing subsets using a 50% cutoff (vRNA$^{hi}$ and vRNA$^{lo}$) (Table 2).

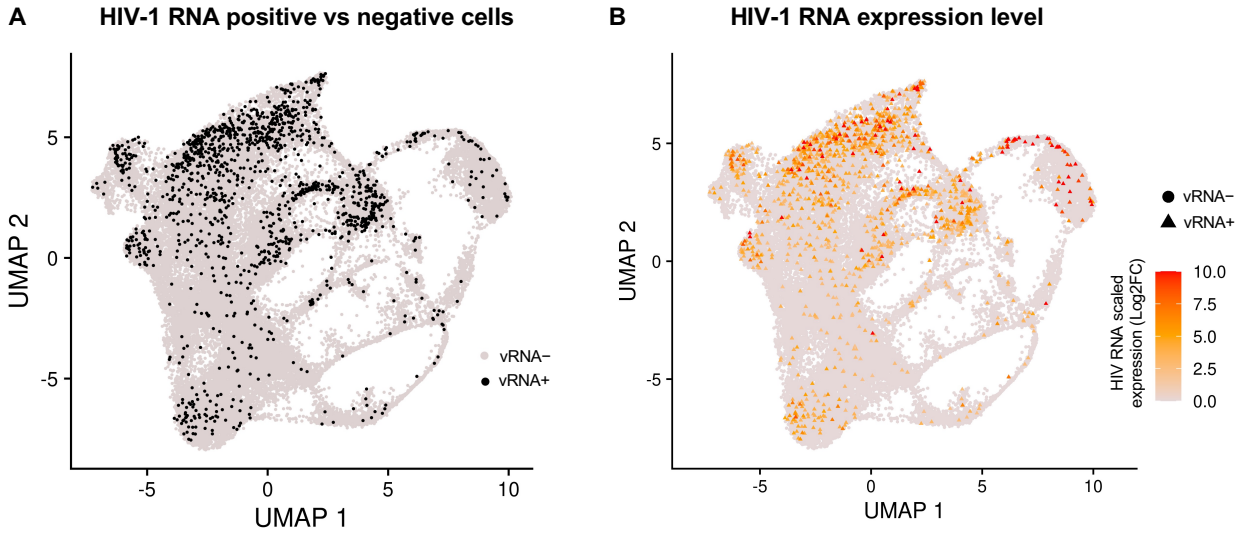


**Figure 24. HIV-1 RNA expression in primary CD4+ T cells.**
**A** UMAP shows clustering of vRNA+ cells and vRNA- cells. **B** UMAP shows viral RNA expression level per cell. Both UMAPs show all combined samples from scRNAseq analysis (CD4+ T cells from two healthy human donors, mock-infected or NanoLuc HIV-infected, +/-IFNβ).

This cutoff was determined as the median HIV-1 RNA count of vRNA+ cells. Cells classified as $vRNA^{hi}$ express more HIV-1 RNA than the median count, and $vRNA^{lo}$ cells express less HIV-1 RNA than median. $vRNA^{hi}$ cells from each donor express HIV-1 RNA levels (mean 4.9 and 3.4 HIV RNA counts) that might be expected from cells undergoing low levels of viral replication, whereas the reduced HIV-1 RNA abundance in $vRNA^{lo}$ cells (mean one HIV-1 RNA count) suggests this population has undergone some degree of transcriptional suppression as in latent cells. While we cannot exclude the possibility of latent cells within the vRNA- subset, our ddPCR data revealed a low total percentage HIV-1 DNA+ cells in the bulk HIV-infected population (see Table 1), suggesting that latent cells are either absent from or are an insignificant fraction of the larger vRNA- population.

**Table 2. scRNA-seq HIV-1 RNA read counts**

| DONOR | Cell subset | Percent of cells | HIV RNA counts per cell | |
|---|---|---|---|---|
| | | | Mean | Range |
| Donor 1 | $vRNA^{hi}$ | 5.34 | 4.88 | 1 - 134 |
| | $vRNA^{lo}$ | 4.54 | 1.01 | 1 - 2 |
| | vRNA- | 90.12 | 0 | 0 - 0 |
| Donor 2 | $vRNA^{hi}$ | 1.76 | 3.35 | 1 - 51 |
| | $vRNA^{lo}$ | 2.63 | 1.01 | 1 - 2 |
| | vRNA- | 95.61 | 0 | 0 - 0 |

T cell subset analysis showed that sequenced cells were predominantly CD4+ T cells, and a minority of these CD4+ T cells could be categorized into specific T cell subsets according to the markers listed below (Fig. 25A, B). Interestingly, analysis of CD4+ T cell subsets showed that HIV-1 RNA expression was enriched in inducible regulatory T cells (Fig. 25C). Regulatory T (Treg) cells are characterized by elevated expression of inhibitory receptors and have immunosuppressive characteristics that might predispose them for HIV-1 infection.

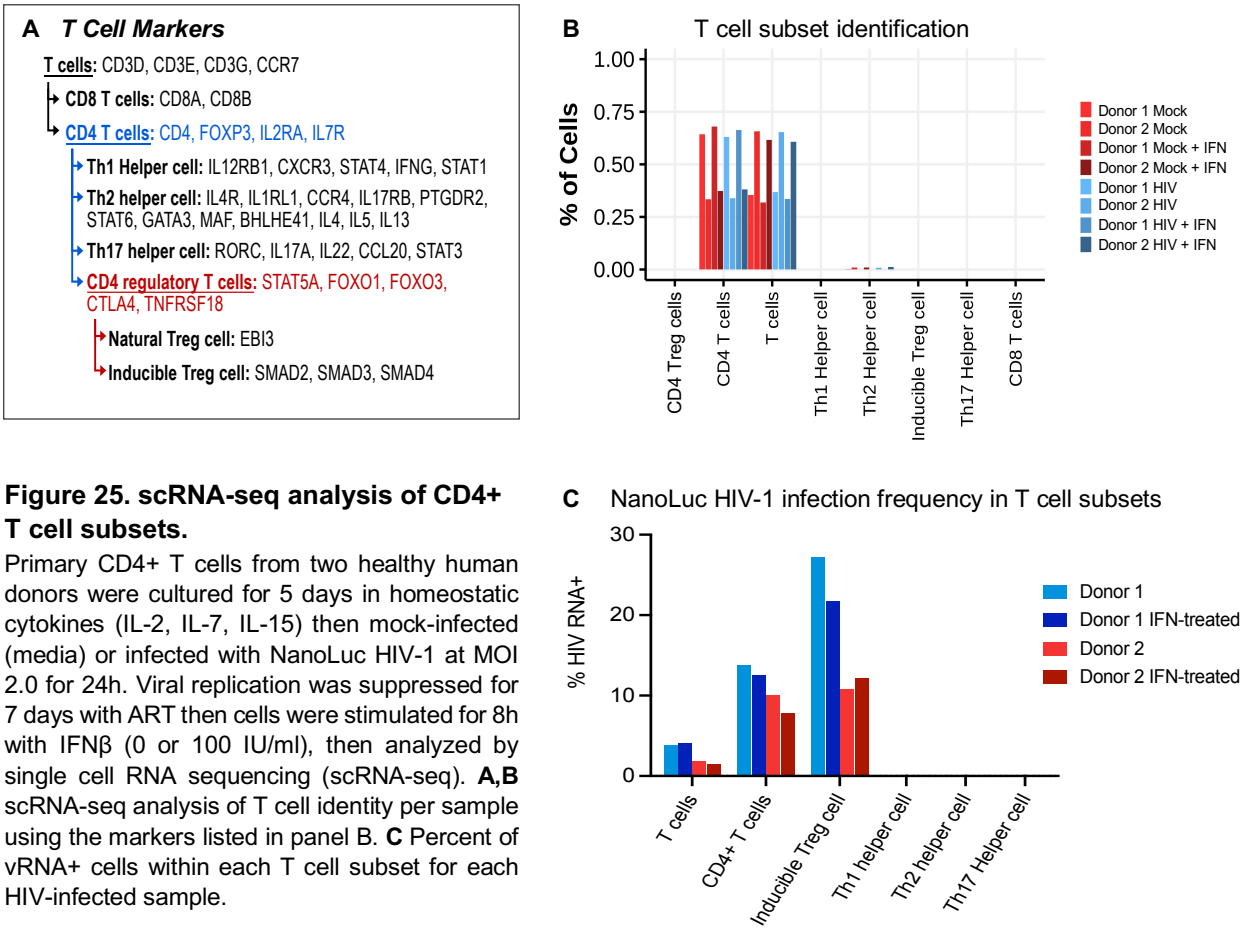


**Figure 25. scRNA-seq analysis of CD4+ T cell subsets.**

Primary CD4+ T cells from two healthy human donors were cultured for 5 days in homeostatic cytokines (IL-2, IL-7, IL-15) then mock-infected (media) or infected with NanoLuc HIV-1 at MOI 2.0 for 24h. Viral replication was suppressed for 7 days with ART then cells were stimulated for 8h with IFNβ (0 or 100 IU/ml), then analyzed by single cell RNA sequencing (scRNA-seq). **A,B** scRNA-seq analysis of T cell identity per sample using the markers listed in panel B. **C** Percent of vRNA+ cells within each T cell subset for each HIV-infected sample.

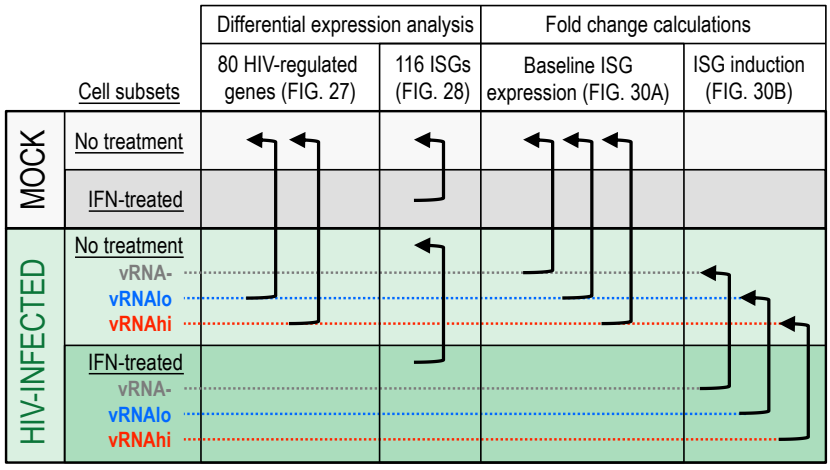


**Figure 26. Guide to scRNA-seq comparisons and analyses.**

Two differential expression analyses were performed to identify the following gene lists: 1) HIV-regulated genes (80 genes), and 2) interferon-induced ISGs (116 genes). Expression of the 116 identified ISGs was then measured in various cell populations, and fold change calculated as depicted above. Arrows indicate specific comparisons between cell populations.

I performed two differential expression analyses to identify genes that: 1) were expressed differently in HIV-infected samples at baseline, “HIV-regulated genes”, or 2) were significantly induced by IFNβ in any sample, “ISGs”. These scRNA-seq DE analyses are mapped in Fig. 26, and specific comparisons between cell populations are indicated by arrows.

**scRNA-seq identification of HIV-regulated genes in CD4+ T cells**

The goal of the first DE analysis was to determine how HIV-1 influences global gene expression in the context of ART suppression and define HIV-regulated genes. I analyzed gene expression in vRNA$^{hi}$ and vRNA$^{lo}$ cells from untreated (no IFNβ), HIV-infected samples for both donors, and identified 80 HIV-regulated genes that were differentially expressed in one or both cell subsets relative to mock-infected cells (Fig. 27A; Table 8). Genes that were significantly downregulated in vRNA$^{hi}$ and vRNA$^{lo}$ subpopulations relative to mock-infected cells include *STAT1*, which is critically important for all type 1 IFN signaling. Other downregulated type 1 IFN response genes include *ISG20* and *IFITM2*. Genes that were significantly elevated in both vRNA$^{hi}$ and vRNA$^{lo}$ subsets at baseline relative to mock-infected cells include *LAG3/CD223*, an inhibitory receptor of lymphocyte activation known to be induced in response to HIV-1 infection and to contribute to HIV-1 persistence (Andrews et al. 2017; Pardons et al. 2019; Fromentin et al. 2016). This is especially remarkable, as inducible Treg cells, which express high levels of *LAG3*, were preferentially infected by HIV-1 in this model (Fig. 25C). Also upregulated in vRNA$^{hi}$ and vRNA$^{lo}$ cells were several granzyme-encoding genes (*GZMA, GZMB, GZMH*), *LGALS3* (encoding Galactin-3) which is known to be induced by HIV-1 (Okamoto et al. 2019), and *RNF213*, an E3 ubiquitin ligase (Ahel et al. 2020). Genes that were significantly differentially expressed in vRNA$^{hi}$ or vRNA$^{lo}$ cells relative to mock-infected cells for each treatment condition (+/- IFNβ) are listed in Table 9. Analysis of significantly enriched pathways revealed that many of these HIV-regulated genes are involved in processes relating to RNA translation, protein localization, and protein

targeting (Fig. 27B), indicating that in our primary cell model of virologic suppression, HIV-1 infection modulates protein and RNA metabolism.

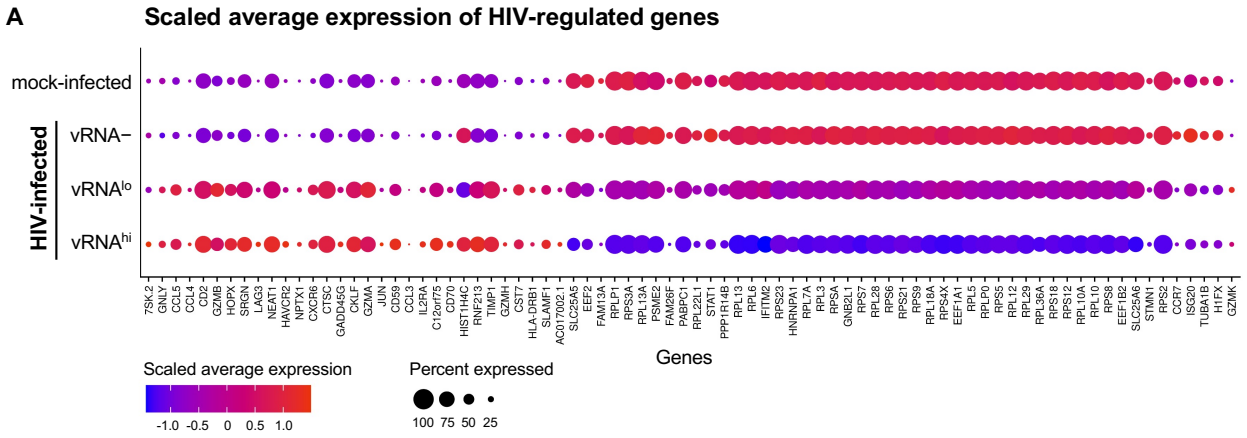


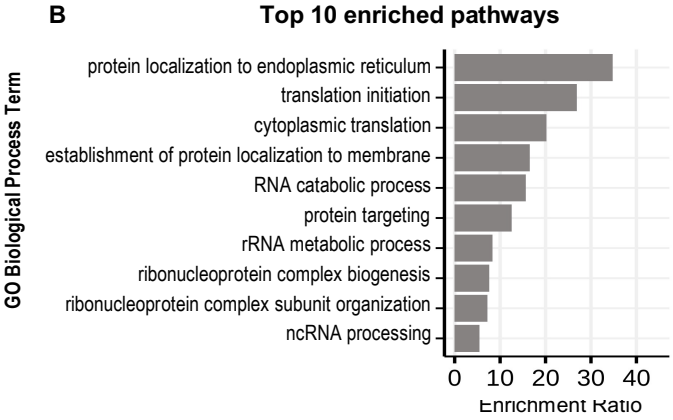


**Figure 27. scRNA-seq identification of HIV-regulated genes.**
Primary CD4+ T cells (donors #1 & 2) were mock-infected (media) or HIV-infected (NanoLuc HIV-1, MOI 2.0) for 24h, then suppressed with ART (10μm Raltegravir and 1μm Efavirenz) for 7d and analyzed by scRNA-seq. **A** HIV-regulated genes were identified through differential expression analysis of vRNA$^{hi}$ and vRNA$^{lo}$ cells relative to mock-infected cells (FC > 1.2, p < 0.05). 80 significant genes were identified across both donors. Dot plot shows scaled average expression and percent of cells expressing each gene. See Tables 8 and 9 for significant genes and expression values. **B** Top ten significantly enriched pathways of HIV-regulated genes.

## scRNA-seq analysis of ISG induction in HIV-suppressed CD4+ T cells

Since bulk RNA-seq of latent cell lines revealed broad disruption of the interferon transcriptome (see Figs. 11-13), I next focused the scRNA-seq analysis on IFNβ-responsive genes. I performed an additional differential expression (DE) analysis comparing IFNβ-treated cultures (mock or HIV-infected) to corresponding untreated cultures (see scRNA-seq guide in Fig. 26). I identified 116 ISGs that were significantly induced by IFNβ in any sample relative to its corresponding untreated control, independent of HIV-1 infection status (Fig. 28). Of these 116

ISGs, 98 were significantly induced by IFNβ in both mock-infected and HIV-infected samples, 16 were significant only in mock samples, and 2 were significant only in HIV-infected samples. The magnitude of ISG induction seemed to be globally reduced in HIV-infected cultures, which is consistent with our qRT-PCR analysis of this model (see Fig. 21). Because a small percentage of cells within the HIV-infected population actually harbors HIV-1 (see Table 1), it follows that this bulk population of cells would generally mimic the mock-treated population, underscoring the value of single cell approaches. These 116 ISGs were identified through combined analysis of both T cell donors; average expression of these ISGs for individual donor samples is shown in the heat map in Fig. 29. Overall, this heat map demonstrates that HIV-1 infection is associated with increased expression of some ISGs relative to mock-infected cells, and that gene induction patterns vary somewhat between donors in this model. IFNβ induction of these genes is pronounced in both mock- and HIV-infected cells and also varies between donors.

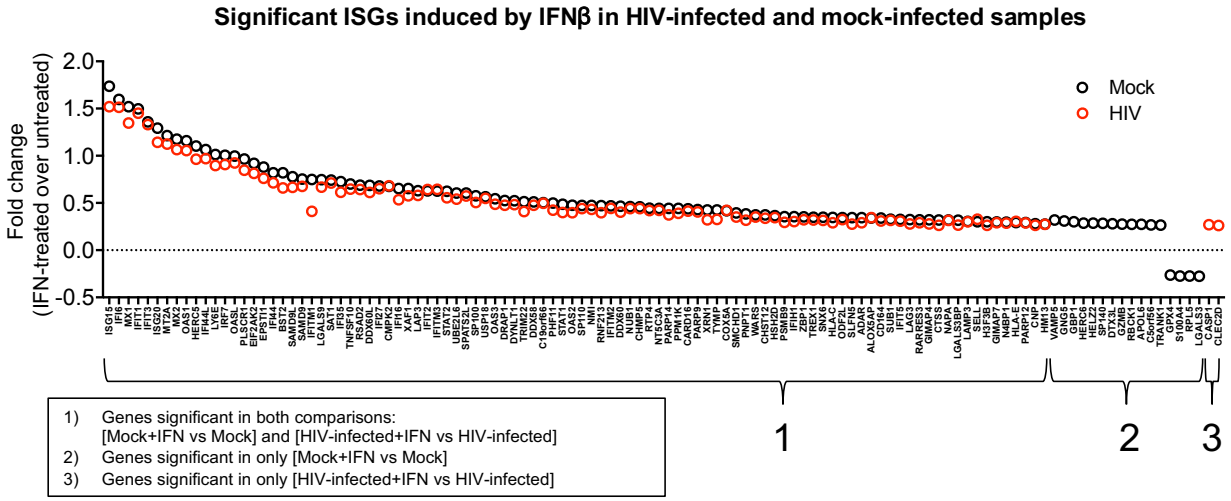


**Figure 28. scRNA-seq analysis of ISG induction in HIV-suppressed, primary CD4+ T cells.**
CD4+ T cells (donors #1 & 2) were mock-infected (media) or HIV-infected (NanoLuc HIV-1 MOI 2.0) for 24h, suppressed with ART for 7 days, then treated +/- IFNβ (100 IU/ml, 8h) and analyzed by scRNA-seq (see protocol in Fig. 17). Differential expression (DE) analysis of IFNβ-treated mock vs. untreated mock cells (black circles); and IFNβ-treated HIV-infected vs. untreated HIV-infected cells (red circles). 116 ISGs were significantly differentially expressed in any IFNβ-treated sample relative to corresponding untreated control (Log2 FC > 0.25, p < 0.05). Brackets denote significance in mock- and/or HIV-infected populations. Log2 FC values are listed in Table 10.

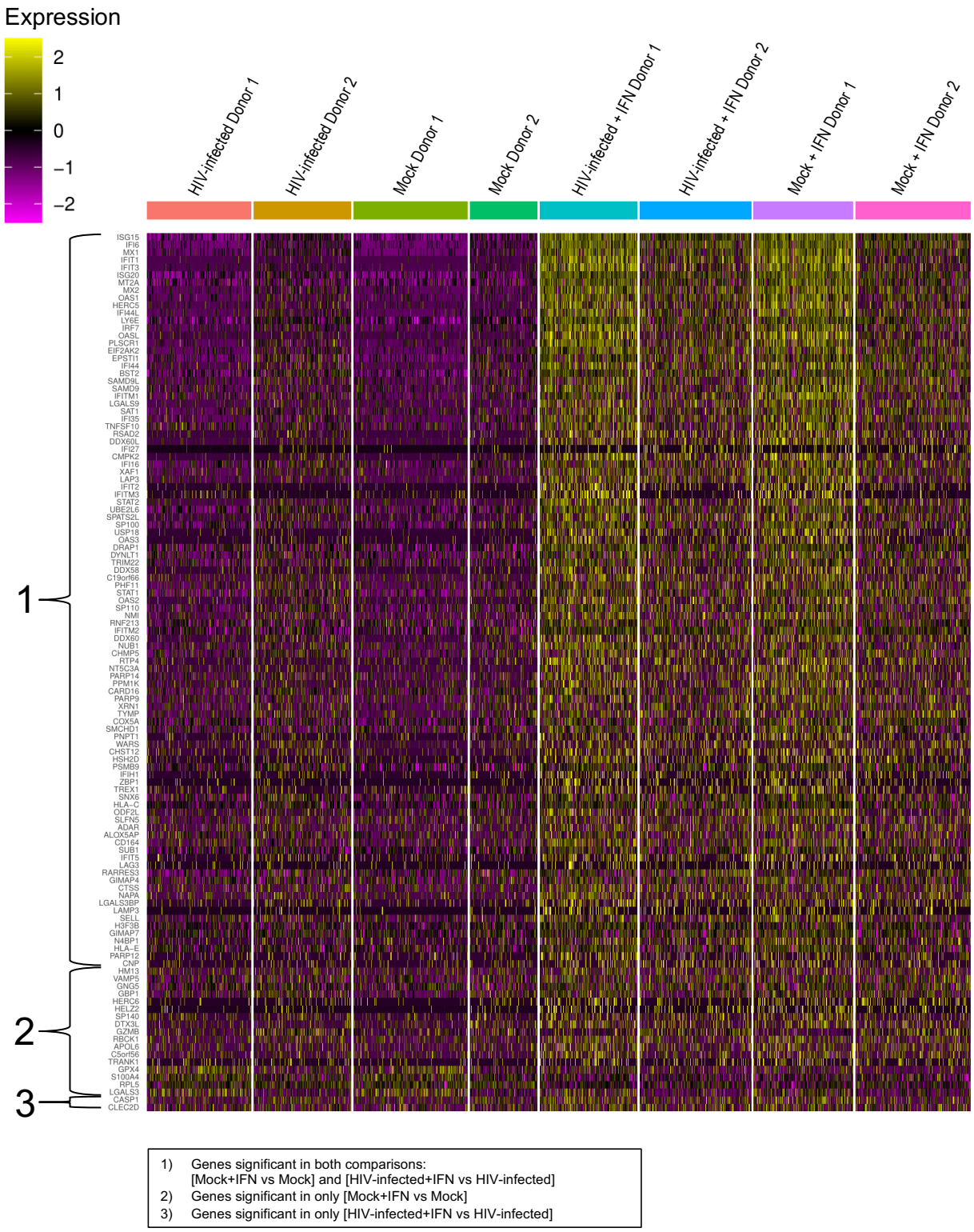


**Figure 29. Heat map showing average expression of significant ISGs in each separate sample.**
Heat map showing single cell RNA sequencing (scRNA-seq) analysis of average expression of 116 ISGs in all samples tested. Each pixel column is the expression of an individual cell. Brackets denote genes significant in mock-infected and/or NanoLuc HIV-1-infected populations (see Fig. 28).

UMAP projections suggested that vRNA$^{hi}$ and vRNA$^{lo}$ cells might have transcriptional differences beyond HIV-1 RNA expression (see Fig. 24B), so I evaluated relative expression of the 116 previously identified ISGs (see Fig. 28) in subpopulations at baseline. I calculated log2 fold change gene expression in each untreated subpopulation (vRNA$^{hi}$, vRNA$^{lo}$, vRNA-) relative to untreated, mock-infected cells (Fig. 30A). ISG expression was generally similar between vRNA- cells (grey circles) and mock-infected cells (represented by dotted line), suggesting that HIV-1 exposure without infection had little impact on ISG expression in this model. Some ISGs were elevated at baseline in vRNA$^{hi}$ or vRNA$^{lo}$ cells relative to mock (*LAG3, IFI27, ZBP1, GZMB, RNF213*), while others were downregulated (*ISG20, STAT1, RPL5, IFIT2, IFITM3, IFIT3*).

My previous studies suggest that latent cell lines are deficient in IFNβ-induced gene expression, so I next compared ISG expression between infected and uninfected cells after IFNβ stimulation. I determined log2 fold change ISG expression in each subpopulation from IFNβ-treated, HIV-infected cultures relative to IFNβ-treated, mock-infected cells (Fig. 30B). Strikingly, vRNA$^{hi}$ cells demonstrate an overall pattern of greater ISG induction relative to all other cell populations (vRNA$^{lo}$, vRNA-, and mock), suggesting that higher levels of viral products might enhance type 1 IFN responses, as demonstrated in both ACH2 cells (see Fig. 10) and productively infected cells from the RGH model (see Fig. 15). For most ISGs examined, induction levels were variable but generally comparable between mock-infected, vRNA-, and vRNA$^{lo}$ cells. Several ISGs (*IFIT3, GBP1, RPL5*) were downregulated in both vRNA$^{hi}$ and vRNA$^{lo}$ cells relative to mock cells regardless of IFNβ treatment. Notably, *LAG3*, an inhibitory receptor expressed highly in Treg cells (Huang et al. 2004), was highly elevated in both vRNA$^{hi}$ and vRNA$^{lo}$ relative to mock-infected cells under any treatment condition.

Earlier experiments in this study evaluate expression of a panel of canonical, antiviral ISGs. Figure 30C shows average expression of these ISGs (*STAT1, MX1, IFIT1, IFITM1, OAS1*) in mock-infected cells and HIV-infected subpopulations from the scRNA-seq study. Importantly,

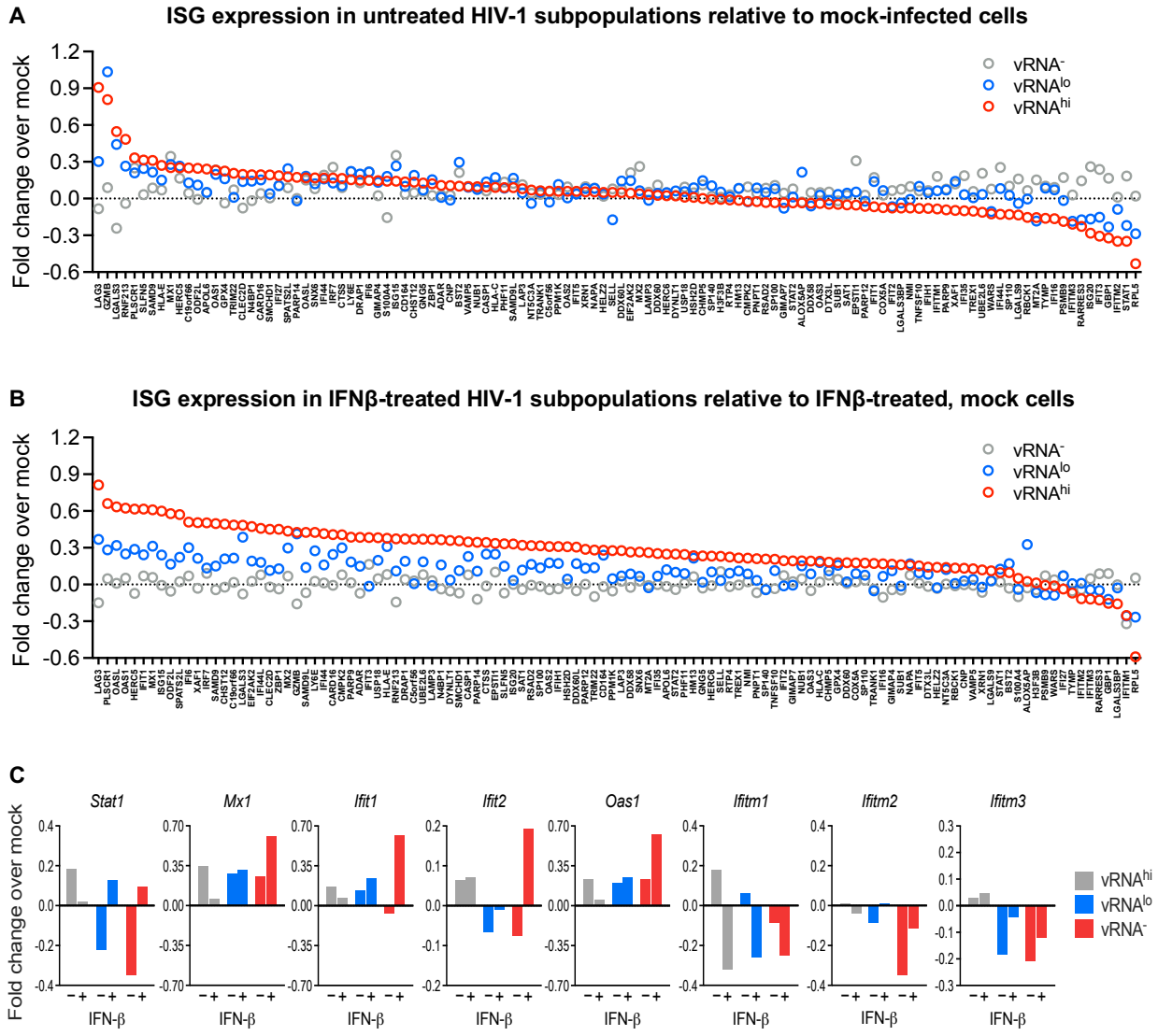


**Figure 30. scRNA-seq analysis of ISG expression before and after IFNβ treatment.**

**A** CD4+ T cells (donors #1 & 2) were infected with NanoLuc HIV-1 (MOI 2.0) for 24h, suppressed with ART for 7 days, then ISG expression in HIV-infected subpopulations assessed through scRNA-seq. Circles represent Log2 fold change (FC) gene expression in each subpopulation (vRNA$^{hi}$, vRNA$^{lo}$, or vRNA$^{-}$) relative to mock-infected cells. **B** ISG expression in cells treated with 100 IU/ml IFNβ for 8h after ART suppression (see protocol in Fig. 17). Circles represent Log2 FC gene expression in each IFNβ-treated subpopulation (vRNA$^{hi}$, vRNA$^{lo}$, or vRNA$^{-}$) relative to IFNβ-treated, mock-infected cells. ISGs shown in Graphs A & B were previously identified through differential expression analysis of mock-infected and HIV-infected cells (see Fig. 28) and are ordered according to expression level in vRNA$^{hi}$ cells. Dotted line represents gene expression in mock-infected cells. **C** Bar graphs summarize expression of select ISGs from Graphs A and B. Bars represent log2FC gene expression relative to similarly-treated, mock-infected cells. See Table 11 for Log2 FC expression values.

*STAT1* gene expression is significantly downregulated in vRNA$^{hi}$ and vRNA$^{lo}$ cells at baseline, but is induced by IFNβ treatment in all cells (Fig. 30C). vRNA$^{lo}$, vRNA-, and mock-infected cells express similar *MX1, IFIT1,* and *OAS1* at baseline, and similarly upregulate these ISGs in response to IFNβ treatment. Despite normal baseline expression of *MX1, IFIT1*, and *OAS1*, vRNA$^{hi}$ cells upregulate very high levels of these genes in response to IFNβ. Interestingly, *IFITM1, IFITM2,* and *IFITM3* are downregulated in vRNA$^{hi}$ and vRNA$^{lo}$ cells at baseline, and are poorly induced by IFNβ. IFITM proteins, including IFITM1-3, specifically disrupt the function of HIV-1 Env to hinder HIV-1 virus particle assembly and release from productively infected cells (Lu et al. 2011; Yu et al. 2015). It is unclear what role IFITM proteins may have in a latently infected cell that has shut down viral replication.

Overall, the single cell transcriptome of primary CD4+ T cells under ART conditions of HIV-1 suppression reveals that vRNA$^{hi}$ and vRNA$^{lo}$ cells display altered baseline expression and IFNβ-induced expression of select ISGs, with increased ISG induction revealed in vRNA$^{hi}$ cells.

*SUMMARY OF RESULTS*

In this study I examined the response to type 1 interferon in HIV-infected compared to uninfected (mock) primary CD4+ T cells after 7 days of ART suppression. This study was performed using CD4+ T cells from three different healthy human donors. I selected a panel of five canonical ISGs (*MX1, IFIT1, IFIT2, IFITM1, OAS1*) as indicators of the overall antiviral IFNβ response, and measured ISG mRNA upregulation by qRT-PCR in IFNβ-treated relative to untreated cells from each infection group. qRT-PCR analysis of these cultures showed that HIV-infected cells upregulated ISGs in response to IFNβ, but the magnitude of this response was diminished for select ISGs compared to that of uninfected CD4+ T cells. The specific genes impaired varied between cells from different donors, suggesting multiple possible mechanisms for ISG restriction in HIV-suppressed cells.

Further scRNA-seq analysis of cells from donors 1 and 2 revealed that a small percentage of total cells expressed viral RNA (vRNA), approximately 6.9% (average across cells from two donors). Remarkably, scRNAseq T cell subset analysis revealed that HIV-1 preferentially infected inducible Treg cells (Fig. 25C), which are characterized by elevated expression of inhibitory receptors and a generally immunosuppressive phenotype. Because vRNA+ cells expressed a wide range of HIV-1 RNA levels (1 – 134 copies), this population was categorized into two groups for further analysis (vRNA$^{hi}$ and vRNA$^{lo}$). Differential expression analysis of vRNA$^{hi}$ and vRNA$^{lo}$ cells relative to mock-infected (vRNA-) cells (no IFNβ treatment) yielded 80 HIV-regulated genes, of which many were involved in processes related to RNA metabolism, translation, and protein localization.

In a separate differential expression analysis of IFNβ-treated relative to IFNβ-untreated cells, 116 ISGs were identified that were significantly upregulated in mock-infected and/or HIV-infected cultures (Fig. 28). Further analysis of these 116 ISGs in HIV-infected cell subsets showed that for most ISGs, baseline expression levels were similar between vRNA$^{hi}$, vRNA$^{lo}$, vRNA-, and mock-infected cells (Fig. 30A). Several ISGs were upregulated (*LAG3, GZMB, LGALS3, RNF213)* or downregulated (*STAT1, IFITM2, IFITM3, GBP1, IFIT3, RPL5, ISG20)* in vRNA$^{hi}$ or vRNA$^{lo}$ cells relative to mock-infected cells at baseline. In contrast, IFNβ-induced expression levels varied considerably between these cell populations (Fig. 30B). ISG induction in IFNβ-treated vRNA$^{hi}$ cells was elevated compared to all other cell populations, suggesting HIV-1 RNA may activate cellular mechanisms that prime these cells for an enhanced response to type 1 IFN. IFITM genes were downregulated in vRNA$^{hi}$ and vRNA$^{lo}$ cells regardless of IFNβ treatment.

# CHAPTER 4: DISCUSSION

Innate immunity plays an important role in early control of HIV-1 infection *in vivo*, but it is not well understood whether latent cells have functional innate immune and interferon responses. Here I investigated responses to RIG-I agonists and type 1 interferon in a variety of different *in vitro* models of HIV-1 latent infection or virologic suppression, including a model of HIV-1 suppression in primary CD4+ T cells.

The HIV-1 latent reservoir *in vivo* is a diverse population that includes multiple CD4+ T cell subsets, distributed in different tissues, and with distinct proviral integration sites. A major challenge to understanding HIV-1 latency has been the availability of *in vitro* models that capture the heterogeneity of the *in vivo* HIV-1 reservoir. I sought to overcome this obstacle by comparing type 1 IFN responses in a variety of cell culture models representing various aspects of HIV-1 latent infection. Latent cell lines are clonal populations that proliferate, representing latent cells that might arise from clonal expansion *in vivo*, but each cell line represents only a single unique latent cell with one integrated provirus. The RGH fluorophore reporter system models acute infection with heterogenous provirus integration, and enables direct comparison of latent and productively infected cells, though virus-driven transcriptional repression may impact fluorophore expression and influence the integrity of each population. The NanoLuc HIV-1 primary cell model represents productive infection of activated CD4+ T cells that are then suppressed by ART. While this model approximates HIV-1 latency it does not represent latent infection arising from complete transcriptional silencing or clonal expansion. However, this model represents a diverse population of primary cells and accounts for the effects of ART, mimicking the diverse reservoir of suppressed cells in ART-treated patients. I discovered that the expression of select ISGs was dysregulated in all cell models examined, though the specific ISGs impaired varied between latency models and primary cell donors. I also identified distinct transcriptional changes within the type 1 IFN-induced

ISG network in each model. Considering the vast biological diversity of the latently infected cell population *in vivo* (Vanhamel, Bruggemans, and Debyser 2019), it is likely that type 1 IFN response regulation might also occur through multiple mechanisms. These mechanisms are not limited to virus-mediated processes, but might also be linked with cell-specific differences in innate immune signaling programs that serve as the basis for supporting latent HIV-1 infection.

When I examined the response to RIG-I agonists or IFNβ in latent cell lines, I found that J-Lat9.2, JLat11.1, and ACH2 latent cell lines demonstrate reduced ISG induction compared to uninfected control cells, suggesting that the establishment of long-term latency in these models may be linked with a dysregulated response to IFNβ. This phenotype was less pronounced in ACH2 cells, which constitutively produce residual HIV-1 and express elevated ISGs at baseline. Jurkat T cells that were latently infected with a dual color reporter HIV-1 also showed reduced induction of select ISGs. Primary CD4+ T cells infected with NanoLuc HIV-1 and suppressed by ART demonstrate variable but overall reduced responses to IFNβ stimulation compared to mock-infected cells. Single cell transcriptomic profiling of these HIV-suppressed CD4+ T cells revealed that viral RNA positive (vRNA+) and negative (vRNA-) cells from the same culture have distinct gene expression profiles, with altered expression of genes involved in RNA processing, translation, and type 1 IFN response. My observations in multiple models of HIV-1 latency or primary cells undergoing virologic suppression suggest that HIV-1 latent infection is associated with transcriptional changes that impair type 1 IFN responses. However, the ISGs impaired varied considerably between models, thwarting discovery of a single, unique mechanism that suppresses antiviral immunity in latent cells.

Several studies suggest that HIV-1 RNA triggers RIG-I activation leading to a type 1 IFN response (Solis et al. 2011; Berg et al. 2012; Li et al. 2016). A recent study also showed that stimulating the RIG-I pathway with Acitretin in reactivated, latent cells led to a RIG-I-induced innate immune response that culminated in the specific death of latent cells (Li et al. 2016). This exciting study highlighted RIG-I as a potential target for therapeutic eradication, prompting a new

wave of research viral RNA sensors for HIV-1 latency eradication. However, these exciting findings could not be repeated by myself or any others (Garcia-Vidal et al. 2017). Reactivating HIV-1 RNA production by various means in my latent cell line models failed to activate RIG-I-mediated innate immunity (Figs. 5, 6), raising the question of whether RIG-I truly can recognize host-transcribed HIV-1 RNA.

These data also highlight the possibility that HIV-1 latent infection obstructs viral RNA sensors like RIG-I, thus protecting latent cells from innate immune activation. In fact, latent cell lines stimulated with RIG-I agonists induced lower levels of select ISGs than uninfected cells, most notably *MX1* (Fig. 7). However, Sendai virus induced similar levels of IRF3 phosphorylation and nuclear translocation in latent JLat9.2 and control Jurkat cells (Fig. 8), suggesting that IRF3 and thus RIG-I activation are probably functional in this model. Latent cell lines transcribed less IFNβ than uninfected cells following treatment with RIG-I agonists (Fig. 7), potentially contributing to poor ISG induction. Latent cell lines treated with IFNβ also induced lower levels of ISGs than IFNβ-treated control cells, supporting a model in which HIV-1 latency somehow disrupts antiviral innate immunity (Fig. 10). Because I observed no loss of IFNAR1 expression or JAK/STAT activation in latent cell lines (Fig. 9, 10), ISG dysregulation might occur downstream of these pathways, possibly at a transcriptional level. A dysregulated type 1 IFN response may support latency persistence, though it is unclear if this phenotype is driven by HIV-1 infection or an inherent property of a pre-latent cell, and my findings support both distinct models.

Functional genomics analysis of latent JLat9.2 and Jurkat cells revealed that latent cells had reduced mRNA abundance for many genes involved in innate antiviral immunity and type 1 interferon responses. As both JLat9.2 and Jurkat cell lines were derived from a single common cell line, these broad transcriptional differences were more likely due to HIV-1 than to stochastic variation between individual cells within a clonal population. scRNA-seq identified many HIV-regulated genes that were common between cells from two individual human donors. Many of these HIV-regulated genes are involved in RNA biogenesis, RNA metabolism, and translation

processes, indicating that HIV latent infection drives changes to RNA transcription and translation machinery. Indeed, latent HIV-1 infection drives many cellular changes that could contribute to transcriptional repression of select ISGs, including modulation of transcription factors like STAT1, NF-κB, and IRF1 (Marsili et al. 2003); suppressive chromatin modifications that downregulate proviral genes (Siliciano and Greene 2011); and alteration of ribosomal proteins (Kleinman et al. 2014). This evidence favors a model in which antiviral innate immunity is inhibited through virus-driven changes to a latent cell.

A key unanswered question is why some productively infected cells die while others progress to HIV-1 latency. Most cells that are productively infected with HIV-1 will die from virus cytopathic effects, innate antiviral immunity, or adaptive immune responses; yet a small number of these cells survive to become latent. The cellular determinants of survival to latency are not known, and if discovered would hugely impact research for HIV-1 cure. The magnitude and efficacy of the intracellular innate immune response depends on many factors such as expression and abundance of signaling proteins (PRRs, STATs, IRFs, IFNAR1, etc.), post-translational modifications of these proteins, and transcriptional regulation of ISGs (Diamond and Farzan 2013). These factors vary between individual cells and may predispose cells with poor antiviral responses to latent infection, supporting an alternate model of cell selection rather than virus reprogramming for latency. This model favors the possibility that HIV-1 latency is supported by many different, cell-specific mechanisms of ISG suppression, and helps explain the considerable variation in ISG regulation observed between latency models in this study.

My single cell sequencing study revealed that vRNA+ cells (including $vRNA^{hi}$ and/or $vRNA^{lo}$ subpopulations) have a distinct transcriptional program that suppresses markers of cell proliferation (*JUN, LAMP3, RPL5*) (Goudarzi and Lindstrom 2016; Shaulian and Karin 2002; Tanaka et al. 2020), regulates NF-κB signaling (*LGALS3, RNF213*) (Okamoto et al. 2019; Ahel et al. 2020), and promotes expression of markers of T cell exhaustion (*LAG3*) (Andrews et al.

2017). These properties might be explained by preferential infection of Tregs over other CD4+ T cell subsets, which is shown in my model (Fig. 25C) and others, and suggests that the epigenetic programming of T cells destined for resting and suppressive fates might impact latency outcomes. A recent single cell sequencing study similarly linked HIV-1 latency in primary CD4+ T cells to T cell subset identity, finding that HIV-1 provirus suppression was associated with a central memory transcriptional phenotype (Bradley et al. 2018). Thus, cells with immune suppressive transcriptomes, whether from stochastic expression of antiviral genes or predetermined T cell fates, may be selected for HIV-1 latency.

Beyond latency establishment, the biological factors contributing to reservoir maintenance are unclear. Constitutive type 1 IFN signaling is pathogenic in chronic HIV-1 infection and may promote formation and maintenance of the latent reservoir. Several studies have linked failure to downregulate type 1 IFN signaling to SIV and HIV-1 pathogenesis in non-human primates and humans, respectively (Bosinger et al. 2009; Jacquelin et al. 2009; Rotger et al. 2011). IFNAR blockade during chronic HIV-1 infection in humanized mice correlated with reduced viral reservoir size, increased reactivation, and delayed rebound following ART cessation (Zhen et al. 2017; Cheng, Ma, et al. 2017), suggesting that sustained type 1 IFN signaling promotes reservoir maintenance. Furthermore, latent cells are often located in immune tissues where they are more likely to be exposed to type 1 IFN and other immune stimulatory cytokines from nearby cells (Vanhamel, Bruggemans, and Debyser 2019). Constitutive, aberrant type 1 IFN signaling has been shown to support other chronic infections, including that caused by hepatitis C virus (HCV). In HCV infection the sustained type 1 IFN production and signaling driven by liver-resident macrophages and infiltrating myeloid cells promotes a state of "innate immune tolerance" that desensitizes infected cells to type 1 IFN and restricts ISG activation, mediating cell survival and chronic infection (Lau et al. 2013; Horner and Gale 2013). I propose that HIV-induced type 1 IFN signaling similarly creates a selective pressure through which latent cells must survive and escape, and that sustained type 1 IFN exposure promotes IFN desensitization in latently infected

cells long-term. The latency models in this study do not recapitulate the immune environment around latent cells, and further studies are needed to resolve how type 1 IFN affects established latent cells.

Integration of data sets of my sequencing studies identified ISGs that were downregulated in latent or HIV-suppressed cells and but do not yet have clearly defined roles in HIV-1 latency (Table 3). These include genes that were downregulated in $vRNA^{hi}$ and/or $vRNA^{lo}$ relative to mock-infected CD4+ T cells (*STAT1, IFITM1, IFITM2, IFITM3, GBP1, RPL5, ISG20*), or were poorly induced by IFNβ in one or more cell line models of latency (*STAT1, MX1, IFITM1, IFITM3, IFIT1, IFIT2, MT2A, OAS1, ISG15, RSAD2*). I propose that these genes (summarized below in Table 3) are candidate latency restriction factors, and are modulated by HIV-1 to promote a cellular environment that is conducive to the establishment and long-term maintenance of latency. By this model, the high or sustained expression of these specific ISGs would be predicted to disrupt one or more essential biological processes within CD4+ T cells that otherwise facilitate the establishment and/or persistence of HIV-1 latency.

Several of these ISGs are already known to restrict HIV-1 replication in productively infected cells, including *IFIT1, IFIT2, IFITM1, IFITM2, IFITM3* (Lu et al. 2011; Yu et al. 2015; Altfeld and Gale 2015). However, it is unclear whether these ISGs have specific antiviral functions in the context of HIV-1 latent infection. Remarkably, *IFITM1* was poorly induced by IFNβ in JLat9.2 cells (Fig. 10D), RGH latently infected Jurkat cells (Fig. 15C), and HIV-suppressed CD4+ T cells positive for viral RNA (Fig. 30C). The similar antiviral *IFITM2* and *IFITM3* genes were also downregulated in vRNA+ cells in my single cell sequencing analysis, highlighting a novel role for IFITM proteins in HIV-1 latency restriction. IFITM proteins, including IFITM1-3, specifically disrupt the function of HIV-1 Env to hinder HIV-1 virus particle assembly and release from productively infected cells (Lu et al. 2011; Yu et al. 2015). It is unclear what role IFITM proteins may have in a latently infected cell that has shut down viral replication.

*STAT1* was downregulated in latent or HIV-suppressed cells in both of my sequencing studies (Figs. 13, 30), which makes sense as the STAT1 protein is well known to restrict HIV-1 infection and may even impart HIV-1 latency reversal (Khanal et al. 2021). STAT1 is a critical mediator of JAK/STAT signaling and an essential effector of interferons (see Fig. 2); loss of STAT1 cripples intracellular antiviral immunity. Beyond its role as an IFN effector, STAT1 also inhibits NF-κB activation and can potentiate TNFα-induced apoptosis (Khanal et al. 2021; Kumar et al. 1997); both of these actions would antagonize latent cell survival. Reduced expression of *STAT1* may facilitate latency, possibly by reducing the intracellular effects of exogenous interferon; this is certainly a promising candidate for latency eradication strategies.

Several other ISGs were identified that do not yet have known roles in HIV-1 infection or latency. GBP1 is a well-characterized guanylate binding protein with potent antiviral activity against dengue, hepatitis C, vesicular stromatitis, and encephalomyocarditis viruses (Anderson et al. 1999; Itsui et al. 2009; Pan et al. 2012). Interestingly, a recent study showed that while GBP1 only weakly inhibited HIV-1 replication, the closely related protein GBP5 potently blocked HIV-1 infectivity in a variety of cell types through interference with Env (Krapp et al. 2016). In the present study, *GBP1* was downregulated in $vRNA^{hi}$ and $vRNA^{lo}$ CD4+ T cells at baseline and after IFNβ stimulation (Figs. 30A,B), suggesting that guanylate binding proteins may have an overlooked role in HIV-1 latent infection.

Indeed, further research will resolve how these different ISGs might inhibit latent HIV-1 infection. A fascinating future experiment might evaluate relative frequencies of latent infection in cells overexpressing or deficient in some of the key ISGs identified in the present work.

**Concluding remarks**

In conclusion, we evaluated innate immune activation and type 1 IFN responses in multiple distinct *in vitro* models of HIV-1 latency, and observed that latent cells have impaired induction of select ISGs. These ISGs varied between latency models, suggesting that HIV-1 latent infection

might be associated with multiple mechanisms of type 1 IFN escape. This study highlights a role for type 1 IFN in the formation, composition, and long-term maintenance of the HIV-1 reservoir. Here we also identified ISGs that may have unique and distinct roles in latently infected cells, though additional studies are needed to elucidate their functions and determine how enrichment of these genes could disrupt latent infection. Our observations contribute to the understanding of how cells might be selected by HIV-1 for latency and have important implications for therapeutic strategies aimed at eradicating the latent HIV-1 reservoir. Restoring and/or enhancing specific ISG function in latent cells will be critical for the success of any latency reversal therapies targeting innate immune programs.

**Table 3. Candidate IFNβ-responsive latency restriction factors**

| | ScRNA-seq | Bulk RNA-seq | qRT-PCR studies | Gene function | References |
|---|---|---|---|---|---|
| Reference figures | Figs. 27A, 28, 29, 30A-C<br>Tables 8-11 | Fig. 13<br>Table 7 | Figs. 7A-C, 10A-F, 15C | | |
| **GBP1** | downreg. in vRNAhi & vRNAlo (+/- IFNβ) | not significant | not tested | inhibits viral glycoproteins | Anderson et al., 2009;<br>Krapp et al. 2016 |
| **IFIT1** | downreg. in vRNAhi | poor induction by IFNβ in JLat9.2* | poor induction by IFNβ in JLat9.2* | inhibits viral RNA expression | Diamond and Farzan, 2013 |
| **IFIT2** | downreg. in vRNAhi & vRNAlo | poor induction by IFNβ in JLat9.2* | poor IFNβ induction in JLat9.2 | inhibits viral RNA expression | Diamond and Farzan, 2013 |
| **IFITM1** | downreg. in vRNAhi & vRNAlo (+/- IFNβ) | poor induction by IFNβ in JLat9.2* | poor induction by IFNβ in all latent cell lines* and RGH latent cells* | blocks viral fusion and release | Lu et al., 2011;<br>Yu et al., 2015;<br>Raftery & Stevenson, 2017 |
| **IFITM2** | downreg. in vRNAhi & vRNAlo (+/- IFNβ)* | not significant | not tested | inhibits viral entry & induces apoptosis | Lu et al., 2011;<br>Yu et al., 2015;<br>Raftery & Stevenson, 2017 |
| **IFITM3** | downreg. in vRNAhi & vRNAlo (+/- IFNβ) | poor induction by IFNβ in JLat9.2* | not tested | inhibits viral entry | Lu et al., 2011;<br>Yu et al., 2015;<br>Raftery & Stevenson, 2017 |
| **ISG15** | not significant | poor induction by IFNβ in JLat9.2* | poor induction by SeV in JLat9.2* and ACH2 | isgylates antiviral proteins to enhance activity; antiviral activity against many viruses | Okumura et al., 2006;<br>Kim et al., 2016;<br>Raftery & Stevenson, 2017 |
| **ISG20** | downreg. in vRNAlo (+/- IFNβ)* | not significant | not tested | degrades viral RNA | Schoggins et al., 2011 |
| **MT2A** | downreg. in vRNAhi & vRNAlo | poor induction by IFNβ in JLat9.2* | not tested | anti-oxidant; regulates intracellular conc. of heavy metals; regulates apoptosis | Ling et al., 2016 |
| **MX1** | not significant | poor induction by IFNβ in JLat9.2* | poor induction by IFNβ in JLat9.2* and JLat11.1* | binding/inactivation of viral ribonucleocapsid | Raftery & Stevenson, 2017 |
| **OAS1** | not significant | poor induction by IFNβ in JLat9.2* | poor induction by IFNβ in all latent cell lines* and RGH latent cells* | activates Rnase L to degrade viral RNA | Raftery & Stevenson, 2017 |
| **RNF213** | upreg. in vRNAhi & vRNAlo (+/- IFNβ)* | not significant | not tested | E3 ubiquitin ligase | Ahel et al., 2020 |
| **RPL5** | downreg. in vRNAhi & vRNAlo (+/- IFNβ)* | not significant | not tested | ribosome component; binds 5S RNA | Goudarzi et al., 2016 |
| **RSAD2 (viperin)** | not significant | poor induction by IFNβ in JLat9.2* | not tested | inhibits viral RNA replication, binds viral proteins, dysregulates lipid metabolism | Fitzgerald, 2011 |
| **STAT1** | downreg. in vRNAhi & vRNAlo (+/- IFNβ)* | poor induction by IFNβ in JLat9.2* | not tested | IFN effector; critical part of JAK/STAT pathway; inhibits NF-KB; potentiates TNFα-mediated apoptosis | Stark and Darnell, 2012;<br>Raftery & Stevenson, 2017;<br>Khanal et al., 2021 |

**Legend:**

| | |
|---|---|
| * | statistically significant ($p < 0.05$) |
| downreg. | downregulated gene expression |
| upreg. | upregulated gene expression |
| +/- IFNβ | refers to untreated and IFNβ-treated samples |
| vRNAhi | HIV-infected CD4+ T cells expressing high HIV-1 RNA levels |
| vRNAlo | HIV-infected CD4+ T cells expressing low HIV-1 RNA levels |
| RGH | Cells infected with Red-Green-HIV-1 reporter |
| SeV | Sendai virus |

# CHAPTER 5: MATERIALS AND METHODS

## Cells lines and culture methods

The following cell lines were used in this study: Jurkat E6-1 (ATCC), A3.01 (NIH ARP), HEK-293T (ATCC), and TZM-bl cells (ATCC), as well as the latent cell lines JLat9.2 (NIH ARP), JLat11.1 (gift from Dr. Florian Hladik), and ACH2 (NIH ARP). All cell lines were cultured under standard cell culture conditions at 37°C and 5% CO2. Jurkat, JLat9.2, JLat11.1, A3.01, and ACH2 cells were cultured in RPMI supplemented with 10% FBS, 1% L-glutamine, 1% non-essential amino acids, 1% sodium pyruvate, and 1% antibiotic/antimycotic cocktail (all Fisher Scientific), hereafter referred to as complete RPMI. HEK-293T and TZM-bl cells were cultured in DMEM supplemented with 10% FBS, 1% L-glutamine, 1% non-essential amino acids, 1% sodium pyruvate, and 1% antibiotic/antimycotic cocktail. Cell lines were thawed from early passages and kept in culture no longer than 4 weeks. All cell lines have tested negative for mycoplasma contamination.

## Primary CD4+ T cell isolation and culture

PBMC from three healthy human donors were isolated from half leuko packs (Bloodworks Northwest) by Ficoll-Paque gradient centrifugation. Briefly, cells were collected from half leuko packs and diluted in 200ml complete RPMI with 2mM EDTA. 30ml of diluted PBMC were layered over 15ml Ficoll-Paque PLUS (GE Healthcare) in 50ml conical tubes, then centrifuged at 400xG for 30 min at 20°C. PBMC were collected and transferred to 50ml conical tubes, washed with complete RPMI, then residual red blood cells lysed for 5 min with RBC lysis buffer. PBMC were washed with complete RPMI and passed through mesh filters. CD4+ T cells were purified from PBMC by negative magnetic separation with a CD4+ T cell isolation kit (Miltenyi) using a QuadroMACS separator (Miltenyi) according to the manufacturer's instructions. Purified CD4+ T

cells were cultured at 37°C and 5% CO2 in RPMI media supplemented with 10% FBS, 1% L-glutamine, 1% non-essential amino acids, 1% sodium pyruvate, and 1% antibiotic/antimycotic cocktail (complete RPMI). Cells were cryopreserved in FBS containing 10% DMSO and stored in liquid nitrogen. CD4+ T cells were genotyped for the CCR5Δ32 polymorphism and confirmed CCR5 wild-type homozygous (Donor #1 & 2), or CCR5Δ32 heterozygous (Donor #3).

**Innate Immune Stimulations**

The following innate immune agonists were used in this study: human recombinant IFNβ (Toray Industries), human recombinant IFNγ (Peprotech), PMA (Sigma), ionomycin, Sendai virus (Charles River Laboratories). Sendai virus infection and PAMP RNA transfection are described below. For innate immune or interferon stimulation studies, cells were seeded at a density of $5x10^5$ cells/ml in 1ml complete RPMI per well in 12-well plates. This was accomplished by diluting cells to $10^6$ cells/ml in complete RPMI, and adding 500ul media alone or media containing 2x desired agonist in amounts described in figure legends, then mixing with a pipette. Cells were cultured for desired times at 37°C, then lysates harvested for protein and RNA analysis as described below.

**Sendai virus infection**

Sendai virus (SeV) Cantrell Strain was obtained from Charles River Laboratories. Cells were seeded at a density of $5x10^5$ cells/ml in 1ml complete RPMI per well in 12-well plates, then 25ul media (mock control) or concentrated SeV stock (4000 HAU/ml) was added directly to each well for a final SeV infection dose of 100 HAU/ml. Wells were pipette mixed then cultured for desired times at 37°C, then lysates harvested for protein and RNA analysis.

**PAMP RNA synthesis and transfection**

HCV Con1 nonstimulatory RNA (xRNA) and HCV Con1 pU/UC RNA (PAMP RNA) were synthesized from T7 promoter-linked complementary oligonucleotides (Integrated DNA Technologies). All *in vitro*-transcribed RNAs contained a 5' triphosphate (5'-ppp) and three guanine nucleotides at the 5' end to enhance T7 polymerase transcription. RNA products were generated using T7 RNA polymerase and a T7 MEGAshortscript kit (Ambion) according to the manufacturer's instructions. Following *in vitro* transcription, DNA templates were removed with DNase treatment and unincorporated nucleotides and protein were removed from the reaction mixture by phenol-chloroform extraction. RNA was then precipitated using ethanol and ammonium acetate as described by the manufacturer and resuspended in nuclease-free water. RNA concentrations were determined by absorbance using a Nanodrop spectrophotometer. RNA quality was assessed on denaturing 2% agarose formaldehyde gels (Kell et al. 2015).

For RNA transfection experiments, cells were seeded at 5 x $10^5$ cells/ml in 12-well plates and cultured overnight at 37°C. Transfections were performed using 10 pmol RNA with a TransIT-mRNA transfection kit (Mirus) according to the manufacturer's instructions. RNA lysates were harvested 24h post transfection and analyzed by qRT-PCR as described below.

**IRF3 nuclear translocation**

Following Sendai virus infection (100 HAU/ml, 24h), IRF3 nuclear localization was measured in cell lines by ImageStreamX technology as described elsewhere (Rustagi et al. 2013). Briefly, cells were washed in PBS, fixed and permeabilized using the BD Cytofix/Cytoperm kit per the manufacturer's instructions (BD Biosciences), then stained with mouse monoclonal anti-IRF3 AR1 antibody on ice for 30 min. Cells were washed twice with PBS + 0.1% sodium azide, then stained with AF647 anti-mouse secondary antibody on ice for 30 min. Cells were washed with PBS + 0.1% sodium azide, stained with 0.05 µg/ml DAPI (ThermoFisher) for 10 min, washed twice with PBS + 0.1% sodium azide, then resuspended in 50 µl Perm/Wash (BD Biosciences)

for analysis by an Annis ImageStreamX Mk II imaging cytometer. IRF3 expression and DAPI nuclei were measured in 20,000 cells per sample, and expression similarity above an arbitrary cutoff determined using IDEAS software (Luminex) as shown in Supplemental Fig. 2A.

**qRT-PCR analysis**

For quantification of HIV-1 RNA or host gene expression, Cell lysates were digested in RLT and total cellular RNA extracted using the miRNeasy Micro kit (Qiagen) or miRNeasy Mini kit (Qiagen) according to the manufacturer's instructions, and residual genomic DNA removed by DNAse treatment. RNA concentrations were determined by absorbance using the NanoDrop 2000 Spectrophotometer. cDNA was synthesized using the iScript Select cDNA Synthesis kit (Biorad).

Quantitative real-time PCR (qRT-PCR) analysis of cDNA was performed using SYBR Green PCR master mix (ABI) and primers (Table 4), on a ViiA 7 Real-Time PCR System (Applied Biosystems) with QuantStudio software (Applied Biosystems). For all qRT-PCR analysis, $\Delta\Delta$Ct values were calculated relative to housekeeping gene RPL13A and to control (untreated or mock-infected) cells as described in figure legends. Mean fold change (FC) was calculated relative to control cells as indicated in figure legends. Multiple independent experiments were performed for each study, and presented data represent mean FC ± SD of biological replicates from multiple combined independent experiments or from a single representative experiment as indicated in figure legends.

**Table 4. Oligonucleotides used in this study**

| Primer ID | Full primer sequence |
|---|---|
| *RT-PCR primers:* | |
| HIV gag fwd | GAAGCTGCAGAATGGGATAGAT |
| HIV gag rev | GGTTCCTTTGGTCCTTGTCTTA |
| hIFIT1 fwd | AGAAGCAGGCAATCACAGAAAA |
| hIFIT1 rev | CTGAAACCGACCATAGTGGAAAT |
| hIFIT2 fwd | GTTTCCGAAGTGGACATCGCA |
| hIFIT2 rev | CTGCACAGGTTGTTCTCAGC |
| hIFITM1 fwd | TACTCCGTGAAGTCTAGGGACAG |
| hIFITM1 rev | AACAGGATGAATCCAATGGTCA |
| hIFNB fwd | TGCATTACCTGAAGGCCAAG |
| hIFNB rev | AAGCAATTGTCCAGTCCA |
| hISG15 fwd | TGAGCGGGCCCTGAGA |
| hISG15 rev | ATATCTGGGTGCCTAAGGACCTT |
| hMX1 fwd | GTTTCCGAAGTGGACATCGCA |
| hMX1 rev | CTGCACAGGTTGTTCTCAGC |
| hOAS1 fwd | TGGGTGGTGGAGACCCAA |
| hOAS1 rev | AATTCAGCCAGGCCTCAGC |
| hRPL13A fwd | GCCCTACGACAAGAAAAAGCG |
| hRPL13A rev | TACTTCCAGCCAACCTCGTGA |
| *ddPCR primers:* | |
| HIV gag sense | GACTAGCGGAGGCTAGAAGGAGAGA |
| HIV gag antisense | CTAATTCTCCCCCGCTTAATAYTGACG |

## Immunoblotting

Whole cell lysates were prepared with RIPA buffer (25mM Tris, HCl pH 7.6, 150mM NaCl, 1% NP-40, 1% sodium deoxycholate, 0.1% SDS) supplemented with 1% protease inhibitor, 1% phosphatase inhibitor, and 0.1% okadaic acid. Ten micrograms of protein were loaded in equal volumes and separated on a 4-20% Mini-Protean TGX precast gel (Biorad), then transferred to a nitrocellulose membrane and blocked for 1h at room temp with 5% BSA (Sigma) in TBST. Blots were incubated overnight at 4°C with primary antibodies from Cell Signaling Technology: rabbit (Rb) anti-MX1, Rb anti-OAS1, Rb anti-phospho-STAT1 Y701, Rb anti-STAT1, Rb anti-STAT2, Rb anti-phospho-STAT3 S727, or Rb anti-STAT3, Rb anti-phospho-IRF3 S386. The following primary antibodies were also used: Rb anti-MX2 (Novus Bio), Rb anti-IFIT1 (gift from G. Sen at the Cleveland Clinic), mouse (Ms) anti-IFITM1 (ProteinTech), Ms anti-Actin (Sigma), Rb anti phospho-JAK1 Y1022/1023 (Abcam), Rb anti phospho-STAT2 Y689 (Millipore), and Ms anti-IRF3 clone AR1 (Rustagi et al. 2013). Following primary antibody incubation, blots were washed with

TBST then incubated with the appropriate horseradish peroxidase (HRP)-conjugated secondary antibody (Jackson Immunoresearch Labs) for 1h at room temp. Blots were washed in TBST then target proteins detected with a chemiluminescent kit (ThermoFisher) and imaged using a ChemiDoc XRS+ system (Bio-Rad) with Image Lab Software (Bio-Rad). Target protein abundance relative to actin was quantified using ImageJ software.

**Flow cytometry analysis of IFNAR1 surface expression**

IFNAR1 surface expression on unstimulated cell lines was measured by flow cytometry. Cells were collected in eppendorf tubes, washed once in cold FACS buffer (PBS with 2% FBS and 0.02% sodium azide), then stained for 30 min with mouse anti-IFNAR1 4G8 antibody (Sigma) or purified mouse IgG2a K isotype control (BioLegend). Cells were washed twice with FACS buffer then incubated for 30 min with rat anti-mouse IgK light chain APC-Cy7 secondary antibody (BD Biosciences). Cells were washed twice with cold FACS buffer then stained with 0.05 µg/ml DAPI (ThermoFisher) for 10 min. Cells were washed three times in DPBS then resuspended in FACS buffer. Data were acquired on a Canto RUO cytometer (BD Biosciences) and analyzed using FlowJo software (FlowJo LLC).

**Bulk RNA sequencing**

*Cell stimulation and RNA extraction*

Jurkat and JLat9.2 cells were treated with cell culture media for 4h (mock) or 100 IU/ml IFNβ for 4, 8, or 12h as described in figure legends. Cells were digested in RLT buffer then RNA extracted using a miRNeasy Micro kit (Qiagen) as described above. The quality and concentration of the recovered RNA was determined using a LabChip GXII (PerkinElmer) instrument and a ribogreen-based RNA assay, respectively.

*Sequencing and data analysis*

mRNA-seq libraries were constructed using KAPA Stranded mRNA-Seq Kit (Roche, Indianapolis, IN) following the manufacturer's recommended protocol. Libraries were sequenced on an Illumina NextSeq500 sequencer using Illumina NextSeq 500/550 High Output v2 kits (150 cycles) following the manufacturer's protocol for sample handling and loading.

Sequencing run metrics were visualized for quality assurance using Illumina's BaseSpace platform, and the quality of mRNA-seq reads were assessed using FastQC version 0.11.3 (http://www.bioinformatics.babraham.ac.uk/projects/fastqc). Adapters were digitally removed using cutadapt, version 1.8.3 (Martin 2011). Subsequently, raw RNA-seq reads were demultiplexed, checked for quality with FastQC v0.11.5 (Andrews 2010), and ribosomal RNA reads were digitally removed with bowtie2 v2.3.4 (Langmead and Salzberg 2012). Reads were then mapped to the human genome (GRCh37) with STAR v2.4.0h1 (Dobin et al. 2013), resulting in at least 20 million uniquely mapped reads per sample. Gene counts were quantified with htseq-count v 0.6.1p1 (Anders, Pyl, and Huber 2015) specifying –stranded=reverse and --mode=intersection-nonempty. Gene counts were loaded into the R statistical programming language (v4.0.0, R Core Team 2020) using RStudio v1.2.1335. I first removed genes with less than 10 raw counts averaged across all samples leaving 13,849 genes for analyses. Counts were then normalized via trimmed mean of M values implemented in edgeR and transformed into log2 counts per million with the voom function of the limma package (Law et al. 2014; Ritchie et al. 2015). Samples then underwent principal component analysis and results were visualized with ggplot2 v3.3.2 (Wickham 2011). All differential expression analyses were performed with limma. To assess functional differences between Jurkat and JLat9.2 mock samples, we performed gene set enrichment analysis (GSEA) using WebGestaltR (Liao et al. 2019). Genes were ranked by descending t-statistic values calculated in limma and were tested for enrichment among KEGG pathways and the non-redundant Gene Ontology database. I designed contrast matrices to test for the effect of IFNβ treatment in each cell line over time relative to mock (e.g. Jurkat IFNβ 4h –

Jurkat Mock 4h) and to directly compare cell lines while accounting for baseline differences (e.g. [(Jurkat IFNβ 4h – Jurkat Mock 4h) – (JLat9.2 IFNβ 4h – JLat9.2 Mock 4h)]). A gene was considered differentially expressed if the absolute Fold Change > 1.5 and Benjamini-Hochberg-adjusted p-value < 0.05 in at least one comparison (Benjamini and Hochberg 1995). The union of all differentially expressed genes were grouped into co-expression modules (ward.D clustering, Euclidean distance) with WGCNA (Langfelder and Horvath 2008; Langfelder, Zhang, and Horvath 2008) and gplots heatmap.2. These modules were uploaded into Ingenuity Pathway Analysis software (Kramer et al. 2014) to assess pathway enrichment and upstream regulators among co-expressed genes.

**RGH virus infection studies**

*Virus stock preparation and titer*

The Red-Green-HIV-1 (RGH) virus and ΔINT control virus were generated from the following viral molecular clones obtained from the NIH AIDS Reagent Program: pRGH-WT and pRGH-Integrase D116A (ΔINT). The RGH virus stably expresses mCherry under the control of a CMV promoter, and conditionally expresses GFP under the control of the HIV-1 LTR promoter upon productive HIV-1 replication (Dahabieh et al. 2013). Vesicular stomatitis virus G (VSV-G) pseudotyped stocks were generated by transfecting HEK293T cells with viral molecular clones and pHEF-VSVg in a 10:1 ratio using the Fugene HD Transfection Reagent according to manufacturer's instructions. Cell supernatant containing virus was collected at 48h post infection and virus titer determined on TZM-bl cells.

*RGH spinfection and flow sort*

Jurkat cells were seeded at a concentration of 5 x $10^5$ cells in 6 well plates in complete RPMI supplemented with 4 μg/ml polybrene, and spinoculated with HEK-293T conditioned media (mock) or VSV-pseudotyped RGH viral stocks (MOI 0.2) for 1.5h at 500xG. Cells were cultured

for 24h, washed twice with DPBS, then cultured in complete RPMI for an additional 4 days to allow establishment of latency. Infected cells were washed in FACS buffer (DPBS + 2% FBS + 0.02% sodium azide), stained with 0.05 µg/ml DAPI (ThermoFisher) to identify dead cells, and viably sorted based on mCherry and GFP expression on a FACSAria II cytometer (BD Biosciences). Sorted cells were resuspended in complete RPMI, seeded at 3 x $10^5$ cells/ml in 0.5ml in 12-well plates, cultured overnight, then stimulated for 8h with 100 IU/ml IFNβ or reactivated for 24h with 10 nM PMA and 1 µM ionomycin.

**NanoLuc HIV-1 preparation, infection, and ART suppression**

*Generation of replication competent NanoLuc-expressing HIV-1 molecular clone*

We generated the HIV-1 infectious molecular clone (IMC) vNL-sNLuc.6ATRi-B-Bal.Ecto, a secreted nanoluciferase (sNLuc) reporter virus (hereafter referred to as "NanoLuc HIV-1"), which expresses the Env ectodomain of HIV-$1_{BaL}$ within the NL4-3-derived proviral backbone, based on our previously described HIV-1 proviral constructs encoding either the sNLuc.T2A or LucR.6ATRi reporter cassettes (Astronomo et al. 2016; Alberti et al. 2015). The T2A “ribosomal skip peptide” was replaced with the modified encephalomyocarditis virus (EMCV) 6ATR internal ribosome entry site (IRES) element (6ATRi), which enables physiological Nef expression and function (Alberti et al. 2015; Cavrois et al. 2017; Prévost et al. 2018; Ventura et al. 2019). I replaced the LucR reporter with secreted NanoLuc® (Astronomo et al. 2016), inserting sNLuc ORF upstream of 6ATRi. Upon replication, the sNLuc reporter is secreted into the culture supernatant, facilitating kinetic monitoring of infection (Astronomo et al. 2016). The reporter IMC is replication competent and encodes all the viral open reading frames, allowing for multiple rounds of viral replication.

*Plasmid description*

The ectodomain of Env BaL (Genbank accession number: AY426110.1) derives from the HIV-1 isolate BaL. In the previously described reporter IMC, pNL-LucR.6ATRi-B.BaL.ecto (Alberti et al. 2015), the Renilla luciferase gene (LucR) was replaced by InFusion® (Takara Bio) cloning methods with the soluble nanoluciferase-expressing sNLuc gene. Fusion of the NLuc gene to an N-terminal secretion signal generates a secreted, 19.1 kDa, form of the NanoLuc® luciferase, secNLuc (Promega, under limited use label license). In the current IMC, the sNLuc IRES cassette was inserted between the NL4-3 env and nef genes. The sNLuc ORF is located downstream of the stop codon (taa) of env and a Kozak sequence (ccacc); it is followed by a 26 nt "spacer", the IRES element and the nef gene. The IRES I used is derived from encephalomyocarditis virus (EMCV) (GenBank: EMCV IRES, NC_001479), contains the "wild type" $(A)_6$ ("6A") bifurcation loop, and encompasses a truncated EMCV IRES fragment ("TR", nucleotides 399 to 833). The proviral plasmid was generated and provided by Dr. Christina Ochsenbauer (University of Alabama at Birmingham, Department of Medicine).

*Virus stock preparation and titer*

The NanoLuc HIV-1 viral stock was generated by Dr. Rena Astronomo and collaborators at the Vaccine Infectious Disease Division, Fred Hutchinson Cancer Research Center (Seattle, WA). The methods and reagents used for the generation of virus stock and calculation of virus infectivity were described previously (Astronomo et al. 2016). In brief, the vNL-sNLuc.6ATRi-B.Bal.Ecto reporter virus was generated by transfection of proviral DNA into 293T/17 cells (ATCC) using Lipofectamine 2000 according to the manufacturer's protocol (Thermo-Fisher). Viral supernatants were harvested 60h post-transfection, clarified at 1200×g for 10 min, and frozen at −70°C. Virus stocks were analyzed for nanoluciferase expression using Nano-glo luciferase (Promega) and were titered on sub-confluent TZM-bl cells (NIH ARP). Virus was diluted in DMEM supplemented with 1% FBS and 40 μg/ml DEAE-Dextran and added to cells for 4h. Growth

medium (DMEM, 10% FBS, Pen/Strep, glutamine) was added to the cells and incubated for 48 hours. Cell monolayers were fixed (0.8% glutaraldehyde, 2.2% Formaldehyde in DPBS) for 8 minutes and stained for β-galactosidase expression (4 mM potassium ferricyanide, 4mM potassium ferrocyanide, 400 µg/ml magnesium chloride, 400 µg/ml X-gal in DPBS) for 2 hours. Titer (2.5 x $10^7$ PFU/ml) was calculated by counting "Blue" β-gal expressing cells.

*NanoLuc HIV-1 infection and ART suppression of CD4+ T cells*

Purified CD4+ T cells were thawed and cultured at $10^6$ cells/ml for 5 days in complete RPMI media supplemented with cytokines that aid in homeostatic proliferation and HIV-1 susceptibility: 20 U/ml IL-2, 10 ng/ml IL-7, and 50 ng/ml recombinant human IL-15 (all from Peprotech). CD4+ T cells were then seeded at a concentration of 2 x $10^6$ cells/ml in 6-well plates and were spinoculated with complete RPMI media (mock control) or NanoLuc HIV-1 (MOI 1.0 or 2.0, see figure legends) for 2h at 2400 rpm. Cells were washed three times with RPMI and cultured in T25 flasks for 24h in complete RPMI supplemented 20 U/ml IL-2, 10 ng/ml IL-7, and 50 ng/ml IL-15. HIV-1 replication was then suppressed for 7 days by treatment with ART consisting of 10 µM Raltegravir (NIH AIDS Reagent Program) and 1 µM Efavirenz (NIH AIDS Reagent Program). During the week of ART suppression, cells were washed and resuspended in fresh medium, cytokines, and ART every two days. Aliquots of supernatants were withdrawn and frozen throughout the ART time course to monitor ART suppression. To determine percent of infected cells, genomic DNA was isolated from cells before ART (24h post infection) and after ART (8 days post infection), and number of HIV-1 copies/cell measured by ddPCR (Table 1). At 8 days post infection (dpi), suppressed cells were seeded in 12-well plates at 5 x $10^5$ cells/ml in complete RPMI + cytokines +/- ART, and were treated with or without 100 IU/ml IFNβ. At 8h following IFNβ treatment, cells were fixed in methanol for single cell sequencing analysis, or lysates collected for qRT-PCR or Immunoblot analysis. For reactivation studies at 8 dpi, suppressed cells were seeded

in 12-well plates at 5 x $10^5$ cells/ml in complete RPMI + cytokines +/- ART, and were treated for 24h with 10 nM PMA and 1 µM ionomycin, then lysates collected for qRT-PCR analysis.

**Luciferase Reporter Assay**

Supernatant samples were brought to room temperature and an aliquot of 20 µl of each sample was mixed with 20 µl of 1X Nano-Glo® luciferase assay reagent (Nano-Glo® Luciferase Assay System, Promega) in a white flat-bottom polystyrene 96-well plate (Corning, Sigma-Aldrich). The mixtures were incubated for 10 min in the dark and luminescence was read on an MLX 96 well Plate Luminometer (1 sec/well, read height: 1 mm, Dynex Technologies) and reported in relative light units (RLU).

**Droplet digital PCR (ddPCR) analysis of HIV-1 proviral DNA**

To quantify the number of HIV-1 genomes per infected cell, I used a droplet digital PCR (ddPCR) assay detecting the HIV-1 gag gene. Genomic DNA was purified from frozen cellular pellets using PureLinkTM Genomic DNA Mini Kit (Thermo Fisher Scientific), following manufacturer's instructions. The concentration of DNA of each sample was determined using NanoDrop™ One-W (Thermo Scientific). Five µl of undiluted and/or 1:10 diluted gDNA were used per reaction. To normalize for total genomic DNA and estimate the number of cells per reaction, I quantified copy numbers of the cellular peptidylprolyl isomerase A (PPIA) gene using a specific FAM-conjugated primers/probe assay (cyclophilin A; assay ID: Hs.571 PT.58v.38887593.g; FAM/ZEN/3IABkFQ configuration). For the amplification of the HIV-1 gag region, I used the following primers and probe: Gag sense 5'GACTAGCGGAGGCTAGAAGGAGAGA 3'; Gag antisense 5' CTAATTCTCCCCCGCTTAATAYTGACG 3'; Gag probe 5' HEX AT+G+GGT+GC+GAGA/3BHQ_1 3', wherein "+" indicates locked nucleic acids and BHQ denotes 3' Black quencher©-1 (Levy et al. 2021).

The ddPCR reaction was done in a total volume of 22 µl of a mixture containing 11 µl of 2X ddPCR Supermix for Probes (BioRad), 1.1 µl 20X hexachlorofluorescein (HEX) HIV-1 gag specific Taqman assay (Integrated DNA Technologies), 1.1 µl of 20X 6-carboxyfluorescein (FAM)-labeled PPIA target qPCR assay and genomic DNA. Each assembled ddPCR reaction mixture was loaded in duplicate into the sample wells of an eight-channel disposable droplet generator cartridge (BioRad) and droplet generation oil (BioRad) was added. After droplet generation, the samples were amplified to the endpoint in 96-well PCR plates on a conventional thermal cycler (C1000, Biorad) using the following conditions: denaturation/enzyme activation for 10 min at 95°C, 40 cycles of 30s denaturation at 94°C and 60 s annealing/amplification at 60°C, followed by a final 10 min incubation step at 98°C. After PCR, the droplets were read on the QX100 Droplet Reader (BioRad). Analysis of the ddPCR data was performed with QuantaSoft analysis software version 1.3.1.0 (BioRad). A non-template control well containing ddPCR reaction mix but no cDNA and a mock-infected control were included to adjust the reaction threshold.

**Single cell RNA-sequencing (scRNA-seq)**

*Cell preparation*

Purified CD4+ T cells were thawed, activated with cytokines, infected with NanoLuc HIV-1, suppressed with ART for 7 days, then stimulated with 100 IU/ml IFNβ for 8h as described above. At 8 hours post IFNβ stimulation, cells were washed twice with cold PBS then viability assessed by Trypan Blue exclusion. Viable cell suspension was adjusted to 5 x 106 cells/ml in 200 µl cold PBS, then 800 µl cold methanol slowly added. Methanol-fixed cells were stored at -20°C until further sample processing. After two weeks, fixed cells were thawed, centrifuged and supernatant removed, then resuspended in rehydration buffer (SSC buffer supplemented with 1% BSA, 20 U/µl Superasein, and 1 M DTT). Single-cell suspensions were diluted to a cell concentration of 1,000 cells/µl for single-cell RNAseq.

*Library preparation and sequencing*

Single-cell RNA sequencing was performed according to the manufacturer's instructions (10x Genomics). Single-cell suspensions were loaded onto a Chromium Single Cell Chip G at a target capture rate of ~8000 individual cells per sample. Barcoded, full-length cDNAs from poly-adenylated mRNAs were produced following reverse transcription of the resulting Gel Beads-in-emulsion (GEMs). All samples for a given donor were processed simultaneously with the Chromium Controller (10x Genomics) to create purified cDNA. Indexed libraries were prepared from 10 µl of cDNA using Chromium Next GEM Single Cell 3' Reagent Kits v3 (10x Genomics). Library and cDNA quality were evaluated using the Agilent 2100 Bioanalyzer Instrument (Agilent) and quantified using the ViiA 7 Real-Time PCR system (ThermoFisher). Constructed libraries were sequenced on an Illumina NextSeq 500/550 High Output v2 kit (Illumina). Each sample was sequenced to a depth of 40,000 reads per cell.

*Data processing and analysis*

Single cell reads were aligned to the hg19 genome with CellRanger v4.0.0 (Zheng et al. 2017). In the hg19 genome I integrated the HIV-1 vector PNL4-3 (GenBank AF324493.2) and only counted reads that map to the HIV-1 region of the vector. I used Seurat 3.2.3 to normalize, perform dimensionality reduction (UMAPs), and identify differentially expressed genes (Butler et al. 2018). Using Seurat I filtered out cells from the analysis that had less than 200 or greater than 2,500 genes detected and a mitochondrial DNA percentage greater than 10%. Cells were classified as HIV+ if they had at least one read mapping to the HIV-1 genome (one UMI count). Differential gene analyses were performed through Seurat using MAST (Finak et al. 2015; Trapnell et al. 2014) and significant differentially expressed genes had an absolute log fold change of ≧ 1.2 and an adjusted P value of less than 0.05. Over-representation analysis using non-redundant biological process gene-ontology terms on viral induced genes (Fig. 6C) was

performed using the tool web-based Gene Set Analysis Toolkit (http://www.lbgestalt.org). Cells were classified into T cell subtypes using Monocle3/Garnett (Pliner, Shendure, and Trapnell 2019) using the markers listed in Fig. S7B. Code for this analysis is available at: https://github.com/galelab/Olson_Latent_HIV_Infection.

**Quantification and Statistical Analysis**

For qRT-PCR analyses and protein abundance quantification, statistical tests were performed using Prism 8.0 software (GraphPad). Data are presented as the values ± standard deviation (SD). Statistical significance was determined using a two-tailed Student's t test with multiple comparisons (Holm-Sidak post-test) or by two-way ANOVA with multiple comparisons (Holm-Sidak post-test) as indicated in figure legends. For these tests, $p < 0.05$ was considered statistically significant. *$p < 0.05$, **$p < 0.01$, ***$p < 0.001$. For bulk RNA-seq and scRNA-seq analysis, statistical analysis was performed using RStudio v1.2.1335 (R Core Team) as described in corresponding methods sections. In this study, n is defined as the number of independent, non-technical biological replicates within a single representative experiment, or as the number of independent experiments included in a data set, as detailed in figure legends.

**Data and Code Availability**

Transcriptomic data sets are available through the Gene Expression Omnibus (https://www.ncbi.nlm.nih.gov/geo/) under access numbers GSE174380 (bulk RNA sequencing) and GSE176386 (single cell RNA sequencing). Code for the single cell RNA sequencing analysis is available at: https://github.com/galelab/Olson_Latent_HIV_Infection.

**Research funding**

Research reported in this publication was supported by the National Institutes of Health grants R01AI127563, R01AI118916, and P51 OD010425 (Michael Gale, Jr.), and under the Ruth

L. Kirschstein National Research Service Award grant T32 AI07140 (Rebecca Olson). This work was also supported by the National Center For Advancing Translational Sciences of the National Institutes of Health under Award Number KL2 TR002317 (Germán Gornalusse). The content is solely the responsibility of the authors and does not necessarily represent the official views of the National Institutes of Health.

# LIST OF ABBREVIATIONS

ART: Antiretroviral therapy

CMV: Cytomegalovirus

ddPCR: Droplet digital PCR

DE: Differential expression

DDE: Differential of differential expression

DMSO: Dimethyl sulfoxide

EMCV: Encephalomyocarditis virus

FC: Fold change

GFP: Green fluorescent protein

GO: Gene ontology

HCV: Hepatitis C virus

HDAC: Histone deacetylase

HIV-1: Human immunodeficiency virus 1

IFN: Interferon

IFNα: Interferon alpha

IFNβ: Interferon beta

IFNγ: Interferon gamma

IFNAR1: Interferon alpha/beta receptor 1

IRES: Internal ribosome entry site

IRF3: Interferon regulatory factor 3

ISG: Interferon-stimulated gene

NanoLuc HIV-1: Nanoluciferase-expressing reporter HIV-1

NF-κB: Nuclear Factor kappa-light-chain-enhancer of activated B cells

P/I: PMA + ionomycin

PAMP: Pathogen-associated molecular pattern

PBMC: Peripheral blood mononuclear cells

PCA: Principal component analysis

PMA: Phorbol 12-myristate 13-acetate

PRR: Pathogen recognition receptor

RIG-I: Retinoic acid inducible gene I

RGH: Red Green HIV-1

RNA-seq: RNA sequencing

scRNA-seq: Single cell RNA sequencing

SeV: Sendai virus

SIV: Simian immunodeficiency virus

TNFα: Tumor necrosis factor alpha

UMAP: Uniform manifold approximation and projection

vRNA: Viral RNA

# APPENDIX

**Table 5. RNA-seq identification of DE genes in IFNβ-treated Jurkat or JLat9.2 cells**

| | Log2 Fold Change (IFNβ - mock) | | | | | | Adjusted p Value (Benjamini-Hochberg FDR corrected) | | | | | |
|---|---|---|---|---|---|---|---|---|---|---|---|---|
| | Jurkat | | | JLat9.2 | | | Jurkat | | | JLat9.2 | | |
| GENE | 4h | 8h | 12h | 4h | 8h | 12h | 4h | 8h | 12h | 4h | 8h | 12h |
| ABCA1 | -0.5780 | 0.3390 | 0.0510 | -0.0050 | -0.2160 | 1.0210 | 0.3894 | 0.7434 | 0.9671 | 0.9980 | 0.6813 | 0.0111 |
| ABCA5 | -0.1410 | -0.0780 | -0.0390 | -0.1600 | -0.6190 | -0.1590 | 0.6922 | 0.9110 | 0.9425 | 0.7305 | 0.0028 | 0.4801 |
| ABCG1 | 0.0380 | 0.0780 | 0.1740 | 0.0710 | 0.4180 | 0.6250 | 0.7810 | 0.6769 | 0.1225 | 0.7202 | 0.0000 | 0.0000 |
| ABLIM2 | 0.4970 | 0.7240 | 0.1850 | 0.6080 | 0.8730 | 0.2230 | 0.3427 | 0.1719 | 0.8409 | 0.4649 | 0.0202 | 0.6744 |
| ABTB2 | -0.1630 | -0.5360 | -0.3350 | 0.1650 | -0.4050 | -0.7250 | 0.6472 | 0.1145 | 0.4017 | 0.8286 | 0.2102 | 0.0365 |
| ACAT2 | 0.0090 | 0.2600 | 0.4120 | 0.0130 | 0.3460 | 0.6210 | 0.9089 | 0.0000 | 0.0000 | 0.9323 | 0.0000 | 0.0000 |
| ACOT11 | -0.0340 | 0.0800 | 0.1800 | 0.0780 | -0.1250 | -0.5800 | 0.9433 | 0.9145 | 0.7019 | 0.9047 | 0.6248 | 0.0231 |
| ACSBG1 | 2.0600 | 2.7090 | 1.9300 | 1.4190 | 4.2630 | 3.6810 | 0.0166 | 0.0001 | 0.0225 | 0.4798 | 0.0000 | 0.0000 |
| ACSS2 | 0.0720 | 0.0660 | 0.2800 | -0.1600 | 0.4700 | 0.6720 | 0.8761 | 0.9371 | 0.5286 | 0.7605 | 0.0124 | 0.0005 |
| ADAR | 0.6700 | 0.9580 | 0.7160 | 0.4920 | 0.8160 | 0.6660 | 0.0000 | 0.0000 | 0.0000 | 0.0000 | 0.0000 | 0.0000 |
| ADC | -0.1950 | -0.2030 | -0.0660 | 0.0690 | 0.1110 | 0.6120 | 0.6268 | 0.7555 | 0.9153 | 0.9295 | 0.7112 | 0.0127 |
| ADSSL1 | 0.2180 | -0.7880 | 0.0200 | 0.6230 | 0.9940 | 0.5570 | 0.8235 | 0.5336 | 0.9887 | 0.5752 | 0.0373 | 0.3318 |
| AFAP1L2 | -0.1470 | 0.0470 | 0.1640 | 0.2450 | 0.4250 | 0.5880 | 0.7070 | 0.9542 | 0.7330 | 0.6180 | 0.0408 | 0.0056 |
| AGBL2 | -0.1640 | 0.3110 | 0.5030 | 0.2530 | 0.7390 | 0.4940 | 0.7122 | 0.5400 | 0.1546 | 0.7488 | 0.0122 | 0.1343 |
| AK7 | 0.1640 | -0.3170 | -0.1080 | 0.0490 | 0.3760 | 0.8410 | 0.8108 | 0.7703 | 0.9117 | 0.9650 | 0.2585 | 0.0070 |
| ALDOC | 0.0870 | 0.0390 | 0.1020 | 0.0940 | 0.7000 | 0.7590 | 0.6430 | 0.9215 | 0.6701 | 0.8188 | 0.0000 | 0.0000 |
| ALPK1 | 0.3940 | 0.5450 | 0.3780 | -0.0100 | 0.3120 | 0.6430 | 0.3411 | 0.2140 | 0.4694 | 0.9920 | 0.2366 | 0.0107 |
| AMOTL2 | 1.8300 | 1.5840 | 0.6030 | 1.6590 | 1.6380 | 0.4980 | 0.0000 | 0.0000 | 0.2109 | 0.0245 | 0.0025 | 0.4919 |
| AMT | 0.3620 | 0.1870 | 0.2370 | 0.1320 | 0.6020 | 0.4680 | 0.2872 | 0.7746 | 0.6234 | 0.8485 | 0.0093 | 0.0626 |
| ANKRD18A | -0.1960 | -0.1810 | -0.0120 | -0.2970 | -0.7150 | -0.4720 | 0.5122 | 0.7032 | 0.9828 | 0.3739 | 0.0001 | 0.0064 |
| ANKRD20B | 0.0550 | -0.0400 | 0.2150 | -0.2840 | -0.8780 | -0.5330 | 0.9352 | 0.9793 | 0.7689 | 0.7313 | 0.0171 | 0.1612 |
| ANKRD9 | 0.3410 | 0.3940 | 0.6040 | 0.0110 | 0.9040 | -0.0670 | 0.6472 | 0.7349 | 0.4566 | 0.9952 | 0.0180 | 0.9164 |
| APOL1 | 1.4920 | 1.5540 | 0.9080 | 0.8980 | 1.3160 | 0.6920 | 0.0000 | 0.0000 | 0.0000 | 0.2247 | 0.0007 | 0.1138 |
| APOL2 | 0.6570 | 0.5300 | 0.0910 | 0.3350 | 0.3520 | 0.1230 | 0.0000 | 0.0000 | 0.3537 | 0.0000 | 0.0000 | 0.0755 |
| APOL6 | 1.2790 | 1.2880 | 0.6710 | 0.9740 | 1.0160 | 0.7770 | 0.0000 | 0.0000 | 0.0000 | 0.0000 | 0.0000 | 0.0000 |
| APOLD1 | -0.0760 | -0.0610 | -0.0740 | 0.2710 | 0.5550 | 0.7380 | 0.8325 | 0.9264 | 0.8789 | 0.5726 | 0.0064 | 0.0004 |
| ATG16L2 | 0.0390 | -0.0200 | 0.1140 | 0.2710 | 0.6230 | 0.5610 | 0.8488 | 0.9596 | 0.5890 | 0.4439 | 0.0001 | 0.0006 |
| ATHL1 | 0.1810 | 0.4000 | 0.4120 | 0.3630 | 0.6190 | 0.3840 | 0.1900 | 0.0002 | 0.0002 | 0.0115 | 0.0000 | 0.0007 |
| ATP10A | 1.5830 | 2.3680 | 1.6790 | 0.4090 | 0.8310 | 0.6250 | 0.0000 | 0.0000 | 0.0000 | 0.0017 | 0.0000 | 0.0000 |
| ATP10D | 0.4360 | -0.0470 | 0.4100 | 1.8710 | 2.1290 | 1.2940 | 0.6286 | 0.9855 | 0.7404 | 0.2187 | 0.0081 | 0.1646 |
| B4GALNT4 | 0.2320 | 0.1760 | 0.3930 | 0.2160 | 0.5940 | 0.3010 | 0.2635 | 0.5747 | 0.0340 | 0.7161 | 0.0090 | 0.2589 |
| BBC3 | 0.0450 | 0.3390 | 0.3030 | -0.0310 | 0.8030 | 0.7340 | 0.9326 | 0.5106 | 0.5284 | 0.9815 | 0.0087 | 0.0240 |
| BHLHE23 | -0.1270 | -0.0480 | 0.2630 | -0.1520 | 0.9790 | 0.4830 | 0.7992 | 0.9629 | 0.6173 | 0.9242 | 0.0310 | 0.3875 |
| BRUNOL6 | 0.1290 | 0.0800 | 0.4040 | -0.1440 | -0.7730 | -0.5110 | 0.8422 | 0.9494 | 0.5248 | 0.8692 | 0.0223 | 0.1478 |
| BST2 | 1.4330 | 2.4810 | 2.3230 | 1.0320 | 2.2420 | 2.2690 | 0.0000 | 0.0000 | 0.0000 | 0.0000 | 0.0000 | 0.0000 |
| C10orf75 | -0.0930 | -0.0300 | 0.2550 | 0.2290 | 0.8880 | 1.4920 | 0.8276 | 0.9758 | 0.5418 | 0.6821 | 0.0001 | 0.0000 |
| C11orf66 | 0.3570 | -0.0920 | 0.3830 | 0.6660 | 0.8550 | 0.6080 | 0.5171 | 0.9458 | 0.5815 | 0.4018 | 0.0192 | 0.1356 |
| C11orf71 | -0.0090 | -0.2550 | -0.1260 | 0.3120 | 0.2120 | 0.9780 | 0.9814 | 0.5344 | 0.7689 | 0.6488 | 0.5180 | 0.0004 |
| C12orf76 | -0.2080 | 0.0660 | -0.0520 | 0.1370 | 0.3210 | 0.6180 | 0.4468 | 0.9087 | 0.9076 | 0.8220 | 0.1565 | 0.0053 |
| C14orf128 | 0.2660 | 0.0950 | 0.1930 | -0.1240 | 0.0330 | 0.8240 | 0.7395 | 0.9561 | 0.8685 | 0.9244 | 0.9521 | 0.0374 |
| C14orf39 | -0.1620 | -0.0870 | -0.1040 | -0.0710 | -0.0490 | 0.6960 | 0.6305 | 0.8946 | 0.8377 | 0.9350 | 0.8918 | 0.0072 |
| C14orf83 | 0.6810 | 0.7870 | 0.4260 | 0.3600 | 0.3780 | 0.2370 | 0.0000 | 0.0000 | 0.0000 | 0.0101 | 0.0005 | 0.0386 |
| C16orf75 | 0.1970 | 0.3980 | 0.2920 | 0.1400 | 0.6410 | 0.7000 | 0.2270 | 0.0019 | 0.0540 | 0.6584 | 0.0000 | 0.0000 |
| C17orf103 | -0.0400 | 0.1050 | 0.1480 | 0.2210 | 0.5440 | 0.7000 | 0.9277 | 0.8815 | 0.7631 | 0.4493 | 0.0000 | 0.0000 |
| C17orf89 | 0.4830 | -0.1470 | 0.5270 | 0.3020 | 0.7380 | -0.3600 | 0.2599 | 0.8905 | 0.2748 | 0.7045 | 0.0171 | 0.4001 |
| C17orf90 | 0.0390 | -0.0050 | 0.0620 | 0.2800 | 0.7210 | 0.7050 | 0.8793 | 0.9945 | 0.8546 | 0.4303 | 0.0000 | 0.0000 |
| C19orf23 | -0.1600 | 0.0720 | -0.3370 | -0.0340 | -0.4630 | -0.8130 | 0.7018 | 0.9280 | 0.4732 | 0.9723 | 0.1168 | 0.0124 |
| C19orf66 | 1.1760 | 1.7530 | 1.3110 | 0.9220 | 1.4580 | 1.1420 | 0.0000 | 0.0000 | 0.0000 | 0.0000 | 0.0000 | 0.0000 |
| C1RL | -0.1830 | -0.0380 | 0.1280 | 0.2050 | 0.5460 | 0.7080 | 0.7387 | 0.9778 | 0.8673 | 0.5604 | 0.0003 | 0.0000 |
| C1orf213 | 0.0420 | 0.1040 | 0.3680 | 0.5070 | 0.6990 | 0.7380 | 0.9141 | 0.8632 | 0.2258 | 0.3316 | 0.0048 | 0.0040 |
| C21orf119 | 0.0060 | 0.0370 | 0.1940 | 0.4250 | 0.8740 | 0.8090 | 0.9909 | 0.9724 | 0.7260 | 0.4798 | 0.0010 | 0.0033 |
| C22orf24 | 0.1390 | 0.0580 | 0.0510 | -0.4780 | -1.6660 | -2.1120 | 0.9221 | 0.9855 | 0.9814 | 0.8188 | 0.0731 | 0.0303 |
| C2orf27A | -1.0500 | -0.1800 | -0.6200 | -0.4110 | -0.1680 | 0.0260 | 0.0265 | 0.8476 | 0.2436 | 0.5299 | 0.6106 | 0.9508 |
| C2orf52 | 0.0580 | 0.3530 | 0.2570 | 0.3560 | 0.5880 | 1.0560 | 0.9386 | 0.6727 | 0.7423 | 0.7513 | 0.1931 | 0.0146 |
| C3AR1 | 1.1730 | 1.3980 | 1.7390 | 0.3340 | 0.1560 | 0.0790 | 0.1498 | 0.0710 | 0.0102 | 0.7624 | 0.7782 | 0.9032 |
| C4orf48 | 0.8100 | 0.3650 | 1.0670 | 0.8630 | 1.3790 | -0.0670 | 0.2701 | 0.8062 | 0.1477 | 0.4452 | 0.0050 | 0.9388 |
| C5orf41 | 0.2970 | 0.4310 | 0.3810 | 0.2860 | 0.5810 | 0.8130 | 0.2654 | 0.0920 | 0.1684 | 0.4560 | 0.0008 | 0.0000 |
| C5orf56 | 0.4060 | 0.4870 | 0.5020 | 0.6530 | 0.4560 | 0.4430 | 0.0116 | 0.0005 | 0.0005 | 0.0057 | 0.0164 | 0.0278 |
| C6orf223 | 0.1520 | 0.4970 | 0.7610 | -0.1260 | 0.8920 | 1.0360 | 0.2572 | 0.0000 | 0.0000 | 0.6217 | 0.0000 | 0.0000 |
| C8orf85 | -0.2650 | 0.0270 | 0.3730 | -0.1400 | 0.6460 | 0.5360 | 0.6033 | 0.9836 | 0.4891 | 0.8943 | 0.0422 | 0.1226 |
| C9orf147 | -0.6900 | 0.0990 | 0.0040 | 0.6460 | 1.1440 | 0.0930 | 0.2655 | 0.9410 | 0.9966 | 0.5172 | 0.0084 | 0.8940 |
| CAPN2 | 2.4520 | 4.4350 | 3.9910 | 1.8790 | 3.4010 | 3.2740 | 0.0000 | 0.0000 | 0.0000 | 0.0383 | 0.0000 | 0.0000 |
| CAPS | 0.4280 | 0.4170 | 0.5520 | 0.2950 | 0.7450 | 0.4670 | 0.3380 | 0.5016 | 0.2573 | 0.7016 | 0.0124 | 0.1665 |
| CCDC135 | 0.2350 | 0.1490 | -0.0240 | 0.7830 | 1.3590 | 1.1200 | 0.7999 | 0.9348 | 0.9872 | 0.5962 | 0.0278 | 0.0979 |
| CCDC151 | 0.4420 | 0.3460 | 0.5970 | 0.7850 | 1.4730 | 1.0060 | 0.5774 | 0.8062 | 0.5227 | 0.5942 | 0.0150 | 0.1410 |
| CCNG2 | -0.2240 | 0.1450 | 0.0820 | -0.0090 | 0.2360 | 0.6180 | 0.1665 | 0.5073 | 0.7300 | 0.9822 | 0.0231 | 0.0000 |
| CCR8 | -0.1350 | 0.1770 | 0.1470 | -0.0630 | 0.3660 | 0.7560 | 0.7889 | 0.8147 | 0.8225 | 0.9506 | 0.2426 | 0.0112 |
| CD244 | -0.0130 | -0.3080 | -0.1540 | -0.1370 | -0.4380 | -0.6290 | 0.9724 | 0.3780 | 0.6976 | 0.7768 | 0.0307 | 0.0045 |
| CD274 | 1.3720 | 0.6040 | 0.5110 | 0.5870 | 0.3570 | 0.3910 | 0.0293 | 0.5881 | 0.6218 | 0.7100 | 0.6424 | 0.6427 |
| CD38 | 0.1710 | 0.8360 | 0.7310 | 0.1570 | 0.4260 | 0.6040 | 0.4540 | 0.0000 | 0.0000 | 0.7478 | 0.0215 | 0.0014 |
| CD48 | 0.5240 | 0.7830 | 0.5370 | 0.4480 | 0.9680 | 0.9920 | 0.0000 | 0.0000 | 0.0000 | 0.0000 | 0.0000 | 0.0000 |
| CD58 | -0.3130 | -0.1870 | -0.1680 | -0.1920 | -0.6200 | -0.2960 | 0.2085 | 0.6305 | 0.6218 | 0.6662 | 0.0026 | 0.1550 |

**Table 5. RNA-seq identification of DE genes in IFNβ-treated Jurkat or JLat9.2 cells** - *Page 2*

| | Log2 Fold Change (IFNβ - mock) | | | | | | Adjusted p Value (Benjamini-Hochberg FDR corrected) | | | | | |
|---|---|---|---|---|---|---|---|---|---|---|---|---|
| | Jurkat | | | JLat9.2 | | | Jurkat | | | JLat9.2 | | |
| GENE | 4h | 8h | 12h | 4h | 8h | 12h | 4h | 8h | 12h | 4h | 8h | 12h |
| CD68 | 0.5990 | 1.1770 | 0.9700 | 0.7010 | 1.0690 | 0.9160 | 0.0414 | 0.0000 | 0.0000 | 0.1218 | 0.0001 | 0.0009 |
| CD93 | -0.3040 | -0.3730 | -0.5570 | -0.4510 | -0.6150 | -1.2970 | 0.3687 | 0.3773 | 0.1121 | 0.6456 | 0.1585 | 0.0093 |
| CDH23 | -0.0300 | 0.0930 | 0.0090 | 1.7850 | 2.2750 | 2.1140 | 0.9723 | 0.9506 | 0.9937 | 0.3177 | 0.0074 | 0.0190 |
| CDKN1C | -0.0240 | 0.1430 | 0.3000 | 0.9300 | 1.1620 | 1.2340 | 0.9752 | 0.9087 | 0.7078 | 0.3033 | 0.0088 | 0.0074 |
| CEACAM1 | 1.2480 | 1.7380 | 1.3030 | 0.5900 | 0.2300 | 0.1360 | 0.0149 | 0.0000 | 0.0067 | 0.7273 | 0.7927 | 0.8940 |
| CEACAM21 | -0.0980 | -0.0220 | 0.3800 | 0.4630 | 0.6850 | 0.4250 | 0.8823 | 0.9887 | 0.5411 | 0.5407 | 0.0386 | 0.2671 |
| CEBPB | 0.3360 | -0.1150 | 0.5500 | 0.2600 | 0.7900 | 0.5400 | 0.3118 | 0.8847 | 0.0754 | 0.6609 | 0.0008 | 0.0314 |
| CECR2 | -0.5590 | 0.6230 | 0.1980 | 0.3120 | 0.5030 | 0.6640 | 0.4466 | 0.4410 | 0.8596 | 0.6899 | 0.1180 | 0.0426 |
| CG030 | -0.6260 | -0.2200 | -0.1260 | -0.0340 | -0.8480 | -0.4190 | 0.3924 | 0.8808 | 0.9117 | 0.9807 | 0.0449 | 0.3523 |
| CHAC1 | 0.1960 | -0.0170 | 0.3070 | 0.0400 | 0.2620 | 0.6350 | 0.6658 | 0.9889 | 0.5582 | 0.9359 | 0.0863 | 0.0000 |
| CHI3L2 | 0.0410 | 0.1990 | 0.2690 | 0.0370 | 0.6080 | 0.9440 | 0.4949 | 0.0000 | 0.0000 | 0.7305 | 0.0000 | 0.0000 |
| CHMP5 | 0.6560 | 1.1650 | 0.8720 | 0.3260 | 0.7630 | 0.7080 | 0.0000 | 0.0000 | 0.0000 | 0.0000 | 0.0000 | 0.0000 |
| CHST12 | 0.8620 | 0.7650 | 0.3910 | 0.7540 | 0.7790 | 0.4240 | 0.0000 | 0.0000 | 0.0000 | 0.0000 | 0.0000 | 0.0002 |
| CMPK2 | 2.4520 | 2.6750 | 1.5770 | 1.7540 | 2.0100 | 1.3470 | 0.0000 | 0.0000 | 0.0000 | 0.0000 | 0.0000 | 0.0000 |
| CMTM8 | 0.2010 | 0.4020 | 0.2780 | 0.6440 | 0.8280 | 0.5730 | 0.5357 | 0.2151 | 0.4677 | 0.0039 | 0.0000 | 0.0021 |
| CNKSR2 | -0.1660 | -0.3110 | -0.9490 | -0.0600 | -1.7240 | -0.5490 | 0.8038 | 0.7525 | 0.1166 | 0.9741 | 0.0055 | 0.3868 |
| CNP | 0.5980 | 0.6150 | 0.2490 | 0.3170 | 0.3140 | 0.1360 | 0.0000 | 0.0000 | 0.0000 | 0.0000 | 0.0000 | 0.0068 |
| COBL | 0.5080 | 0.9160 | 0.7690 | 0.0970 | 0.4710 | 0.5660 | 0.0420 | 0.0000 | 0.0002 | 0.9167 | 0.1001 | 0.0567 |
| CRABP2 | 0.4690 | 0.6220 | 0.7700 | -0.0140 | 0.2830 | 1.0370 | 0.5988 | 0.6208 | 0.4281 | 0.9952 | 0.6452 | 0.0428 |
| CRELD1 | 0.1450 | 0.3250 | 0.4420 | 0.2100 | 0.6890 | 0.4280 | 0.5070 | 0.0999 | 0.0092 | 0.5100 | 0.0000 | 0.0037 |
| CRIP2 | -0.5930 | -0.8570 | -0.8020 | -0.1740 | -1.4860 | -0.3030 | 0.3306 | 0.2163 | 0.2529 | 0.9240 | 0.0374 | 0.6970 |
| CSMD1 | -0.2100 | -0.3570 | -0.2500 | -0.2910 | -1.7980 | -0.4300 | 0.7176 | 0.6671 | 0.7404 | 0.9135 | 0.0387 | 0.7014 |
| CTRL | 0.1240 | -0.0140 | -0.2990 | 0.1340 | -0.5410 | -1.1230 | 0.7851 | 0.9903 | 0.5812 | 0.8984 | 0.1777 | 0.0134 |
| CXCR3 | 0.1020 | -0.1000 | -0.2400 | -0.2490 | -1.1470 | -0.7490 | 0.7183 | 0.8476 | 0.4564 | 0.8054 | 0.0097 | 0.0918 |
| CXCR7 | 0.2440 | 0.1850 | 0.1690 | 0.4120 | 0.5310 | 0.5930 | 0.3532 | 0.6714 | 0.6478 | 0.4598 | 0.0384 | 0.0267 |
| DAPP1 | 1.0780 | 1.9580 | 1.1000 | 0.1480 | 0.2860 | -0.0500 | 0.0349 | 0.0000 | 0.0236 | 0.9244 | 0.6209 | 0.9488 |
| DDX58 | 2.4670 | 3.1540 | 1.9160 | 1.6310 | 2.0270 | 1.4420 | 0.0000 | 0.0000 | 0.0000 | 0.0000 | 0.0000 | 0.0000 |
| DDX60 | 1.6110 | 3.0350 | 2.9870 | 1.4180 | 2.7210 | 3.0280 | 0.0000 | 0.0000 | 0.0000 | 0.0000 | 0.0000 | 0.0000 |
| DDX60L | 1.4170 | 2.7450 | 2.3340 | 1.2140 | 2.0650 | 2.0060 | 0.0000 | 0.0000 | 0.0000 | 0.0000 | 0.0000 | 0.0000 |
| DERL3 | 0.9070 | 0.7100 | 0.6120 | 0.2170 | 1.2000 | 0.9890 | 0.1329 | 0.3579 | 0.4368 | 0.9016 | 0.0238 | 0.0877 |
| DHRS12 | -0.2000 | 0.0930 | 0.0450 | 0.3970 | 0.5770 | 0.9190 | 0.6887 | 0.9243 | 0.9546 | 0.6600 | 0.1249 | 0.0131 |
| DHX58 | 1.9920 | 2.0500 | 1.6550 | 1.5430 | 1.7830 | 1.5270 | 0.0000 | 0.0000 | 0.0000 | 0.0000 | 0.0000 | 0.0000 |
| DPEP2 | 0.7420 | 0.7540 | 0.3490 | 0.5580 | 0.8010 | 1.4420 | 0.2666 | 0.3639 | 0.7428 | 0.7016 | 0.1881 | 0.0128 |
| DPY19L2 | -0.1630 | -0.0380 | 0.1200 | -0.2830 | -0.6000 | -0.1640 | 0.7616 | 0.9768 | 0.8715 | 0.6571 | 0.0342 | 0.6199 |
| DTX3L | 1.7540 | 1.8360 | 1.1650 | 1.6290 | 1.7080 | 1.3340 | 0.0000 | 0.0000 | 0.0000 | 0.0000 | 0.0000 | 0.0000 |
| ECE1 | 0.5020 | 0.7010 | 0.3010 | 0.2560 | 0.3610 | 0.1590 | 0.0000 | 0.0000 | 0.0000 | 0.0000 | 0.0000 | 0.0023 |
| EHD4 | 0.6400 | 1.0440 | 0.4550 | 0.1120 | 0.3530 | 0.2030 | 0.0000 | 0.0000 | 0.0000 | 0.4865 | 0.0000 | 0.0085 |
| EID3 | 0.6940 | 0.4780 | 0.9700 | -0.4030 | -2.4290 | 0.4470 | 0.5667 | 0.8365 | 0.4837 | 0.8632 | 0.0158 | 0.6415 |
| EIF2AK2 | 1.1080 | 2.0350 | 1.6960 | 0.9880 | 1.5030 | 1.4710 | 0.0000 | 0.0000 | 0.0000 | 0.0000 | 0.0000 | 0.0000 |
| ENPEP | -0.1720 | -0.6620 | -0.8110 | -2.8500 | -1.3310 | -1.7700 | 0.8197 | 0.4317 | 0.2748 | 0.0126 | 0.1330 | 0.0521 |
| EPHX2 | 0.0240 | 0.0120 | -0.0170 | 0.0450 | 0.5030 | 0.6410 | 0.8423 | 0.9592 | 0.9201 | 0.8028 | 0.0000 | 0.0000 |
| EPSTI1 | 3.0000 | 4.2790 | 3.8560 | 2.4890 | 3.8720 | 3.8260 | 0.0000 | 0.0000 | 0.0000 | 0.0000 | 0.0000 | 0.0000 |
| ERBB2 | -0.0510 | -0.0230 | 0.2760 | 0.3560 | 0.5670 | 0.6690 | 0.9116 | 0.9820 | 0.5068 | 0.5602 | 0.0302 | 0.0133 |
| ETV5 | -0.2880 | 0.0090 | -0.0670 | 0.2140 | 0.7010 | 0.8280 | 0.3395 | 0.9908 | 0.8905 | 0.7499 | 0.0050 | 0.0012 |
| EXPH5 | 0.0790 | 0.3630 | 0.1190 | -0.0480 | 0.3500 | 0.7120 | 0.9042 | 0.6272 | 0.8868 | 0.9649 | 0.2703 | 0.0182 |
| F2RL2 | -0.0240 | -0.1530 | 0.0030 | -0.7700 | -0.7030 | -0.2090 | 0.9248 | 0.5978 | 0.9922 | 0.1392 | 0.0203 | 0.5387 |
| FAM132B | 0.1670 | -1.3190 | -0.2080 | 0.4850 | 0.2290 | -0.3680 | 0.8077 | 0.0276 | 0.8300 | 0.5898 | 0.6289 | 0.4846 |
| FAM19A2 | 0.1710 | 0.2750 | 0.3970 | -0.1050 | -1.5290 | -0.2300 | 0.8577 | 0.8587 | 0.7099 | 0.9520 | 0.0213 | 0.7550 |
| FAR2 | 0.0430 | 0.6970 | 0.9120 | 0.0200 | 0.4660 | 0.1250 | 0.9063 | 0.0004 | 0.0000 | 0.9856 | 0.0767 | 0.7291 |
| FBLN1 | -0.2610 | -0.4730 | 0.1460 | 0.4420 | 0.7600 | 0.3630 | 0.7721 | 0.7209 | 0.9055 | 0.5962 | 0.0318 | 0.4040 |
| FBXO32 | 0.0910 | 0.0030 | 0.2490 | 0.0640 | 0.5870 | 0.5320 | 0.8516 | 0.9988 | 0.6260 | 0.9355 | 0.0115 | 0.0311 |
| FBXO39 | 2.2490 | 2.4160 | 2.2540 | 2.2230 | 2.2590 | 1.9200 | 0.0000 | 0.0000 | 0.0000 | 0.0000 | 0.0000 | 0.0002 |
| FCHSD2 | 0.2400 | 0.7900 | 0.4190 | 0.1500 | 0.3900 | 0.3690 | 0.0000 | 0.0000 | 0.0000 | 0.0269 | 0.0000 | 0.0000 |
| FDFT1 | 0.0340 | 0.2400 | 0.3360 | 0.0040 | 0.5000 | 0.6830 | 0.5375 | 0.0000 | 0.0000 | 0.9798 | 0.0000 | 0.0000 |
| FDPSL2A | -0.2770 | 0.0130 | 0.0960 | -0.0610 | 0.3380 | 0.6020 | 0.4510 | 0.9902 | 0.8678 | 0.9450 | 0.2227 | 0.0251 |
| FLJ10038 | 0.0580 | 0.3250 | 0.4480 | 0.5310 | 0.6050 | 0.6080 | 0.8483 | 0.1690 | 0.0229 | 0.0203 | 0.0004 | 0.0005 |
| FLJ32255 | 0.6270 | 0.6090 | 0.2580 | 0.0590 | 0.0140 | 0.1280 | 0.0274 | 0.0250 | 0.5480 | 0.9524 | 0.9725 | 0.7506 |
| FLJ32810 | -0.1210 | -0.1520 | -0.0650 | -0.1200 | -0.5950 | -0.4800 | 0.6001 | 0.6635 | 0.8587 | 0.7452 | 0.0003 | 0.0037 |
| FLJ40125 | -0.1140 | 0.1310 | 0.6160 | 0.7360 | 1.0880 | 0.9550 | 0.8656 | 0.9087 | 0.2322 | 0.4317 | 0.0091 | 0.0320 |
| FLJ40606 | 0.9190 | 0.8140 | 0.3630 | 0.4850 | 0.5310 | 1.2380 | 0.1623 | 0.3011 | 0.7350 | 0.7452 | 0.4136 | 0.0337 |
| FLJ45422 | 0.2470 | 0.7080 | 0.8180 | 0.2110 | 0.4940 | 0.4340 | 0.3745 | 0.0005 | 0.0000 | 0.6586 | 0.0097 | 0.0328 |
| FTSJD2 | 0.4960 | 0.8320 | 0.5920 | 0.3120 | 0.6980 | 0.5540 | 0.0000 | 0.0000 | 0.0000 | 0.0000 | 0.0000 | 0.0000 |
| GALNT9 | 0.9050 | -0.1520 | 0.1330 | 0.5970 | 0.2780 | 0.7410 | 0.1668 | 0.9317 | 0.9163 | 0.2699 | 0.3789 | 0.0096 |
| GBP1 | 1.1860 | 1.6960 | 1.1280 | 0.9340 | 1.2810 | 0.8700 | 0.0000 | 0.0000 | 0.0000 | 0.0000 | 0.0000 | 0.0000 |
| GBP2 | 1.2660 | 1.9090 | 1.1250 | 1.5380 | 1.4310 | 1.5830 | 0.2400 | 0.0412 | 0.3963 | 0.2552 | 0.0432 | 0.0305 |
| GBP3 | 0.9100 | 0.7670 | 0.4260 | 0.3850 | 0.3410 | 0.2150 | 0.0000 | 0.0000 | 0.0000 | 0.0029 | 0.0013 | 0.0562 |
| GBP4 | 0.5250 | 1.8210 | 1.5270 | -0.3320 | -0.1290 | 0.6270 | 0.6211 | 0.0117 | 0.0636 | 0.9009 | 0.9138 | 0.5681 |
| GCET2 | 0.0930 | 0.2270 | 0.0810 | 0.3200 | 0.5450 | 0.8030 | 0.7192 | 0.4162 | 0.8255 | 0.6794 | 0.0853 | 0.0118 |
| GEFT | 0.2720 | 0.3440 | 0.4900 | 0.2830 | 0.8020 | 0.5140 | 0.6718 | 0.7214 | 0.4818 | 0.7208 | 0.0070 | 0.1249 |
| GIMAP8 | 0.0810 | -0.0450 | 0.3160 | -1.4000 | -2.4300 | -0.5480 | 0.9054 | 0.9769 | 0.6521 | 0.4844 | 0.0093 | 0.6265 |
| GLMN | -0.1920 | -0.0770 | -0.1250 | -0.1410 | -0.5840 | -0.2180 | 0.3279 | 0.8476 | 0.6458 | 0.6631 | 0.0001 | 0.1402 |
| GPC5 | -1.3540 | -2.1900 | -2.6170 | 0.3690 | 0.5900 | 0.0770 | 0.2702 | 0.0591 | 0.0147 | 0.6866 | 0.1152 | 0.8921 |

**Table 5. RNA-seq identification of DE genes in IFNβ-treated Jurkat or JLat9.2 cells** - *Page 3*

| | Log2 Fold Change (IFNβ - mock) | | | | | | Adjusted p Value (Benjamini-Hochberg FDR corrected) | | | | | |
|---|---|---|---|---|---|---|---|---|---|---|---|---|
| | Jurkat | | | JLat9.2 | | | Jurkat | | | JLat9.2 | | |
| GENE | 4h | 8h | 12h | 4h | 8h | 12h | 4h | 8h | 12h | 4h | 8h | 12h |
| GPR135 | 0.7540 | 0.7690 | 1.4130 | -0.3590 | -0.1980 | 0.3970 | 0.3307 | 0.4540 | 0.0293 | 0.7768 | 0.7373 | 0.4594 |
| GPR162 | -0.1400 | 0.1210 | 0.1420 | 0.3890 | 0.8390 | 0.5540 | 0.7435 | 0.8690 | 0.7947 | 0.3694 | 0.0000 | 0.0085 |
| GPR17 | 0.1550 | -0.2000 | -0.1690 | -0.0730 | -1.2200 | -1.3140 | 0.7306 | 0.7935 | 0.7904 | 0.9151 | 0.0000 | 0.0000 |
| GPR75 | -0.3300 | -0.1800 | -0.2420 | -0.1040 | -0.4540 | -0.7810 | 0.2160 | 0.6779 | 0.4725 | 0.8451 | 0.0278 | 0.0008 |
| GRK5 | 0.2220 | 0.6750 | 0.3270 | 0.1430 | 0.3420 | 0.0040 | 0.0188 | 0.0000 | 0.0001 | 0.4566 | 0.0001 | 0.9785 |
| GRM4 | 1.0060 | 0.5020 | 0.4330 | -0.3880 | -1.3850 | -1.2170 | 0.1463 | 0.6860 | 0.6911 | 0.7658 | 0.0197 | 0.0475 |
| GSDMD | 0.2690 | 0.4230 | 0.3330 | 0.3450 | 0.6550 | 0.4160 | 0.0345 | 0.0001 | 0.0031 | 0.0326 | 0.0000 | 0.0005 |
| GTPBP2 | 0.4260 | 0.5080 | 0.4260 | 0.2770 | 0.6140 | 0.5070 | 0.0000 | 0.0000 | 0.0000 | 0.0008 | 0.0000 | 0.0000 |
| GZMM | 0.5650 | 0.4440 | 0.1100 | 0.0290 | -0.1890 | -0.7150 | 0.2733 | 0.5718 | 0.9078 | 0.9806 | 0.5987 | 0.0476 |
| HAR1A | 0.0890 | 0.0580 | 0.2900 | 0.2390 | 0.4220 | 0.6100 | 0.8090 | 0.9334 | 0.4042 | 0.6753 | 0.0718 | 0.0102 |
| HBP1 | 0.0070 | 0.1910 | 0.0990 | 0.1190 | 0.3800 | 0.6420 | 0.9741 | 0.2921 | 0.6633 | 0.6484 | 0.0005 | 0.0000 |
| HCG27 | 0.4360 | 0.1570 | 0.2520 | 0.4860 | 0.9400 | 1.3330 | 0.3951 | 0.8929 | 0.7509 | 0.5726 | 0.0089 | 0.0002 |
| HCP5 | 1.7810 | 1.6960 | 2.6970 | -2.3450 | 0.1450 | -0.0530 | 0.1724 | 0.2649 | 0.0116 | 0.1313 | 0.8800 | 0.9651 |
| HEPACAM | 0.0440 | -0.0300 | -0.0230 | -0.0590 | -0.6120 | -0.1570 | 0.9314 | 0.9794 | 0.9779 | 0.9467 | 0.0484 | 0.6715 |
| HERC5 | 0.6650 | 1.6700 | 1.3570 | 0.4120 | 0.8260 | 0.8760 | 0.0000 | 0.0000 | 0.0000 | 0.0000 | 0.0000 | 0.0000 |
| HERC6 | 1.7770 | 3.4250 | 3.3150 | 1.6450 | 2.8400 | 2.9090 | 0.0000 | 0.0000 | 0.0000 | 0.0000 | 0.0000 | 0.0000 |
| HES4 | 0.4760 | 0.3490 | 0.8390 | 0.4070 | 0.7860 | 0.0720 | 0.1294 | 0.3922 | 0.0007 | 0.2942 | 0.0001 | 0.7951 |
| HLA-B | 0.4760 | 0.9170 | 1.0290 | 0.4140 | 0.9350 | 1.0080 | 0.0000 | 0.0000 | 0.0000 | 0.0000 | 0.0000 | 0.0000 |
| HLA-C | 0.3070 | 0.6140 | 0.6800 | 0.2100 | 0.5670 | 0.5710 | 0.0000 | 0.0000 | 0.0000 | 0.0122 | 0.0000 | 0.0000 |
| HLA-DOA | 0.2320 | 0.2270 | 0.1940 | 0.1790 | 0.4090 | 0.6880 | 0.4060 | 0.5763 | 0.6051 | 0.7627 | 0.0749 | 0.0026 |
| HLA-F | 0.1860 | 0.5590 | 0.7800 | 0.1050 | 0.5010 | 0.5760 | 0.4439 | 0.0017 | 0.0000 | 0.8360 | 0.0045 | 0.0015 |
| HLA-G | 0.3680 | 0.6170 | 0.8590 | 0.2460 | 0.4770 | 0.4060 | 0.1432 | 0.0019 | 0.0000 | 0.6295 | 0.0237 | 0.0745 |
| HLA-J | 0.4460 | 0.8250 | 1.1500 | -0.0060 | 0.4710 | 0.3250 | 0.3700 | 0.0599 | 0.0020 | 0.9970 | 0.2204 | 0.4676 |
| HMGCS1 | -0.1210 | 0.4960 | 0.6530 | -0.0840 | 0.5340 | 1.0490 | 0.1013 | 0.0000 | 0.0000 | 0.5044 | 0.0000 | 0.0000 |
| HSD17B14 | -0.2460 | -0.0720 | -0.1590 | 0.3950 | 0.1930 | 0.7760 | 0.6675 | 0.9536 | 0.8535 | 0.5948 | 0.6202 | 0.0174 |
| HSH2D | 2.6130 | 2.9950 | 2.2890 | 2.0570 | 2.5450 | 2.2150 | 0.0000 | 0.0000 | 0.0000 | 0.0000 | 0.0000 | 0.0000 |
| HSPA1B | 0.1970 | 0.5950 | 0.2930 | 0.0500 | 0.2250 | -0.0630 | 0.0047 | 0.0000 | 0.0000 | 0.7637 | 0.0007 | 0.4241 |
| HTR2B | -0.2960 | -0.2100 | -0.3070 | -1.2840 | -1.2210 | -2.4950 | 0.7308 | 0.8938 | 0.7873 | 0.5898 | 0.2693 | 0.0228 |
| HTR7P | 0.1110 | -0.1720 | 0.0910 | 0.0710 | 0.2380 | 0.6410 | 0.7510 | 0.7576 | 0.8579 | 0.9368 | 0.4302 | 0.0189 |
| HYDIN | -0.1310 | 0.0700 | 0.2480 | 0.0110 | 0.4130 | 0.7040 | 0.8516 | 0.9588 | 0.7521 | 0.9898 | 0.0307 | 0.0003 |
| ICA1 | -0.2360 | -0.2330 | -0.1860 | 0.0580 | 0.2340 | 0.7470 | 0.2474 | 0.3579 | 0.4713 | 0.9149 | 0.1837 | 0.0000 |
| ICAM4 | -0.0100 | -0.1600 | 0.0900 | 0.0100 | 0.4870 | 0.6230 | 0.9723 | 0.6016 | 0.7595 | 0.9892 | 0.0029 | 0.0002 |
| ID1 | 0.0530 | 0.0560 | 0.1920 | -0.1610 | 0.0650 | -0.5950 | 0.8879 | 0.9360 | 0.6236 | 0.6644 | 0.7160 | 0.0007 |
| IFI16 | 0.7150 | 1.0150 | 0.6510 | 0.5130 | 0.6880 | 0.6450 | 0.0000 | 0.0000 | 0.0000 | 0.0000 | 0.0000 | 0.0000 |
| IFI27 | 1.8200 | 3.5550 | 3.6150 | -0.2200 | 0.3530 | 0.5890 | 0.0317 | 0.0000 | 0.0000 | 0.8990 | 0.5632 | 0.3240 |
| IFI35 | 2.0520 | 3.1710 | 3.2100 | 1.2170 | 2.3260 | 2.3820 | 0.0000 | 0.0000 | 0.0000 | 0.0000 | 0.0000 | 0.0000 |
| IFI44 | 3.4290 | 4.7580 | 4.3440 | 2.7610 | 4.1110 | 4.1620 | 0.0000 | 0.0000 | 0.0000 | 0.0000 | 0.0000 | 0.0000 |
| IFI44L | 10.5190 | 12.8320 | 12.8910 | 9.3620 | 11.6860 | 12.0190 | 0.0000 | 0.0000 | 0.0000 | 0.0000 | 0.0000 | 0.0000 |
| IFI6 | 2.5170 | 4.0820 | 4.2590 | 2.0490 | 3.7460 | 4.0110 | 0.0000 | 0.0000 | 0.0000 | 0.0000 | 0.0000 | 0.0000 |
| IFIH1 | 2.2360 | 3.0640 | 2.3910 | 2.0250 | 2.8070 | 2.4180 | 0.0000 | 0.0000 | 0.0000 | 0.0000 | 0.0000 | 0.0000 |
| IFIT1 | 6.5210 | 7.3590 | 5.8610 | 5.3570 | 6.2130 | 5.2210 | 0.0000 | 0.0000 | 0.0000 | 0.0000 | 0.0000 | 0.0000 |
| IFIT1L | 6.1220 | 6.9330 | 5.5210 | 4.1050 | 5.3120 | 4.3030 | 0.0000 | 0.0000 | 0.0000 | 0.0000 | 0.0000 | 0.0000 |
| IFIT2 | 3.5500 | 3.4250 | 1.6550 | 2.5020 | 2.3340 | 1.2440 | 0.0000 | 0.0000 | 0.0000 | 0.0000 | 0.0000 | 0.0000 |
| IFIT3 | 6.2270 | 6.9120 | 5.4110 | 6.4350 | 7.5060 | 6.1820 | 0.0000 | 0.0000 | 0.0000 | 0.0000 | 0.0000 | 0.0000 |
| IFIT5 | 2.4940 | 2.4840 | 1.4630 | 1.7720 | 1.8040 | 1.1840 | 0.0000 | 0.0000 | 0.0000 | 0.0000 | 0.0000 | 0.0000 |
| IFITM1 | 2.5080 | 3.7110 | 3.6680 | 1.5220 | 2.4890 | 2.5110 | 0.0000 | 0.0000 | 0.0000 | 0.0000 | 0.0000 | 0.0000 |
| IFITM2 | 0.4350 | 0.7470 | 0.7510 | 0.2220 | 0.5310 | 0.5300 | 0.0000 | 0.0000 | 0.0000 | 0.3511 | 0.0000 | 0.0000 |
| IFITM3 | 1.1380 | 1.9040 | 1.8980 | 0.4960 | 1.0350 | 1.1490 | 0.0000 | 0.0000 | 0.0000 | 0.3712 | 0.0001 | 0.0000 |
| IFT74 | -0.1260 | -0.2430 | -0.2820 | -0.2810 | -0.9290 | -0.6570 | 0.8229 | 0.7734 | 0.6690 | 0.6970 | 0.0054 | 0.0522 |
| IGFBP5 | 0.3450 | -0.2650 | 0.9800 | -0.6330 | 1.0650 | 0.1290 | 0.8108 | 0.9245 | 0.4785 | 0.6387 | 0.0212 | 0.8597 |
| IL10RA | 0.0470 | 0.3740 | 0.1180 | 0.4710 | 0.5820 | 0.7490 | 0.9227 | 0.3821 | 0.8459 | 0.3996 | 0.0236 | 0.0043 |
| IL17RD | 0.8830 | 0.9630 | 0.9290 | 0.1440 | 0.4130 | 0.6070 | 0.3378 | 0.4078 | 0.3998 | 0.8286 | 0.0882 | 0.0130 |
| IL21R | 0.1150 | -0.6960 | -0.1820 | -0.4050 | 0.7780 | 1.0440 | 0.8564 | 0.2751 | 0.8321 | 0.7154 | 0.0443 | 0.0077 |
| IL4I1 | 1.6440 | 1.8760 | 1.8850 | 0.6780 | -0.0870 | 0.4380 | 0.1074 | 0.0452 | 0.0453 | 0.6288 | 0.9205 | 0.5639 |
| IL7R | -0.0900 | 0.1140 | 0.1360 | 0.1220 | 0.5250 | 0.6250 | 0.7083 | 0.7497 | 0.6233 | 0.8015 | 0.0026 | 0.0005 |
| INSIG1 | -0.1010 | 0.2600 | 0.3900 | -0.0780 | 0.4310 | 0.7970 | 0.0746 | 0.0000 | 0.0000 | 0.3597 | 0.0000 | 0.0000 |
| IPCEF1 | -0.1510 | -0.1370 | 0.0970 | -0.3230 | -0.6190 | -0.2820 | 0.5971 | 0.7751 | 0.8122 | 0.1288 | 0.0000 | 0.0336 |
| IRF7 | 3.4710 | 4.3570 | 3.9240 | 3.0880 | 4.0520 | 3.7280 | 0.0000 | 0.0000 | 0.0000 | 0.0000 | 0.0000 | 0.0000 |
| IRF9 | 3.5090 | 3.2260 | 2.8910 | 3.3010 | 3.0490 | 2.7010 | 0.0000 | 0.0000 | 0.0000 | 0.0000 | 0.0000 | 0.0000 |
| ISG15 | 2.1960 | 3.3300 | 3.2210 | 1.8210 | 3.0370 | 2.9740 | 0.0000 | 0.0000 | 0.0000 | 0.0000 | 0.0000 | 0.0000 |
| ISG20 | 0.8430 | 1.6610 | 1.4300 | 0.5860 | 1.4140 | 1.2690 | 0.0004 | 0.0000 | 0.0000 | 0.2590 | 0.0000 | 0.0000 |
| ITPKA | -0.4230 | -0.6020 | -0.4460 | -0.0740 | -0.6710 | -0.4290 | 0.1850 | 0.0506 | 0.2008 | 0.9160 | 0.0078 | 0.0973 |
| JAK3 | 0.7310 | 0.3920 | 0.2270 | 0.5710 | 0.2110 | -0.0390 | 0.0000 | 0.0000 | 0.0085 | 0.0000 | 0.0623 | 0.8072 |
| JUN | 0.2410 | -0.2380 | -0.1980 | 0.0590 | -0.4800 | -0.6840 | 0.2346 | 0.3931 | 0.4782 | 0.8286 | 0.0000 | 0.0000 |
| KBTBD10 | -0.2920 | 1.0410 | 0.1810 | -0.4920 | -1.9070 | -0.3590 | 0.8164 | 0.3088 | 0.9114 | 0.7562 | 0.0136 | 0.6524 |
| KCNJ10 | 1.0780 | 0.5480 | 0.9330 | 0.1160 | 0.7290 | 0.7420 | 0.1371 | 0.6714 | 0.2661 | 0.9203 | 0.0327 | 0.0394 |
| KCNN4 | 0.0670 | -0.6610 | 0.4800 | 1.0140 | 1.5140 | 1.2230 | 0.9584 | 0.6808 | 0.6976 | 0.5565 | 0.0389 | 0.1311 |
| KIAA1618 | 0.8140 | 1.4000 | 1.0360 | 0.5080 | 0.9190 | 0.7420 | 0.0000 | 0.0000 | 0.0000 | 0.0004 | 0.0000 | 0.0000 |
| KLHL24 | -0.2820 | 0.0570 | 0.0620 | 0.0200 | 0.2160 | 0.5910 | 0.0259 | 0.8253 | 0.7544 | 0.9433 | 0.0148 | 0.0000 |
| KRT73 | -0.6950 | -1.6010 | -0.6700 | -0.1650 | -0.3810 | -0.2970 | 0.3501 | 0.0330 | 0.4694 | 0.9037 | 0.4601 | 0.6091 |
| LAMP3 | 0.4460 | 0.8070 | 0.4390 | 0.2580 | 0.5840 | 0.4470 | 0.0000 | 0.0000 | 0.0000 | 0.0001 | 0.0000 | 0.0000 |
| LAP3 | 0.5810 | 1.0260 | 0.9660 | 0.4080 | 0.7540 | 0.7620 | 0.0000 | 0.0000 | 0.0000 | 0.0000 | 0.0000 | 0.0000 |

**Table 5. RNA-seq identification of DE genes in IFNβ-treated Jurkat or JLat9.2 cells** - *Page 4*

| | Log2 Fold Change (IFNβ - mock) | | | | | | Adjusted p Value (Benjamini-Hochberg FDR corrected) | | | | | |
|---|---|---|---|---|---|---|---|---|---|---|---|---|
| | Jurkat | | | JLat9.2 | | | Jurkat | | | JLat9.2 | | |
| GENE | 4h | 8h | 12h | 4h | 8h | 12h | 4h | 8h | 12h | 4h | 8h | 12h |
| LBA1 | 1.0690 | 2.0950 | 1.4370 | 0.5070 | 1.1400 | 0.9010 | 0.0000 | 0.0000 | 0.0000 | 0.0000 | 0.0000 | 0.0000 |
| LGALS3BP | 0.8440 | 1.4050 | 1.1470 | 0.6340 | 1.0960 | 0.9100 | 0.0000 | 0.0000 | 0.0000 | 0.0000 | 0.0000 | 0.0000 |
| LGALS9 | 0.4010 | 0.8450 | 0.8030 | 0.2810 | 0.6450 | 0.7310 | 0.0000 | 0.0000 | 0.0000 | 0.0000 | 0.0000 | 0.0000 |
| LGALS9B | 0.3560 | 0.7520 | 0.8160 | 0.4520 | 0.7310 | 0.7510 | 0.0325 | 0.0000 | 0.0000 | 0.1008 | 0.0000 | 0.0000 |
| LGALS9C | 0.3140 | 0.8070 | 0.8520 | 0.4210 | 0.8410 | 0.8720 | 0.0488 | 0.0000 | 0.0000 | 0.1126 | 0.0000 | 0.0000 |
| LGMN | 0.0180 | 0.1100 | 0.1800 | 0.1760 | 0.7300 | 0.7140 | 0.9269 | 0.6116 | 0.2367 | 0.6402 | 0.0000 | 0.0000 |
| LIF | 2.8980 | 3.0910 | 2.6850 | 0.9750 | 2.0020 | 1.0810 | 0.0005 | 0.0001 | 0.0012 | 0.6977 | 0.0351 | 0.3632 |
| LNP1 | 0.1100 | -0.4110 | 0.3210 | 0.6700 | 0.2650 | 1.1790 | 0.9121 | 0.7845 | 0.7756 | 0.6033 | 0.7062 | 0.0376 |
| LOC100008589 | 0.4800 | 0.0640 | 0.5270 | 0.5120 | 1.0040 | -0.1190 | 0.6062 | 0.9820 | 0.6607 | 0.6933 | 0.0491 | 0.8874 |
| LOC100049716 | 0.1050 | 0.4710 | 0.2990 | 0.5950 | 0.9460 | 1.2480 | 0.8568 | 0.3728 | 0.6213 | 0.4598 | 0.0088 | 0.0006 |
| LOC100125556 | 0.0870 | 0.2570 | 0.1380 | 0.4990 | 0.7110 | 0.3930 | 0.7254 | 0.2725 | 0.6383 | 0.0861 | 0.0001 | 0.0486 |
| LOC100128288 | 0.2530 | 0.1820 | 0.3460 | 0.4520 | 0.4260 | 0.6290 | 0.5192 | 0.7971 | 0.4447 | 0.4543 | 0.1389 | 0.0291 |
| LOC100128822 | 0.3630 | 0.1480 | 0.5960 | 0.0730 | 0.4260 | 0.2910 | 0.2402 | 0.8101 | 0.0262 | 0.9151 | 0.0413 | 0.2153 |
| LOC100128895 | -0.0550 | 0.0650 | -0.1910 | -0.1610 | -0.8280 | -0.5690 | 0.9351 | 0.9580 | 0.8142 | 0.8712 | 0.0333 | 0.1618 |
| LOC100129104 | -0.1560 | 0.1390 | 0.6810 | 0.8690 | 1.3360 | 1.2530 | 0.8660 | 0.9318 | 0.3757 | 0.5091 | 0.0208 | 0.0408 |
| LOC100129122 | 0.4790 | 0.3980 | 0.3410 | 0.0800 | 0.8910 | 1.2790 | 0.6447 | 0.8339 | 0.8293 | 0.9722 | 0.1298 | 0.0286 |
| LOC100129518 | 0.3600 | 0.7200 | 0.5560 | 0.4090 | 0.4120 | 1.1940 | 0.6148 | 0.3394 | 0.4936 | 0.7702 | 0.5069 | 0.0263 |
| LOC100129917 | 0.1880 | 0.3740 | 0.5910 | 0.1170 | 0.7130 | 0.5410 | 0.6056 | 0.3382 | 0.0388 | 0.8909 | 0.0073 | 0.0624 |
| LOC100130691 | 0.0280 | 0.0280 | -0.1150 | 0.2730 | 0.5520 | 0.7220 | 0.9606 | 0.9814 | 0.8658 | 0.6970 | 0.0471 | 0.0110 |
| LOC100130855 | 0.1930 | 0.2610 | 0.3300 | 1.0390 | 0.1760 | 1.5420 | 0.8516 | 0.8806 | 0.7904 | 0.5068 | 0.8597 | 0.0334 |
| LOC100130872 | 0.0210 | 0.2960 | 0.4830 | 0.0670 | 0.5240 | 0.8240 | 0.9032 | 0.0044 | 0.0000 | 0.8225 | 0.0000 | 0.0000 |
| LOC100131257 | -0.0100 | 0.1560 | 0.2790 | -0.8040 | -1.1150 | -0.5410 | 0.9878 | 0.8884 | 0.6980 | 0.2216 | 0.0030 | 0.1383 |
| LOC100131354 | -0.4600 | -0.3670 | -0.3450 | 0.6150 | 1.3530 | 1.2640 | 0.5893 | 0.8036 | 0.7705 | 0.7214 | 0.0365 | 0.0686 |
| LOC100131507 | 0.0920 | 0.0730 | 0.3440 | 0.3810 | 0.4230 | 0.7010 | 0.8572 | 0.9390 | 0.4785 | 0.5689 | 0.1590 | 0.0180 |
| LOC100132652 | -0.1930 | 0.0180 | -0.1820 | -0.3650 | -0.6700 | -0.9020 | 0.5449 | 0.9834 | 0.6709 | 0.5051 | 0.0122 | 0.0023 |
| LOC100133167 | 0.0450 | 0.2870 | 0.4120 | 0.0610 | 0.6630 | 0.5330 | 0.9326 | 0.6208 | 0.3339 | 0.9478 | 0.0145 | 0.0707 |
| LOC100133264 | -0.4510 | 0.0110 | -0.3150 | 0.2780 | -0.7470 | -1.0340 | 0.4244 | 0.9954 | 0.6859 | 0.7682 | 0.0882 | 0.0305 |
| LOC100287062 | 0.7200 | 1.3980 | 1.0510 | 0.5040 | 0.9380 | 0.7710 | 0.0000 | 0.0000 | 0.0000 | 0.0050 | 0.0000 | 0.0000 |
| LOC100287126 | -0.4860 | -0.0330 | -0.2360 | 0.6580 | 1.2690 | 0.8650 | 0.5171 | 0.9862 | 0.8373 | 0.6867 | 0.0497 | 0.2441 |
| LOC100287226 | -0.3030 | -0.1730 | -0.4360 | -0.1440 | -0.7080 | -0.2990 | 0.5091 | 0.8427 | 0.4225 | 0.8748 | 0.0417 | 0.4361 |
| LOC100287563 | 0.2830 | 0.0380 | 0.0440 | 0.6190 | 0.6170 | 0.3930 | 0.3878 | 0.9665 | 0.9414 | 0.1489 | 0.0137 | 0.1618 |
| LOC100287569 | 0.3990 | -0.4010 | 0.6290 | 0.7820 | 2.4450 | 2.0640 | 0.7176 | 0.8531 | 0.6204 | 0.7495 | 0.0045 | 0.0256 |
| LOC100287659 | 0.0150 | 0.3470 | -0.1190 | 0.4200 | 0.6020 | 0.6870 | 0.9802 | 0.5480 | 0.8730 | 0.5749 | 0.0636 | 0.0411 |
| LOC100287960 | 0.3900 | 0.4100 | 0.4350 | 0.8970 | 1.1800 | 0.9850 | 0.6068 | 0.7349 | 0.6511 | 0.4018 | 0.0155 | 0.0623 |
| LOC100288196 | 0.4010 | 0.3230 | 0.6120 | 0.3490 | 0.0590 | 0.1260 | 0.0960 | 0.2489 | 0.0018 | 0.4177 | 0.8232 | 0.6359 |
| LOC100288594 | 0.8180 | 1.0610 | 0.4290 | 1.0780 | 1.0040 | 0.3750 | 0.0139 | 0.0002 | 0.3512 | 0.2092 | 0.0334 | 0.5436 |
| LOC100288640 | 0.3570 | 0.6170 | 0.4840 | -0.2730 | 0.6730 | 0.3740 | 0.3895 | 0.1176 | 0.2869 | 0.7707 | 0.0392 | 0.3368 |
| LOC100288682 | 0.1270 | 0.2230 | 0.4150 | 1.2250 | 0.6790 | 0.8160 | 0.8289 | 0.7972 | 0.4605 | 0.0099 | 0.0825 | 0.0424 |
| LOC100288926 | 0.3400 | 0.4600 | 0.5600 | 0.3300 | 0.7780 | 0.5870 | 0.5860 | 0.5963 | 0.4101 | 0.7499 | 0.0471 | 0.1788 |
| LOC100289002 | 0.9840 | 0.8810 | 0.6920 | 0.2620 | 0.4130 | 0.6200 | 0.0317 | 0.0602 | 0.2071 | 0.8171 | 0.3603 | 0.1629 |
| LOC100289008 | 0.1450 | 0.3570 | 0.3390 | 0.8640 | 0.6790 | 1.1130 | 0.8473 | 0.7142 | 0.6817 | 0.3081 | 0.1241 | 0.0100 |
| LOC100289060 | -0.3370 | -0.2120 | -0.1280 | -0.4900 | -0.5990 | -0.1300 | 0.2611 | 0.6607 | 0.7763 | 0.1324 | 0.0026 | 0.5571 |
| LOC100289210 | -0.3870 | -0.3140 | -0.1360 | 0.9190 | 0.6450 | 1.2090 | 0.4786 | 0.7282 | 0.8773 | 0.2541 | 0.1442 | 0.0043 |
| LOC100289218 | -0.2820 | 0.5470 | 0.0250 | 1.7560 | 1.5930 | 1.7290 | 0.7896 | 0.6727 | 0.9873 | 0.2788 | 0.0607 | 0.0498 |
| LOC100289230 | 0.2500 | 0.2930 | 0.5790 | 0.4040 | 0.6980 | 0.7420 | 0.6298 | 0.7131 | 0.2410 | 0.6274 | 0.0435 | 0.0402 |
| LOC100289274 | 0.5520 | 0.5830 | 0.8370 | 0.1850 | 0.5200 | 1.3690 | 0.3181 | 0.4077 | 0.1157 | 0.8969 | 0.2785 | 0.0015 |
| LOC100289316 | -0.1140 | -0.4010 | 0.2470 | 1.1410 | 1.1140 | 1.5900 | 0.8894 | 0.7225 | 0.7942 | 0.3768 | 0.0731 | 0.0100 |
| LOC100289608 | -0.4010 | -0.1570 | -0.0970 | -0.3540 | -0.6850 | -0.1980 | 0.3555 | 0.8555 | 0.8886 | 0.5344 | 0.0128 | 0.5161 |
| LOC100289653 | -0.0860 | 0.1560 | 0.1810 | 0.2780 | 0.5750 | 0.6600 | 0.8234 | 0.7747 | 0.6670 | 0.6265 | 0.0148 | 0.0068 |
| LOC100289656 | 0.3430 | 0.0370 | 0.9960 | 0.4550 | 1.1320 | 0.2440 | 0.7061 | 0.9881 | 0.2005 | 0.7502 | 0.0333 | 0.7525 |
| LOC201229 | -0.2010 | -0.2600 | 0.2320 | 0.0340 | 0.5390 | 0.7530 | 0.6114 | 0.6622 | 0.6174 | 0.9734 | 0.0420 | 0.0050 |
| LOC220930 | -0.0970 | 0.0500 | 0.1750 | 0.0340 | 0.3000 | 0.6230 | 0.6883 | 0.9168 | 0.4962 | 0.9498 | 0.0692 | 0.0002 |
| LOC255512 | 1.0800 | 0.7000 | 1.0960 | 1.3750 | 0.6000 | 1.6130 | 0.1922 | 0.6025 | 0.2322 | 0.4122 | 0.5237 | 0.0463 |
| LOC255783 | 0.3680 | 0.0330 | 0.4750 | 0.4480 | 0.8940 | 0.0560 | 0.4786 | 0.9835 | 0.4362 | 0.6309 | 0.0179 | 0.9287 |
| LOC26010 | 1.0790 | 2.5750 | 2.0740 | 0.2740 | 0.7100 | 0.7540 | 0.0001 | 0.0000 | 0.0000 | 0.5251 | 0.0002 | 0.0001 |
| LOC283314 | 0.3170 | 0.2290 | 0.6310 | 0.1280 | -0.1570 | 0.0550 | 0.3882 | 0.7142 | 0.0482 | 0.6977 | 0.2999 | 0.7669 |
| LOC284801 | 0.2910 | -0.3470 | 0.6760 | 1.1730 | 1.3840 | 0.1210 | 0.7752 | 0.8573 | 0.5115 | 0.2033 | 0.0053 | 0.8853 |
| LOC338598 | -0.6160 | -0.2860 | -0.3560 | -0.6540 | -1.1170 | -0.3000 | 0.2608 | 0.7634 | 0.6302 | 0.3380 | 0.0021 | 0.4055 |
| LOC342918 | 0.0870 | -0.1010 | 0.7240 | 0.2030 | 0.9780 | 0.3180 | 0.9098 | 0.9430 | 0.1981 | 0.8676 | 0.0114 | 0.5311 |
| LOC387763 | 0.5270 | 0.0420 | 1.0360 | -0.1420 | 0.2400 | -0.3850 | 0.2974 | 0.9801 | 0.0119 | 0.9063 | 0.5763 | 0.4265 |
| LOC388559 | -0.3250 | -0.1870 | -0.1830 | -0.3170 | -0.6310 | -0.2740 | 0.1430 | 0.5705 | 0.5248 | 0.3597 | 0.0005 | 0.1250 |
| LOC389705 | 0.3740 | 0.2940 | 0.5710 | -0.1450 | -0.7620 | 0.2300 | 0.4346 | 0.7142 | 0.2591 | 0.8796 | 0.0364 | 0.5501 |
| LOC389813 | -0.0190 | -0.3640 | 0.1120 | 0.0520 | 0.1380 | -1.0270 | 0.9757 | 0.6264 | 0.8814 | 0.9563 | 0.6848 | 0.0055 |
| LOC390424 | -0.0610 | -0.1140 | 0.0540 | -0.7980 | -0.4010 | -0.7780 | 0.9147 | 0.9057 | 0.9416 | 0.1429 | 0.1947 | 0.0203 |
| LOC400752 | 0.1960 | -0.1320 | -0.0950 | 1.5000 | 1.5250 | 1.2360 | 0.8090 | 0.9360 | 0.9365 | 0.2716 | 0.0291 | 0.1093 |
| LOC400759 | 1.2090 | 1.7760 | 1.5370 | 1.5640 | 1.5580 | 1.1740 | 0.0000 | 0.0000 | 0.0000 | 0.0078 | 0.0008 | 0.0177 |
| LOC441455 | 0.9460 | 1.2240 | 0.6780 | -0.0360 | 0.1710 | 0.1010 | 0.1489 | 0.0356 | 0.4186 | 0.9833 | 0.7404 | 0.8707 |
| LOC441548 | -0.4560 | -0.1250 | 0.0400 | -0.0850 | -1.0080 | -0.0200 | 0.3745 | 0.9089 | 0.9671 | 0.9307 | 0.0066 | 0.9679 |
| LOC492303 | -0.1090 | -0.0190 | -0.0780 | 0.0930 | 0.5420 | 0.7770 | 0.6592 | 0.9760 | 0.8325 | 0.8748 | 0.0046 | 0.0001 |
| LOC554206 | 0.6310 | 0.3670 | 0.1780 | 1.8440 | 0.8610 | 0.7460 | 0.4369 | 0.8147 | 0.9011 | 0.0356 | 0.2204 | 0.3383 |
| LOC642441 | 0.0200 | -0.1560 | 0.3730 | 0.5590 | 0.2660 | 1.1720 | 0.9801 | 0.9070 | 0.6230 | 0.5344 | 0.5825 | 0.0032 |
| LOC642648 | 0.3050 | -0.1310 | -0.1810 | 0.5970 | 1.4000 | 0.4630 | 0.7047 | 0.9396 | 0.8854 | 0.7363 | 0.0348 | 0.6138 |

**Table 5. RNA-seq identification of DE genes in IFNβ-treated Jurkat or JLat9.2 cells** - *Page 5*

| | Log2 Fold Change (IFNβ - mock) | | | | | | Adjusted p Value (Benjamini-Hochberg FDR corrected) | | | | | |
|---|---|---|---|---|---|---|---|---|---|---|---|---|
| | Jurkat | | | JLat9.2 | | | Jurkat | | | JLat9.2 | | |
| GENE | 4h | 8h | 12h | 4h | 8h | 12h | 4h | 8h | 12h | 4h | 8h | 12h |
| LOC645405 | -0.6260 | -0.2240 | -0.1350 | 0.3390 | 0.4950 | 0.6290 | 0.0717 | 0.6895 | 0.7986 | 0.4941 | 0.0280 | 0.0065 |
| LOC645676 | 0.2070 | -0.1230 | 0.0090 | 0.6190 | 0.3430 | 0.7280 | 0.6114 | 0.8883 | 0.9893 | 0.3511 | 0.3322 | 0.0278 |
| LOC654433 | -0.4020 | -0.4230 | -0.0420 | 2.2340 | 1.4320 | 3.0290 | 0.5416 | 0.6811 | 0.9726 | 0.1311 | 0.1211 | 0.0004 |
| LOC728739 | 0.0960 | -0.0410 | -0.1220 | 0.6220 | 0.9390 | 0.5010 | 0.8688 | 0.9760 | 0.8793 | 0.4393 | 0.0084 | 0.2301 |
| LOC729255 | 0.2150 | 0.2640 | -0.0320 | 0.3080 | 0.6310 | 0.3610 | 0.5861 | 0.6499 | 0.9671 | 0.6613 | 0.0246 | 0.2707 |
| LOC729920 | 0.0620 | 0.7260 | -0.0430 | 0.2750 | 0.0340 | 0.8920 | 0.9654 | 0.6116 | 0.9830 | 0.8135 | 0.9549 | 0.0380 |
| LOC730101 | -0.0820 | -0.0250 | 0.0830 | 0.1880 | 0.3260 | 0.5900 | 0.6422 | 0.9489 | 0.7217 | 0.5414 | 0.0161 | 0.0000 |
| LOC730153 | -0.0020 | 0.1780 | 0.0260 | -0.4280 | -0.9200 | -0.6970 | 0.9978 | 0.8969 | 0.9842 | 0.6399 | 0.0276 | 0.1100 |
| LOC85389 | -0.2500 | -0.4010 | -0.1700 | -0.3360 | -0.5300 | -0.7480 | 0.4283 | 0.2624 | 0.7026 | 0.5948 | 0.0654 | 0.0160 |
| LOC85391 | 1.3470 | 1.5010 | 1.2560 | 1.3050 | 1.2740 | 1.3440 | 0.0220 | 0.0037 | 0.0317 | 0.1970 | 0.0229 | 0.0216 |
| LQK1 | -0.1660 | 0.0610 | 0.2410 | 0.6930 | 1.0090 | 1.0670 | 0.8289 | 0.9696 | 0.7893 | 0.5272 | 0.0369 | 0.0346 |
| LRRC46 | -0.0170 | -0.1400 | -0.0550 | -0.2680 | -0.3370 | -0.8330 | 0.9757 | 0.8738 | 0.9395 | 0.7642 | 0.3851 | 0.0430 |
| LSS | 0.0430 | 0.3750 | 0.5850 | 0.0330 | 0.5430 | 0.6770 | 0.5765 | 0.0000 | 0.0000 | 0.8225 | 0.0000 | 0.0000 |
| LTA | -0.0850 | 0.0610 | -0.1820 | 1.3900 | 1.5490 | 2.0580 | 0.8289 | 0.9331 | 0.6976 | 0.4575 | 0.0797 | 0.0204 |
| LY6E | 0.5880 | 1.1480 | 1.1560 | 0.3760 | 0.8980 | 0.8070 | 0.0000 | 0.0000 | 0.0000 | 0.0000 | 0.0000 | 0.0000 |
| LY9 | -0.0670 | -0.0950 | 0.1870 | 0.1580 | 0.5810 | 0.7350 | 0.7442 | 0.7601 | 0.3328 | 0.6834 | 0.0002 | 0.0000 |
| MAGIX | -0.0170 | 0.2160 | 0.2350 | -0.4560 | -0.8750 | -0.3880 | 0.9804 | 0.8065 | 0.7383 | 0.6403 | 0.0495 | 0.4234 |
| MBLAC1 | 0.9530 | 0.6170 | 0.8330 | 0.0660 | 0.0530 | -0.1710 | 0.0355 | 0.2961 | 0.0819 | 0.9517 | 0.9056 | 0.7116 |
| MFAP4 | -0.1970 | -0.2530 | -0.0200 | 0.2690 | 0.5700 | 0.8790 | 0.7490 | 0.7993 | 0.9842 | 0.5071 | 0.0016 | 0.0000 |
| MGAT3 | -0.2870 | -0.0510 | 0.0370 | 0.2480 | 0.5470 | 0.6210 | 0.4817 | 0.9579 | 0.9609 | 0.7452 | 0.0629 | 0.0419 |
| MGC12982 | 0.0520 | 0.2150 | 0.1860 | 0.2280 | 0.5420 | 0.6150 | 0.8566 | 0.4584 | 0.5096 | 0.5604 | 0.0012 | 0.0003 |
| MGC13005 | 0.0130 | 0.2160 | 0.1720 | 0.0300 | 0.7150 | 0.9650 | 0.9854 | 0.8450 | 0.8522 | 0.9886 | 0.1109 | 0.0329 |
| MGC16384 | 0.4030 | 0.3030 | 0.1650 | 0.5950 | 0.7150 | 0.3420 | 0.4381 | 0.7353 | 0.8545 | 0.4500 | 0.0446 | 0.4392 |
| MLC1 | -0.0640 | -0.1030 | 0.1580 | -0.2400 | -0.3950 | -0.6450 | 0.8659 | 0.8687 | 0.7019 | 0.5463 | 0.0309 | 0.0015 |
| MOV10 | 0.2840 | 0.6410 | 0.6070 | 0.1860 | 0.4770 | 0.4880 | 0.0000 | 0.0000 | 0.0000 | 0.0080 | 0.0000 | 0.0000 |
| MT2A | 0.3660 | 0.6250 | 0.6080 | 0.0250 | 0.0840 | -0.0440 | 0.0054 | 0.0000 | 0.0000 | 0.9450 | 0.5087 | 0.7785 |
| MX1 | 8.8150 | 11.6750 | 11.3930 | 2.3140 | 4.7900 | 3.8400 | 0.0000 | 0.0000 | 0.0000 | 0.3189 | 0.0000 | 0.0003 |
| MX2 | 2.7350 | 4.7780 | 4.2220 | 2.0590 | 3.2830 | 3.0030 | 0.0000 | 0.0000 | 0.0000 | 0.0000 | 0.0000 | 0.0000 |
| MYD88 | 0.5610 | 0.6920 | 0.3480 | 0.3780 | 0.3530 | 0.1050 | 0.0000 | 0.0000 | 0.0000 | 0.0000 | 0.0000 | 0.0217 |
| MYLIP | -0.1060 | 0.2050 | 0.4470 | 0.1850 | 0.2500 | 0.6600 | 0.8572 | 0.8063 | 0.3778 | 0.6971 | 0.2153 | 0.0005 |
| NAPA | 0.2930 | 0.5870 | 0.5180 | 0.1970 | 0.4430 | 0.3610 | 0.0000 | 0.0000 | 0.0000 | 0.0043 | 0.0000 | 0.0000 |
| NCRNA00115 | 0.2340 | 0.0290 | 0.5880 | 1.0020 | 0.7090 | 0.5580 | 0.6211 | 0.9829 | 0.1675 | 0.0166 | 0.0279 | 0.1155 |
| NCRNA00164 | 0.0270 | -0.5880 | 0.0850 | 0.7840 | 0.8150 | 0.2240 | 0.9696 | 0.3892 | 0.9205 | 0.1750 | 0.0125 | 0.6185 |
| NEGR1 | -0.1360 | 0.1750 | 0.2280 | -0.4380 | -0.9400 | -0.3500 | 0.9020 | 0.9268 | 0.8698 | 0.5602 | 0.0090 | 0.3551 |
| NEK5 | 2.0150 | 1.9770 | 2.0370 | -0.1100 | 0.4380 | 0.2160 | 0.0068 | 0.0052 | 0.0042 | 0.9115 | 0.1485 | 0.5672 |
| NEXN | 1.7640 | 2.7770 | 1.9510 | 0.0550 | -0.1050 | -0.8690 | 0.0000 | 0.0000 | 0.0000 | 0.9898 | 0.9376 | 0.5096 |
| NFATC4 | 0.1980 | 0.3280 | 0.5020 | 0.2020 | 0.7170 | 0.6750 | 0.5449 | 0.3837 | 0.0743 | 0.4315 | 0.0000 | 0.0000 |
| NGFR | 0.4380 | -0.7350 | 0.3180 | -0.7700 | -1.2730 | -3.0010 | 0.5356 | 0.4986 | 0.7575 | 0.6701 | 0.1145 | 0.0003 |
| NHLH1 | -0.1150 | -0.0830 | -0.2020 | 0.0340 | -0.7440 | -1.1340 | 0.8702 | 0.9506 | 0.8248 | 0.9819 | 0.0915 | 0.0203 |
| NKX2-1 | -0.0200 | 0.7280 | 0.0200 | 0.6030 | 0.4970 | 1.1550 | 0.9912 | 0.7747 | 0.9937 | 0.6553 | 0.4286 | 0.0394 |
| NLRC5 | 1.5420 | 1.7820 | 1.0810 | 1.4990 | 1.8090 | 1.3390 | 0.0000 | 0.0000 | 0.0000 | 0.0000 | 0.0000 | 0.0000 |
| NOL3 | 0.0380 | 0.0540 | 0.0910 | 0.3540 | 0.6820 | 0.3470 | 0.9516 | 0.9609 | 0.9031 | 0.6077 | 0.0175 | 0.3155 |
| NPAS4 | -0.3630 | -0.2580 | -0.0670 | -0.2640 | -0.2130 | -1.1370 | 0.4113 | 0.7268 | 0.9250 | 0.7794 | 0.6174 | 0.0121 |
| NPM2 | 0.0980 | 0.3680 | -0.0820 | -0.2820 | -0.6280 | -1.1020 | 0.8957 | 0.6937 | 0.9365 | 0.8075 | 0.1871 | 0.0355 |
| NT5E | 0.0310 | 0.6220 | 0.7760 | 0.0660 | -0.0670 | 0.0580 | 0.9629 | 0.1563 | 0.0413 | 0.8896 | 0.7380 | 0.7951 |
| NTRK3 | 0.1700 | 0.3080 | 0.3640 | 0.3620 | 0.7140 | 0.9300 | 0.7737 | 0.7043 | 0.5632 | 0.7170 | 0.0668 | 0.0190 |
| NUB1 | 0.4140 | 0.8330 | 0.4820 | 0.0950 | 0.3220 | 0.1830 | 0.0000 | 0.0000 | 0.0000 | 0.2984 | 0.0000 | 0.0001 |
| NUDT19 | 0.2250 | 0.1580 | 0.0870 | 0.5410 | 0.6000 | 0.1510 | 0.7142 | 0.8929 | 0.9259 | 0.4081 | 0.0480 | 0.7211 |
| OAS1 | 6.1490 | 7.4470 | 6.9970 | 3.5890 | 4.7910 | 4.5360 | 0.0000 | 0.0000 | 0.0000 | 0.0000 | 0.0000 | 0.0000 |
| OAS2 | 3.1390 | 4.3270 | 3.8210 | 3.1900 | 4.5450 | 4.2250 | 0.0000 | 0.0000 | 0.0000 | 0.0000 | 0.0000 | 0.0000 |
| OAS3 | 1.9000 | 3.1480 | 2.9160 | 1.3550 | 2.5280 | 2.4050 | 0.0000 | 0.0000 | 0.0000 | 0.0000 | 0.0000 | 0.0000 |
| OASL | 4.6540 | 5.2210 | 3.9890 | 3.5700 | 3.8670 | 3.2440 | 0.0000 | 0.0000 | 0.0000 | 0.0000 | 0.0000 | 0.0000 |
| OGFR | 0.6830 | 0.6750 | 0.3170 | 0.4730 | 0.5320 | 0.1180 | 0.0000 | 0.0000 | 0.0000 | 0.0000 | 0.0000 | 0.0326 |
| OLFM2 | -0.3140 | -0.2680 | -0.2130 | 0.2070 | 0.4820 | 0.6550 | 0.4376 | 0.6758 | 0.7095 | 0.7208 | 0.0314 | 0.0041 |
| ORAI3 | 0.6810 | 0.2980 | 0.3510 | -0.0020 | 0.1970 | 0.0400 | 0.0482 | 0.6211 | 0.4694 | 0.9988 | 0.5797 | 0.9336 |
| OSM | 1.4100 | 0.8780 | 0.4480 | 0.9330 | 0.5700 | -0.2540 | 0.0000 | 0.0122 | 0.3978 | 0.2963 | 0.2461 | 0.7102 |
| OTOF | 1.1250 | 2.5380 | 2.9020 | 0.4850 | 1.2900 | 1.4600 | 0.0006 | 0.0000 | 0.0000 | 0.4503 | 0.0000 | 0.0000 |
| PACSIN1 | 0.1660 | -0.0310 | 0.0120 | 0.2230 | 0.4620 | 0.8260 | 0.8378 | 0.9871 | 0.9914 | 0.7793 | 0.1339 | 0.0060 |
| PAPLN | 0.0590 | -0.0580 | 0.3050 | -0.2040 | 0.2560 | 0.6420 | 0.9148 | 0.9561 | 0.5647 | 0.7419 | 0.2863 | 0.0042 |
| PAR5 | -0.2470 | -0.5870 | -0.4280 | -0.1270 | -0.4340 | -0.2840 | 0.3752 | 0.0216 | 0.1454 | 0.6944 | 0.0022 | 0.0510 |
| PARP10 | 1.2510 | 1.9400 | 1.3770 | 1.0550 | 2.0020 | 1.6000 | 0.0000 | 0.0000 | 0.0000 | 0.0000 | 0.0000 | 0.0000 |
| PARP12 | 1.1920 | 1.7460 | 1.1730 | 0.8510 | 1.4170 | 1.0850 | 0.0000 | 0.0000 | 0.0000 | 0.0000 | 0.0000 | 0.0000 |
| PARP14 | 1.1260 | 2.0530 | 1.4880 | 0.7690 | 1.3270 | 1.2410 | 0.0000 | 0.0000 | 0.0000 | 0.0000 | 0.0000 | 0.0000 |
| PARP8 | 0.3500 | 0.6920 | 0.3850 | 0.0570 | 0.3040 | 0.3230 | 0.0000 | 0.0000 | 0.0000 | 0.7526 | 0.0000 | 0.0000 |
| PARP9 | 2.6670 | 3.2870 | 2.5290 | 2.1150 | 2.8350 | 2.4080 | 0.0000 | 0.0000 | 0.0000 | 0.0000 | 0.0000 | 0.0000 |
| PAX6 | 0.2560 | 0.4020 | -0.1280 | 0.0330 | 0.6460 | 0.4690 | 0.5618 | 0.4528 | 0.8661 | 0.9775 | 0.0229 | 0.1365 |
| PCDH21 | 0.0120 | 0.1340 | -0.0580 | 0.1250 | 0.3710 | 0.6650 | 0.9813 | 0.8549 | 0.9262 | 0.7798 | 0.0275 | 0.0001 |
| PCDHB14 | -2.3400 | -0.6970 | -0.8520 | 0.6640 | 0.1370 | 0.4120 | 0.0342 | 0.6797 | 0.5282 | 0.6823 | 0.8821 | 0.6427 |
| PCK2 | 0.2550 | 0.2510 | 0.2470 | 0.1850 | 0.5740 | 0.7970 | 0.1227 | 0.1477 | 0.1544 | 0.4371 | 0.0000 | 0.0000 |
| PCOLCE | 0.0950 | 0.0950 | 0.1190 | 0.3060 | 0.5840 | 0.4350 | 0.7434 | 0.8518 | 0.7476 | 0.3707 | 0.0003 | 0.0094 |
| PDE5A | 2.5690 | 2.4310 | 1.5360 | -0.6430 | -0.7410 | 0.1800 | 0.0338 | 0.0447 | 0.3308 | 0.6540 | 0.2444 | 0.8055 |
| PEX5L | 0.2940 | 0.9530 | 0.7650 | 0.1270 | 0.6420 | 0.5160 | 0.1390 | 0.0000 | 0.0000 | 0.8825 | 0.0204 | 0.0860 |

**Table 5. RNA-seq identification of DE genes in IFNβ-treated Jurkat or JLat9.2 cells** - *Page 6*

| | Log2 Fold Change (IFNβ - mock) | | | | | | Adjusted p Value (Benjamini-Hochberg FDR corrected) | | | | | |
|---|---|---|---|---|---|---|---|---|---|---|---|---|
| | Jurkat | | | JLat9.2 | | | Jurkat | | | JLat9.2 | | |
| GENE | 4h | 8h | 12h | 4h | 8h | 12h | 4h | 8h | 12h | 4h | 8h | 12h |
| PHF11 | 0.3960 | 0.9520 | 0.7200 | 0.4090 | 0.5730 | 0.7140 | 0.0004 | 0.0000 | 0.0000 | 0.0016 | 0.0000 | 0.0000 |
| PIK3IP1 | -0.2400 | 0.1050 | 0.5480 | -0.2740 | 1.1040 | 0.9930 | 0.7974 | 0.9547 | 0.5466 | 0.8856 | 0.0485 | 0.0997 |
| PLCD1 | 0.1810 | 0.2670 | 0.3370 | 0.3400 | 0.6920 | 0.6960 | 0.6787 | 0.6671 | 0.4766 | 0.5652 | 0.0054 | 0.0073 |
| PLEKHG3 | -1.1490 | -0.1740 | 0.1470 | 0.0020 | 0.0970 | 1.7290 | 0.1319 | 0.9087 | 0.8931 | 0.9990 | 0.9258 | 0.0130 |
| PLSCR1 | 1.7780 | 2.6840 | 2.0640 | 1.1820 | 1.7890 | 1.5570 | 0.0000 | 0.0000 | 0.0000 | 0.0000 | 0.0000 | 0.0000 |
| PLXNC1 | 0.2050 | 0.1670 | 0.1640 | 0.3670 | 0.8490 | 0.3360 | 0.5573 | 0.7845 | 0.7404 | 0.6397 | 0.0067 | 0.3874 |
| PML | 0.8700 | 0.8330 | 0.4460 | 0.6330 | 0.6960 | 0.3690 | 0.0000 | 0.0000 | 0.0000 | 0.0000 | 0.0000 | 0.0000 |
| PNPT1 | 0.3390 | 0.9790 | 0.6400 | 0.2250 | 0.3710 | 0.4190 | 0.0000 | 0.0000 | 0.0000 | 0.0295 | 0.0000 | 0.0000 |
| PPAPDC2 | 0.1210 | 0.1530 | 0.2690 | 0.2160 | 0.3660 | 0.6340 | 0.7462 | 0.7972 | 0.4956 | 0.6741 | 0.0850 | 0.0028 |
| PPM1K | 0.4220 | 0.7930 | 0.4060 | 0.2630 | 0.3630 | 0.4390 | 0.0000 | 0.0000 | 0.0000 | 0.0005 | 0.0000 | 0.0000 |
| PPP4R1L | 0.3190 | 0.1310 | -0.0390 | 0.5530 | 0.6110 | 1.2530 | 0.5443 | 0.9087 | 0.9706 | 0.6809 | 0.3005 | 0.0222 |
| PRDM1 | -0.3270 | -0.4500 | -0.1900 | 0.3830 | 0.3010 | 0.8570 | 0.4468 | 0.4079 | 0.7615 | 0.5969 | 0.3923 | 0.0064 |
| PRDM11 | 0.6090 | 0.2610 | 0.4080 | -0.2980 | -0.8490 | -0.3610 | 0.1003 | 0.6983 | 0.3814 | 0.7002 | 0.0147 | 0.3318 |
| PRG4 | -0.3020 | -0.4640 | -0.1060 | -0.3590 | -0.0130 | -2.0450 | 0.4055 | 0.2649 | 0.8584 | 0.8246 | 0.9873 | 0.0121 |
| PRIC285 | 3.6980 | 3.8290 | 2.8210 | 3.3460 | 3.5370 | 2.8020 | 0.0000 | 0.0000 | 0.0000 | 0.0000 | 0.0000 | 0.0000 |
| PRKD2 | 0.5260 | 0.5750 | 0.2800 | 0.3910 | 0.6410 | 0.3990 | 0.0000 | 0.0000 | 0.0000 | 0.0000 | 0.0000 | 0.0000 |
| PSD3 | 0.2180 | -0.7270 | -0.3520 | -0.3350 | -1.7130 | -0.5210 | 0.8501 | 0.6567 | 0.8235 | 0.8286 | 0.0152 | 0.4615 |
| PSMB9 | 0.3260 | 0.5300 | 0.4520 | 0.3670 | 0.6280 | 0.5840 | 0.0003 | 0.0000 | 0.0000 | 0.0180 | 0.0000 | 0.0000 |
| PTGER3 | -0.6040 | -0.8800 | -0.3600 | -0.2040 | -0.5410 | -0.1350 | 0.1041 | 0.0084 | 0.4179 | 0.7086 | 0.0234 | 0.6323 |
| RAB26 | -0.1150 | 0.0220 | 0.2320 | 0.1680 | 0.5810 | 0.5980 | 0.7771 | 0.9820 | 0.5868 | 0.8018 | 0.0144 | 0.0162 |
| RAB33A | -0.0220 | 0.4360 | 0.3030 | -0.0610 | 0.6020 | 0.8830 | 0.9711 | 0.3811 | 0.5757 | 0.9373 | 0.0063 | 0.0001 |
| RASGRP3 | 1.7680 | 3.0790 | 2.2640 | 1.4280 | 2.0900 | 1.6630 | 0.0000 | 0.0000 | 0.0000 | 0.0001 | 0.0000 | 0.0000 |
| RASSF4 | -0.1000 | -0.0750 | -0.0750 | 0.0050 | -0.0040 | 0.7220 | 0.7297 | 0.8915 | 0.8599 | 0.9952 | 0.9895 | 0.0005 |
| RBM43 | 0.5600 | 0.7930 | 0.4940 | 0.5550 | 0.5110 | 0.8100 | 0.0059 | 0.0000 | 0.0175 | 0.2590 | 0.0475 | 0.0017 |
| REC8 | 2.8140 | 2.6980 | 2.4650 | 2.6900 | 2.5430 | 2.2940 | 0.0000 | 0.0000 | 0.0000 | 0.0000 | 0.0000 | 0.0000 |
| RGL4 | 0.0300 | -0.1070 | -0.0410 | -0.0050 | -0.1940 | -0.6270 | 0.8765 | 0.6662 | 0.8760 | 0.9953 | 0.3704 | 0.0065 |
| RHBDL3 | 2.6970 | 2.2420 | 2.7840 | -0.0120 | -0.2920 | 0.2020 | 0.0259 | 0.0915 | 0.0139 | 0.9960 | 0.7314 | 0.8235 |
| RHEBL1 | 0.1530 | 0.1090 | -0.1490 | -0.1820 | 0.7740 | 1.0050 | 0.6602 | 0.8681 | 0.7676 | 0.8090 | 0.0020 | 0.0001 |
| RIMS4 | -0.3350 | -0.3870 | -0.8300 | 0.1140 | -0.0590 | -0.0510 | 0.3632 | 0.4108 | 0.0185 | 0.8272 | 0.8157 | 0.8579 |
| RN7SL2 | 0.2040 | 0.3250 | 0.4050 | 0.5500 | 0.5880 | 0.4660 | 0.5125 | 0.3620 | 0.1819 | 0.0781 | 0.0035 | 0.0292 |
| RNF213 | 0.7900 | 1.4120 | 1.0220 | 0.5140 | 0.9930 | 0.7790 | 0.0000 | 0.0000 | 0.0000 | 0.0000 | 0.0000 | 0.0000 |
| RNF31 | 0.7090 | 0.6270 | 0.5750 | 0.6900 | 0.7370 | 0.4820 | 0.0000 | 0.0000 | 0.0000 | 0.0000 | 0.0000 | 0.0000 |
| RSAD2 | 4.7290 | 5.1930 | 3.5150 | 3.4320 | 3.7610 | 2.6790 | 0.0000 | 0.0000 | 0.0000 | 0.0000 | 0.0000 | 0.0000 |
| RTP4 | 3.7700 | 3.8260 | 2.8410 | 1.3780 | 2.9820 | 0.6270 | 0.0000 | 0.0000 | 0.0003 | 0.5971 | 0.0098 | 0.6722 |
| RUNDC3A | -0.0490 | 0.3780 | 0.4560 | 0.6800 | 0.4540 | 0.9150 | 0.9576 | 0.7104 | 0.5626 | 0.4274 | 0.2883 | 0.0233 |
| SAMD9 | 1.9630 | 2.7990 | 2.1350 | 1.5460 | 1.8680 | 1.7580 | 0.0000 | 0.0000 | 0.0000 | 0.0000 | 0.0000 | 0.0000 |
| SAMD9L | 2.7240 | 3.5510 | 2.7860 | 2.3060 | 2.9640 | 2.6630 | 0.0000 | 0.0000 | 0.0000 | 0.0000 | 0.0000 | 0.0000 |
| SC4MOL | -0.1120 | 0.3160 | 0.4800 | -0.1570 | 0.0860 | 0.7530 | 0.5053 | 0.0158 | 0.0001 | 0.4986 | 0.4577 | 0.0000 |
| SCARNA16 | -0.0310 | 0.3160 | 0.2090 | -1.0990 | -0.7020 | -0.9890 | 0.9729 | 0.7907 | 0.8478 | 0.1975 | 0.1201 | 0.0435 |
| SCARNA7 | -1.2380 | 0.0000 | 0.2870 | 1.1440 | 1.0740 | 1.7220 | 0.2983 | 0.9999 | 0.8663 | 0.5348 | 0.2233 | 0.0405 |
| SCN3B | 0.3600 | 0.2610 | 0.0660 | 0.2380 | -0.3840 | -2.0200 | 0.3948 | 0.7178 | 0.9298 | 0.8327 | 0.4472 | 0.0009 |
| SERPINB9 | -0.0760 | 0.1670 | 0.3500 | 0.0770 | 0.5460 | 0.6950 | 0.8485 | 0.7519 | 0.2804 | 0.8984 | 0.0037 | 0.0003 |
| SHC4 | -0.7640 | 0.0000 | 0.5810 | -0.5820 | -0.6480 | -0.4930 | 0.4247 | 0.9999 | 0.5879 | 0.2263 | 0.0125 | 0.0666 |
| SHISA5 | 0.4990 | 0.8830 | 0.7500 | 0.3370 | 0.6230 | 0.5090 | 0.0000 | 0.0000 | 0.0000 | 0.0000 | 0.0000 | 0.0000 |
| SIDT1 | 0.9300 | 1.2930 | 0.9210 | 0.4460 | 0.8240 | 0.6590 | 0.0005 | 0.0000 | 0.0005 | 0.4838 | 0.0034 | 0.0290 |
| SIX3 | -0.0120 | -0.2770 | 0.2210 | 0.3730 | 0.6650 | 0.2950 | 0.9840 | 0.7309 | 0.7300 | 0.6540 | 0.0485 | 0.4884 |
| SLC16A6 | -0.0740 | -0.0220 | -0.1340 | -0.7120 | -1.2470 | -0.5830 | 0.9314 | 0.9903 | 0.9018 | 0.4629 | 0.0117 | 0.2402 |
| SLC17A9 | 0.0970 | -0.1470 | 0.1370 | -0.4640 | -1.6450 | -1.3140 | 0.8580 | 0.8752 | 0.8491 | 0.7305 | 0.0097 | 0.0409 |
| SLC18A2 | -0.1450 | -0.1920 | 0.3600 | 1.2190 | 1.1390 | 0.8380 | 0.8568 | 0.8915 | 0.6680 | 0.2590 | 0.0449 | 0.1886 |
| SLC25A27 | 0.2410 | 0.1850 | 0.0670 | 0.0230 | 0.5840 | 0.4860 | 0.6767 | 0.8623 | 0.9434 | 0.9838 | 0.0291 | 0.0970 |
| SLC29A2 | -0.0170 | 0.2850 | 0.3730 | -0.1250 | 0.3780 | 0.5900 | 0.9655 | 0.3791 | 0.1607 | 0.8612 | 0.1099 | 0.0128 |
| SLC37A4 | -0.2450 | 0.2870 | 0.4960 | 0.0880 | 1.0220 | 0.9310 | 0.7509 | 0.8036 | 0.5162 | 0.9613 | 0.0373 | 0.0772 |
| SLC44A5 | -0.0770 | -0.1720 | -0.1220 | -0.2480 | -0.7060 | -0.3920 | 0.8286 | 0.7286 | 0.7814 | 0.6863 | 0.0112 | 0.1724 |
| SLC6A9 | 0.6360 | 0.0380 | 0.0050 | 0.3000 | 0.6060 | 0.6850 | 0.3520 | 0.9859 | 0.9966 | 0.7190 | 0.0619 | 0.0418 |
| SLFN5 | 1.0480 | 1.4660 | 0.9540 | 0.7520 | 1.0590 | 0.8950 | 0.0000 | 0.0000 | 0.0000 | 0.0000 | 0.0000 | 0.0000 |
| SNIP | 0.7840 | 0.4580 | 0.3040 | 0.3760 | 0.2940 | 1.0600 | 0.1971 | 0.6644 | 0.7615 | 0.7104 | 0.5327 | 0.0079 |
| SNORA10 | -0.0570 | -0.1310 | -0.2030 | 0.8900 | 0.4140 | 0.3210 | 0.9080 | 0.8691 | 0.7233 | 0.0378 | 0.2106 | 0.3924 |
| SNORA23 | 0.0650 | -0.0090 | -0.1070 | 1.5370 | 1.0460 | 1.3340 | 0.9496 | 0.9973 | 0.9326 | 0.1267 | 0.1004 | 0.0387 |
| SNORA29 | -0.6650 | 0.1820 | -0.1450 | -0.5480 | -1.1890 | -0.3220 | 0.3749 | 0.9034 | 0.9040 | 0.5726 | 0.0117 | 0.5225 |
| SNORA32 | -0.3550 | -0.1620 | 0.1330 | -0.5390 | -0.8600 | -0.6870 | 0.4460 | 0.8605 | 0.8539 | 0.4018 | 0.0068 | 0.0354 |
| SNORA56 | 0.5610 | 0.4810 | 0.2940 | 1.1300 | 0.6990 | 1.0010 | 0.3446 | 0.5984 | 0.7515 | 0.1135 | 0.1326 | 0.0311 |
| SNORA63 | -0.5310 | 0.0360 | 0.0470 | -0.1870 | -0.7910 | -0.5630 | 0.2591 | 0.9785 | 0.9548 | 0.8184 | 0.0188 | 0.1097 |
| SNORA71C | 0.1870 | -0.0990 | 0.1050 | 1.0110 | 1.0520 | 0.4600 | 0.7908 | 0.9465 | 0.9173 | 0.3368 | 0.0384 | 0.4752 |
| SNORA73B | -0.2300 | -0.1620 | -0.2140 | -0.2250 | -1.2830 | -0.3700 | 0.7553 | 0.9074 | 0.8368 | 0.8476 | 0.0087 | 0.4704 |
| SNORD14B | -0.6360 | -0.5990 | -0.7420 | -0.6030 | -1.3770 | -0.6690 | 0.3135 | 0.4945 | 0.3201 | 0.5344 | 0.0051 | 0.1667 |
| SNORD34 | 0.0070 | 0.4430 | -0.1120 | -0.7990 | -1.1380 | -0.7160 | 0.9934 | 0.6608 | 0.9231 | 0.4641 | 0.0332 | 0.1977 |
| SNORD38A | -0.0730 | -0.5240 | -0.0930 | -0.4500 | -0.6710 | -1.1880 | 0.9321 | 0.6090 | 0.9326 | 0.6646 | 0.1429 | 0.0191 |
| SNORD45A | -0.8020 | -0.3080 | -0.3690 | -0.6670 | -0.6090 | -1.3720 | 0.1305 | 0.7214 | 0.5890 | 0.4354 | 0.1269 | 0.0028 |
| SNORD45B | -0.2370 | -0.1020 | -0.0680 | -0.8830 | -0.9300 | -0.9950 | 0.7499 | 0.9459 | 0.9531 | 0.3177 | 0.0345 | 0.0335 |
| SNORD80 | -0.2100 | -0.1100 | -0.0780 | -0.1240 | -0.7130 | -0.0010 | 0.7219 | 0.9245 | 0.9273 | 0.8960 | 0.0426 | 0.9992 |
| SNORD83A | -0.1890 | -0.1940 | -0.2790 | -0.1890 | -0.5390 | -1.7380 | 0.8304 | 0.9022 | 0.8096 | 0.8984 | 0.3252 | 0.0064 |
| SNTB1 | 0.3040 | 0.7230 | 0.4690 | 0.0710 | 0.3800 | 0.4560 | 0.1445 | 0.0000 | 0.0078 | 0.8219 | 0.0010 | 0.0001 |

**Table 5. RNA-seq identification of DE genes in IFNβ-treated Jurkat or JLat9.2 cells** - *Page 7*

| | Log2 Fold Change (IFNβ - mock) | | | | | | Adjusted p Value (Benjamini-Hochberg FDR corrected) | | | | | |
|---|---|---|---|---|---|---|---|---|---|---|---|---|
| | Jurkat | | | JLat9.2 | | | Jurkat | | | JLat9.2 | | |
| GENE | 4h | 8h | 12h | 4h | 8h | 12h | 4h | 8h | 12h | 4h | 8h | 12h |
| SOCS1 | 1.7210 | 0.8210 | 0.7400 | 3.3520 | 3.3610 | 1.9120 | 0.0010 | 0.3175 | 0.3758 | 0.0016 | 0.0002 | 0.0573 |
| SP100 | 1.1840 | 1.9580 | 1.5040 | 0.8160 | 1.4170 | 1.2220 | 0.0000 | 0.0000 | 0.0000 | 0.0000 | 0.0000 | 0.0000 |
| SP110 | 1.3480 | 2.0450 | 1.3850 | 1.0190 | 1.7110 | 1.2920 | 0.0000 | 0.0000 | 0.0000 | 0.0000 | 0.0000 | 0.0000 |
| SPINK2 | 0.0910 | -0.1610 | -0.4740 | 0.0580 | 0.9220 | 0.5850 | 0.7983 | 0.7719 | 0.1530 | 0.9734 | 0.0346 | 0.2466 |
| SPRY4 | 0.0310 | -0.0060 | -0.0550 | 1.0690 | 1.6850 | 1.2140 | 0.9612 | 0.9973 | 0.9456 | 0.4909 | 0.0139 | 0.1148 |
| SPTB | 0.3120 | 0.5300 | 0.3430 | 0.2720 | 0.5880 | 0.7940 | 0.5289 | 0.3260 | 0.5812 | 0.6061 | 0.0076 | 0.0004 |
| SPTLC3 | -0.2670 | 0.6240 | 0.7520 | 1.4310 | 1.5590 | 1.2140 | 0.8475 | 0.7083 | 0.5560 | 0.1392 | 0.0059 | 0.0484 |
| STAT1 | 2.4270 | 3.2540 | 2.6660 | 2.0720 | 2.6330 | 2.4010 | 0.0000 | 0.0000 | 0.0000 | 0.0000 | 0.0000 | 0.0000 |
| STAT2 | 1.4920 | 1.7910 | 0.9400 | 1.1580 | 1.7450 | 1.1980 | 0.0000 | 0.0000 | 0.0000 | 0.0000 | 0.0000 | 0.0000 |
| SYNM | 0.7340 | 1.6810 | 1.2200 | 0.0650 | 0.7060 | 0.4740 | 0.5624 | 0.1247 | 0.3610 | 0.9462 | 0.0104 | 0.1238 |
| TAGAP | 0.6950 | 0.5430 | 0.2740 | 0.3900 | 0.4100 | 0.4300 | 0.0000 | 0.0000 | 0.0074 | 0.0000 | 0.0000 | 0.0000 |
| TAP1 | 0.9150 | 1.3070 | 0.8200 | 0.5980 | 0.8140 | 0.5780 | 0.0000 | 0.0000 | 0.0000 | 0.0000 | 0.0000 | 0.0000 |
| TAP2 | 0.3200 | 0.6090 | 0.3970 | 0.2120 | 0.3290 | 0.2700 | 0.0000 | 0.0000 | 0.0000 | 0.0000 | 0.0000 | 0.0000 |
| TC2N | 0.1030 | 0.0010 | 0.4050 | -0.1230 | -1.2430 | 0.0400 | 0.8659 | 0.9994 | 0.4785 | 0.8812 | 0.0004 | 0.9231 |
| TDRD7 | 0.8590 | 1.3390 | 0.8260 | 0.5110 | 0.9290 | 0.8140 | 0.0000 | 0.0000 | 0.0000 | 0.0000 | 0.0000 | 0.0000 |
| TECTA | 0.3820 | 1.0530 | 0.6210 | 0.0270 | -0.0120 | -0.3670 | 0.5675 | 0.0440 | 0.3919 | 0.9856 | 0.9822 | 0.4465 |
| TLR3 | 0.8110 | 0.9590 | 0.7930 | 0.3590 | 0.2220 | 0.2000 | 0.0003 | 0.0000 | 0.0003 | 0.3786 | 0.2874 | 0.3878 |
| TLR9 | -0.3520 | -0.1580 | 0.2300 | -0.0380 | -0.1420 | -0.6790 | 0.5210 | 0.8874 | 0.7491 | 0.9546 | 0.5458 | 0.0051 |
| TM6SF1 | -0.0140 | 0.1420 | 0.1310 | 0.2140 | 0.2590 | 0.7430 | 0.9711 | 0.7697 | 0.7431 | 0.5752 | 0.1327 | 0.0000 |
| TMEM133 | 0.1350 | -0.2280 | -0.1810 | -0.5420 | -1.1180 | -0.4160 | 0.8059 | 0.7972 | 0.8121 | 0.4129 | 0.0015 | 0.2134 |
| TMEM140 | 2.5130 | 3.1300 | 1.9470 | 2.3250 | 2.1530 | 1.3940 | 0.0000 | 0.0000 | 0.0005 | 0.0191 | 0.0039 | 0.1015 |
| TMEM187 | 0.1440 | 0.5590 | 0.2500 | 0.3150 | 0.5850 | 0.8330 | 0.7445 | 0.1059 | 0.6230 | 0.7388 | 0.1152 | 0.0252 |
| TNFSF10 | 1.5320 | 1.5010 | 0.8990 | 0.7420 | 0.2620 | 0.3620 | 0.0000 | 0.0000 | 0.0000 | 0.0041 | 0.2572 | 0.1234 |
| TP53INP1 | 0.0190 | 0.1170 | 0.3310 | -0.1170 | 0.2450 | 0.5980 | 0.9629 | 0.8299 | 0.2634 | 0.8056 | 0.1584 | 0.0004 |
| TPM2 | 0.2720 | 0.3210 | 0.5080 | 0.1970 | 0.8810 | 0.5300 | 0.1879 | 0.1277 | 0.0025 | 0.6132 | 0.0000 | 0.0017 |
| TPPP | -0.9830 | -0.0640 | -0.0770 | 0.7270 | 1.3530 | 0.9380 | 0.3256 | 0.9820 | 0.9658 | 0.4849 | 0.0031 | 0.0615 |
| TRAF1 | -0.1120 | 0.0120 | 0.1640 | 0.6810 | 1.0140 | 0.7600 | 0.8182 | 0.9917 | 0.7736 | 0.3694 | 0.0036 | 0.0437 |
| TRIM14 | 0.5490 | 1.0510 | 0.8430 | 0.3540 | 0.7500 | 0.5330 | 0.0000 | 0.0000 | 0.0000 | 0.0000 | 0.0000 | 0.0000 |
| TRIM2 | -0.1120 | -0.3200 | -0.1480 | -0.1330 | -0.5950 | -0.3430 | 0.7326 | 0.3669 | 0.7234 | 0.7371 | 0.0008 | 0.0529 |
| TRIM21 | 1.6730 | 1.4750 | 0.6840 | 1.2410 | 1.1910 | 0.7520 | 0.0000 | 0.0000 | 0.0000 | 0.0000 | 0.0000 | 0.0000 |
| TRIM22 | 3.8600 | 5.8390 | 5.2510 | 3.4510 | 5.0220 | 4.5210 | 0.0000 | 0.0000 | 0.0000 | 0.0000 | 0.0000 | 0.0000 |
| TRIM25 | 1.3260 | 1.4770 | 0.9640 | 0.9630 | 1.0420 | 0.7460 | 0.0000 | 0.0000 | 0.0000 | 0.0000 | 0.0000 | 0.0000 |
| TRIM34 | 0.3980 | 0.5540 | 0.7330 | 1.1110 | 1.6380 | 1.6210 | 0.5184 | 0.4765 | 0.2287 | 0.4089 | 0.0065 | 0.0100 |
| TRIM38 | 0.7490 | 0.7570 | 0.4340 | 0.5170 | 0.5070 | 0.3090 | 0.0000 | 0.0000 | 0.0000 | 0.0000 | 0.0000 | 0.0000 |
| TRIM5 | 0.6120 | 1.1550 | 0.7220 | 0.3970 | 0.6640 | 0.5170 | 0.0000 | 0.0000 | 0.0000 | 0.0000 | 0.0000 | 0.0000 |
| TRIM56 | 0.7760 | 0.6710 | 0.3300 | 0.5500 | 0.5780 | 0.3480 | 0.0000 | 0.0000 | 0.0000 | 0.0000 | 0.0000 | 0.0000 |
| TRIM69 | 1.8550 | 2.5520 | 1.5780 | 0.7700 | 1.3490 | 1.0790 | 0.0001 | 0.0000 | 0.0012 | 0.1977 | 0.0000 | 0.0012 |
| TRPM4 | 0.3190 | 0.5460 | 0.6440 | 0.0460 | 0.7200 | 0.5140 | 0.7236 | 0.6499 | 0.4943 | 0.9728 | 0.0348 | 0.1792 |
| TSLP | -0.2230 | 0.0430 | 0.2480 | 0.0870 | 0.4280 | 0.7360 | 0.4495 | 0.9498 | 0.4536 | 0.8787 | 0.0224 | 0.0001 |
| TTC21A | 0.3790 | 0.6000 | 0.3920 | 0.2130 | 0.7280 | 0.6770 | 0.1463 | 0.0044 | 0.1524 | 0.6809 | 0.0004 | 0.0013 |
| TTC39B | 0.1780 | 0.9040 | 0.6630 | 0.2140 | 0.6270 | 0.6730 | 0.3385 | 0.0000 | 0.0000 | 0.4598 | 0.0000 | 0.0000 |
| TTLL9 | 0.7810 | 1.0910 | 1.2500 | 0.5470 | 1.3480 | 0.8650 | 0.3269 | 0.1812 | 0.0900 | 0.7590 | 0.0417 | 0.2598 |
| TUBA8 | -0.1640 | -0.1140 | -0.0660 | -0.3370 | -0.3360 | -0.6710 | 0.6379 | 0.8610 | 0.9018 | 0.4598 | 0.1204 | 0.0052 |
| TXLNB | -0.0210 | 0.2100 | -0.0820 | 0.0470 | 0.5570 | 0.8300 | 0.9629 | 0.6647 | 0.8781 | 0.9552 | 0.0206 | 0.0006 |
| UBA7 | 0.3720 | 0.7820 | 0.5390 | 0.1990 | 0.0350 | -0.2550 | 0.0444 | 0.0000 | 0.0005 | 0.8170 | 0.9376 | 0.5526 |
| UBE2L6 | 0.9920 | 1.5700 | 1.4130 | 0.5450 | 1.1390 | 1.1200 | 0.0000 | 0.0000 | 0.0000 | 0.0000 | 0.0000 | 0.0000 |
| UBE2S | 0.5290 | -0.1670 | 0.7050 | 0.1540 | 0.6780 | -0.2750 | 0.2110 | 0.8612 | 0.0838 | 0.8569 | 0.0199 | 0.4657 |
| UNC93B1 | 0.4220 | 0.8170 | 0.7780 | 0.3740 | 0.6680 | 0.5320 | 0.0745 | 0.0000 | 0.0000 | 0.3177 | 0.0003 | 0.0049 |
| USP18 | 1.5370 | 2.7550 | 2.2240 | 0.7260 | 1.7090 | 1.4520 | 0.0000 | 0.0000 | 0.0000 | 0.0000 | 0.0000 | 0.0000 |
| USP41 | 1.3460 | 2.5360 | 1.9590 | 0.6410 | 1.4020 | 1.2120 | 0.0000 | 0.0000 | 0.0000 | 0.0357 | 0.0000 | 0.0000 |
| UTRN | 0.1140 | 0.7280 | 0.5860 | 0.0490 | 0.3150 | 0.3040 | 0.1889 | 0.0000 | 0.0000 | 0.7642 | 0.0000 | 0.0000 |
| WDR78 | 0.1330 | 0.0970 | 0.2560 | -0.1050 | 0.0970 | 0.8400 | 0.8569 | 0.9448 | 0.7676 | 0.9254 | 0.8275 | 0.0133 |
| WTIP | 0.1690 | 0.3810 | 0.2800 | 0.3910 | 0.7460 | 0.0730 | 0.7691 | 0.5865 | 0.6814 | 0.6592 | 0.0355 | 0.8951 |
| XAF1 | 2.0470 | 2.5660 | 2.1370 | 1.7480 | 2.2600 | 2.0260 | 0.0000 | 0.0000 | 0.0000 | 0.0000 | 0.0000 | 0.0000 |
| ZBTB16 | -0.0940 | -0.2890 | -0.0360 | -1.9170 | -1.9590 | -1.3660 | 0.8289 | 0.5987 | 0.9562 | 0.2059 | 0.0183 | 0.1252 |
| ZCCHC2 | 1.0530 | 1.0960 | 0.5640 | 0.4690 | 0.4180 | 0.0960 | 0.0000 | 0.0000 | 0.0000 | 0.0000 | 0.0000 | 0.1238 |
| ZFHX3 | 0.0830 | -0.1650 | -0.0960 | -0.2490 | -0.2380 | -0.7580 | 0.7184 | 0.6013 | 0.7599 | 0.7140 | 0.4300 | 0.0182 |
| ZFP2 | 0.1850 | 0.5700 | 0.3900 | -0.3600 | -0.6210 | -0.9800 | 0.8630 | 0.6618 | 0.7532 | 0.7313 | 0.1733 | 0.0498 |
| ZMAT1 | 0.0610 | 0.2490 | 0.5920 | 0.2660 | 0.2480 | 0.5050 | 0.8833 | 0.5963 | 0.0222 | 0.5948 | 0.2880 | 0.0241 |
| ZMAT3 | -0.1800 | -0.6430 | -0.5830 | -0.3070 | -0.5110 | -0.6330 | 0.1642 | 0.0000 | 0.0000 | 0.0121 | 0.0000 | 0.0000 |
| ZNF117 | -0.2200 | 0.0090 | -0.0460 | -0.2300 | -0.6030 | -0.3120 | 0.2312 | 0.9859 | 0.8817 | 0.3870 | 0.0000 | 0.0203 |
| ZNF347 | 0.0000 | -0.1260 | -0.1090 | 0.8400 | -0.3850 | 0.8740 | 0.9991 | 0.6824 | 0.6857 | 0.2725 | 0.4448 | 0.0341 |
| ZNF425 | -0.2630 | -0.2520 | -0.1380 | -0.1240 | -0.3740 | -0.7110 | 0.4935 | 0.6746 | 0.8141 | 0.8782 | 0.2199 | 0.0300 |
| ZNF583 | -0.1390 | -0.2710 | -0.2350 | -0.1100 | -0.3480 | -0.5820 | 0.4809 | 0.1885 | 0.2767 | 0.7972 | 0.0415 | 0.0019 |
| ZNF606 | -0.1620 | 0.1290 | -0.0330 | -0.6590 | -1.6010 | -0.5900 | 0.8213 | 0.9192 | 0.9784 | 0.6257 | 0.0156 | 0.3796 |
| ZNF676 | -0.4520 | -0.2800 | -0.1630 | -0.5830 | -1.0230 | -0.2760 | 0.3135 | 0.7061 | 0.8174 | 0.4018 | 0.0037 | 0.4538 |
| ZNF728 | -0.5850 | -1.4840 | -0.1570 | -0.1700 | -0.2980 | 0.0550 | 0.4064 | 0.0366 | 0.8874 | 0.9135 | 0.6127 | 0.9390 |
| ZNF771 | 0.5410 | -0.0080 | 0.3540 | 0.4400 | 0.6930 | 0.4940 | 0.1980 | 0.9960 | 0.5400 | 0.5236 | 0.0227 | 0.1460 |
| ZNF98 | -0.6350 | -0.3640 | -0.0840 | -0.8890 | -0.8510 | -0.2950 | 0.2499 | 0.6811 | 0.9246 | 0.2140 | 0.0271 | 0.4851 |
| ZNF99 | -0.8430 | -0.3430 | -0.2120 | -0.3410 | -0.8370 | -0.5410 | 0.1850 | 0.7517 | 0.8304 | 0.7289 | 0.0489 | 0.2302 |
| ZNFX1 | 1.2480 | 0.8870 | 0.5020 | 0.8520 | 0.6300 | 0.2530 | 0.0000 | 0.0000 | 0.0000 | 0.0000 | 0.0000 | 0.0000 |

**Table 6. RNA-seq identification of DE genes in IFNγ-treated Jurkat or JLat9.2 cells**

| | Log2 Fold Change (IFNγ - mock) | | | | | | Adjusted p Value (Benjamini-Hochberg FDR corrected) | | | | | |
|---|---|---|---|---|---|---|---|---|---|---|---|---|
| | Jurkat | | | JLat9.2 | | | Jurkat | | | JLat9.2 | | |
| GENE | 4h | 8h | 12h | 4h | 8h | 12h | 4h | 8h | 12h | 4h | 8h | 12h |
| ABCA1 | -0.3130 | -0.1900 | 0.0670 | -0.2010 | -0.2610 | 1.0060 | 0.9063 | 0.8960 | 0.9534 | 0.8148 | 0.6228 | 0.0071 |
| ABTB2 | -0.7380 | -0.8630 | -0.9580 | -0.2090 | -0.6310 | -1.3450 | 0.0360 | 0.0048 | 0.0014 | 0.6917 | 0.0475 | 0.0002 |
| ACAT2 | 0.0260 | 0.2160 | 0.4160 | -0.0300 | 0.3500 | 0.6220 | 0.9312 | 0.0000 | 0.0000 | 0.7360 | 0.0000 | 0.0000 |
| ACSBG1 | 1.2310 | 0.3070 | 0.6570 | 1.3620 | 2.3450 | 1.6860 | 0.4625 | 0.9055 | 0.6340 | 0.3379 | 0.0129 | 0.0727 |
| AGBL2 | 0.3710 | 0.2250 | 0.3330 | -0.0170 | 0.5890 | 0.8010 | 0.5865 | 0.7113 | 0.4066 | 0.9825 | 0.0500 | 0.0047 |
| AK7 | 0.0660 | 0.4370 | 0.1310 | -0.4710 | 0.5000 | 0.7000 | 0.9888 | 0.5759 | 0.8845 | 0.3891 | 0.1155 | 0.0179 |
| AKAP2 | 0.2480 | 0.4490 | 0.3670 | 0.2740 | 0.6180 | 0.4300 | 0.4481 | 0.0055 | 0.0333 | 0.2627 | 0.0001 | 0.0063 |
| AKR1C3 | -0.2570 | -2.3150 | 0.3620 | -0.4490 | -0.3640 | 0.0830 | 0.9716 | 0.0373 | 0.8105 | 0.6775 | 0.6153 | 0.9124 |
| ALDOC | -0.0710 | 0.0890 | 0.2330 | 0.2200 | 0.4130 | 0.7740 | 0.9360 | 0.7782 | 0.1498 | 0.3275 | 0.0042 | 0.0000 |
| ALPK1 | 0.8440 | 1.6020 | 1.5720 | 0.8320 | 1.5260 | 1.8940 | 0.0221 | 0.0000 | 0.0000 | 0.0025 | 0.0000 | 0.0000 |
| AMICA1 | -0.4620 | -1.7140 | -0.5970 | -0.0200 | 0.3230 | 0.3280 | 0.8394 | 0.0254 | 0.4853 | 0.9806 | 0.3443 | 0.3298 |
| AMT | 0.1180 | 0.5870 | 0.2890 | 0.1370 | 0.6770 | 0.7080 | 0.9506 | 0.0576 | 0.4748 | 0.7641 | 0.0027 | 0.0014 |
| APC2 | 0.6220 | 0.5730 | 0.2130 | -0.8340 | -2.7320 | -0.6760 | 0.7977 | 0.6828 | 0.8833 | 0.5136 | 0.0022 | 0.4242 |
| APOBEC3F | 0.3050 | 0.6080 | 0.6050 | 0.3130 | 0.6650 | 0.9630 | 0.0411 | 0.0000 | 0.0000 | 0.0660 | 0.0000 | 0.0000 |
| APOBEC3G | 0.3500 | 0.6890 | 0.8430 | 0.1590 | 0.8960 | 1.1600 | 0.1198 | 0.0000 | 0.0000 | 0.6432 | 0.0000 | 0.0000 |
| APOL1 | 1.4750 | 2.0000 | 2.1320 | 2.3750 | 3.7320 | 4.0990 | 0.0000 | 0.0000 | 0.0000 | 0.0000 | 0.0000 | 0.0000 |
| APOL2 | 1.0250 | 1.1290 | 0.9780 | 1.1540 | 1.4470 | 1.2010 | 0.0000 | 0.0000 | 0.0000 | 0.0000 | 0.0000 | 0.0000 |
| APOL3 | 1.2190 | 1.5220 | 1.4660 | 1.5710 | 2.3260 | 2.3700 | 0.0000 | 0.0000 | 0.0000 | 0.0000 | 0.0000 | 0.0000 |
| APOL6 | 2.2390 | 2.4200 | 2.2900 | 2.7690 | 3.1610 | 3.0710 | 0.0000 | 0.0000 | 0.0000 | 0.0000 | 0.0000 | 0.0000 |
| APOLD1 | -0.3450 | 0.0000 | -0.3300 | 0.4490 | 0.3930 | 0.6560 | 0.5228 | 0.9990 | 0.3032 | 0.1162 | 0.0576 | 0.0008 |
| ARAP2 | 0.3480 | 0.5620 | 0.5280 | 0.3460 | 0.4840 | 0.7390 | 0.0000 | 0.0000 | 0.0000 | 0.0164 | 0.0000 | 0.0000 |
| ARID3B | -0.4400 | -0.7250 | -0.7180 | -0.4520 | -0.6540 | -0.8170 | 0.0000 | 0.0000 | 0.0000 | 0.0002 | 0.0000 | 0.0000 |
| ARL10 | 0.3730 | 0.0180 | 0.6430 | -0.0330 | -1.4520 | 2.6870 | 0.8980 | 0.9946 | 0.4176 | 0.9877 | 0.1447 | 0.0014 |
| ATF3 | 0.3020 | 0.2930 | 0.3050 | 0.5760 | 0.6690 | 0.6810 | 0.1112 | 0.0682 | 0.0449 | 0.0001 | 0.0000 | 0.0000 |
| ATF5 | -0.0640 | -0.1430 | -0.2380 | -0.0920 | -0.5200 | -0.6070 | 0.8391 | 0.1744 | 0.0037 | 0.4192 | 0.0000 | 0.0000 |
| ATP10A | 0.3910 | 0.5390 | 0.6900 | 0.2650 | 0.4950 | 0.4890 | 0.0024 | 0.0000 | 0.0000 | 0.0666 | 0.0000 | 0.0000 |
| ATP10D | -0.0410 | 0.3320 | -0.0050 | 1.1340 | 1.8760 | 0.6840 | 0.9961 | 0.8447 | 0.9986 | 0.3963 | 0.0224 | 0.4987 |
| ATP6AP1L | 0.3870 | 0.2700 | 0.3120 | 0.3690 | 0.2920 | 0.6420 | 0.6960 | 0.7154 | 0.5530 | 0.3817 | 0.3341 | 0.0137 |
| B2M | 0.3030 | 0.6420 | 0.9030 | 0.2680 | 0.6950 | 1.1250 | 0.0000 | 0.0000 | 0.0000 | 0.0000 | 0.0000 | 0.0000 |
| BATF | 0.3720 | 0.3400 | 0.5060 | 0.4370 | 0.6010 | 0.3870 | 0.1257 | 0.1118 | 0.0032 | 0.0251 | 0.0001 | 0.0093 |
| BATF3 | 0.7660 | 0.9480 | 1.0290 | 0.6910 | 0.9170 | 0.7280 | 0.0000 | 0.0000 | 0.0000 | 0.0000 | 0.0000 | 0.0000 |
| BCL2L2 | -0.0090 | -0.3780 | -0.3070 | 0.4380 | 0.4810 | 0.7580 | 0.9983 | 0.5078 | 0.5294 | 0.4321 | 0.1976 | 0.0250 |
| BCL6 | 2.2270 | 2.4760 | 2.3340 | 1.9320 | 2.2820 | 2.4140 | 0.0000 | 0.0000 | 0.0000 | 0.0000 | 0.0000 | 0.0000 |
| BHLHE23 | 0.1810 | -0.0080 | 0.2020 | 1.0520 | 0.9830 | 0.4690 | 0.9169 | 0.9954 | 0.7066 | 0.0881 | 0.0302 | 0.3658 |
| BST2 | 0.5560 | 1.3310 | 1.5550 | 0.5840 | 1.9130 | 2.2840 | 0.0000 | 0.0000 | 0.0000 | 0.0000 | 0.0000 | 0.0000 |
| BTG1 | 0.5000 | 0.4470 | 0.6980 | 0.2030 | 0.4110 | 0.5570 | 0.0000 | 0.0000 | 0.0000 | 0.0392 | 0.0000 | 0.0000 |
| BTN3A1 | 0.4150 | 0.6320 | 0.8060 | 0.3890 | 0.9440 | 1.1510 | 0.0000 | 0.0000 | 0.0000 | 0.0000 | 0.0000 | 0.0000 |
| BTN3A2 | 0.2480 | 0.4710 | 0.6180 | 0.3350 | 0.8290 | 0.9320 | 0.0000 | 0.0000 | 0.0000 | 0.0000 | 0.0000 | 0.0000 |
| BTN3A3 | 0.2320 | 0.5180 | 0.6600 | 0.3880 | 0.8050 | 1.0160 | 0.1400 | 0.0000 | 0.0000 | 0.0010 | 0.0000 | 0.0000 |
| C10orf75 | -0.5080 | 0.2300 | 0.2170 | 0.1900 | 0.9170 | 1.4980 | 0.3460 | 0.6506 | 0.5915 | 0.6339 | 0.0000 | 0.0000 |
| C11orf66 | 0.4360 | 0.3230 | -0.0280 | 0.3540 | 0.8150 | 0.4140 | 0.7343 | 0.7170 | 0.9801 | 0.5852 | 0.0254 | 0.3106 |
| C11orf71 | -0.2290 | 0.0000 | 0.0080 | 0.3010 | 0.7390 | 0.8460 | 0.7626 | 0.9992 | 0.9896 | 0.5174 | 0.0058 | 0.0012 |
| C14orf145 | 0.2660 | 0.7930 | 0.9270 | 0.1210 | 0.7980 | 1.0300 | 0.0001 | 0.0000 | 0.0000 | 0.2156 | 0.0000 | 0.0000 |
| C14orf181 | 0.2690 | 0.4180 | 0.4500 | 0.3800 | 0.3110 | 0.6320 | 0.8762 | 0.5134 | 0.3782 | 0.4674 | 0.3976 | 0.0448 |
| C14orf39 | -0.1380 | 0.1090 | -0.0840 | 0.1780 | 0.3310 | 0.7930 | 0.9244 | 0.8620 | 0.8597 | 0.7051 | 0.2259 | 0.0008 |
| C14orf83 | 0.7380 | 0.8760 | 0.8010 | 0.6700 | 0.7340 | 0.6900 | 0.0000 | 0.0000 | 0.0000 | 0.0000 | 0.0000 | 0.0000 |
| C14orf93 | 0.1010 | 0.1310 | -0.0600 | 0.1040 | 0.2170 | 0.5910 | 0.9399 | 0.7925 | 0.8934 | 0.7880 | 0.3152 | 0.0014 |
| C16orf75 | 0.1860 | 0.3430 | 0.4310 | 0.1910 | 0.5920 | 0.9570 | 0.5323 | 0.0139 | 0.0008 | 0.3252 | 0.0000 | 0.0000 |
| C17orf89 | 0.5600 | 0.2900 | 0.7680 | 0.2950 | 0.3530 | -0.2550 | 0.4064 | 0.6969 | 0.0384 | 0.5902 | 0.3143 | 0.5216 |
| C19orf71 | 0.2160 | 0.4590 | 0.2060 | 0.2490 | 0.5600 | 1.0960 | 0.9421 | 0.5990 | 0.8207 | 0.7581 | 0.2026 | 0.0044 |
| C1R | 0.5380 | 0.9580 | 1.0010 | 0.4300 | 1.0220 | 1.1740 | 0.4159 | 0.0036 | 0.0017 | 0.4632 | 0.0031 | 0.0005 |
| C1RL | -0.5270 | 0.0660 | 0.1620 | 0.1630 | 0.7430 | 0.8390 | 0.5711 | 0.9546 | 0.8069 | 0.5199 | 0.0000 | 0.0000 |
| C1orf203 | 0.0740 | 0.1330 | 0.1290 | 0.7360 | 0.9960 | 0.8990 | 0.9873 | 0.9193 | 0.8819 | 0.3068 | 0.0353 | 0.0565 |
| C1orf213 | -0.0210 | 0.1250 | 0.1130 | 0.7000 | 0.7270 | 0.7550 | 0.9930 | 0.8276 | 0.7993 | 0.0276 | 0.0027 | 0.0015 |
| C20orf201 | 0.0410 | 0.0270 | 0.6760 | -0.1270 | -0.0370 | -1.0300 | 0.9952 | 0.9886 | 0.3032 | 0.8904 | 0.9521 | 0.0357 |
| C20orf26 | 0.0130 | 0.2210 | -0.5590 | -0.2030 | -0.8110 | -1.5480 | 0.9994 | 0.8980 | 0.5858 | 0.8715 | 0.2398 | 0.0283 |
| C21orf119 | -0.0930 | 0.1690 | 0.1440 | 0.3470 | 0.6790 | 0.9340 | 0.9718 | 0.8160 | 0.7997 | 0.4200 | 0.0105 | 0.0003 |
| C22orf37 | 0.2040 | 0.0890 | 0.1460 | 0.3260 | 0.4490 | 0.7450 | 0.7265 | 0.8649 | 0.6373 | 0.3213 | 0.0365 | 0.0003 |
| C2CD2 | 0.5330 | 0.5370 | 0.5510 | 0.3420 | 0.7600 | 0.7970 | 0.0017 | 0.0008 | 0.0005 | 0.2448 | 0.0001 | 0.0000 |
| C4orf34 | -0.1270 | 0.1330 | 0.0530 | -0.0280 | 0.2370 | 0.5980 | 0.8172 | 0.6168 | 0.8477 | 0.9194 | 0.0523 | 0.0000 |
| C4orf48 | 1.1760 | 0.7280 | 1.4800 | 0.4990 | 0.9450 | 0.2360 | 0.1601 | 0.4671 | 0.0099 | 0.5815 | 0.0688 | 0.7286 |
| C5orf39 | 0.4670 | 0.4200 | 0.5090 | 0.7300 | 1.0050 | 0.9570 | 0.0012 | 0.0028 | 0.0001 | 0.0000 | 0.0000 | 0.0000 |
| C5orf41 | 0.7260 | 0.8720 | 0.9740 | 0.4650 | 0.8550 | 1.1910 | 0.0007 | 0.0000 | 0.0000 | 0.0392 | 0.0000 | 0.0000 |
| C5orf56 | 0.9380 | 1.0150 | 1.0050 | 1.3550 | 1.7410 | 1.7030 | 0.0000 | 0.0000 | 0.0000 | 0.0000 | 0.0000 | 0.0000 |
| C6orf138 | -1.5820 | -1.6030 | -1.6140 | -0.2480 | -0.6170 | -0.8910 | 0.4251 | 0.2576 | 0.2007 | 0.7330 | 0.1550 | 0.0393 |
| C6orf223 | 0.1650 | 0.4370 | 0.6620 | -0.0260 | 0.7030 | 0.9980 | 0.4676 | 0.0000 | 0.0000 | 0.9117 | 0.0000 | 0.0000 |
| C7orf29 | 0.6730 | 0.7250 | 0.7110 | 0.7690 | 0.7140 | 0.8200 | 0.0000 | 0.0000 | 0.0000 | 0.0000 | 0.0000 | 0.0000 |
| C7orf53 | -0.1270 | -0.4130 | -0.2800 | 0.5820 | 0.8160 | 0.3640 | 0.9724 | 0.6716 | 0.7394 | 0.3421 | 0.0406 | 0.4260 |
| C8orf85 | -0.1150 | -0.2460 | -0.1370 | -0.6610 | 0.3060 | 0.6920 | 0.9702 | 0.7790 | 0.8504 | 0.2377 | 0.4010 | 0.0244 |
| CABLES1 | -0.1320 | -0.1070 | -0.2440 | -0.3440 | -0.4720 | -0.8020 | 0.9768 | 0.9509 | 0.8057 | 0.3476 | 0.0581 | 0.0019 |
| CALCOCO2 | 0.1530 | 0.2870 | 0.2850 | 0.1210 | 0.5150 | 0.6090 | 0.0006 | 0.0000 | 0.0000 | 0.0359 | 0.0000 | 0.0000 |
| CAPN2 | -0.3080 | 0.2780 | -0.4620 | -0.9560 | -1.6480 | -0.9610 | 0.9429 | 0.8739 | 0.7047 | 0.4588 | 0.0496 | 0.2656 |

**Table 6. RNA-seq identification of DE genes in IFNγ-treated Jurkat or JLat9.2 cells** - *Page 2*

| | Log2 Fold Change (IFNγ - mock) | | | | | | Adjusted p Value (Benjamini-Hochberg FDR corrected) | | | | | |
|---|---|---|---|---|---|---|---|---|---|---|---|---|
| | Jurkat | | | JLat9.2 | | | Jurkat | | | JLat9.2 | | |
| GENE | 4h | 8h | 12h | 4h | 8h | 12h | 4h | 8h | 12h | 4h | 8h | 12h |
| CARD9 | 0.5880 | 0.7410 | 0.0350 | -0.1660 | -1.2050 | -1.3060 | 0.7370 | 0.3903 | 0.9819 | 0.8767 | 0.0402 | 0.0257 |
| CASP10 | 0.1030 | 0.0420 | 0.0250 | 0.3270 | 0.6600 | 0.5740 | 0.4689 | 0.7982 | 0.8550 | 0.0300 | 0.0000 | 0.0000 |
| CCDC102B | 0.1930 | 0.6580 | 0.4510 | 0.2290 | 0.4900 | 0.5720 | 0.7970 | 0.0008 | 0.0442 | 0.4022 | 0.0038 | 0.0006 |
| CCDC135 | -0.2470 | -0.1730 | 0.1570 | 0.7000 | 1.1640 | 1.2810 | 0.9558 | 0.9321 | 0.9029 | 0.5090 | 0.0684 | 0.0365 |
| CCDC7 | -0.2950 | -0.6020 | -0.4880 | -0.1160 | 0.3510 | 0.7130 | 0.8398 | 0.2799 | 0.3458 | 0.8793 | 0.3451 | 0.0264 |
| CCNG2 | -0.1330 | 0.1960 | 0.1250 | -0.1300 | 0.3410 | 0.8460 | 0.7513 | 0.2753 | 0.5021 | 0.4415 | 0.0009 | 0.0000 |
| CD244 | 0.1010 | 0.0300 | 0.0880 | -0.1480 | -0.7630 | -1.0850 | 0.9399 | 0.9669 | 0.8279 | 0.6502 | 0.0003 | 0.0000 |
| CD248 | -0.0660 | -0.1970 | -0.1870 | 0.0070 | -0.3600 | -0.6070 | 0.9716 | 0.6694 | 0.6003 | 0.9898 | 0.1705 | 0.0202 |
| CD274 | 1.9200 | 2.4540 | 2.0940 | 2.0140 | 3.0520 | 3.1270 | 0.0004 | 0.0000 | 0.0000 | 0.0027 | 0.0000 | 0.0000 |
| CD38 | 0.0770 | 0.3230 | 0.1710 | 0.1830 | 0.3800 | 0.7440 | 0.9484 | 0.1513 | 0.5174 | 0.5614 | 0.0407 | 0.0000 |
| CD48 | 0.1630 | 0.2980 | 0.3190 | 0.2720 | 0.7580 | 0.7980 | 0.0975 | 0.0000 | 0.0000 | 0.0295 | 0.0000 | 0.0000 |
| CD93 | -0.1720 | -0.5740 | -0.6790 | -0.0130 | -0.5520 | -1.2400 | 0.8980 | 0.1040 | 0.0360 | 0.9877 | 0.2085 | 0.0062 |
| CDGAP | 0.0810 | -0.2520 | -0.0930 | -0.0890 | -0.5910 | -0.3480 | 0.9479 | 0.4491 | 0.8029 | 0.7480 | 0.0003 | 0.0248 |
| CDH23 | 0.0630 | 0.0600 | -0.1460 | 1.5020 | 1.8860 | 2.5870 | 0.9907 | 0.9704 | 0.8860 | 0.2617 | 0.0321 | 0.0014 |
| CDKN1C | 0.4710 | 0.0070 | 0.0360 | 0.5870 | 0.7740 | 1.1920 | 0.7095 | 0.9967 | 0.9748 | 0.4192 | 0.1007 | 0.0056 |
| CDS1 | -2.7720 | -2.3020 | -1.1220 | -0.0140 | -0.4000 | 0.4610 | 0.0040 | 0.0152 | 0.3521 | 0.9895 | 0.5109 | 0.3706 |
| CEACAM1 | 1.3290 | 2.2290 | 2.4150 | 1.1210 | 2.5790 | 2.2710 | 0.0095 | 0.0000 | 0.0000 | 0.2377 | 0.0000 | 0.0001 |
| CEACAM21 | -0.0850 | 0.8700 | 0.0000 | 0.0560 | 0.4400 | 0.9840 | 0.9820 | 0.0281 | 0.9999 | 0.9428 | 0.2197 | 0.0015 |
| CEBPA | -0.1840 | -0.3270 | -0.0850 | -0.1640 | -0.1280 | -0.6140 | 0.8441 | 0.3728 | 0.8484 | 0.5668 | 0.5163 | 0.0009 |
| CEBPB | 0.4180 | 0.2700 | 0.8260 | 0.3160 | 0.4230 | 0.2060 | 0.4314 | 0.5932 | 0.0010 | 0.3992 | 0.0823 | 0.4516 |
| CECR4 | 0.4500 | 0.7970 | -0.1150 | 1.1930 | 1.0060 | 1.2730 | 0.8980 | 0.4908 | 0.9473 | 0.2172 | 0.1504 | 0.0499 |
| CFTR | -0.0360 | -0.5560 | -0.8290 | -0.1480 | -0.1510 | -0.0900 | 0.9920 | 0.2691 | 0.0433 | 0.5427 | 0.3515 | 0.5972 |
| CHAC1 | 0.1650 | 0.0190 | -0.1150 | 0.0780 | 0.1940 | 0.6140 | 0.9363 | 0.9849 | 0.8654 | 0.7896 | 0.2236 | 0.0000 |
| CHAT | 0.2130 | 0.2840 | 0.1080 | 0.6710 | 0.8210 | 1.2490 | 0.9595 | 0.8452 | 0.9359 | 0.4128 | 0.1278 | 0.0111 |
| CHI3L2 | -0.0050 | 0.1090 | 0.1980 | 0.0510 | 0.5350 | 0.8070 | 0.9920 | 0.0280 | 0.0000 | 0.4588 | 0.0000 | 0.0000 |
| CLEC2B | 0.6280 | 0.8610 | 0.6180 | 0.5760 | 1.0660 | 1.0840 | 0.0001 | 0.0000 | 0.0001 | 0.0008 | 0.0000 | 0.0000 |
| CLIC2 | 0.2890 | 0.6660 | 0.7150 | -0.1980 | 0.2040 | 0.6530 | 0.9221 | 0.3720 | 0.2514 | 0.7736 | 0.6197 | 0.0436 |
| CLYBL | -0.1080 | 0.0050 | 0.2880 | 0.1160 | 0.4300 | 0.6050 | 0.9524 | 0.9966 | 0.4126 | 0.8234 | 0.0984 | 0.0131 |
| CMPK2 | 0.6630 | 0.6830 | 0.6160 | 0.5350 | 0.7590 | 0.6700 | 0.0000 | 0.0000 | 0.0000 | 0.0000 | 0.0000 | 0.0000 |
| CMTM8 | 0.2370 | 0.2270 | 0.2690 | 0.4350 | 0.5990 | 0.4790 | 0.7768 | 0.6368 | 0.4386 | 0.0761 | 0.0007 | 0.0064 |
| CNPY1 | -2.6410 | -0.8230 | 0.2610 | 0.2660 | 0.4660 | 0.8820 | 0.0067 | 0.6098 | 0.8591 | 0.7989 | 0.4336 | 0.0839 |
| CPA4 | 0.0700 | -1.1840 | -1.7270 | -0.3620 | -0.4410 | -0.8620 | 0.9932 | 0.4149 | 0.1120 | 0.2389 | 0.0358 | 0.0002 |
| CPNE2 | -0.1630 | -0.4990 | -0.5820 | 0.2250 | 0.0690 | -0.1370 | 0.7970 | 0.0146 | 0.0030 | 0.2891 | 0.7020 | 0.4074 |
| CRIP2 | -0.2700 | -0.6290 | -0.6880 | -0.3300 | -0.8090 | -2.7650 | 0.9177 | 0.4244 | 0.3001 | 0.7688 | 0.2300 | 0.0010 |
| CTHRC1 | 0.0930 | -0.1470 | 0.2570 | 0.4690 | 0.1360 | 0.7140 | 0.9635 | 0.8238 | 0.4867 | 0.3631 | 0.7625 | 0.0272 |
| CTRL | 0.5800 | 0.7300 | 0.7150 | 0.8530 | 0.9980 | 0.7390 | 0.1627 | 0.0135 | 0.0141 | 0.0392 | 0.0012 | 0.0180 |
| CTSO | 0.5740 | 0.8690 | 0.6950 | 0.4770 | 1.0210 | 1.1990 | 0.5581 | 0.0674 | 0.1756 | 0.6339 | 0.0671 | 0.0235 |
| CUBN | -0.1940 | 0.0490 | -0.2310 | 0.3040 | 0.7110 | 0.2440 | 0.9360 | 0.9677 | 0.7297 | 0.5041 | 0.0073 | 0.4350 |
| CXCR3 | -0.0120 | -0.0010 | 0.0010 | 0.1650 | -0.9070 | -1.0730 | 0.9961 | 0.9988 | 0.9988 | 0.8082 | 0.0294 | 0.0112 |
| CYP1B1 | 1.4510 | 1.7050 | 1.9010 | 1.6790 | 2.0440 | 2.0570 | 0.0002 | 0.0000 | 0.0000 | 0.0000 | 0.0000 | 0.0000 |
| CYTH4 | 0.0600 | -1.5480 | -0.3790 | 0.6090 | -0.1040 | -0.7020 | 0.9920 | 0.0293 | 0.6729 | 0.4514 | 0.8930 | 0.2673 |
| DDX58 | 0.5020 | 0.6440 | 0.6660 | 0.6730 | 0.9560 | 0.9810 | 0.0000 | 0.0000 | 0.0000 | 0.0000 | 0.0000 | 0.0000 |
| DDX60 | 0.2330 | 0.6120 | 0.7440 | 0.3400 | 0.8740 | 1.4530 | 0.0989 | 0.0000 | 0.0000 | 0.0311 | 0.0000 | 0.0000 |
| DDX60L | 0.3020 | 0.4680 | 0.4320 | 0.2300 | 0.4690 | 0.7310 | 0.0423 | 0.0001 | 0.0002 | 0.2699 | 0.0006 | 0.0000 |
| DENND2D | 0.1660 | 0.1230 | 0.1250 | 0.4440 | 0.5130 | 0.6020 | 0.7604 | 0.7360 | 0.6458 | 0.3377 | 0.0977 | 0.0425 |
| DEPDC6 | -0.3630 | -1.4490 | -0.6110 | -0.0430 | -0.0850 | 0.2420 | 0.8381 | 0.0106 | 0.3321 | 0.9594 | 0.8674 | 0.5446 |
| DERL3 | 0.3280 | 0.5190 | 0.3600 | 0.7680 | 1.3730 | 1.3640 | 0.9020 | 0.5868 | 0.6830 | 0.3585 | 0.0084 | 0.0075 |
| DHX58 | 0.1690 | 0.4520 | 0.4750 | 0.3810 | 0.7350 | 0.7370 | 0.7827 | 0.0130 | 0.0065 | 0.1135 | 0.0000 | 0.0000 |
| DKFZP434I0714 | 0.4730 | 0.4800 | 0.5120 | 0.4320 | 0.4020 | 0.9250 | 0.0740 | 0.0330 | 0.0159 | 0.1417 | 0.0548 | 0.0000 |
| DLL3 | -0.0730 | -0.0310 | 0.1900 | 0.2120 | 0.0250 | -0.9650 | 0.9774 | 0.9750 | 0.6920 | 0.7842 | 0.9677 | 0.0432 |
| DLX3 | -0.1550 | -0.3970 | -0.1960 | -0.0090 | 0.2330 | -0.8080 | 0.9116 | 0.3278 | 0.6429 | 0.9898 | 0.5349 | 0.0298 |
| DNAH3 | 1.4920 | 2.6140 | 2.6340 | 3.6670 | 4.2150 | 5.0170 | 0.4251 | 0.0036 | 0.0027 | 0.0005 | 0.0000 | 0.0000 |
| DNAH6 | -0.0520 | 0.5070 | 0.3340 | -0.0100 | 1.6990 | 1.2950 | 0.9931 | 0.6448 | 0.7459 | 0.9954 | 0.0016 | 0.0177 |
| DNHD1 | 0.2140 | 0.2220 | 0.4640 | 0.0420 | 0.5990 | 0.6740 | 0.7385 | 0.5439 | 0.0335 | 0.9221 | 0.0009 | 0.0001 |
| DOCK9 | 0.1380 | 0.6590 | 0.5830 | 0.0130 | 0.5370 | 0.6410 | 0.4745 | 0.0000 | 0.0000 | 0.9422 | 0.0000 | 0.0000 |
| DOK3 | 0.2600 | 0.2860 | 0.1790 | -0.1090 | -0.2530 | -0.6060 | 0.5365 | 0.2875 | 0.5234 | 0.7213 | 0.1564 | 0.0009 |
| DPY19L2P4 | -0.8650 | -0.5240 | -1.7570 | -0.8770 | -0.7330 | -0.4200 | 0.4911 | 0.6238 | 0.0123 | 0.2992 | 0.2136 | 0.4810 |
| DTX1 | -0.0790 | -0.2060 | -0.1330 | -0.0570 | -0.4060 | -0.6020 | 0.5878 | 0.0008 | 0.0492 | 0.5230 | 0.0000 | 0.0000 |
| DTX3L | 1.4830 | 1.6900 | 1.5590 | 1.8640 | 2.2710 | 2.1540 | 0.0000 | 0.0000 | 0.0000 | 0.0000 | 0.0000 | 0.0000 |
| DUSP16 | 0.2840 | 0.7400 | 0.7220 | 0.2530 | 0.7730 | 0.8560 | 0.3194 | 0.0000 | 0.0000 | 0.0262 | 0.0000 | 0.0000 |
| EGLN3 | 0.4780 | 0.4920 | 0.6720 | 0.3290 | 0.7980 | 0.7050 | 0.6276 | 0.4192 | 0.1353 | 0.3715 | 0.0005 | 0.0016 |
| EIF4E3 | 0.3210 | 0.7050 | 0.7520 | 0.1820 | 0.2270 | 0.6280 | 0.3816 | 0.0001 | 0.0000 | 0.5707 | 0.2684 | 0.0004 |
| EML1 | 0.0010 | -0.6380 | -0.2730 | -0.1630 | -0.5560 | -0.8130 | 0.9994 | 0.1855 | 0.6138 | 0.7465 | 0.0580 | 0.0064 |
| ENPEP | 0.3650 | 0.9880 | 0.7400 | 1.0880 | 1.7250 | 2.3110 | 0.8370 | 0.0321 | 0.1536 | 0.3282 | 0.0143 | 0.0005 |
| EPAS1 | 0.1400 | 0.3340 | 0.4590 | 0.3120 | 0.5730 | 0.5860 | 0.8308 | 0.0902 | 0.0051 | 0.3282 | 0.0047 | 0.0033 |
| EPB41L4B | -0.0570 | -0.6420 | -0.5780 | -0.1380 | -0.5590 | -0.6750 | 0.9448 | 0.0000 | 0.0001 | 0.3350 | 0.0000 | 0.0000 |
| EPSTI1 | 1.1600 | 2.6950 | 3.1480 | 0.9400 | 3.0330 | 3.7130 | 0.0000 | 0.0000 | 0.0000 | 0.0002 | 0.0000 | 0.0000 |
| ERAP1 | 0.2650 | 0.4900 | 0.5220 | 0.3040 | 0.6630 | 0.8150 | 0.0000 | 0.0000 | 0.0000 | 0.0000 | 0.0000 | 0.0000 |
| ERAP2 | 0.3750 | 0.6950 | 0.7680 | 0.3540 | 0.8650 | 1.0330 | 0.0000 | 0.0000 | 0.0000 | 0.0000 | 0.0000 | 0.0000 |
| ETV5 | -0.0850 | 0.1390 | 0.2120 | 0.4480 | 0.8260 | 1.1290 | 0.9616 | 0.7929 | 0.5210 | 0.2343 | 0.0007 | 0.0000 |
| EVI1 | -0.8000 | -1.0810 | 0.4960 | 0.3650 | 0.3950 | 1.0720 | 0.7951 | 0.4434 | 0.7106 | 0.7292 | 0.5577 | 0.0437 |
| EXPH5 | 0.0180 | 0.2270 | 0.3940 | -0.0770 | 0.2570 | 0.8940 | 0.9978 | 0.8112 | 0.4775 | 0.9108 | 0.4459 | 0.0010 |

**Table 6. RNA-seq identification of DE genes in IFNγ-treated Jurkat or JLat9.2 cells** - *Page 3*

| | Log2 Fold Change (IFNγ - mock) | | | | | | Adjusted p Value (Benjamini-Hochberg FDR corrected) | | | | | |
|---|---|---|---|---|---|---|---|---|---|---|---|---|
| | Jurkat | | | JLat9.2 | | | Jurkat | | | JLat9.2 | | |
| GENE | 4h | 8h | 12h | 4h | 8h | 12h | 4h | 8h | 12h | 4h | 8h | 12h |
| F2RL2 | -0.0010 | -0.1720 | -0.1050 | -0.1330 | -0.9720 | -0.3940 | 0.9994 | 0.5246 | 0.6810 | 0.7975 | 0.0017 | 0.1752 |
| FAM122C | 0.2620 | 0.3590 | 0.3690 | 0.4710 | 0.5750 | 0.7840 | 0.6026 | 0.1747 | 0.1210 | 0.0873 | 0.0034 | 0.0000 |
| FAM176B | 1.0100 | 0.5490 | 0.9780 | 0.3570 | 0.5820 | 1.2580 | 0.5239 | 0.7360 | 0.3035 | 0.7687 | 0.4056 | 0.0307 |
| FAR2 | 0.2670 | 0.0420 | 0.3450 | -0.0060 | 0.4770 | 0.6380 | 0.6428 | 0.9552 | 0.2000 | 0.9926 | 0.0678 | 0.0099 |
| FAT3 | -0.2860 | 0.1740 | -0.5510 | -0.6910 | -1.2130 | -2.4680 | 0.9244 | 0.9003 | 0.4771 | 0.5924 | 0.1528 | 0.0020 |
| FBXL13 | -0.2320 | -0.2300 | -0.2380 | -0.0970 | -0.7260 | -0.3350 | 0.9266 | 0.8238 | 0.7574 | 0.8908 | 0.0500 | 0.3730 |
| FBXO32 | 0.0970 | 0.0380 | 0.3260 | 0.0320 | 0.6790 | 0.6550 | 0.9702 | 0.9705 | 0.4342 | 0.9559 | 0.0026 | 0.0033 |
| FBXO39 | 1.0650 | 1.5860 | 1.6210 | 1.7360 | 1.6970 | 1.8340 | 0.0624 | 0.0002 | 0.0001 | 0.0028 | 0.0006 | 0.0001 |
| FDFT1 | 0.0130 | 0.2170 | 0.3370 | 0.0230 | 0.4950 | 0.6520 | 0.9702 | 0.0000 | 0.0000 | 0.7409 | 0.0000 | 0.0000 |
| FDPSL2A | -0.1640 | 0.1160 | 0.0890 | 0.1850 | 0.3870 | 0.7170 | 0.9182 | 0.8743 | 0.8673 | 0.7007 | 0.1523 | 0.0033 |
| FER1L4 | -0.0280 | -1.3220 | 0.1830 | -0.0780 | 0.3530 | 0.8490 | 0.9978 | 0.3280 | 0.9106 | 0.9333 | 0.4322 | 0.0224 |
| FLJ10038 | 0.2390 | 0.3880 | 0.5000 | 0.3200 | 0.6290 | 0.8450 | 0.5982 | 0.0661 | 0.0062 | 0.2030 | 0.0002 | 0.0000 |
| FLJ32255 | 0.8400 | 0.7190 | 1.0990 | 0.7000 | 0.8400 | 1.0190 | 0.0010 | 0.0048 | 0.0000 | 0.0602 | 0.0020 | 0.0001 |
| FLJ35776 | 0.1140 | 0.2910 | 0.0920 | 0.1950 | 0.5140 | 0.8750 | 0.9812 | 0.8071 | 0.9367 | 0.8341 | 0.2940 | 0.0426 |
| FLJ40125 | -0.4360 | 0.1140 | -0.0580 | 0.6630 | 0.3970 | 0.8580 | 0.7625 | 0.9298 | 0.9534 | 0.3062 | 0.4286 | 0.0414 |
| FLJ45244 | -0.1720 | 0.1860 | -0.1790 | 0.1780 | 0.6260 | 0.7390 | 0.9506 | 0.8604 | 0.8218 | 0.7915 | 0.0638 | 0.0226 |
| FLJ45248 | 1.0760 | 1.2190 | 1.2810 | 1.2290 | 1.4630 | 1.5820 | 0.0000 | 0.0000 | 0.0000 | 0.0000 | 0.0000 | 0.0000 |
| FLJ45422 | 0.2980 | 0.6420 | 0.8690 | 0.2510 | 0.5870 | 1.0260 | 0.5624 | 0.0028 | 0.0000 | 0.4068 | 0.0016 | 0.0000 |
| FLT3LG | 0.5530 | 0.5920 | 0.6530 | 0.2890 | 0.4250 | 0.4650 | 0.0037 | 0.0007 | 0.0001 | 0.2645 | 0.0127 | 0.0053 |
| FOXD1 | -0.3270 | -0.7590 | -0.8240 | -0.3140 | -1.0310 | -0.9960 | 0.8975 | 0.3526 | 0.2385 | 0.6818 | 0.0330 | 0.0356 |
| FRMPD4 | -0.1120 | -0.1210 | -0.1030 | -0.3760 | -0.3170 | -0.8590 | 0.8867 | 0.7316 | 0.7158 | 0.5310 | 0.4350 | 0.0269 |
| FZD5 | 2.0180 | 2.1000 | 1.9910 | 1.3790 | 1.3360 | 1.4160 | 0.0000 | 0.0000 | 0.0000 | 0.0000 | 0.0000 | 0.0000 |
| GABRB2 | 0.9550 | 0.9530 | 0.2350 | 0.3370 | 0.5650 | 0.6540 | 0.2269 | 0.1266 | 0.8189 | 0.3782 | 0.0197 | 0.0052 |
| GADD45B | 0.6140 | 0.5790 | 0.5420 | 0.7890 | 0.8170 | 0.5300 | 0.0007 | 0.0009 | 0.0019 | 0.0000 | 0.0000 | 0.0003 |
| GALT | 0.1640 | 0.1960 | 0.3280 | 0.1790 | 0.6160 | 0.5770 | 0.6848 | 0.3683 | 0.0315 | 0.4317 | 0.0000 | 0.0000 |
| GBP1 | 1.9300 | 3.1410 | 3.2680 | 2.3330 | 4.1360 | 4.4580 | 0.0000 | 0.0000 | 0.0000 | 0.0000 | 0.0000 | 0.0000 |
| GBP2 | 3.7130 | 5.5480 | 6.0440 | 3.7390 | 5.9220 | 6.5710 | 0.0000 | 0.0000 | 0.0000 | 0.0000 | 0.0000 | 0.0000 |
| GBP3 | 1.5590 | 1.7400 | 1.6880 | 1.6900 | 2.3690 | 2.1880 | 0.0000 | 0.0000 | 0.0000 | 0.0000 | 0.0000 | 0.0000 |
| GBP4 | 3.7330 | 5.3770 | 5.8140 | 2.7810 | 6.4330 | 7.6140 | 0.0000 | 0.0000 | 0.0000 | 0.0062 | 0.0000 | 0.0000 |
| GBP5 | 1.7480 | 3.1760 | 3.2940 | 3.4550 | 5.7070 | 6.5140 | 0.0000 | 0.0000 | 0.0000 | 0.0000 | 0.0000 | 0.0000 |
| GCET2 | 0.2420 | 0.2230 | 0.1590 | 0.2120 | 0.2080 | 0.6760 | 0.5431 | 0.4280 | 0.5547 | 0.7167 | 0.5853 | 0.0249 |
| GEFT | 0.3260 | 0.2550 | 0.7220 | 0.2570 | 0.5870 | 0.6940 | 0.8724 | 0.8176 | 0.1717 | 0.6392 | 0.0547 | 0.0180 |
| GIMAP2 | 0.4810 | 0.4610 | 0.3720 | 0.7150 | 1.0030 | 1.0740 | 0.0000 | 0.0000 | 0.0000 | 0.0000 | 0.0000 | 0.0000 |
| GLDC | 0.5630 | 0.7300 | 0.7410 | 0.2900 | 0.4390 | 0.5880 | 0.0000 | 0.0000 | 0.0000 | 0.0881 | 0.0003 | 0.0000 |
| GLIS2 | -0.4400 | -0.5770 | -0.3160 | -0.3720 | -0.8180 | -0.4090 | 0.6192 | 0.2509 | 0.5359 | 0.4995 | 0.0263 | 0.2590 |
| GNG10 | -0.0580 | -0.1110 | 0.0620 | -0.0780 | 0.1520 | 0.5960 | 0.9820 | 0.8875 | 0.9148 | 0.8904 | 0.6218 | 0.0128 |
| GNRHR2 | 0.6320 | 0.4000 | 0.3830 | 0.3470 | 0.3850 | 0.7080 | 0.4133 | 0.5968 | 0.5256 | 0.5864 | 0.3506 | 0.0493 |
| GPR113 | 0.4090 | 0.5030 | 0.5530 | 0.4300 | 0.7760 | 0.8290 | 0.2212 | 0.0293 | 0.0101 | 0.1721 | 0.0002 | 0.0001 |
| GPR17 | 0.1030 | 0.0100 | -0.0960 | 0.1780 | -1.0760 | -0.9190 | 0.9671 | 0.9943 | 0.8842 | 0.6195 | 0.0001 | 0.0003 |
| GPR19 | 0.8700 | 1.1250 | 0.6590 | 0.4250 | 0.6040 | 0.7890 | 0.5079 | 0.1240 | 0.4519 | 0.5332 | 0.1535 | 0.0454 |
| GPR81 | 1.2700 | 1.3930 | 1.8260 | -0.2230 | 1.4230 | 0.8000 | 0.1601 | 0.0432 | 0.0019 | 0.9163 | 0.1445 | 0.4576 |
| GRID2IP | 0.1410 | 0.9970 | 0.6240 | 0.1970 | 1.0590 | 0.9060 | 0.9855 | 0.3324 | 0.5700 | 0.8505 | 0.0254 | 0.0576 |
| GSDMD | 0.2180 | 0.4210 | 0.4640 | 0.4270 | 0.8210 | 0.7920 | 0.2083 | 0.0001 | 0.0000 | 0.0012 | 0.0000 | 0.0000 |
| GTF2IRD2 | 0.0260 | 0.1870 | 0.4270 | -0.6720 | -0.2730 | -1.0280 | 0.9974 | 0.9059 | 0.6075 | 0.3745 | 0.6250 | 0.0463 |
| GVIN1 | 0.6830 | 0.8650 | 0.7790 | 1.0310 | 1.8240 | 1.8620 | 0.0000 | 0.0000 | 0.0000 | 0.0000 | 0.0000 | 0.0000 |
| GZMM | 0.1570 | 0.2440 | 0.2970 | 0.0410 | -0.2960 | -0.7480 | 0.9635 | 0.8169 | 0.6812 | 0.9502 | 0.3890 | 0.0241 |
| H1F0 | -0.0260 | 0.0990 | 0.1430 | 0.1090 | 0.3830 | 0.5810 | 0.9639 | 0.3728 | 0.0828 | 0.2108 | 0.0000 | 0.0000 |
| H2AFY2 | 0.2030 | -0.2320 | -0.5630 | 0.0400 | -0.2190 | -0.7290 | 0.9399 | 0.8410 | 0.4065 | 0.9284 | 0.3401 | 0.0014 |
| HAPLN3 | 3.4570 | 4.1670 | 4.0730 | 3.3090 | 4.0800 | 4.1990 | 0.0000 | 0.0000 | 0.0000 | 0.0000 | 0.0000 | 0.0000 |
| HAS3 | -0.0180 | -0.3190 | -0.3090 | -0.1240 | -0.3880 | -0.6320 | 0.9931 | 0.3530 | 0.3032 | 0.6614 | 0.0216 | 0.0003 |
| HBEGF | 0.0670 | -0.2050 | -0.4450 | -0.3620 | -0.3070 | -0.7440 | 0.9413 | 0.3955 | 0.0084 | 0.0213 | 0.0109 | 0.0000 |
| HBP1 | 0.0070 | 0.2170 | 0.1210 | 0.0220 | 0.4190 | 0.7100 | 0.9974 | 0.1991 | 0.5213 | 0.9282 | 0.0001 | 0.0000 |
| HCG27 | 0.6950 | 0.4630 | 0.5670 | 0.5910 | 0.9220 | 1.4530 | 0.3154 | 0.5073 | 0.2781 | 0.2841 | 0.0097 | 0.0000 |
| HCP5 | 1.8940 | 2.2180 | 2.8850 | -0.8100 | 0.3050 | 1.0360 | 0.2877 | 0.0620 | 0.0037 | 0.5542 | 0.7381 | 0.1301 |
| HDAC6 | -0.0080 | 0.0640 | 0.1420 | 0.1950 | 0.4990 | 0.6570 | 0.9921 | 0.6726 | 0.1004 | 0.0466 | 0.0000 | 0.0000 |
| HELB | 0.8810 | 0.8820 | 0.7180 | 0.6540 | 0.7490 | 0.9060 | 0.0000 | 0.0000 | 0.0000 | 0.0000 | 0.0000 | 0.0000 |
| HEPACAM | -0.4640 | -0.6470 | 0.1620 | -0.3640 | -0.6770 | -0.6710 | 0.5181 | 0.1220 | 0.7596 | 0.4206 | 0.0272 | 0.0267 |
| HES1 | -0.9550 | -1.3430 | -1.3080 | -1.1310 | -2.0180 | -1.7770 | 0.0000 | 0.0000 | 0.0000 | 0.0952 | 0.0004 | 0.0009 |
| HIST1H2AJ | -0.3000 | -0.4330 | -1.5040 | -0.2500 | -0.4100 | -0.4920 | 0.9311 | 0.7213 | 0.0399 | 0.8196 | 0.5434 | 0.4438 |
| HIST1H2AM | -0.1810 | 0.0230 | -0.7950 | 0.0030 | -0.5620 | -0.5710 | 0.9244 | 0.9815 | 0.0451 | 0.9960 | 0.0657 | 0.0581 |
| HIVEP3 | 0.4370 | 0.6640 | 0.7610 | 0.6660 | 0.9660 | 0.9040 | 0.0000 | 0.0000 | 0.0000 | 0.0000 | 0.0000 | 0.0000 |
| HKDC1 | 0.2420 | 0.3670 | 0.6610 | 0.1540 | 0.8320 | 0.7940 | 0.6744 | 0.1679 | 0.0006 | 0.6835 | 0.0000 | 0.0001 |
| HLA-A | -0.0310 | 0.2200 | 0.6460 | 0.0610 | 0.3780 | 0.8180 | 0.9376 | 0.0003 | 0.0000 | 0.5248 | 0.0000 | 0.0000 |
| HLA-B | 0.1470 | 0.7590 | 1.4640 | 0.2720 | 1.0400 | 1.8890 | 0.1076 | 0.0000 | 0.0000 | 0.0004 | 0.0000 | 0.0000 |
| HLA-C | 0.0560 | 0.4180 | 0.9360 | 0.2240 | 0.7010 | 1.1690 | 0.8244 | 0.0000 | 0.0000 | 0.0028 | 0.0000 | 0.0000 |
| HLA-DOB | 0.5110 | 0.6100 | 0.7720 | 0.8580 | 1.2310 | 1.0010 | 0.2542 | 0.0456 | 0.0039 | 0.0098 | 0.0000 | 0.0001 |
| HLA-E | 1.6110 | 2.0190 | 2.0490 | 1.9850 | 2.4150 | 2.5300 | 0.0000 | 0.0000 | 0.0000 | 0.0000 | 0.0000 | 0.0000 |
| HLA-F | 0.0480 | 0.7590 | 1.3990 | 0.0740 | 0.7280 | 1.6210 | 0.9774 | 0.0000 | 0.0000 | 0.8429 | 0.0000 | 0.0000 |
| HLA-G | 0.6210 | 0.9790 | 1.4520 | 0.8300 | 1.1930 | 1.5350 | 0.0048 | 0.0000 | 0.0000 | 0.0003 | 0.0000 | 0.0000 |
| HLA-J | 0.3430 | 1.0070 | 1.2110 | 0.2180 | 0.4400 | 1.3100 | 0.8197 | 0.0102 | 0.0008 | 0.7560 | 0.2627 | 0.0001 |
| HMGCS1 | 0.0530 | 0.5110 | 0.5430 | -0.0110 | 0.6150 | 1.0460 | 0.8008 | 0.0000 | 0.0000 | 0.9329 | 0.0000 | 0.0000 |
| HOTAIR | 0.6150 | 0.2780 | 1.0040 | 0.9460 | 0.8170 | 1.1870 | 0.8308 | 0.9003 | 0.2842 | 0.2019 | 0.1227 | 0.0146 |

**Table 6. RNA-seq identification of DE genes in IFNγ-treated Jurkat or JLat9.2 cells** - *Page 4*

| | Log2 Fold Change (IFNγ - mock) | | | | | | Adjusted p Value (Benjamini-Hochberg FDR corrected) | | | | | |
|---|---|---|---|---|---|---|---|---|---|---|---|---|
| | Jurkat | | | JLat9.2 | | | Jurkat | | | JLat9.2 | | |
| GENE | 4h | 8h | 12h | 4h | 8h | 12h | 4h | 8h | 12h | 4h | 8h | 12h |
| HOXA3 | -0.1570 | -0.0290 | -0.3410 | -0.2600 | -0.2220 | -0.5850 | 0.9139 | 0.9731 | 0.3711 | 0.3893 | 0.2858 | 0.0042 |
| ICAM1 | 3.4010 | 3.8820 | 3.7970 | 2.9380 | 3.5150 | 3.5510 | 0.0000 | 0.0000 | 0.0000 | 0.0000 | 0.0000 | 0.0000 |
| ICOS | -0.1180 | -0.0870 | -0.1170 | 0.4190 | 1.0160 | 1.5170 | 0.9815 | 0.9627 | 0.9222 | 0.7152 | 0.0992 | 0.0068 |
| ID1 | -0.0240 | -0.1040 | -0.0710 | -0.1470 | -0.0990 | -0.7920 | 0.9924 | 0.8740 | 0.8839 | 0.5594 | 0.5783 | 0.0000 |
| IFI30 | 0.3170 | 0.7780 | 0.9350 | 0.3570 | 0.9360 | 1.0310 | 0.1336 | 0.0000 | 0.0000 | 0.0544 | 0.0000 | 0.0000 |
| IFI35 | 0.7800 | 1.5770 | 1.8230 | 0.6440 | 1.4410 | 1.7740 | 0.0001 | 0.0000 | 0.0000 | 0.0343 | 0.0000 | 0.0000 |
| IFI44 | 0.6060 | 0.9040 | 0.9980 | 0.4880 | 1.0880 | 1.5440 | 0.0015 | 0.0000 | 0.0000 | 0.0466 | 0.0000 | 0.0000 |
| IFI44L | 0.0590 | 3.9240 | 3.4490 | 0.3050 | 3.2350 | 4.5380 | 0.9978 | 0.0043 | 0.0200 | 0.9229 | 0.0064 | 0.0000 |
| IFI6 | 0.3710 | 0.8900 | 1.2970 | 0.3830 | 1.2330 | 1.5470 | 0.0052 | 0.0000 | 0.0000 | 0.0207 | 0.0000 | 0.0000 |
| IFIH1 | 0.6120 | 1.0840 | 1.1240 | 0.8330 | 1.5600 | 1.7050 | 0.0000 | 0.0000 | 0.0000 | 0.0000 | 0.0000 | 0.0000 |
| IFIT1 | 1.0970 | 1.3140 | 1.1140 | 0.8420 | 1.2790 | 1.2730 | 0.0000 | 0.0000 | 0.0000 | 0.0148 | 0.0000 | 0.0000 |
| IFIT2 | 1.2190 | 1.3000 | 1.2410 | 1.3790 | 1.8450 | 1.8010 | 0.0000 | 0.0000 | 0.0000 | 0.0000 | 0.0000 | 0.0000 |
| IFIT3 | 2.0960 | 2.8200 | 2.8220 | 3.2540 | 4.8340 | 5.1100 | 0.0000 | 0.0000 | 0.0000 | 0.0000 | 0.0000 | 0.0000 |
| IFIT5 | 0.6880 | 0.6870 | 0.5580 | 0.6720 | 0.8230 | 0.7160 | 0.0000 | 0.0000 | 0.0000 | 0.0000 | 0.0000 | 0.0000 |
| IFITM1 | 0.3580 | 0.9980 | 1.3410 | 0.3810 | 1.0350 | 1.4500 | 0.0087 | 0.0000 | 0.0000 | 0.0029 | 0.0000 | 0.0000 |
| IFITM3 | 0.4410 | 0.4810 | 0.7090 | -0.1070 | 0.4930 | 0.2270 | 0.3662 | 0.1497 | 0.0059 | 0.8521 | 0.0620 | 0.4485 |
| IL10RA | 0.1820 | 0.3210 | 0.5820 | 0.4060 | 0.7640 | 1.0140 | 0.8980 | 0.5003 | 0.0526 | 0.2937 | 0.0020 | 0.0000 |
| IL12RB1 | 0.5500 | 0.9360 | 1.2680 | 1.5610 | 2.6320 | 2.9300 | 0.0360 | 0.0000 | 0.0000 | 0.0771 | 0.0000 | 0.0000 |
| IL15 | 1.2040 | 1.3430 | 1.3150 | 1.2180 | 2.2700 | 2.5710 | 0.0061 | 0.0006 | 0.0007 | 0.0257 | 0.0000 | 0.0000 |
| IL15RA | 0.7070 | 1.0230 | 0.9670 | 0.9600 | 1.9520 | 1.6430 | 0.2624 | 0.0081 | 0.0128 | 0.1853 | 0.0000 | 0.0004 |
| IL17RD | 0.3940 | 0.9940 | 0.9040 | 0.2270 | 0.4580 | 0.6340 | 0.9360 | 0.3706 | 0.3734 | 0.5754 | 0.0541 | 0.0048 |
| IL7R | -0.1050 | 0.1860 | 0.0160 | 0.2430 | 0.5730 | 0.6770 | 0.9020 | 0.4993 | 0.9673 | 0.3722 | 0.0008 | 0.0001 |
| INSIG1 | -0.0210 | 0.2270 | 0.2630 | -0.0940 | 0.3790 | 0.7190 | 0.9421 | 0.0000 | 0.0000 | 0.0975 | 0.0000 | 0.0000 |
| IRF1 | 1.5900 | 1.5820 | 1.5300 | 2.3430 | 2.4070 | 2.2910 | 0.0000 | 0.0000 | 0.0000 | 0.0000 | 0.0000 | 0.0000 |
| IRF2 | 0.6010 | 0.6960 | 0.6300 | 0.5590 | 0.8910 | 0.8070 | 0.0000 | 0.0000 | 0.0000 | 0.0000 | 0.0000 | 0.0000 |
| IRF7 | 0.4240 | 0.5720 | 0.5540 | 0.3480 | 0.7050 | 0.8640 | 0.4472 | 0.0689 | 0.0707 | 0.5032 | 0.0212 | 0.0033 |
| IRF9 | 2.5150 | 2.4830 | 2.3580 | 2.4990 | 2.3930 | 2.2670 | 0.0000 | 0.0000 | 0.0000 | 0.0000 | 0.0000 | 0.0000 |
| ISG15 | -0.0640 | 0.2760 | 0.3870 | 0.4290 | 0.6320 | 0.5370 | 0.9584 | 0.2164 | 0.0264 | 0.0761 | 0.0003 | 0.0018 |
| ISG20 | -0.1570 | 0.2980 | 0.4680 | -0.0090 | 0.4050 | 0.7090 | 0.9200 | 0.4900 | 0.1064 | 0.9895 | 0.1553 | 0.0059 |
| ITPKA | -0.4340 | -0.8470 | -0.3760 | -0.3290 | -0.2950 | -0.4040 | 0.3946 | 0.0043 | 0.2705 | 0.3498 | 0.2264 | 0.0869 |
| JAK3 | 0.4590 | 0.5530 | 0.5600 | 0.6140 | 0.7190 | 0.7110 | 0.0000 | 0.0000 | 0.0000 | 0.0000 | 0.0000 | 0.0000 |
| JUN | 0.1510 | -0.5210 | -0.1270 | -0.2150 | -0.7010 | -0.8620 | 0.7999 | 0.0103 | 0.6620 | 0.1539 | 0.0000 | 0.0000 |
| KALRN | 0.1280 | 0.6530 | 1.1350 | -0.1660 | -0.3310 | -1.5200 | 0.9878 | 0.6610 | 0.2064 | 0.8887 | 0.6291 | 0.0212 |
| KCTD19 | -0.0010 | 0.0380 | 0.2020 | -0.0480 | 0.5870 | 0.5000 | 0.9994 | 0.9479 | 0.3966 | 0.8666 | 0.0000 | 0.0001 |
| KDSR | 0.2960 | 0.3730 | 0.4220 | 0.3600 | 0.6400 | 0.7720 | 0.0016 | 0.0000 | 0.0000 | 0.0000 | 0.0000 | 0.0000 |
| KEL | -0.0470 | 0.3300 | 0.4720 | 0.3260 | 0.8800 | 0.9970 | 0.9930 | 0.7829 | 0.5322 | 0.6914 | 0.0435 | 0.0177 |
| KIAA1618 | 0.2930 | 0.4840 | 0.4960 | 0.2070 | 0.5930 | 0.5420 | 0.1141 | 0.0002 | 0.0001 | 0.2595 | 0.0000 | 0.0000 |
| KIAA1632 | 0.3390 | 0.3650 | 0.3500 | 0.3450 | 0.6480 | 0.7290 | 0.0000 | 0.0000 | 0.0000 | 0.0000 | 0.0000 | 0.0000 |
| KLF10 | 0.5140 | 0.5870 | 0.5290 | 0.5850 | 0.4590 | 0.3300 | 0.0000 | 0.0000 | 0.0000 | 0.0000 | 0.0000 | 0.0012 |
| KLF15 | 0.0170 | -0.1310 | -0.0220 | -0.7660 | -0.2440 | -0.3550 | 0.9978 | 0.9341 | 0.9870 | 0.0330 | 0.3728 | 0.1767 |
| KLF9 | -0.2720 | 0.3400 | 0.1320 | 0.4160 | 0.8760 | 1.2140 | 0.9447 | 0.8089 | 0.9198 | 0.7036 | 0.1492 | 0.0292 |
| KLHL24 | -0.2190 | 0.0300 | 0.0340 | -0.1680 | 0.2600 | 0.6970 | 0.1980 | 0.9298 | 0.8707 | 0.2156 | 0.0029 | 0.0000 |
| KLHL35 | 0.3400 | -0.0690 | 0.1540 | -0.0100 | -0.1620 | -0.8680 | 0.8308 | 0.9627 | 0.8509 | 0.9898 | 0.7367 | 0.0408 |
| KLRG1 | 0.0240 | 0.1680 | 0.1120 | 0.3210 | 0.6820 | 0.3920 | 0.9961 | 0.8509 | 0.8721 | 0.5534 | 0.0290 | 0.2507 |
| KRT1 | 0.0190 | -0.2940 | -0.5190 | 0.0250 | -0.2610 | -0.9390 | 0.9888 | 0.0669 | 0.0003 | 0.9303 | 0.0612 | 0.0000 |
| LAMB2L | -0.7590 | -1.1140 | -0.5330 | 0.0350 | -0.2680 | 0.0980 | 0.1319 | 0.0046 | 0.2183 | 0.9619 | 0.4738 | 0.8042 |
| LBA1 | 0.2860 | 0.7260 | 0.8810 | 0.1260 | 0.7570 | 0.9290 | 0.0282 | 0.0000 | 0.0000 | 0.2423 | 0.0000 | 0.0000 |
| LGALS1 | -0.3990 | -1.0090 | -1.1000 | 0.1370 | -0.1760 | -0.2450 | 0.7625 | 0.0456 | 0.0240 | 0.8351 | 0.6811 | 0.5429 |
| LGALS3BP | 0.6810 | 1.1690 | 1.2640 | 0.8200 | 1.2410 | 1.2070 | 0.0000 | 0.0000 | 0.0000 | 0.0000 | 0.0000 | 0.0000 |
| LGALS9 | 0.1780 | 0.5390 | 0.6600 | 0.2620 | 0.7090 | 0.9400 | 0.0041 | 0.0000 | 0.0000 | 0.0001 | 0.0000 | 0.0000 |
| LGALS9B | 0.1790 | 0.3960 | 0.5990 | 0.3400 | 0.7310 | 0.9650 | 0.6625 | 0.0099 | 0.0000 | 0.1676 | 0.0000 | 0.0000 |
| LGALS9C | 0.2380 | 0.4350 | 0.7700 | 0.4680 | 0.8430 | 1.0130 | 0.3437 | 0.0014 | 0.0000 | 0.0214 | 0.0000 | 0.0000 |
| LGMN | -0.0040 | 0.0630 | 0.1050 | 0.0930 | 0.6490 | 0.8030 | 0.9978 | 0.8212 | 0.5358 | 0.7533 | 0.0000 | 0.0000 |
| LINGO4 | -0.7380 | -0.1310 | -0.3780 | -1.3150 | -1.8210 | -1.8060 | 0.6519 | 0.9417 | 0.7044 | 0.2866 | 0.0322 | 0.0283 |
| LINS1 | 0.9690 | 1.0410 | 0.8540 | 0.8660 | 0.7380 | 0.7770 | 0.0000 | 0.0000 | 0.0000 | 0.0000 | 0.0000 | 0.0000 |
| LOC100049716 | 0.1300 | 0.1450 | 0.2360 | 0.4260 | 0.6930 | 1.1020 | 0.9635 | 0.8866 | 0.7008 | 0.4868 | 0.0642 | 0.0014 |
| LOC100128028 | -1.1310 | -0.4730 | -0.4580 | 0.0440 | 0.6050 | 1.4420 | 0.4064 | 0.7298 | 0.6590 | 0.9814 | 0.4720 | 0.0327 |
| LOC100128288 | 0.3710 | 0.0970 | 0.1060 | 0.2150 | 0.3890 | 0.6850 | 0.6148 | 0.9165 | 0.8583 | 0.6697 | 0.1828 | 0.0093 |
| LOC100128822 | 0.2150 | 0.1680 | 0.7120 | 0.0070 | 0.1010 | 0.1650 | 0.8302 | 0.7812 | 0.0033 | 0.9888 | 0.7023 | 0.4919 |
| LOC100128895 | -0.0400 | -0.1500 | -0.2340 | -0.1920 | -0.4630 | -0.8500 | 0.9921 | 0.8962 | 0.7478 | 0.7675 | 0.2229 | 0.0248 |
| LOC100129083 | -0.0360 | 0.4910 | -0.0750 | 0.6030 | 0.7120 | 1.3310 | 0.9961 | 0.6292 | 0.9561 | 0.5518 | 0.2766 | 0.0180 |
| LOC100129104 | -0.1460 | 0.2910 | -0.2680 | 0.1540 | 0.6500 | 1.3490 | 0.9768 | 0.8271 | 0.8066 | 0.9136 | 0.3325 | 0.0171 |
| LOC100129122 | 0.7520 | 1.0720 | 1.0110 | 0.5290 | 0.4180 | 1.4070 | 0.7390 | 0.2963 | 0.2762 | 0.5990 | 0.5530 | 0.0086 |
| LOC100129518 | -0.1630 | 0.3920 | 0.4690 | 0.7900 | 0.8780 | 1.1900 | 0.9718 | 0.7275 | 0.5477 | 0.3218 | 0.1035 | 0.0176 |
| LOC100129917 | 0.0680 | 0.3300 | 0.4520 | 0.3290 | 0.4820 | 0.6030 | 0.9774 | 0.4352 | 0.1486 | 0.4499 | 0.0798 | 0.0219 |
| LOC100130107 | 0.2820 | -0.2360 | -0.0070 | 0.4630 | 0.5230 | 0.6280 | 0.6928 | 0.6655 | 0.9949 | 0.2871 | 0.0762 | 0.0262 |
| LOC100130557 | 0.1990 | 0.6400 | 0.8210 | 0.1180 | 0.2090 | 0.5500 | 0.9242 | 0.1232 | 0.0170 | 0.8441 | 0.5435 | 0.0494 |
| LOC100130691 | -0.0020 | 0.3310 | -0.2800 | 0.4420 | 0.6720 | 0.6600 | 0.9994 | 0.5134 | 0.5771 | 0.2848 | 0.0124 | 0.0129 |
| LOC100130855 | 0.2960 | 0.2630 | 0.0010 | 1.7740 | 0.8500 | 0.4950 | 0.9400 | 0.8814 | 0.9999 | 0.0487 | 0.2803 | 0.5674 |
| LOC100130872 | -0.0150 | 0.2160 | 0.3130 | -0.0050 | 0.5990 | 0.7400 | 0.9897 | 0.0784 | 0.0023 | 0.9863 | 0.0000 | 0.0000 |
| LOC100131354 | -0.6360 | -0.8710 | -0.3600 | 1.2010 | 0.9990 | 1.4160 | 0.7676 | 0.4118 | 0.7485 | 0.2108 | 0.1504 | 0.0249 |
| LOC100131507 | 0.0540 | -0.0820 | -0.0060 | 0.3160 | 0.6290 | 0.8810 | 0.9875 | 0.9377 | 0.9961 | 0.5050 | 0.0250 | 0.0010 |

**Table 6. RNA-seq identification of DE genes in IFNγ-treated Jurkat or JLat9.2 cells** - *Page 5*

| | Log2 Fold Change (IFNγ - mock) | | | | | | Adjusted p Value (Benjamini-Hochberg FDR corrected) | | | | | |
|---|---|---|---|---|---|---|---|---|---|---|---|---|
| | Jurkat | | | JLat9.2 | | | Jurkat | | | JLat9.2 | | |
| GENE | 4h | 8h | 12h | 4h | 8h | 12h | 4h | 8h | 12h | 4h | 8h | 12h |
| LOC100131733 | 2.1490 | 3.2580 | 3.2110 | 2.9260 | 4.8290 | 4.9670 | 0.0160 | 0.0000 | 0.0000 | 0.0086 | 0.0000 | 0.0000 |
| LOC100131871 | 0.1340 | -0.3310 | -0.0160 | -0.2580 | 0.1120 | -0.7510 | 0.9560 | 0.6555 | 0.9876 | 0.6607 | 0.7852 | 0.0356 |
| LOC100132707 | 0.1150 | 0.4030 | 0.4340 | 0.2460 | 0.7740 | 0.6580 | 0.8295 | 0.0027 | 0.0009 | 0.2376 | 0.0000 | 0.0000 |
| LOC100133019 | 0.1810 | -0.1210 | -0.1100 | 0.0870 | 0.1040 | -0.9130 | 0.9513 | 0.9348 | 0.9107 | 0.9141 | 0.8338 | 0.0304 |
| LOC100133211 | 0.2890 | 0.3120 | 0.2210 | 0.4780 | 0.5280 | 0.6330 | 0.2777 | 0.1063 | 0.2956 | 0.0300 | 0.0017 | 0.0001 |
| LOC100216545 | 0.2580 | 0.4640 | 0.4680 | 0.3120 | 0.3960 | 0.6900 | 0.6143 | 0.0350 | 0.0282 | 0.2699 | 0.0357 | 0.0001 |
| LOC100270804 | 0.2080 | 0.0630 | -0.1490 | 0.5800 | 1.0750 | 0.8860 | 0.9162 | 0.9584 | 0.8390 | 0.2707 | 0.0014 | 0.0085 |
| LOC100287062 | 0.2540 | 0.4750 | 0.5320 | 0.2210 | 0.6350 | 0.5500 | 0.4329 | 0.0033 | 0.0006 | 0.3087 | 0.0000 | 0.0001 |
| LOC100287126 | -0.5930 | -0.1520 | 0.0760 | 1.3240 | 1.2790 | 1.6580 | 0.7428 | 0.9301 | 0.9515 | 0.1467 | 0.0506 | 0.0066 |
| LOC100287190 | 0.0130 | -0.1830 | -0.2790 | -0.2460 | -0.4470 | -0.8780 | 0.9976 | 0.7879 | 0.5259 | 0.6029 | 0.1313 | 0.0039 |
| LOC100287569 | -0.5490 | -0.7750 | 0.2710 | 0.7370 | 1.1840 | 2.0300 | 0.8975 | 0.6555 | 0.8564 | 0.6668 | 0.2368 | 0.0193 |
| LOC100287852 | 0.1860 | -0.0190 | 0.0150 | -0.1740 | -0.1130 | -0.5960 | 0.9116 | 0.9846 | 0.9862 | 0.7294 | 0.7388 | 0.0410 |
| LOC100288682 | 0.3000 | 0.6000 | 0.3840 | 0.5040 | 0.6780 | 0.8760 | 0.8334 | 0.2039 | 0.4562 | 0.4053 | 0.0833 | 0.0176 |
| LOC100288735 | -0.8980 | -0.9370 | -0.5980 | 1.7300 | 1.6980 | 1.0710 | 0.7311 | 0.5263 | 0.6492 | 0.0873 | 0.0218 | 0.1802 |
| LOC100289008 | 0.2730 | 0.5110 | 0.5830 | -0.0200 | 0.4100 | 0.9390 | 0.9158 | 0.5128 | 0.3358 | 0.9859 | 0.4043 | 0.0224 |
| LOC100289098 | 0.1410 | -0.0270 | 0.2800 | 0.9300 | 1.1300 | 0.5860 | 0.9718 | 0.9881 | 0.7521 | 0.2355 | 0.0309 | 0.3213 |
| LOC100289210 | 0.1090 | -0.2960 | 0.0790 | 0.8330 | 0.9260 | 0.9020 | 0.9718 | 0.7501 | 0.9290 | 0.1685 | 0.0265 | 0.0281 |
| LOC100289230 | 0.1400 | -0.0700 | 0.4560 | 0.3980 | 0.3920 | 0.9130 | 0.9610 | 0.9573 | 0.3665 | 0.4834 | 0.3083 | 0.0051 |
| LOC100289274 | 0.4010 | 0.4740 | 0.5400 | 0.7280 | 0.6070 | 1.3460 | 0.8095 | 0.5581 | 0.3836 | 0.2647 | 0.1986 | 0.0009 |
| LOC100289316 | -0.1400 | 0.2970 | -0.0010 | 1.5930 | 1.8470 | 0.9850 | 0.9724 | 0.7912 | 0.9999 | 0.0402 | 0.0015 | 0.1179 |
| LOC100289608 | 0.0590 | 0.0330 | -0.0160 | -0.5420 | -0.5890 | -0.0340 | 0.9858 | 0.9750 | 0.9854 | 0.1481 | 0.0248 | 0.9148 |
| LOC120364 | -0.0690 | -0.3900 | 0.0300 | -0.3830 | -0.3870 | -0.7610 | 0.9864 | 0.6322 | 0.9757 | 0.4800 | 0.2880 | 0.0317 |
| LOC201229 | -0.2190 | -0.1440 | -0.0570 | -0.0330 | 0.3150 | 0.6040 | 0.8642 | 0.8449 | 0.9274 | 0.9598 | 0.2758 | 0.0178 |
| LOC220930 | 0.0970 | 0.2350 | 0.1910 | 0.0650 | 0.3000 | 0.7350 | 0.9156 | 0.3268 | 0.4011 | 0.8466 | 0.0671 | 0.0000 |
| LOC255512 | 0.9720 | 0.3660 | -0.1390 | 1.2750 | 1.0430 | 1.6070 | 0.5181 | 0.8442 | 0.9373 | 0.2731 | 0.2208 | 0.0337 |
| LOC283314 | 0.4610 | 0.6410 | 0.4500 | 0.2120 | 0.3510 | 0.3880 | 0.4125 | 0.0413 | 0.2133 | 0.2866 | 0.0070 | 0.0024 |
| LOC284297 | -0.5090 | -0.1740 | -0.0780 | -0.6190 | -0.6700 | -0.9640 | 0.8660 | 0.9341 | 0.9608 | 0.3883 | 0.1682 | 0.0486 |
| LOC284805 | 0.2000 | -0.1260 | -0.6880 | 0.3270 | 0.4280 | 0.9890 | 0.9556 | 0.9420 | 0.4036 | 0.7360 | 0.4702 | 0.0414 |
| LOC338598 | -0.1280 | -0.0640 | 0.0730 | -0.6670 | -1.1680 | -0.1080 | 0.9702 | 0.9634 | 0.9364 | 0.1498 | 0.0009 | 0.7671 |
| LOC388692 | 0.5210 | 0.3530 | 0.7260 | 0.3370 | 0.5300 | 0.3860 | 0.3236 | 0.5002 | 0.0181 | 0.4881 | 0.0760 | 0.2160 |
| LOC389043 | 0.6350 | 1.1410 | 1.2240 | 0.3050 | 0.9430 | 1.0560 | 0.1690 | 0.0001 | 0.0000 | 0.5620 | 0.0013 | 0.0002 |
| LOC389791 | 0.5430 | 0.4620 | 0.3450 | 1.5620 | 2.1610 | 1.3230 | 0.8669 | 0.7904 | 0.8069 | 0.1664 | 0.0040 | 0.0999 |
| LOC389813 | 0.0030 | 0.1090 | 0.5580 | -0.3250 | 0.0180 | -0.8720 | 0.9994 | 0.9216 | 0.1752 | 0.5174 | 0.9664 | 0.0086 |
| LOC390424 | 0.2390 | 0.3630 | -0.0430 | -0.5060 | -0.6960 | -0.4830 | 0.8675 | 0.5134 | 0.9587 | 0.2536 | 0.0245 | 0.1103 |
| LOC390806 | 0.3240 | 0.0520 | 0.2360 | -0.2560 | -0.5290 | -0.8630 | 0.7510 | 0.9639 | 0.6564 | 0.5630 | 0.0588 | 0.0031 |
| LOC400682 | 0.0680 | 0.0120 | 0.1450 | -0.0500 | 0.3700 | 0.5810 | 0.9484 | 0.9821 | 0.5510 | 0.8850 | 0.0168 | 0.0001 |
| LOC400752 | 0.2900 | 0.1660 | 0.2060 | 1.1550 | 1.6020 | 2.2360 | 0.9244 | 0.9188 | 0.8410 | 0.2783 | 0.0216 | 0.0006 |
| LOC400759 | 2.0940 | 3.3650 | 3.4170 | 2.6860 | 4.5760 | 4.9330 | 0.0000 | 0.0000 | 0.0000 | 0.0000 | 0.0000 | 0.0000 |
| LOC400931 | 0.0360 | -0.0970 | 0.1640 | -0.4730 | -0.2470 | -1.0050 | 0.9930 | 0.9395 | 0.8231 | 0.4193 | 0.5601 | 0.0133 |
| LOC440461 | 0.0750 | -0.0060 | 0.7490 | 0.2280 | 0.6180 | 0.6240 | 0.9824 | 0.9967 | 0.0441 | 0.6129 | 0.0128 | 0.0105 |
| LOC492303 | -0.2060 | 0.0010 | 0.0090 | 0.3470 | 0.6270 | 0.5910 | 0.6959 | 0.9987 | 0.9856 | 0.2235 | 0.0008 | 0.0013 |
| LOC554206 | 0.7200 | 0.5200 | 0.7090 | 0.8550 | 0.6980 | 1.3050 | 0.6829 | 0.6950 | 0.4249 | 0.4072 | 0.3493 | 0.0405 |
| LOC642423 | 0.1790 | 0.2290 | -0.2620 | -0.5970 | -1.1060 | -0.3180 | 0.9645 | 0.8721 | 0.8033 | 0.3891 | 0.0221 | 0.5146 |
| LOC642441 | -0.0150 | 0.0840 | 0.3550 | 0.6450 | 0.4230 | 0.9250 | 0.9978 | 0.9554 | 0.6125 | 0.2763 | 0.3482 | 0.0155 |
| LOC642533 | 0.0300 | -0.0710 | -0.3030 | -0.1860 | -0.3800 | -0.7340 | 0.9850 | 0.8664 | 0.1201 | 0.2851 | 0.0016 | 0.0000 |
| LOC642648 | 0.2440 | 0.1790 | -0.3690 | 1.5510 | 1.5200 | 0.5510 | 0.9437 | 0.9165 | 0.7345 | 0.0824 | 0.0206 | 0.4907 |
| LOC645405 | -0.2800 | -0.3670 | -0.1460 | 0.1460 | 0.1790 | 0.6350 | 0.7480 | 0.4035 | 0.7645 | 0.7346 | 0.5014 | 0.0030 |
| LOC645676 | -0.0990 | 0.2270 | 0.1370 | 0.3980 | 0.6350 | 0.7290 | 0.9702 | 0.7213 | 0.8097 | 0.4317 | 0.0458 | 0.0172 |
| LOC647055 | 0.1240 | -0.0300 | 0.3660 | -0.2080 | -1.0680 | -0.0860 | 0.9815 | 0.9886 | 0.7011 | 0.8237 | 0.0481 | 0.8901 |
| LOC652990 | 0.1170 | 0.3570 | 0.2520 | 0.5030 | 0.4070 | 0.7020 | 0.9696 | 0.5860 | 0.6747 | 0.2938 | 0.2403 | 0.0232 |
| LOC654433 | 0.0700 | -0.2240 | -0.6550 | 2.0210 | 2.5570 | 2.0330 | 0.9888 | 0.8620 | 0.3579 | 0.1067 | 0.0026 | 0.0209 |
| LOC728147 | -0.4320 | -0.1230 | -0.2260 | 0.5740 | 0.0920 | 0.9050 | 0.7744 | 0.9263 | 0.7752 | 0.3910 | 0.8843 | 0.0285 |
| LOC728178 | 1.3370 | 0.4940 | 1.2710 | 1.0610 | 0.7960 | 1.1770 | 0.1255 | 0.7403 | 0.0764 | 0.2298 | 0.2237 | 0.0446 |
| LOC728743 | 0.6190 | 0.6660 | 0.7570 | 0.8560 | 1.0520 | 0.8850 | 0.0000 | 0.0000 | 0.0000 | 0.0000 | 0.0000 | 0.0000 |
| LOC728752 | 0.0560 | -0.0470 | 0.2530 | 0.0070 | 0.4080 | 0.7190 | 0.9785 | 0.9533 | 0.4311 | 0.9923 | 0.1503 | 0.0051 |
| LOC729225 | 0.2470 | 0.1460 | -0.1420 | -0.3590 | -0.3870 | -0.9010 | 0.9162 | 0.9078 | 0.8731 | 0.6017 | 0.3888 | 0.0406 |
| LOC729324 | 0.2490 | 0.7210 | 0.5810 | 0.9140 | 0.3970 | 0.9280 | 0.9181 | 0.1759 | 0.2814 | 0.1127 | 0.4122 | 0.0209 |
| LOC729421 | 0.1680 | -0.1430 | 0.1740 | 0.0590 | 0.8190 | 0.4400 | 0.9360 | 0.8764 | 0.7642 | 0.9438 | 0.0175 | 0.2449 |
| LOC729859 | -0.2150 | -0.1590 | -0.0590 | 0.1350 | 0.6690 | 0.4050 | 0.8308 | 0.7879 | 0.9107 | 0.7943 | 0.0072 | 0.1248 |
| LOC730020 | 0.3850 | 0.7180 | 0.0230 | -0.1940 | -0.0750 | -0.1170 | 0.6644 | 0.0394 | 0.9787 | 0.7025 | 0.8424 | 0.7304 |
| LOC730101 | 0.1090 | 0.0580 | -0.0560 | 0.0520 | 0.2450 | 0.5900 | 0.8163 | 0.8614 | 0.8171 | 0.8533 | 0.0747 | 0.0000 |
| LOC81691 | 0.4190 | 0.8210 | 0.7680 | 0.0810 | 0.4690 | 1.2120 | 0.7898 | 0.1270 | 0.1405 | 0.9287 | 0.2609 | 0.0006 |
| LOC85391 | 1.3010 | 1.3520 | 1.2240 | 1.4910 | 1.0730 | 1.1690 | 0.0423 | 0.0145 | 0.0315 | 0.0389 | 0.0637 | 0.0354 |
| LOH12CR2 | 0.0900 | -0.0250 | 0.5710 | 0.6480 | 1.5130 | 0.5710 | 0.9888 | 0.9919 | 0.5136 | 0.5707 | 0.0175 | 0.4549 |
| LOXL1 | 0.0620 | -0.1280 | -0.1620 | -0.3210 | -0.2060 | -0.8000 | 0.9812 | 0.8666 | 0.7540 | 0.4995 | 0.5413 | 0.0112 |
| LOXL2 | 0.1590 | -0.0600 | 0.0210 | -0.3750 | -0.5470 | -0.6920 | 0.9228 | 0.9509 | 0.9772 | 0.2583 | 0.0168 | 0.0030 |
| LQK1 | 0.0620 | 0.1040 | 0.0580 | 0.8390 | 0.5700 | 1.0310 | 0.9907 | 0.9474 | 0.9603 | 0.2448 | 0.2937 | 0.0290 |
| LRRIQ4 | -0.2750 | 0.0290 | 0.0120 | -0.4500 | -0.2530 | -0.9570 | 0.9189 | 0.9829 | 0.9949 | 0.5459 | 0.6314 | 0.0484 |
| LTA | 0.2260 | -0.0260 | 0.0040 | 1.5810 | 2.3690 | 1.8340 | 0.7844 | 0.9750 | 0.9966 | 0.2221 | 0.0037 | 0.0306 |
| LY96 | 0.5750 | 0.5440 | 0.6630 | 0.2610 | 0.4890 | 0.8450 | 0.1699 | 0.1240 | 0.0284 | 0.5249 | 0.0458 | 0.0002 |
| MAFB | 2.5510 | 1.1910 | 1.2050 | 0.3390 | -0.3500 | -0.6470 | 0.0210 | 0.5003 | 0.4085 | 0.7107 | 0.5939 | 0.2912 |
| MAFF | 0.6590 | 0.7400 | 0.7050 | 0.8120 | 0.9870 | 0.9600 | 0.0002 | 0.0000 | 0.0000 | 0.0000 | 0.0000 | 0.0000 |

**Table 6. RNA-seq identification of DE genes in IFNγ-treated Jurkat or JLat9.2 cells** - *Page 6*

| | Log2 Fold Change (IFNγ - mock) | | | | | | Adjusted p Value (Benjamini-Hochberg FDR corrected) | | | | | |
|---|---|---|---|---|---|---|---|---|---|---|---|---|
| | Jurkat | | | JLat9.2 | | | Jurkat | | | JLat9.2 | | |
| GENE | 4h | 8h | 12h | 4h | 8h | 12h | 4h | 8h | 12h | 4h | 8h | 12h |
| MAGEL2 | -0.0740 | -0.0710 | 0.1540 | 0.4160 | 1.0030 | 0.6500 | 0.9921 | 0.9750 | 0.9197 | 0.6438 | 0.0416 | 0.2190 |
| MAP3K8 | 0.8460 | 0.8600 | 1.0910 | 0.4480 | 0.6990 | 0.5510 | 0.2393 | 0.1235 | 0.0181 | 0.4532 | 0.0619 | 0.1523 |
| MAT1A | 0.3610 | 0.4450 | 0.3010 | 0.3800 | 0.7950 | 0.7620 | 0.1847 | 0.0219 | 0.1807 | 0.1635 | 0.0000 | 0.0000 |
| MDGA1 | 0.9000 | 1.5100 | 1.6950 | 0.9570 | 2.2620 | 2.8770 | 0.2537 | 0.0009 | 0.0001 | 0.3327 | 0.0002 | 0.0000 |
| MGC12916 | 0.3180 | 0.2220 | 0.5010 | 0.3590 | 1.0580 | 1.2030 | 0.8987 | 0.8720 | 0.4788 | 0.7499 | 0.0658 | 0.0285 |
| MGC13005 | 0.2740 | 0.3860 | 0.1820 | 0.3760 | 0.5360 | 1.0090 | 0.8980 | 0.6358 | 0.8240 | 0.6332 | 0.2636 | 0.0159 |
| MGC23284 | 0.0620 | 0.3430 | 0.3400 | -0.1090 | 0.6110 | 0.6480 | 0.9684 | 0.1366 | 0.1152 | 0.8212 | 0.0058 | 0.0029 |
| MGC24975 | -0.0960 | -0.1630 | -0.1670 | 0.0660 | -0.1930 | -0.5930 | 0.9020 | 0.5616 | 0.4535 | 0.8140 | 0.2281 | 0.0002 |
| MLC1 | 0.0220 | -0.1810 | -0.1560 | -0.2180 | -0.3800 | -0.7630 | 0.9930 | 0.7312 | 0.7081 | 0.4173 | 0.0338 | 0.0001 |
| MN1 | -0.4000 | -0.3190 | -0.2580 | -0.5020 | -0.3750 | -0.8950 | 0.8443 | 0.7836 | 0.7769 | 0.3233 | 0.2910 | 0.0120 |
| MOV10 | 0.1230 | 0.3930 | 0.5630 | 0.1920 | 0.6130 | 0.7590 | 0.1304 | 0.0000 | 0.0000 | 0.0027 | 0.0000 | 0.0000 |
| MSX1 | 0.3920 | -0.0740 | 0.6160 | -0.3050 | -0.1820 | -0.5460 | 0.4806 | 0.9348 | 0.0242 | 0.2292 | 0.3149 | 0.0019 |
| MUC1 | 0.7150 | 1.2230 | 1.4380 | 0.6850 | 1.0720 | 1.2000 | 0.0563 | 0.0000 | 0.0000 | 0.0965 | 0.0002 | 0.0000 |
| MVD | -0.0370 | 0.3220 | 0.4560 | 0.0730 | 0.5250 | 0.6630 | 0.9400 | 0.0000 | 0.0000 | 0.6028 | 0.0000 | 0.0000 |
| MVP | 0.4060 | 0.8680 | 1.1420 | 0.3490 | 0.9540 | 1.2040 | 0.0560 | 0.0000 | 0.0000 | 0.0392 | 0.0000 | 0.0000 |
| MXD3 | -0.1090 | -0.0320 | 0.0460 | 0.1620 | 0.4820 | 0.5820 | 0.8370 | 0.9394 | 0.8578 | 0.4113 | 0.0001 | 0.0000 |
| MYC | -0.2600 | -0.2250 | -0.2110 | -0.3120 | -0.5340 | -0.7150 | 0.0000 | 0.0000 | 0.0000 | 0.0000 | 0.0000 | 0.0000 |
| MYCBPAP | 0.0570 | 0.2600 | -0.0930 | 0.2050 | 0.6000 | 0.4920 | 0.9815 | 0.5698 | 0.8583 | 0.6438 | 0.0134 | 0.0439 |
| MYCN | -0.2100 | -0.0950 | -0.1670 | -0.1410 | -0.6030 | -0.1450 | 0.5268 | 0.7782 | 0.4243 | 0.7053 | 0.0072 | 0.5408 |
| MYLIP | 0.1590 | 0.2500 | 0.5350 | 0.1100 | 0.3410 | 0.6670 | 0.9428 | 0.7487 | 0.2088 | 0.7632 | 0.0745 | 0.0002 |
| NBPF7 | 0.0640 | 0.0850 | 0.4130 | -0.2160 | -0.3380 | -0.7090 | 0.9875 | 0.9477 | 0.4308 | 0.7184 | 0.3606 | 0.0454 |
| NCRNA00084 | 0.5390 | 0.5820 | 0.5130 | 0.1550 | 0.3650 | 0.8180 | 0.1890 | 0.0619 | 0.1060 | 0.7334 | 0.1457 | 0.0003 |
| NCRNA00115 | 0.1580 | 0.4580 | 0.5930 | 0.5220 | 0.7970 | 0.8780 | 0.9421 | 0.3749 | 0.1332 | 0.2820 | 0.0114 | 0.0041 |
| NCRNA00120 | 0.0710 | 0.1250 | -0.0290 | 0.1780 | 0.1480 | 0.7260 | 0.9768 | 0.8671 | 0.9653 | 0.7233 | 0.6583 | 0.0039 |
| NDRG1 | 1.1980 | 1.6380 | 1.7060 | 1.1040 | 1.6430 | 1.8790 | 0.0000 | 0.0000 | 0.0000 | 0.0000 | 0.0000 | 0.0000 |
| NEDD9 | 0.2030 | 0.3080 | 0.2800 | 0.4220 | 0.6730 | 0.5620 | 0.7323 | 0.2407 | 0.2513 | 0.2566 | 0.0054 | 0.0204 |
| NEK5 | 1.9190 | 1.6640 | 1.1200 | -0.1150 | -0.1130 | -0.0880 | 0.0162 | 0.0338 | 0.2342 | 0.8575 | 0.7813 | 0.8256 |
| NELF | -0.0620 | -0.1850 | -0.2200 | -0.2630 | -0.5230 | -0.6410 | 0.9815 | 0.7821 | 0.6383 | 0.5212 | 0.0461 | 0.0154 |
| NEXN | 2.1870 | 2.9400 | 2.8880 | 0.7430 | 2.6550 | 2.5960 | 0.0000 | 0.0000 | 0.0000 | 0.6417 | 0.0010 | 0.0009 |
| NFATC4 | 0.1960 | 0.2590 | 0.5580 | 0.0620 | 0.5370 | 0.6750 | 0.8452 | 0.5609 | 0.0292 | 0.7833 | 0.0000 | 0.0000 |
| NGFR | -0.5550 | -0.0090 | -1.2080 | -1.3150 | -1.4860 | -2.4330 | 0.7990 | 0.9967 | 0.1339 | 0.2676 | 0.0702 | 0.0019 |
| NKX3-1 | -0.2510 | -0.3480 | -0.4340 | -0.4200 | -0.5950 | -0.6630 | 0.0001 | 0.0000 | 0.0000 | 0.0000 | 0.0000 | 0.0000 |
| NLRC5 | 3.1600 | 3.4520 | 3.3950 | 3.9260 | 4.4440 | 4.3470 | 0.0000 | 0.0000 | 0.0000 | 0.0000 | 0.0000 | 0.0000 |
| NMI | 0.4280 | 0.5760 | 0.5550 | 0.5280 | 0.8730 | 0.9690 | 0.0000 | 0.0000 | 0.0000 | 0.0000 | 0.0000 | 0.0000 |
| NOL3 | -0.1600 | -0.2400 | 0.2780 | 0.2580 | 0.5830 | 0.5470 | 0.9430 | 0.7795 | 0.6025 | 0.6199 | 0.0438 | 0.0577 |
| NPTXR | -0.3700 | -0.6090 | -0.8150 | -0.0920 | -0.4860 | -0.6940 | 0.7675 | 0.2863 | 0.0853 | 0.7736 | 0.0074 | 0.0003 |
| NRIP1 | -0.1480 | -0.1670 | -0.3860 | -0.1220 | -1.1260 | -0.4460 | 0.9812 | 0.9365 | 0.7521 | 0.9000 | 0.0355 | 0.3993 |
| NRXN3 | -2.7330 | -1.0780 | -1.5510 | 0.2160 | 0.0200 | -0.2320 | 0.0349 | 0.5774 | 0.2619 | 0.8426 | 0.9801 | 0.7432 |
| NUB1 | 0.3490 | 0.5840 | 0.5100 | 0.2070 | 0.5210 | 0.5030 | 0.0000 | 0.0000 | 0.0000 | 0.0001 | 0.0000 | 0.0000 |
| NUCB1 | 0.4580 | 0.9350 | 1.0190 | 0.6130 | 1.1640 | 1.3400 | 0.0000 | 0.0000 | 0.0000 | 0.0000 | 0.0000 | 0.0000 |
| OAS1 | 0.7200 | 1.1950 | 1.1520 | 0.2700 | 0.6760 | 0.7600 | 0.0894 | 0.0001 | 0.0001 | 0.2466 | 0.0000 | 0.0000 |
| OAS2 | 0.3710 | 0.8660 | 0.8990 | 0.2710 | 1.0890 | 1.2600 | 0.0000 | 0.0000 | 0.0000 | 0.0653 | 0.0000 | 0.0000 |
| OAS3 | 0.2770 | 0.6170 | 0.7820 | 0.4020 | 0.9680 | 1.0850 | 0.0001 | 0.0000 | 0.0000 | 0.0000 | 0.0000 | 0.0000 |
| OASL | 0.2360 | 0.8760 | 0.6770 | 0.7480 | 1.1820 | 1.3550 | 0.9099 | 0.0277 | 0.1232 | 0.0655 | 0.0001 | 0.0000 |
| OPTN | 0.1640 | 0.3140 | 0.2200 | -0.0210 | 0.4110 | 0.7500 | 0.8880 | 0.3851 | 0.5344 | 0.9648 | 0.0292 | 0.0000 |
| OSBPL5 | 0.4940 | 0.7100 | 0.8020 | 0.5470 | 0.8940 | 0.9240 | 0.0000 | 0.0000 | 0.0000 | 0.0000 | 0.0000 | 0.0000 |
| PANX2 | 0.3530 | 0.5010 | 1.2240 | 0.2680 | 0.3220 | 0.7060 | 0.8967 | 0.6197 | 0.0191 | 0.6796 | 0.4305 | 0.0404 |
| PARP10 | 0.4510 | 0.8040 | 0.7780 | 0.5820 | 1.3390 | 1.1540 | 0.0000 | 0.0000 | 0.0000 | 0.0000 | 0.0000 | 0.0000 |
| PARP12 | 0.5130 | 0.6720 | 0.7010 | 0.5360 | 0.9350 | 0.7660 | 0.0000 | 0.0000 | 0.0000 | 0.0000 | 0.0000 | 0.0000 |
| PARP14 | 1.0040 | 1.6800 | 1.6310 | 1.0510 | 2.0410 | 2.2880 | 0.0000 | 0.0000 | 0.0000 | 0.0000 | 0.0000 | 0.0000 |
| PARP9 | 2.4300 | 3.0340 | 2.9070 | 2.4580 | 3.4680 | 3.4260 | 0.0000 | 0.0000 | 0.0000 | 0.0000 | 0.0000 | 0.0000 |
| PATL2 | 0.2430 | -0.0790 | 0.1880 | 0.6910 | 1.0240 | 1.9250 | 0.9558 | 0.9712 | 0.8847 | 0.5382 | 0.1363 | 0.0013 |
| PCDH19 | -0.2000 | -0.0610 | -0.3520 | -0.2290 | -0.7960 | -0.7090 | 0.9668 | 0.9750 | 0.7513 | 0.3319 | 0.0000 | 0.0000 |
| PCK2 | 0.1680 | 0.0180 | -0.0210 | 0.0220 | 0.4580 | 0.5970 | 0.6491 | 0.9689 | 0.9498 | 0.9284 | 0.0000 | 0.0000 |
| PCSK4 | 0.0590 | 0.1540 | 0.3350 | -0.0340 | 0.4410 | 0.5950 | 0.9718 | 0.7163 | 0.1593 | 0.9337 | 0.0102 | 0.0004 |
| PDE5A | 2.7320 | 2.4190 | 1.9790 | -0.5370 | -0.1540 | 0.0910 | 0.0265 | 0.0441 | 0.1201 | 0.5852 | 0.8380 | 0.8976 |
| PELI1 | 0.2250 | 0.2780 | 0.2680 | 0.2630 | 0.5710 | 0.6380 | 0.0149 | 0.0005 | 0.0007 | 0.0003 | 0.0000 | 0.0000 |
| PHLDA1 | -0.4670 | -0.4260 | -0.2780 | -0.3510 | -0.7460 | -0.4880 | 0.6148 | 0.4981 | 0.6272 | 0.3563 | 0.0050 | 0.0556 |
| PIGZ | 0.2570 | -0.0720 | -0.1590 | -0.0010 | 0.2210 | 0.5900 | 0.7977 | 0.9393 | 0.7741 | 0.9984 | 0.5007 | 0.0282 |
| PIK3IP1 | -0.0910 | 0.5860 | -0.2320 | 0.7360 | 0.3340 | 1.0800 | 0.9888 | 0.5512 | 0.8466 | 0.4068 | 0.6441 | 0.0497 |
| PIK3R6 | 0.5130 | 0.7000 | 0.2980 | -0.1790 | -1.4520 | -0.5360 | 0.7741 | 0.3857 | 0.7634 | 0.8904 | 0.0460 | 0.4509 |
| PIM1 | 0.2770 | 0.2480 | 0.4480 | 0.3340 | 0.6310 | 0.8660 | 0.3607 | 0.3013 | 0.0060 | 0.0955 | 0.0000 | 0.0000 |
| PIM2 | 0.7310 | 0.7690 | 0.6730 | 0.5770 | 0.6110 | 0.4770 | 0.0000 | 0.0000 | 0.0000 | 0.0000 | 0.0000 | 0.0000 |
| PKP1 | -0.5700 | -0.7820 | -1.5090 | 0.1220 | -0.8610 | -1.0490 | 0.6193 | 0.2238 | 0.0051 | 0.9071 | 0.1302 | 0.0632 |
| PLAC2 | 0.1290 | 0.1000 | 0.0290 | 0.3040 | 0.3380 | 0.8810 | 0.9718 | 0.9427 | 0.9796 | 0.7069 | 0.5137 | 0.0345 |
| PLEKHG1 | -0.5960 | -1.3380 | -1.8770 | 0.2020 | 0.6830 | 1.4440 | 0.9360 | 0.5115 | 0.2071 | 0.9095 | 0.4369 | 0.0458 |
| PLEKHH2 | 0.3770 | 0.3890 | 0.3660 | 0.0820 | 0.4640 | 0.6750 | 0.3683 | 0.1930 | 0.1903 | 0.7507 | 0.0005 | 0.0000 |
| PLXNC1 | 0.3390 | 0.2260 | 0.3770 | 0.6580 | 0.9280 | 1.1040 | 0.5871 | 0.6702 | 0.2547 | 0.1464 | 0.0025 | 0.0002 |
| PMAIP1 | 0.2940 | 0.3280 | 0.2960 | 0.3910 | 0.6270 | 0.7550 | 0.0000 | 0.0000 | 0.0000 | 0.0000 | 0.0000 | 0.0000 |
| PML | 0.3100 | 0.4450 | 0.4080 | 0.4640 | 0.6550 | 0.5700 | 0.0000 | 0.0000 | 0.0000 | 0.0000 | 0.0000 | 0.0000 |
| POLD4 | -0.1570 | -0.0130 | 0.0130 | 0.3230 | 0.3520 | 0.5970 | 0.7990 | 0.9794 | 0.9743 | 0.2699 | 0.0781 | 0.0014 |
| POU3F3 | 1.7820 | 1.6590 | 2.2200 | 0.6700 | 1.4680 | 1.0600 | 0.3463 | 0.2669 | 0.0485 | 0.6192 | 0.0470 | 0.1732 |

**Table 6. RNA-seq identification of DE genes in IFNγ-treated Jurkat or JLat9.2 cells** - *Page 7*

| | Log2 Fold Change (IFNγ - mock) | | | | | | Adjusted p Value (Benjamini-Hochberg FDR corrected) | | | | | |
|---|---|---|---|---|---|---|---|---|---|---|---|---|
| | Jurkat | | | JLat9.2 | | | Jurkat | | | JLat9.2 | | |
| GENE | 4h | 8h | 12h | 4h | 8h | 12h | 4h | 8h | 12h | 4h | 8h | 12h |
| PPFIBP2 | 1.0800 | 0.6520 | 0.4480 | -0.1250 | 0.1970 | 0.1180 | 0.0243 | 0.2925 | 0.4788 | 0.8286 | 0.5427 | 0.7321 |
| PRDM1 | -0.7840 | -0.9650 | -1.0900 | -0.0260 | 0.4690 | 0.3300 | 0.1317 | 0.0194 | 0.0061 | 0.9751 | 0.1482 | 0.3363 |
| PRIC285 | 0.3620 | 0.6080 | 0.6210 | 0.2880 | 0.8050 | 0.7560 | 0.0411 | 0.0000 | 0.0000 | 0.2307 | 0.0000 | 0.0000 |
| PRKCE | 0.3650 | 0.6510 | 0.5470 | 0.6580 | 0.6620 | 0.6820 | 0.0009 | 0.0000 | 0.0000 | 0.0000 | 0.0000 | 0.0000 |
| PRKCG | 0.4530 | 1.3020 | 0.8370 | 0.5180 | 1.0950 | 1.1620 | 0.8923 | 0.0794 | 0.3473 | 0.3910 | 0.0029 | 0.0012 |
| PROM2 | 1.6240 | 1.1630 | 2.0600 | 0.7940 | 0.8660 | 0.6390 | 0.1666 | 0.3526 | 0.0100 | 0.3922 | 0.1674 | 0.3324 |
| PROX1 | 0.4720 | 0.2160 | 0.7230 | 0.6210 | 0.7830 | 0.9770 | 0.4913 | 0.7808 | 0.0326 | 0.0002 | 0.0000 | 0.0000 |
| PRPS2 | 0.4930 | 0.7680 | 0.8020 | 0.5140 | 0.9460 | 1.0900 | 0.0000 | 0.0000 | 0.0000 | 0.0000 | 0.0000 | 0.0000 |
| PSD3 | -0.5830 | -0.1140 | -0.8790 | -0.3470 | -1.1750 | -1.2820 | 0.8675 | 0.9652 | 0.4584 | 0.7452 | 0.0733 | 0.0486 |
| PSMB10 | 0.4010 | 0.8230 | 0.9950 | 0.7640 | 1.5430 | 1.8000 | 0.0000 | 0.0000 | 0.0000 | 0.0000 | 0.0000 | 0.0000 |
| PSMB8 | 0.4410 | 0.8570 | 1.0890 | 0.5370 | 1.1370 | 1.3500 | 0.0000 | 0.0000 | 0.0000 | 0.0000 | 0.0000 | 0.0000 |
| PSMB9 | 0.7140 | 1.4100 | 1.7680 | 1.2360 | 2.3760 | 2.7310 | 0.0000 | 0.0000 | 0.0000 | 0.0000 | 0.0000 | 0.0000 |
| PSME1 | 0.1550 | 0.3610 | 0.4950 | 0.2590 | 0.5920 | 0.7350 | 0.0307 | 0.0000 | 0.0000 | 0.0001 | 0.0000 | 0.0000 |
| PSME2 | 0.3000 | 0.6470 | 0.7720 | 0.5080 | 0.9780 | 1.2290 | 0.0000 | 0.0000 | 0.0000 | 0.0000 | 0.0000 | 0.0000 |
| PSTPIP2 | -0.0700 | 0.8420 | 0.1030 | 1.6780 | 2.0910 | 2.2950 | 0.9920 | 0.3222 | 0.9447 | 0.0951 | 0.0031 | 0.0008 |
| PTGER3 | -0.6940 | -0.5360 | -0.8050 | -0.4370 | -0.8050 | -0.5190 | 0.1113 | 0.1885 | 0.0187 | 0.1910 | 0.0010 | 0.0238 |
| PVT1 | 0.0090 | -0.6190 | -0.2450 | -0.2350 | -0.3340 | -0.3330 | 0.9978 | 0.0328 | 0.4873 | 0.4286 | 0.0891 | 0.0869 |
| RAB26 | 0.1470 | -0.0890 | 0.1450 | 0.0360 | 0.4200 | 0.5900 | 0.9221 | 0.9132 | 0.7596 | 0.9494 | 0.0858 | 0.0103 |
| RAB33A | -0.2200 | 0.0600 | 0.1880 | -0.1650 | 0.4490 | 0.6030 | 0.9060 | 0.9581 | 0.7588 | 0.7077 | 0.0443 | 0.0046 |
| RARRES3 | 0.5580 | 0.8800 | 1.1050 | 1.2170 | 1.7600 | 2.3560 | 0.0252 | 0.0000 | 0.0000 | 0.0273 | 0.0000 | 0.0000 |
| RASGEF1B | 0.5380 | 0.4530 | 0.6690 | 0.2070 | 0.1460 | 0.7740 | 0.1148 | 0.1601 | 0.0070 | 0.5754 | 0.5796 | 0.0001 |
| RASGRP3 | 0.5160 | 1.4210 | 1.8670 | 0.6320 | 1.6520 | 2.3630 | 0.5542 | 0.0000 | 0.0000 | 0.2156 | 0.0000 | 0.0000 |
| RASL11A | -0.4400 | -0.6370 | -0.1330 | 0.2280 | -0.4680 | -0.7020 | 0.6035 | 0.1736 | 0.8325 | 0.6531 | 0.1661 | 0.0357 |
| REC8 | 2.0410 | 1.8740 | 1.9210 | 1.8920 | 1.9090 | 1.7500 | 0.0000 | 0.0000 | 0.0000 | 0.0000 | 0.0000 | 0.0000 |
| RFTN2 | 0.0240 | 0.0850 | 0.0790 | 0.3170 | 0.5270 | 0.9120 | 0.9978 | 0.9671 | 0.9564 | 0.7120 | 0.2935 | 0.0393 |
| RHBDL3 | 1.2740 | 2.5680 | 1.5770 | 0.3120 | -0.1260 | 0.1000 | 0.7245 | 0.0290 | 0.3065 | 0.8034 | 0.8946 | 0.9101 |
| RHEBL1 | 0.0550 | 0.5000 | 0.3270 | -0.0740 | 0.9990 | 1.0040 | 0.9815 | 0.0752 | 0.3166 | 0.8985 | 0.0000 | 0.0000 |
| RIMS4 | -0.6910 | -0.9080 | -0.7240 | -0.0140 | -0.0650 | -0.3120 | 0.1200 | 0.0098 | 0.0407 | 0.9771 | 0.8004 | 0.1404 |
| RIN1 | 0.2790 | 0.2520 | 0.4190 | 0.0420 | -0.1540 | -0.8500 | 0.8701 | 0.7782 | 0.4319 | 0.9589 | 0.7286 | 0.0306 |
| RNASE6 | -0.6920 | -1.7880 | -0.7910 | 0.4040 | 0.0710 | -0.0030 | 0.6928 | 0.0236 | 0.3473 | 0.6753 | 0.9307 | 0.9972 |
| RND1 | 0.4900 | 0.6800 | 0.6350 | 0.1690 | 0.2330 | 0.0330 | 0.3333 | 0.0238 | 0.0366 | 0.6420 | 0.3004 | 0.9072 |
| RNF213 | 0.3110 | 0.4800 | 0.5080 | 0.2040 | 0.6110 | 0.5330 | 0.0145 | 0.0000 | 0.0000 | 0.1563 | 0.0000 | 0.0000 |
| RNF31 | 0.5330 | 0.5700 | 0.5970 | 0.5980 | 0.6470 | 0.4770 | 0.0000 | 0.0000 | 0.0000 | 0.0000 | 0.0000 | 0.0000 |
| RP9P | -0.1620 | -0.1290 | 0.1250 | -0.1930 | -0.1230 | -0.5950 | 0.8519 | 0.7925 | 0.7242 | 0.5213 | 0.5624 | 0.0023 |
| RRAS2 | 0.3230 | 0.3940 | 0.3600 | 0.2760 | 0.4220 | 0.5990 | 0.0012 | 0.0000 | 0.0001 | 0.0327 | 0.0000 | 0.0000 |
| RSAD2 | 1.0840 | 1.4220 | 1.3170 | 0.9520 | 1.5030 | 1.4470 | 0.0000 | 0.0000 | 0.0000 | 0.0000 | 0.0000 | 0.0000 |
| RTP4 | 2.9620 | 3.0260 | 3.1080 | 3.0310 | 4.0800 | 4.8290 | 0.0002 | 0.0001 | 0.0000 | 0.0466 | 0.0001 | 0.0000 |
| RUNX2 | -0.3260 | -0.5660 | -0.7480 | -0.4950 | -0.7660 | -0.5730 | 0.0866 | 0.0001 | 0.0000 | 0.0002 | 0.0000 | 0.0000 |
| RYR2 | 1.0360 | 0.5020 | 2.3730 | 0.7900 | -0.3680 | -2.2320 | 0.8295 | 0.8919 | 0.0593 | 0.5877 | 0.7694 | 0.0433 |
| S1PR1 | -0.2550 | -0.3070 | -0.2280 | -0.4370 | -0.5900 | -0.4460 | 0.0594 | 0.0057 | 0.0528 | 0.0016 | 0.0000 | 0.0001 |
| SAMD9 | 0.2510 | 0.5320 | 0.4240 | 0.1210 | 0.4990 | 0.7230 | 0.1750 | 0.0000 | 0.0004 | 0.5288 | 0.0000 | 0.0000 |
| SAMD9L | 1.2270 | 1.7610 | 1.7320 | 0.8300 | 1.8370 | 2.1630 | 0.0000 | 0.0000 | 0.0000 | 0.0000 | 0.0000 | 0.0000 |
| SBNO2 | 0.3120 | 0.4790 | 0.5250 | 0.4690 | 0.7390 | 0.6170 | 0.0001 | 0.0000 | 0.0000 | 0.0000 | 0.0000 | 0.0000 |
| SC4MOL | 0.0020 | 0.3500 | 0.3430 | -0.2010 | 0.1830 | 0.8110 | 0.9994 | 0.0059 | 0.0062 | 0.2019 | 0.0833 | 0.0000 |
| SCARNA7 | 0.4680 | 0.3710 | 0.3860 | 0.9590 | 0.6570 | 1.9900 | 0.9093 | 0.8566 | 0.7905 | 0.4802 | 0.5150 | 0.0093 |
| SCML1 | 0.0870 | 0.1800 | 0.5530 | 0.0550 | 0.3200 | 0.5870 | 0.9413 | 0.6078 | 0.0016 | 0.8139 | 0.0054 | 0.0000 |
| SEC31B | 0.5690 | 0.7620 | 0.8520 | 0.5630 | 1.0040 | 1.1090 | 0.0000 | 0.0000 | 0.0000 | 0.0000 | 0.0000 | 0.0000 |
| SEMA3F | -0.7680 | 0.2920 | 0.4560 | -0.2210 | 0.5450 | 1.0180 | 0.5316 | 0.7925 | 0.5041 | 0.6675 | 0.0377 | 0.0000 |
| SERPINH1 | 0.3190 | 0.6090 | 0.4950 | 0.3020 | 0.7550 | 0.5560 | 0.1259 | 0.0000 | 0.0006 | 0.0169 | 0.0000 | 0.0000 |
| SESN3 | -0.2980 | 0.2500 | 0.3060 | -0.0210 | 0.2210 | 0.6360 | 0.8550 | 0.7572 | 0.5785 | 0.9777 | 0.5096 | 0.0186 |
| SH2D3C | -0.0880 | -0.0480 | 0.1570 | -0.0240 | 0.5210 | 0.6500 | 0.8992 | 0.9055 | 0.4066 | 0.9505 | 0.0012 | 0.0000 |
| SHC4 | 1.0820 | 0.1450 | 0.3480 | -0.3950 | -0.5840 | -0.2540 | 0.2990 | 0.9484 | 0.7719 | 0.2714 | 0.0196 | 0.3157 |
| SIDT1 | 0.3720 | 0.6170 | 0.5510 | 0.1740 | 0.5530 | 0.7390 | 0.5954 | 0.0504 | 0.0876 | 0.7589 | 0.0572 | 0.0072 |
| SLAMF8 | 2.1060 | 2.4230 | 2.1100 | 2.7120 | 2.8790 | 2.5960 | 0.0000 | 0.0000 | 0.0000 | 0.0000 | 0.0000 | 0.0000 |
| SLC14A1 | 0.3220 | 1.3120 | 0.6230 | 0.4810 | 0.7070 | 0.9490 | 0.9669 | 0.3176 | 0.7016 | 0.1538 | 0.0019 | 0.0000 |
| SLC17A9 | -0.5430 | -0.3510 | -0.5480 | -1.1900 | -2.1330 | -1.6490 | 0.5165 | 0.6127 | 0.2656 | 0.1639 | 0.0013 | 0.0076 |
| SLC25A27 | 0.1650 | 0.2720 | 0.2160 | 0.1680 | 0.4260 | 0.6840 | 0.9539 | 0.7705 | 0.7741 | 0.7473 | 0.1256 | 0.0076 |
| SLC2A12 | 0.1120 | 0.6750 | 0.1490 | -0.7230 | 0.1160 | 1.3060 | 0.9875 | 0.5512 | 0.9198 | 0.4768 | 0.8846 | 0.0089 |
| SLC2A14 | 0.7240 | 0.3850 | 0.7580 | 0.7190 | 1.0480 | 1.2450 | 0.4949 | 0.7302 | 0.2269 | 0.3091 | 0.0224 | 0.0046 |
| SLC2A3 | 0.5880 | 0.6000 | 0.5340 | 0.7830 | 0.9660 | 1.3280 | 0.0000 | 0.0000 | 0.0000 | 0.0000 | 0.0000 | 0.0000 |
| SLC37A1 | 0.3250 | 0.6030 | 0.6670 | 0.2050 | 0.5810 | 0.5960 | 0.0001 | 0.0000 | 0.0000 | 0.0479 | 0.0000 | 0.0000 |
| SLC44A5 | -0.1620 | -0.1970 | -0.3580 | -0.5860 | -0.7430 | -0.4300 | 0.8824 | 0.6803 | 0.2486 | 0.1180 | 0.0062 | 0.1000 |
| SLC6A9 | 0.4030 | 0.3610 | -0.1320 | 0.5150 | 0.6650 | 0.6310 | 0.8731 | 0.7829 | 0.9211 | 0.2821 | 0.0359 | 0.0449 |
| SLC7A7 | -0.0030 | -0.2710 | -0.3090 | -0.0650 | -0.4340 | -0.6130 | 0.9994 | 0.6303 | 0.4651 | 0.8987 | 0.1000 | 0.0203 |
| SLFN5 | 0.0890 | 0.2070 | 0.2900 | 0.0380 | 0.2930 | 0.6470 | 0.6986 | 0.0133 | 0.0001 | 0.8026 | 0.0002 | 0.0000 |
| SMPD3 | 0.3850 | 0.4100 | 0.4640 | 1.9160 | 2.0090 | 1.4710 | 0.7970 | 0.6044 | 0.4311 | 0.1152 | 0.0204 | 0.1042 |
| SNIP | 0.4130 | 0.5410 | 0.3130 | 0.2330 | 0.6730 | 1.0800 | 0.8405 | 0.5537 | 0.7384 | 0.7662 | 0.0976 | 0.0036 |
| SNORA10 | -0.0530 | -0.0350 | 0.1840 | 0.7850 | 0.8810 | 0.3100 | 0.9860 | 0.9720 | 0.7187 | 0.0503 | 0.0031 | 0.3705 |
| SNORA29 | -0.2350 | 0.0500 | 0.3330 | -0.5430 | -1.1390 | -0.4280 | 0.9486 | 0.9771 | 0.7174 | 0.4060 | 0.0130 | 0.3395 |
| SNORA3 | -0.5890 | 0.2810 | -0.1910 | -0.6320 | -1.5950 | -0.9020 | 0.7222 | 0.8119 | 0.8508 | 0.4719 | 0.0100 | 0.1196 |
| SNORA56 | 0.3420 | 0.2350 | 0.4920 | 0.3200 | 0.5780 | 1.2260 | 0.8808 | 0.8556 | 0.4765 | 0.7033 | 0.2365 | 0.0034 |
| SNORA73B | -0.2500 | 0.0730 | -0.6450 | -0.4520 | -0.5950 | -0.9170 | 0.9369 | 0.9652 | 0.3791 | 0.5195 | 0.1967 | 0.0435 |

**Table 6. RNA-seq identification of DE genes in IFNγ-treated Jurkat or JLat9.2 cells** - *Page 8*

| | Log2 Fold Change (IFNγ - mock) | | | | | | Adjusted p Value (Benjamini-Hochberg FDR corrected) | | | | | |
|---|---|---|---|---|---|---|---|---|---|---|---|---|
| | Jurkat | | | JLat9.2 | | | Jurkat | | | JLat9.2 | | |
| GENE | 4h | 8h | 12h | 4h | 8h | 12h | 4h | 8h | 12h | 4h | 8h | 12h |
| SNORD14B | 0.1320 | 0.1200 | -0.0400 | -1.1750 | -1.9730 | -0.4750 | 0.9718 | 0.9348 | 0.9720 | 0.0648 | 0.0002 | 0.2942 |
| SNORD45B | -0.0590 | -0.4290 | -0.3420 | -1.0800 | -0.8680 | -0.2160 | 0.9920 | 0.6851 | 0.6934 | 0.0732 | 0.0443 | 0.6416 |
| SNORD83A | 0.2510 | 0.4280 | 0.0210 | -0.5680 | -0.8110 | -1.3720 | 0.9399 | 0.6915 | 0.9896 | 0.4882 | 0.1368 | 0.0141 |
| SNTB1 | 0.3550 | 0.6390 | 0.5850 | 0.0610 | 0.5940 | 0.6490 | 0.1535 | 0.0001 | 0.0003 | 0.7848 | 0.0000 | 0.0000 |
| SOCS1 | 2.6290 | 2.8330 | 3.1540 | 4.5070 | 5.6320 | 4.9370 | 0.0000 | 0.0000 | 0.0000 | 0.0000 | 0.0000 | 0.0000 |
| SOCS2 | -0.8280 | -1.8620 | -1.8640 | -0.9780 | -2.1860 | -2.7750 | 0.0009 | 0.0000 | 0.0000 | 0.0000 | 0.0000 | 0.0000 |
| SOCS3 | 1.4070 | 1.3860 | 1.4620 | 1.9700 | 2.2780 | 2.0380 | 0.0000 | 0.0000 | 0.0000 | 0.0000 | 0.0000 | 0.0000 |
| SOX7 | 0.2470 | 0.1230 | -0.2590 | -0.7490 | -0.4440 | -1.6000 | 0.9702 | 0.9650 | 0.8783 | 0.5249 | 0.5839 | 0.0471 |
| SP100 | 0.3380 | 0.5900 | 0.6370 | 0.2210 | 0.5730 | 0.6450 | 0.0000 | 0.0000 | 0.0000 | 0.0001 | 0.0000 | 0.0000 |
| SP110 | 0.4270 | 0.8590 | 0.8160 | 0.4270 | 0.9870 | 0.9670 | 0.0000 | 0.0000 | 0.0000 | 0.0000 | 0.0000 | 0.0000 |
| SPRY4 | 0.2270 | 0.1090 | -0.0100 | 0.6340 | 1.0200 | 1.5100 | 0.8914 | 0.9179 | 0.9942 | 0.6248 | 0.1816 | 0.0272 |
| SPTA1 | 0.1370 | 0.2780 | 0.6250 | 1.0460 | 0.3720 | 1.2720 | 0.9772 | 0.8364 | 0.3818 | 0.1376 | 0.5509 | 0.0074 |
| SPTB | 0.1150 | 0.1300 | 0.1990 | 0.2920 | 0.6580 | 0.6840 | 0.9718 | 0.9099 | 0.7761 | 0.4053 | 0.0022 | 0.0012 |
| SPTLC3 | 0.7020 | 1.6940 | 1.3080 | 1.5410 | 2.4290 | 2.3740 | 0.7998 | 0.0329 | 0.1405 | 0.0384 | 0.0000 | 0.0000 |
| SQRDL | 0.1860 | 0.2740 | 0.4330 | 0.2570 | 0.6400 | 0.6780 | 0.2227 | 0.0060 | 0.0000 | 0.0408 | 0.0000 | 0.0000 |
| STARD4 | 0.0030 | 0.2360 | 0.2260 | -0.0630 | 0.3270 | 0.6070 | 0.9987 | 0.0585 | 0.0656 | 0.7360 | 0.0008 | 0.0000 |
| STAT1 | 3.1710 | 3.6680 | 3.6610 | 3.2380 | 3.7510 | 3.8500 | 0.0000 | 0.0000 | 0.0000 | 0.0000 | 0.0000 | 0.0000 |
| STAT2 | 0.7800 | 1.1750 | 1.1140 | 0.6760 | 1.5560 | 1.5070 | 0.0000 | 0.0000 | 0.0000 | 0.0000 | 0.0000 | 0.0000 |
| STAT3 | 0.8340 | 0.9580 | 0.9350 | 0.8330 | 0.9540 | 0.8740 | 0.0000 | 0.0000 | 0.0000 | 0.0000 | 0.0000 | 0.0000 |
| STON1 | -0.6610 | -0.6140 | -0.5140 | 0.9010 | -0.0990 | 1.2520 | 0.7245 | 0.5873 | 0.5819 | 0.2851 | 0.9116 | 0.0207 |
| SULT1B1 | -0.0010 | -0.6080 | -0.5470 | -0.4940 | -0.8250 | -0.4860 | 0.9994 | 0.2388 | 0.2488 | 0.3852 | 0.0354 | 0.2063 |
| SYCE2 | -0.2490 | -0.0260 | 0.0300 | -0.0310 | 0.2850 | 0.5910 | 0.6214 | 0.9677 | 0.9464 | 0.9489 | 0.1760 | 0.0018 |
| TAP1 | 1.7960 | 2.7490 | 2.9450 | 2.0740 | 3.2180 | 3.3720 | 0.0000 | 0.0000 | 0.0000 | 0.0000 | 0.0000 | 0.0000 |
| TAP2 | 0.5500 | 0.9520 | 0.9790 | 0.6500 | 1.2310 | 1.2530 | 0.0000 | 0.0000 | 0.0000 | 0.0000 | 0.0000 | 0.0000 |
| TAPBP | 0.2040 | 0.4150 | 0.4910 | 0.3270 | 0.6210 | 0.6960 | 0.0000 | 0.0000 | 0.0000 | 0.0000 | 0.0000 | 0.0000 |
| TAPBPL | 0.3550 | 0.4380 | 0.5810 | 0.7100 | 0.8330 | 0.8690 | 0.0070 | 0.0002 | 0.0000 | 0.0000 | 0.0000 | 0.0000 |
| TBX19 | 0.9740 | 1.4520 | 0.6550 | 0.0460 | 0.4340 | 0.5300 | 0.4963 | 0.0441 | 0.5181 | 0.9729 | 0.4717 | 0.3513 |
| TBX21 | 1.0180 | 1.3790 | 1.4770 | 1.4570 | 1.9330 | 1.8790 | 0.0053 | 0.0000 | 0.0000 | 0.0012 | 0.0000 | 0.0000 |
| TCEAL5 | -2.3800 | 0.5520 | -1.0120 | -0.2000 | 0.1880 | 0.3340 | 0.0332 | 0.7693 | 0.4385 | 0.8491 | 0.7683 | 0.5489 |
| TCTE3 | 1.0720 | 1.1350 | 0.3360 | 0.4440 | 0.7450 | 0.9760 | 0.2179 | 0.0841 | 0.7575 | 0.5968 | 0.1365 | 0.0359 |
| TEX19 | 0.3060 | 0.3870 | 0.1790 | 0.3800 | 0.5470 | 0.6390 | 0.4885 | 0.1342 | 0.5874 | 0.0202 | 0.0000 | 0.0000 |
| TFPI | -0.6840 | -0.3380 | -0.7150 | -1.0940 | -0.8470 | -1.4490 | 0.9360 | 0.9365 | 0.7695 | 0.2750 | 0.2180 | 0.0409 |
| TIGD5 | 0.0100 | -0.0950 | 0.0440 | -0.1710 | -0.2890 | -0.6690 | 0.9974 | 0.8434 | 0.9102 | 0.5421 | 0.1043 | 0.0003 |
| TIMP1 | -0.5710 | -0.4230 | -1.8640 | -0.0070 | -0.3640 | -0.3220 | 0.7831 | 0.7481 | 0.0065 | 0.9894 | 0.1180 | 0.1641 |
| TLR3 | 0.6190 | 0.7840 | 0.6000 | 0.7270 | 1.0860 | 1.0380 | 0.0208 | 0.0004 | 0.0117 | 0.0005 | 0.0000 | 0.0000 |
| TLR6 | 1.2100 | 0.0070 | -1.0600 | 0.1390 | 0.0750 | 1.1270 | 0.7265 | 0.9981 | 0.5623 | 0.9166 | 0.9323 | 0.0372 |
| TM6SF1 | 0.0090 | 0.0890 | -0.1170 | 0.1060 | 0.3960 | 0.6380 | 0.9978 | 0.8814 | 0.7750 | 0.7371 | 0.0151 | 0.0001 |
| TMEM106A | 0.1210 | 0.1370 | 0.3580 | 0.2610 | 0.5320 | 0.6620 | 0.8315 | 0.6302 | 0.0178 | 0.2573 | 0.0004 | 0.0000 |
| TMEM133 | 0.0720 | -0.2070 | -0.1290 | -0.2890 | -0.4920 | -0.6490 | 0.9838 | 0.8219 | 0.8597 | 0.5451 | 0.1076 | 0.0341 |
| TMEM140 | 0.9990 | 2.0000 | 1.6220 | 2.1050 | 3.3490 | 3.0870 | 0.3946 | 0.0003 | 0.0058 | 0.0296 | 0.0000 | 0.0000 |
| TMEM149 | 0.0240 | 0.2070 | 0.1920 | 0.3110 | 0.6330 | 0.4460 | 0.9920 | 0.6123 | 0.5574 | 0.2383 | 0.0003 | 0.0095 |
| TMEM169 | -0.2830 | -0.2570 | -0.6010 | -0.2400 | 0.1890 | 0.2600 | 0.6817 | 0.5591 | 0.0366 | 0.6218 | 0.5349 | 0.3566 |
| TMEM187 | -0.0120 | 0.0630 | 0.2560 | 0.5120 | 0.7990 | 0.9860 | 0.9978 | 0.9518 | 0.5744 | 0.3547 | 0.0233 | 0.0034 |
| TMEM20 | -0.0690 | -0.0010 | -0.1190 | -0.1800 | -0.6360 | -0.3710 | 0.9636 | 0.9979 | 0.7388 | 0.4661 | 0.0002 | 0.0197 |
| TMPRSS3 | 0.2750 | 0.4550 | 0.2710 | 0.1350 | 0.8420 | 0.8750 | 0.6523 | 0.0858 | 0.3954 | 0.7193 | 0.0000 | 0.0000 |
| TNFRSF14 | 0.6040 | 0.9600 | 1.2300 | 0.6560 | 1.5430 | 2.0460 | 0.0001 | 0.0000 | 0.0000 | 0.0587 | 0.0000 | 0.0000 |
| TNFSF10 | 0.8870 | 1.0190 | 1.0400 | 0.7270 | 0.9620 | 1.1850 | 0.0000 | 0.0000 | 0.0000 | 0.0027 | 0.0000 | 0.0000 |
| TNS4 | -0.1910 | -0.4400 | -0.5530 | -0.1380 | -0.5810 | -1.6550 | 0.9707 | 0.7693 | 0.5978 | 0.9168 | 0.4218 | 0.0265 |
| TP53INP1 | 0.9100 | 1.3090 | 1.4160 | 0.8510 | 1.4820 | 1.8940 | 0.0000 | 0.0000 | 0.0000 | 0.0000 | 0.0000 | 0.0000 |
| TPM2 | 0.2460 | 0.3850 | 0.4610 | 0.4190 | 0.6740 | 0.7120 | 0.5109 | 0.0411 | 0.0067 | 0.0522 | 0.0000 | 0.0000 |
| TRAF1 | -0.0950 | 0.1010 | -0.1440 | 0.0700 | 0.4120 | 1.1210 | 0.9707 | 0.9108 | 0.8095 | 0.9342 | 0.3002 | 0.0008 |
| TRAFD1 | 0.4090 | 0.5650 | 0.6180 | 0.4780 | 0.7310 | 0.6310 | 0.0000 | 0.0000 | 0.0000 | 0.0000 | 0.0000 | 0.0000 |
| TRIB1 | -0.2230 | -0.2260 | -0.0340 | -1.6210 | -1.3980 | -1.0760 | 0.9251 | 0.8169 | 0.9709 | 0.0205 | 0.0078 | 0.0302 |
| TRIM14 | 0.2780 | 0.5370 | 0.5700 | 0.2790 | 0.6300 | 0.5660 | 0.0000 | 0.0000 | 0.0000 | 0.0000 | 0.0000 | 0.0000 |
| TRIM2 | 0.1560 | -0.5320 | -0.1520 | -0.2760 | -0.6890 | -0.1530 | 0.8675 | 0.0616 | 0.6920 | 0.2460 | 0.0001 | 0.3704 |
| TRIM21 | 0.7240 | 0.9700 | 1.0230 | 0.9080 | 1.4170 | 1.3200 | 0.0000 | 0.0000 | 0.0000 | 0.0000 | 0.0000 | 0.0000 |
| TRIM22 | 1.4970 | 2.8750 | 3.3880 | 0.8040 | 3.2290 | 4.4850 | 0.0000 | 0.0000 | 0.0000 | 0.3931 | 0.0000 | 0.0000 |
| TRIM34 | 0.4240 | 0.2660 | -0.0600 | 0.9150 | 1.4440 | 1.5020 | 0.7970 | 0.8160 | 0.9603 | 0.3424 | 0.0183 | 0.0117 |
| TRIM5 | 0.1460 | 0.3560 | 0.4200 | -0.0700 | 0.3990 | 0.6000 | 0.2212 | 0.0000 | 0.0000 | 0.6215 | 0.0000 | 0.0000 |
| TRIM56 | 0.5260 | 0.4860 | 0.4520 | 0.6870 | 0.7660 | 0.6290 | 0.0000 | 0.0000 | 0.0000 | 0.0000 | 0.0000 | 0.0000 |
| TRIM69 | 2.5830 | 2.8030 | 2.8650 | 1.6110 | 1.9980 | 1.8450 | 0.0000 | 0.0000 | 0.0000 | 0.0000 | 0.0000 | 0.0000 |
| TRMT61A | -0.1030 | -0.0930 | -0.1360 | 0.0340 | -0.2850 | -0.6440 | 0.6655 | 0.5443 | 0.2192 | 0.8396 | 0.0013 | 0.0000 |
| TRPM4 | 0.3400 | 0.8020 | 0.2770 | 0.2890 | 0.7310 | 0.5860 | 0.9251 | 0.3683 | 0.8129 | 0.6406 | 0.0307 | 0.0893 |
| TSHR | 0.2470 | 0.5030 | 0.4940 | 0.3400 | 0.9680 | 1.0210 | 0.0000 | 0.0000 | 0.0000 | 0.0000 | 0.0000 | 0.0000 |
| TSLP | -0.0410 | -0.2760 | -0.0840 | -0.0860 | 0.4220 | 0.7000 | 0.9858 | 0.4916 | 0.8504 | 0.8252 | 0.0228 | 0.0001 |
| TTC32 | -0.0250 | 0.0690 | -0.0520 | 0.3370 | 0.2690 | 0.6110 | 0.9888 | 0.8875 | 0.8844 | 0.1701 | 0.1292 | 0.0002 |
| TTC39B | 0.0540 | 0.3740 | 0.4140 | 0.1030 | 0.4940 | 0.6320 | 0.9635 | 0.0169 | 0.0050 | 0.6649 | 0.0002 | 0.0000 |
| TTLL9 | 0.9250 | 1.6020 | 2.2780 | 0.7030 | 2.2930 | 1.7510 | 0.4885 | 0.0103 | 0.0000 | 0.5395 | 0.0003 | 0.0050 |
| TXK | 0.9110 | 0.2160 | 1.3140 | 0.1280 | 0.4690 | 0.4070 | 0.4885 | 0.9145 | 0.0465 | 0.8252 | 0.1058 | 0.1652 |
| TXLNB | 0.3140 | 0.4370 | 0.1320 | 0.0520 | 0.4180 | 0.6500 | 0.5710 | 0.1330 | 0.7641 | 0.9275 | 0.0908 | 0.0048 |
| UBA7 | 0.4050 | 0.9980 | 1.1890 | -0.0880 | 0.7990 | 1.1770 | 0.0366 | 0.0000 | 0.0000 | 0.9003 | 0.0066 | 0.0000 |
| UBE2L6 | 1.1770 | 1.8700 | 2.0570 | 1.3080 | 2.2060 | 2.4010 | 0.0000 | 0.0000 | 0.0000 | 0.0000 | 0.0000 | 0.0000 |

**Table 6. RNA-seq identification of DE genes in IFNγ-treated Jurkat or JLat9.2 cells** - *Page 9*

| | Log2 Fold Change (IFNγ - mock) | | | | | | Adjusted p Value (Benjamini-Hochberg FDR corrected) | | | | | |
|---|---|---|---|---|---|---|---|---|---|---|---|---|
| | Jurkat | | | JLat9.2 | | | Jurkat | | | JLat9.2 | | |
| GENE | 4h | 8h | 12h | 4h | 8h | 12h | 4h | 8h | 12h | 4h | 8h | 12h |
| UBE2S | 0.6060 | 0.2940 | 0.8640 | 0.1310 | 0.2490 | -0.2030 | 0.3033 | 0.6794 | 0.0140 | 0.8252 | 0.4689 | 0.5707 |
| UCP3 | -0.0810 | -0.2580 | -0.1770 | 0.2300 | -0.4150 | -0.6530 | 0.9715 | 0.6316 | 0.7122 | 0.6044 | 0.1679 | 0.0285 |
| UNC5CL | 0.0470 | 0.0830 | -0.0280 | 0.2990 | 0.4230 | 0.6000 | 0.9878 | 0.9277 | 0.9682 | 0.4821 | 0.1130 | 0.0165 |
| USP18 | 0.3470 | 0.6850 | 0.7230 | 0.1120 | 0.5320 | 0.5370 | 0.0024 | 0.0000 | 0.0000 | 0.4804 | 0.0000 | 0.0000 |
| USP41 | 0.2690 | 0.6220 | 0.5740 | 0.2740 | 0.4250 | 0.4360 | 0.7633 | 0.0292 | 0.0467 | 0.4314 | 0.0541 | 0.0440 |
| WDR5B | -0.0690 | -0.0570 | -0.0680 | 0.0860 | 0.1670 | 0.5890 | 0.9541 | 0.9122 | 0.8403 | 0.7859 | 0.3497 | 0.0001 |
| WDR64 | 1.2360 | 1.7440 | 1.6120 | 0.3730 | 0.7500 | 1.4380 | 0.6510 | 0.2073 | 0.2138 | 0.7402 | 0.2296 | 0.0074 |
| WDR78 | 0.3970 | 0.1690 | 0.1040 | 0.5540 | 0.5720 | 0.9350 | 0.8048 | 0.8989 | 0.9170 | 0.2603 | 0.0902 | 0.0026 |
| WIPI1 | 0.9360 | 1.4940 | 1.2390 | 0.1960 | 0.9610 | 1.4690 | 0.0121 | 0.0000 | 0.0001 | 0.7507 | 0.0015 | 0.0000 |
| XAF1 | 0.9650 | 1.2480 | 1.1310 | 1.0100 | 1.7100 | 1.7270 | 0.0000 | 0.0000 | 0.0000 | 0.0000 | 0.0000 | 0.0000 |
| ZBTB16 | -0.1420 | -0.0250 | 0.0000 | -0.5100 | -0.3800 | -2.1000 | 0.9369 | 0.9771 | 0.9999 | 0.7423 | 0.7188 | 0.0107 |
| ZC3H6 | 0.0750 | 0.1320 | 0.0070 | -0.0580 | 0.3220 | 0.6360 | 0.8464 | 0.3673 | 0.9788 | 0.7286 | 0.0003 | 0.0000 |
| ZIC5 | 0.5520 | -0.0040 | -0.6620 | -0.5760 | -0.1750 | -0.7090 | 0.6447 | 0.9979 | 0.3700 | 0.2296 | 0.6273 | 0.0304 |
| ZMAT1 | 0.4870 | 0.5500 | 0.3460 | 0.0960 | 0.3530 | 0.6400 | 0.1768 | 0.0403 | 0.2821 | 0.8252 | 0.1061 | 0.0015 |
| ZNF350 | 0.2670 | 0.3400 | -0.0960 | 0.7910 | 0.9940 | 0.1220 | 0.9413 | 0.8071 | 0.9464 | 0.2730 | 0.0381 | 0.8591 |
| ZNF425 | -0.3240 | -0.1110 | -0.1400 | -0.0810 | -0.5440 | -0.6040 | 0.7265 | 0.8919 | 0.7991 | 0.8882 | 0.0686 | 0.0417 |
| ZNF676 | -0.1190 | 0.1300 | -0.2430 | -0.4160 | -0.8000 | -0.3020 | 0.9639 | 0.8910 | 0.6791 | 0.3888 | 0.0159 | 0.3667 |
| ZNF682 | 0.4510 | 0.1890 | 0.2160 | 0.0240 | 0.1900 | 0.6090 | 0.2215 | 0.7121 | 0.5552 | 0.9711 | 0.5307 | 0.0121 |
| ZNF738 | -0.0580 | 0.1040 | 0.1490 | -0.3150 | -0.6270 | -0.0660 | 0.9815 | 0.8866 | 0.7466 | 0.4200 | 0.0179 | 0.8295 |

**Table 7. RNA-seq identification of ISGs differentially induced by IFNβ in JLat9.2 vs. Jurkat cells**

| GENE | Log2 Fold Change: (JLat9.2 IFNβ Xh - JLat9.2 mock) - (Jurkat IFNβ Xh - Jurkat mock) 4h | 8h | 12h |
|---|---|---|---|
| AGTRAP | 0.1855 | 0.5816 | 0.5595 |
| ALDOC | 0.0071 | 0.6612 | 0.6566 |
| ANKRD19 | 1.3927 | 2.7356 | 1.8985 |
| APOLD1 | 0.3473 | 0.6161 | 0.8127 |
| ATG16L2 | 0.2327 | 0.6428 | 0.4470 |
| ATP10A | -1.1742 | -1.5370 | -1.0539 |
| C10orf75 | 0.3218 | 0.9180 | 1.2371 |
| C11orf71 | 0.3205 | 0.4665 | 1.1036 |
| C17orf90 | 0.2404 | 0.7255 | 0.6422 |
| C19orf20 | 0.0983 | 0.6135 | 0.2751 |
| C1orf122 | -0.3417 | 0.1681 | -0.5968 |
| C6orf57 | 0.3453 | 0.4978 | 0.6002 |
| C7orf53 | 0.8703 | 1.6839 | 0.5339 |
| CEBPB | -0.0756 | 0.9044 | -0.0103 |
| CHI3L2 | -0.0036 | 0.4086 | 0.6751 |
| CMPK2 | -0.6977 | -0.6645 | -0.2301 |
| CPS1 | 0.2869 | 0.9031 | 0.9500 |
| DAPP1 | -0.9301 | -1.6724 | -1.1507 |
| DBP | 0.1129 | 0.6146 | 0.0805 |
| DDX58 | -0.8363 | -1.1271 | -0.4735 |
| DDX60L | -0.2030 | -0.6807 | -0.3279 |
| DHX40P | -0.2949 | -0.7002 | -0.2635 |
| EHD4 | -0.5277 | -0.6910 | -0.2524 |
| EMILIN2 | -0.1379 | -0.1733 | -0.6928 |
| EPHX2 | 0.0211 | 0.4910 | 0.6573 |
| ETV5 | 0.5020 | 0.6914 | 0.8954 |
| EVI2A | 0.1424 | 0.1806 | 0.6052 |
| FAM46A | -0.3641 | -0.6217 | -0.1858 |
| FBLIM1 | -0.7203 | -0.9463 | -2.7356 |
| FRAT1 | 0.4037 | 0.5917 | 0.6413 |
| FZD8 | 0.1112 | 2.0005 | 1.2742 |
| GPC5 | 1.7230 | 2.7803 | 2.6933 |
| GPR17 | -0.2283 | -1.0204 | -1.1457 |
| HDAC11 | -0.0098 | 0.3266 | 0.6354 |
| HERC5 | -0.2531 | -0.8444 | -0.4804 |
| HERC6 | -0.1322 | -0.5844 | -0.4055 |
| HES4 | -0.0693 | 0.4371 | -0.7671 |
| ICA1 | 0.2944 | 0.4661 | 0.9330 |
| ICAM4 | 0.0197 | 0.6477 | 0.5324 |
| ID1 | -0.2138 | 0.0089 | -0.7872 |
| IFI27 | -2.0393 | -3.2020 | -3.0258 |
| IFI35 | -0.8349 | -0.8449 | -0.8286 |
| IFI44 | -0.6676 | -0.6460 | -0.1813 |
| IFIT1 | -1.1641 | -1.1453 | -0.6399 |
| IFIT2 | -1.0482 | -1.0912 | -0.4109 |
| IFIT5 | -0.7222 | -0.6799 | -0.2794 |
| IFITM1 | -0.9854 | -1.2219 | -1.1576 |
| IFITM3 | -0.6425 | -0.8691 | -0.7487 |
| IL21R | -0.5206 | 1.4749 | 1.2259 |
| KBTBD10 | -0.2007 | -2.9475 | -0.5396 |
| LBA1 | -0.5617 | -0.9556 | -0.5355 |
| LGMN | 0.1584 | 0.6194 | 0.5340 |
| LOC100130887 | -1.1923 | -1.1464 | -1.9578 |

| GENE | Log2 Fold Change: (JLat9.2 IFNβ Xh - JLat9.2 mock) - (Jurkat IFNβ Xh - Jurkat mock) 4h | 8h | 12h |
|---|---|---|---|
| LOC100287569 | 0.3835 | 2.8466 | 1.4348 |
| LOC26010 | -0.8044 | -1.8653 | -1.3200 |
| LOC387763 | -0.6689 | 0.1980 | -1.4217 |
| LOC492303 | 0.2017 | 0.5611 | 0.8543 |
| LOC645822 | -0.2734 | -0.6772 | -0.3004 |
| LOC654433 | 2.6353 | 1.8547 | 3.0707 |
| LTA | 1.4758 | 1.4881 | 2.2397 |
| LY9 | 0.2250 | 0.6769 | 0.5480 |
| MLC1 | -0.1764 | -0.2923 | -0.8027 |
| MPV17L | -1.6326 | -1.6556 | -2.4127 |
| MSX1 | -0.6371 | -0.2696 | -1.0019 |
| MT2A | -0.3416 | -0.5408 | -0.6520 |
| MX1 | -6.5018 | -6.8852 | -7.5531 |
| MX2 | -0.6760 | -1.4956 | -1.2195 |
| NCRNA00164 | 0.7568 | 1.4025 | 0.1390 |
| NEK5 | -2.1253 | -1.5390 | -1.8213 |
| NEXN | -1.7089 | -2.8825 | -2.8199 |
| NGFR | -1.2074 | -0.5375 | -3.3197 |
| NLGN3 | -0.2729 | -0.7093 | -0.4779 |
| NUDT14 | 0.3964 | 0.8353 | 0.4399 |
| OAS1 | -2.5601 | -2.6554 | -2.4614 |
| OAS3 | -0.5448 | -0.6201 | -0.5104 |
| OASL | -1.0837 | -1.3539 | -0.7441 |
| OTOF | -0.6400 | -1.2478 | -1.4422 |
| PARP14 | -0.3573 | -0.7261 | -0.2465 |
| PDE5A | -3.2121 | -3.1722 | -1.3560 |
| PLCD3 | -0.0108 | 0.5974 | 0.3244 |
| PLSCR1 | -0.5953 | -0.8955 | -0.5063 |
| PLXNB2 | 0.2098 | 0.8883 | 0.8196 |
| PNPT1 | -0.1139 | -0.6076 | -0.2208 |
| POU6F1 | 0.3502 | 0.3662 | 0.6376 |
| PTTG2 | 0.2414 | 0.4545 | 0.6601 |
| RASSF4 | 0.1059 | 0.0703 | 0.7965 |
| RHEBL1 | -0.3353 | 0.6642 | 1.1531 |
| RSAD2 | -1.2968 | -1.4323 | -0.8360 |
| SAMD9 | -0.4166 | -0.9307 | -0.3769 |
| SAMD9L | -0.4178 | -0.5871 | -0.1228 |
| SCN3B | -0.1215 | -0.6447 | -2.0860 |
| SOCS1 | 1.6308 | 2.5395 | 1.1722 |
| STAT1 | -0.3552 | -0.6211 | -0.2651 |
| STON1 | 1.4882 | 1.2974 | 2.0076 |
| TC2N | -0.2259 | -1.2446 | -0.3651 |
| TLR3 | -0.4526 | -0.7371 | -0.5927 |
| TMSB15A | 0.5393 | 1.7970 | 0.9636 |
| TNFSF10 | -0.7902 | -1.2389 | -0.5367 |
| TXLNB | 0.0681 | 0.3469 | 0.9121 |
| USP18 | -0.8110 | -1.0458 | -0.7719 |
| USP41 | -0.7050 | -1.1334 | -0.7471 |
| WWC1 | 0.2574 | 0.8733 | 0.1908 |
| ZCCHC2 | -0.5840 | -0.6780 | -0.4676 |
| ZNF107 | -0.1221 | -0.6040 | -0.1714 |
| ZNF117 | -0.0103 | -0.6119 | -0.2666 |
| ZNF579 | -0.2275 | 0.3266 | -0.7404 |

**Table 8. scRNA-seq identification of HIV-regulated genes**

| GENE | HIV-infected (pooled donor 1 & 2 data) | | | | | | | | | mock-infected (pooled donor 1 & 2 data) | | |
|---|---|---|---|---|---|---|---|---|---|---|---|---|
| | vRNAhi | | | vRNAlo | | | vRNA- | | | | | |
| | avg.exp. | avg.exp. scaled | percent exp. | avg.exp. | avg.exp. scaled | percent exp. | avg.exp. | avg.exp. scaled | percent exp. | avg.exp. | avg.exp. scaled | percent exp. |
| 7SK.2 | 3.82 | 1.34 | 24.44 | 0.54 | -0.61 | 27.42 | 0.94 | -0.06 | 24.90 | 0.61 | -0.50 | 20.25 |
| AC017002.1 | 0.81 | -0.21 | 19.72 | 0.54 | -0.61 | 19.94 | 0.31 | -1.17 | 9.54 | 0.41 | -0.89 | 11.99 |
| C12orf75 | 3.94 | 1.37 | 66.67 | 2.89 | 1.06 | 73.68 | 1.94 | 0.66 | 45.81 | 2.20 | 0.79 | 50.24 |
| CCL3 | 1.54 | 0.43 | 4.17 | 1.01 | 0.01 | 3.32 | 0.50 | -0.69 | 3.91 | 0.57 | -0.56 | 3.25 |
| CCL4 | 8.29 | 2.11 | 13.61 | 5.34 | 1.68 | 16.34 | 1.78 | 0.58 | 11.99 | 3.22 | 1.17 | 10.72 |
| CCL5 | 15.84 | 2.76 | 54.72 | 16.76 | 2.82 | 55.96 | 6.76 | 1.91 | 33.27 | 7.01 | 1.95 | 35.28 |
| CCR7 | 0.53 | -0.64 | 15.56 | 0.49 | -0.71 | 20.22 | 1.54 | 0.43 | 40.20 | 1.22 | 0.20 | 34.50 |
| CD2 | 11.11 | 2.41 | 88.33 | 9.51 | 2.25 | 94.18 | 5.51 | 1.71 | 78.05 | 5.99 | 1.79 | 79.26 |
| CD59 | 2.86 | 1.05 | 57.50 | 1.99 | 0.69 | 60.39 | 1.27 | 0.24 | 40.00 | 1.41 | 0.34 | 42.67 |
| CD70 | 1.47 | 0.39 | 30.56 | 0.91 | -0.10 | 28.81 | 0.51 | -0.67 | 13.52 | 0.58 | -0.55 | 14.37 |
| CKLF | 6.82 | 1.92 | 80.83 | 6.07 | 1.80 | 86.43 | 3.82 | 1.34 | 66.85 | 4.04 | 1.40 | 69.28 |
| CST7 | 2.23 | 0.80 | 47.78 | 2.29 | 0.83 | 55.40 | 1.59 | 0.47 | 36.88 | 1.63 | 0.49 | 38.65 |
| CTSC | 11.41 | 2.43 | 88.61 | 10.90 | 2.39 | 92.52 | 6.39 | 1.86 | 73.83 | 6.41 | 1.86 | 76.05 |
| CXCR6 | 2.43 | 0.89 | 45.83 | 2.25 | 0.81 | 52.08 | 1.02 | 0.02 | 23.14 | 1.16 | 0.15 | 24.95 |
| EEF1A1 | 72.47 | 4.28 | 99.17 | 90.85 | 4.51 | 100.00 | 108.69 | 4.69 | 99.88 | 107.14 | 4.67 | 99.86 |
| EEF1B2 | 9.32 | 2.23 | 90.00 | 11.48 | 2.44 | 98.06 | 15.83 | 2.76 | 95.44 | 15.78 | 2.76 | 94.89 |
| EEF2 | 1.99 | 0.69 | 55.28 | 2.22 | 0.80 | 69.81 | 2.81 | 1.03 | 70.05 | 2.89 | 1.06 | 70.83 |
| FAM13A | 0.44 | -0.82 | 13.06 | 0.42 | -0.88 | 16.34 | 0.72 | -0.33 | 23.99 | 0.79 | -0.23 | 25.27 |
| FAM26F | 0.31 | -1.18 | 11.39 | 0.51 | -0.67 | 26.04 | 0.86 | -0.15 | 31.35 | 0.77 | -0.27 | 28.15 |
| GADD45G | 1.23 | 0.21 | 24.72 | 0.84 | -0.17 | 27.70 | 0.50 | -0.69 | 14.18 | 0.55 | -0.59 | 14.83 |
| GNB2L1 | 18.78 | 2.93 | 97.78 | 21.87 | 3.09 | 100.00 | 27.12 | 3.30 | 98.88 | 26.19 | 3.27 | 98.85 |
| GNLY | 16.48 | 2.80 | 33.33 | 15.23 | 2.72 | 30.47 | 5.41 | 1.69 | 24.76 | 9.33 | 2.23 | 28.32 |
| GZMA | 26.83 | 3.29 | 80.83 | 29.79 | 3.39 | 82.27 | 16.28 | 2.79 | 69.25 | 16.52 | 2.80 | 71.40 |
| GZMB | 20.83 | 3.04 | 68.61 | 24.54 | 3.20 | 70.91 | 12.27 | 2.51 | 54.20 | 11.47 | 2.44 | 53.25 |
| GZMH | 0.91 | -0.10 | 16.67 | 0.68 | -0.38 | 15.79 | 0.25 | -1.38 | 5.83 | 0.25 | -1.38 | 5.79 |
| GZMK | 2.10 | 0.74 | 20.28 | 3.02 | 1.11 | 26.32 | 1.09 | 0.08 | 12.67 | 0.90 | -0.11 | 12.07 |
| H1FX | 1.48 | 0.39 | 41.11 | 1.49 | 0.40 | 49.86 | 2.11 | 0.75 | 53.45 | 1.89 | 0.64 | 50.02 |
| HAVCR2 | 1.37 | 0.31 | 30.00 | 0.70 | -0.36 | 24.93 | 0.36 | -1.03 | 12.35 | 0.44 | -0.82 | 14.49 |
| HIST1H4C | 4.81 | 1.57 | 74.44 | 2.83 | 1.04 | 80.06 | 4.49 | 1.50 | 78.32 | 3.33 | 1.20 | 72.15 |
| HLA-DRB1 | 1.92 | 0.65 | 17.22 | 2.10 | 0.74 | 27.70 | 1.13 | 0.13 | 18.64 | 0.92 | -0.09 | 15.38 |
| HNRNPA1 | 4.78 | 1.56 | 79.17 | 5.34 | 1.68 | 91.97 | 6.83 | 1.92 | 89.04 | 6.66 | 1.90 | 88.97 |
| HOPX | 6.47 | 1.87 | 62.22 | 5.64 | 1.73 | 60.11 | 2.96 | 1.08 | 33.81 | 3.43 | 1.23 | 36.75 |
| IFITM2 | 6.83 | 1.92 | 86.11 | 8.38 | 2.13 | 96.40 | 9.06 | 2.20 | 91.36 | 8.98 | 2.19 | 90.69 |
| IL2RA | 1.14 | 0.13 | 27.50 | 0.77 | -0.26 | 27.15 | 0.47 | -0.74 | 16.47 | 0.57 | -0.56 | 18.47 |
| ISG20 | 2.75 | 1.01 | 53.89 | 3.06 | 1.12 | 66.20 | 4.46 | 1.50 | 72.93 | 3.56 | 1.27 | 67.08 |
| JUN | 0.73 | -0.32 | 14.44 | 0.34 | -1.07 | 16.90 | 0.29 | -1.22 | 9.82 | 0.27 | -1.31 | 10.33 |
| LAG3 | 1.69 | 0.53 | 22.22 | 0.77 | -0.26 | 19.94 | 0.35 | -1.04 | 8.47 | 0.44 | -0.83 | 9.16 |
| NEAT1 | 12.25 | 2.51 | 83.89 | 9.52 | 2.25 | 89.47 | 5.62 | 1.73 | 72.45 | 6.51 | 1.87 | 75.38 |
| NPTX1 | 0.88 | -0.12 | 19.44 | 0.64 | -0.44 | 21.33 | 0.24 | -1.45 | 8.36 | 0.29 | -1.23 | 9.94 |
| PABPC1 | 4.91 | 1.59 | 83.06 | 5.75 | 1.75 | 92.24 | 6.85 | 1.92 | 88.79 | 6.94 | 1.94 | 88.95 |
| PPP1R14B | 1.35 | 0.30 | 39.44 | 1.55 | 0.44 | 58.45 | 1.94 | 0.67 | 58.20 | 1.96 | 0.67 | 57.97 |
| PSME2 | 6.52 | 1.88 | 86.39 | 8.14 | 2.10 | 94.46 | 10.61 | 2.36 | 93.50 | 9.40 | 2.24 | 93.39 |
| RNF213 | 5.84 | 1.76 | 80.83 | 4.87 | 1.58 | 88.92 | 3.76 | 1.32 | 74.14 | 3.89 | 1.36 | 76.01 |
| RPL10 | 102.62 | 4.63 | 100.00 | 124.07 | 4.82 | 100.00 | 160.47 | 5.08 | 99.94 | 160.72 | 5.08 | 99.99 |
| RPL10A | 11.36 | 2.43 | 94.72 | 13.98 | 2.64 | 98.61 | 16.84 | 2.82 | 97.11 | 17.24 | 2.85 | 97.41 |
| RPL12 | 30.59 | 3.42 | 98.89 | 36.20 | 3.59 | 100.00 | 49.37 | 3.90 | 99.75 | 45.71 | 3.82 | 99.74 |
| RPL13 | 34.99 | 3.56 | 98.89 | 42.49 | 3.75 | 100.00 | 48.33 | 3.88 | 99.73 | 48.28 | 3.88 | 99.76 |
| RPL13A | 11.76 | 2.46 | 96.39 | 12.87 | 2.55 | 99.45 | 15.46 | 2.74 | 97.04 | 14.61 | 2.68 | 97.12 |
| RPL18A | 30.12 | 3.41 | 99.44 | 37.56 | 3.63 | 100.00 | 46.53 | 3.84 | 99.67 | 45.14 | 3.81 | 99.50 |
| RPL22L1 | 0.96 | -0.04 | 32.22 | 1.18 | 0.16 | 45.43 | 1.71 | 0.54 | 50.65 | 1.63 | 0.49 | 50.05 |
| RPL28 | 54.78 | 4.00 | 100.00 | 64.50 | 4.17 | 100.00 | 84.03 | 4.43 | 99.97 | 79.97 | 4.38 | 99.98 |
| RPL29 | 32.02 | 3.47 | 99.44 | 37.82 | 3.63 | 100.00 | 46.76 | 3.84 | 99.45 | 45.25 | 3.81 | 99.49 |
| RPL3 | 11.39 | 2.43 | 91.94 | 13.04 | 2.57 | 98.89 | 15.54 | 2.74 | 95.87 | 16.06 | 2.78 | 96.40 |
| RPL36A | 4.23 | 1.44 | 76.67 | 5.17 | 1.64 | 88.92 | 6.34 | 1.85 | 87.09 | 6.25 | 1.83 | 86.85 |
| RPL5 | 25.11 | 3.22 | 98.33 | 29.91 | 3.40 | 100.00 | 37.25 | 3.62 | 98.98 | 36.73 | 3.60 | 98.91 |
| RPL6 | 32.83 | 3.49 | 99.17 | 39.70 | 3.68 | 100.00 | 45.15 | 3.81 | 99.22 | 44.11 | 3.79 | 99.35 |
| RPL7A | 39.47 | 3.68 | 99.72 | 45.58 | 3.82 | 100.00 | 54.38 | 4.00 | 99.51 | 52.97 | 3.97 | 99.57 |
| RPLP0 | 23.84 | 3.17 | 97.78 | 29.13 | 3.37 | 100.00 | 39.38 | 3.67 | 99.43 | 37.96 | 3.64 | 99.23 |
| RPLP1 | 76.10 | 4.33 | 99.72 | 86.32 | 4.46 | 100.00 | 101.96 | 4.62 | 99.97 | 102.20 | 4.63 | 99.99 |

**Table 8. scRNA-seq identification of HIV-regulated genes** - *Page 2*

| GENE | HIV-infected (pooled donor 1 & 2 data) | | | | | | | | | mock-infected (pooled donor 1 & 2 data) | | |
|---|---|---|---|---|---|---|---|---|---|---|---|---|
| | vRNAhi | | | vRNAlo | | | vRNA- | | | | | |
| | avg.exp. | avg.exp. scaled | percent exp. | avg.exp. | avg.exp. scaled | percent exp. | avg.exp. | avg.exp. scaled | percent exp. | avg.exp. | avg.exp. scaled | percent exp. |
| RPS12 | 75.80 | 4.33 | 100.00 | 92.59 | 4.53 | 100.00 | 117.05 | 4.76 | 100.00 | 113.35 | 4.73 | 100.00 |
| RPS18 | 25.30 | 3.23 | 98.61 | 30.05 | 3.40 | 100.00 | 39.01 | 3.66 | 99.56 | 39.14 | 3.67 | 99.50 |
| RPS2 | 25.71 | 3.25 | 98.89 | 32.54 | 3.48 | 100.00 | 43.39 | 3.77 | 99.63 | 41.56 | 3.73 | 99.58 |
| RPS21 | 17.55 | 2.87 | 98.33 | 19.48 | 2.97 | 100.00 | 25.00 | 3.22 | 98.98 | 24.43 | 3.20 | 99.17 |
| RPS23 | 37.95 | 3.64 | 98.89 | 41.46 | 3.72 | 100.00 | 53.11 | 3.97 | 99.75 | 52.73 | 3.97 | 99.67 |
| RPS3A | 37.77 | 3.63 | 98.89 | 41.52 | 3.73 | 100.00 | 47.16 | 3.85 | 99.34 | 48.47 | 3.88 | 99.45 |
| RPS4X | 45.98 | 3.83 | 100.00 | 53.48 | 3.98 | 100.00 | 58.89 | 4.08 | 99.43 | 60.42 | 4.10 | 99.60 |
| RPS5 | 11.70 | 2.46 | 94.17 | 13.58 | 2.61 | 100.00 | 18.01 | 2.89 | 97.53 | 17.66 | 2.87 | 97.91 |
| RPS6 | 16.89 | 2.83 | 97.50 | 19.96 | 2.99 | 99.72 | 25.23 | 3.23 | 98.51 | 24.63 | 3.20 | 98.70 |
| RPS7 | 30.30 | 3.41 | 97.78 | 36.79 | 3.61 | 100.00 | 43.55 | 3.77 | 99.48 | 42.70 | 3.75 | 99.63 |
| RPS8 | 52.92 | 3.97 | 100.00 | 65.45 | 4.18 | 100.00 | 83.73 | 4.43 | 99.92 | 79.05 | 4.37 | 99.79 |
| RPS9 | 7.69 | 2.04 | 89.72 | 9.15 | 2.21 | 97.23 | 12.42 | 2.52 | 95.24 | 11.96 | 2.48 | 95.47 |
| RPSA | 13.70 | 2.62 | 96.11 | 16.00 | 2.77 | 99.45 | 20.64 | 3.03 | 97.58 | 19.52 | 2.97 | 97.72 |
| SLAMF1 | 1.57 | 0.45 | 44.72 | 1.26 | 0.23 | 47.37 | 0.76 | -0.27 | 29.59 | 0.85 | -0.17 | 30.87 |
| SLC25A5 | 2.74 | 1.01 | 66.67 | 3.46 | 1.24 | 83.93 | 4.24 | 1.44 | 80.00 | 4.18 | 1.43 | 81.00 |
| SLC25A6 | 4.99 | 1.61 | 80.28 | 7.00 | 1.95 | 93.35 | 8.55 | 2.15 | 91.18 | 8.48 | 2.14 | 91.55 |
| SRGN | 6.67 | 1.90 | 76.39 | 5.44 | 1.69 | 84.76 | 3.33 | 1.20 | 68.27 | 3.82 | 1.34 | 69.43 |
| STAT1 | 2.62 | 0.96 | 50.83 | 2.96 | 1.09 | 68.98 | 4.24 | 1.44 | 70.11 | 3.61 | 1.28 | 64.51 |
| STMN1 | 0.72 | -0.33 | 19.17 | 1.16 | 0.15 | 23.27 | 2.28 | 0.82 | 29.05 | 2.07 | 0.73 | 28.54 |
| TIMP1 | 7.30 | 1.99 | 78.89 | 6.75 | 1.91 | 90.03 | 4.32 | 1.46 | 68.04 | 4.68 | 1.54 | 70.77 |
| TUBA1B | 1.48 | 0.39 | 37.50 | 1.44 | 0.36 | 42.94 | 2.26 | 0.82 | 43.41 | 2.06 | 0.72 | 43.11 |

**Table 9. Significant HIV-regulated genes in vRNA$^{hi}$ or vRNA$^{lo}$ cell populations**

| No treatment | | |
|---|---|---|
| vRNAhi vs mock-infected | | vRNAlo vs mock-infected |
| 7SK.2 | RPL13 | CCL4 |
| AC017002.1 | RPL13A | CCL5 |
| C12orf75 | RPL18A | CCR7 |
| CCL3 | RPL22L1 | CD2 |
| CCL4 | RPL28 | CTSC |
| CCL5 | RPL29 | CXCR6 |
| CD2 | RPL3 | EEF1B2 |
| CD59 | RPL36A | FAM13A |
| CD70 | RPL5 | GNLY |
| CKLF | RPL6 | GZMA |
| CST7 | RPL7A | GZMB |
| CTSC | RPLP0 | GZMK |
| CXCR6 | RPLP1 | H1FX |
| EEF1A1 | RPS12 | HIST1H4C |
| EEF1B2 | RPS18 | HLA-DRB1 |
| EEF2 | RPS2 | HOPX |
| FAM13A | RPS21 | ISG20 |
| FAM26F | RPS23 | PPP1R14B |
| GADD45G | RPS3A | RPL12 |
| GNB2L1 | RPS4X | RPL36A |
| GNLY | RPS5 | RPLP0 |
| GZMA | RPS6 | RPS18 |
| GZMB | RPS7 | RPS21 |
| GZMH | RPS8 | RPS21 |
| HAVCR2 | RPS9 | SRGN |
| HIST1H4C | RPSA | STAT1 |
| HLA-DRB1 | SLAMF1 | STMN1 |
| HNRNPA1 | SLC25A5 | TUBA1B |
| HOPX | SLC25A6 | |
| IFITM2 | SRGN | |
| IL2RA | STAT1 | |
| JUN | STMN1 | |
| LAG3 | TIMP1 | |
| NEAT1 | | |
| NPTX1 | | |
| PABPC1 | | |
| PPP1R14B | | |
| PSME2 | | |
| RNF213 | | |
| RPL10 | | |
| RPL10A | | |
| RPL12 | | |

| IFNβ-treated | | |
|---|---|---|
| vRNAhi vs mock-infected | | vRNAlo vs mock-infected |
| 7SK.2 | PTMA | CCL4 |
| AC017002.1 | REEP5 | CCL5 |
| BTG2 | RNF213 | CD2 |
| CCL3 | RPL10 | CTSC |
| CCL4 | RPL10A | EEF1B2 |
| CCL5 | RPL12 | GZMA |
| CD2 | RPL13 | GZMH |
| CD4 | RPL13A | HOPX |
| CD40LG | RPL18A | ISG20 |
| CD59 | RPL22L1 | NEAT1 |
| CD70 | RPL28 | TUBA1B |
| CD82 | RPL29 | |
| CFLAR | RPL3 | |
| CKLF | RPL36A | |
| CTLA4 | RPL5 | |
| CTSC | RPL6 | |
| CXCR6 | RPL7A | |
| EEF1A1 | RPLP0 | |
| EEF1B2 | RPLP1 | |
| F5 | RPS12 | |
| GADD45G | RPS18 | |
| GNB2L1 | RPS2 | |
| GNLY | RPS21 | |
| GZMA | RPS23 | |
| GZMB | RPS3A | |
| HAVCR2 | RPS4X | |
| HNRNPA1 | RPS5 | |
| HOPX | RPS6 | |
| ID2 | RPS7 | |
| IFITM2 | RPS8 | |
| JUN | RPS9 | |
| LAG3 | RPSA | |
| LIMS1 | SDC4 | |
| LINC00152 | SLC25A6 | |
| LPAR6 | SRGN | |
| MLLT4 | STAT1 | |
| NEAT1 | TIPARP | |
| NPTX1 | TNF | |
| OSTF1 | TNFRSF18 | |
| PRDM1 | | |
| PRF1 | | |
| PSME2 | | |

**Table 10. scRNA-seq identification of ISGs induced by IFNβ in mock- or HIV-infected cells**

| GENE | HIV-infected (pooled donor 1 & 2 data) | | | | | | | | | mock-infected (pooled donor 1 & 2 data) | | |
|---|---|---|---|---|---|---|---|---|---|---|---|---|
| | vRNAhi | | | vRNAlo | | | vRNA- | | | | | |
| | avg.exp. | avg.exp. scaled | percent exp. | avg.exp. | avg.exp. scaled | percent exp. | avg.exp. | avg.exp. scaled | percent exp. | avg.exp. | avg.exp. scaled | percent exp. |
| ADAR | 2.26 | 0.82 | 59.08 | 1.77 | 0.57 | 64.72 | 1.38 | 0.32 | 49.72 | 1.50 | 0.40 | 51.28 |
| ALOX5AP | 4.25 | 1.45 | 55.04 | 5.47 | 1.70 | 76.99 | 4.06 | 1.40 | 60.41 | 4.16 | 1.43 | 60.46 |
| APOL6 | 1.82 | 0.60 | 48.99 | 1.59 | 0.46 | 63.50 | 1.35 | 0.30 | 47.84 | 1.38 | 0.32 | 48.24 |
| BST2 | 9.56 | 2.26 | 90.49 | 10.12 | 2.31 | 99.08 | 8.68 | 2.16 | 90.71 | 8.88 | 2.18 | 90.57 |
| C19orf66 | 2.93 | 1.08 | 69.16 | 2.26 | 0.82 | 69.94 | 1.85 | 0.61 | 57.82 | 1.81 | 0.59 | 56.96 |
| C5orf56 | 2.00 | 0.69 | 54.47 | 1.33 | 0.29 | 54.91 | 1.37 | 0.31 | 48.05 | 1.32 | 0.28 | 46.08 |
| CARD16 | 5.49 | 1.70 | 79.25 | 4.79 | 1.57 | 88.96 | 3.86 | 1.35 | 76.17 | 3.89 | 1.36 | 76.25 |
| CASP1 | 2.44 | 0.89 | 63.40 | 2.17 | 0.77 | 68.71 | 1.86 | 0.62 | 57.82 | 1.70 | 0.53 | 54.85 |
| CD164 | 2.75 | 1.01 | 65.42 | 2.65 | 0.97 | 76.99 | 2.05 | 0.72 | 61.65 | 2.09 | 0.74 | 61.62 |
| CHMP5 | 3.39 | 1.22 | 73.49 | 3.18 | 1.16 | 85.28 | 3.07 | 1.12 | 75.77 | 2.87 | 1.05 | 73.32 |
| CHST12 | 1.93 | 0.66 | 49.28 | 1.41 | 0.34 | 57.67 | 1.05 | 0.05 | 40.09 | 1.08 | 0.08 | 40.27 |
| CLEC2D | 3.43 | 1.23 | 68.59 | 2.51 | 0.92 | 70.86 | 2.19 | 0.79 | 60.97 | 2.24 | 0.81 | 60.71 |
| CMPK2 | 2.13 | 0.75 | 57.35 | 1.90 | 0.64 | 66.87 | 1.49 | 0.40 | 50.50 | 1.36 | 0.31 | 47.22 |
| CNP | 0.88 | -0.13 | 31.41 | 0.75 | -0.29 | 36.81 | 0.71 | -0.34 | 30.41 | 0.71 | -0.34 | 30.31 |
| COX5A | 7.45 | 2.01 | 83.29 | 6.96 | 1.94 | 96.63 | 6.59 | 1.89 | 87.67 | 6.48 | 1.87 | 87.68 |
| CTSS | 2.38 | 0.87 | 61.96 | 2.17 | 0.77 | 73.01 | 1.64 | 0.50 | 56.16 | 1.67 | 0.51 | 54.14 |
| DDX58 | 1.56 | 0.44 | 46.97 | 1.26 | 0.23 | 51.53 | 1.09 | 0.09 | 38.95 | 1.13 | 0.12 | 39.51 |
| DDX60 | 1.52 | 0.42 | 44.67 | 1.26 | 0.23 | 54.60 | 1.24 | 0.21 | 45.90 | 1.23 | 0.20 | 44.54 |
| DDX60L | 2.43 | 0.89 | 57.35 | 2.12 | 0.75 | 71.47 | 1.67 | 0.52 | 52.91 | 1.77 | 0.57 | 53.28 |
| DRAP1 | 11.25 | 2.42 | 91.64 | 9.80 | 2.28 | 99.08 | 8.74 | 2.17 | 93.41 | 8.47 | 2.14 | 92.95 |
| DTX3L | 1.33 | 0.29 | 43.80 | 1.24 | 0.21 | 52.15 | 1.09 | 0.09 | 42.06 | 1.11 | 0.11 | 42.99 |
| DYNLT1 | 4.65 | 1.54 | 77.23 | 3.52 | 1.26 | 87.73 | 3.25 | 1.18 | 75.35 | 3.40 | 1.23 | 75.77 |
| EIF2AK2 | 5.46 | 1.70 | 79.25 | 4.31 | 1.46 | 88.34 | 3.74 | 1.32 | 77.79 | 3.65 | 1.30 | 75.95 |
| EPSTI1 | 7.56 | 2.02 | 87.03 | 7.06 | 1.95 | 96.01 | 6.28 | 1.84 | 86.00 | 5.78 | 1.76 | 85.25 |
| GBP1 | 2.09 | 0.74 | 55.04 | 2.16 | 0.77 | 68.40 | 2.65 | 0.98 | 63.37 | 2.44 | 0.89 | 61.67 |
| GIMAP4 | 6.17 | 1.82 | 78.96 | 5.91 | 1.78 | 90.49 | 5.20 | 1.65 | 80.48 | 5.39 | 1.69 | 81.31 |
| GIMAP7 | 18.57 | 2.92 | 91.93 | 16.06 | 2.78 | 97.55 | 16.38 | 2.80 | 92.84 | 16.11 | 2.78 | 92.73 |
| GNG5 | 6.42 | 1.86 | 88.47 | 5.39 | 1.68 | 94.79 | 5.18 | 1.65 | 86.27 | 5.31 | 1.67 | 86.25 |
| GPX4 | 1.91 | 0.64 | 47.84 | 1.86 | 0.62 | 58.59 | 1.65 | 0.50 | 49.24 | 1.57 | 0.45 | 47.49 |
| GZMB | 21.11 | 3.05 | 70.03 | 20.91 | 3.04 | 67.18 | 13.75 | 2.62 | 55.51 | 15.46 | 2.74 | 58.86 |
| H3F3B | 20.61 | 3.03 | 96.54 | 19.43 | 2.97 | 100.00 | 19.77 | 2.98 | 97.50 | 20.41 | 3.02 | 97.55 |
| HELZ2 | 0.58 | -0.55 | 20.46 | 0.41 | -0.90 | 21.47 | 0.40 | -0.91 | 18.29 | 0.43 | -0.84 | 19.27 |
| HERC5 | 6.24 | 1.83 | 80.69 | 4.76 | 1.56 | 87.12 | 3.49 | 1.25 | 68.05 | 3.72 | 1.31 | 66.70 |
| HERC6 | 0.79 | -0.23 | 28.82 | 0.64 | -0.45 | 32.21 | 0.52 | -0.66 | 23.53 | 0.53 | -0.64 | 23.81 |
| HLA-C | 21.88 | 3.09 | 95.10 | 21.71 | 3.08 | 100.00 | 19.35 | 2.96 | 94.94 | 19.06 | 2.95 | 95.01 |
| HLA-E | 11.00 | 2.40 | 92.80 | 10.45 | 2.35 | 99.39 | 8.78 | 2.17 | 91.25 | 8.24 | 2.11 | 91.01 |
| HM13 | 1.87 | 0.63 | 54.47 | 1.83 | 0.61 | 67.79 | 1.55 | 0.44 | 52.83 | 1.44 | 0.36 | 49.88 |
| HSH2D | 1.14 | 0.14 | 40.35 | 0.78 | -0.24 | 35.58 | 0.74 | -0.30 | 30.67 | 0.73 | -0.31 | 29.93 |
| IFI16 | 4.49 | 1.50 | 80.69 | 4.12 | 1.42 | 87.73 | 3.55 | 1.27 | 76.29 | 3.89 | 1.36 | 78.29 |
| IFI27 | 1.18 | 0.16 | 12.10 | 1.35 | 0.30 | 18.10 | 1.34 | 0.30 | 16.40 | 1.23 | 0.21 | 14.88 |
| IFI35 | 3.83 | 1.34 | 76.08 | 3.25 | 1.18 | 84.05 | 3.05 | 1.11 | 73.09 | 3.05 | 1.12 | 72.78 |
| IFI44 | 3.62 | 1.29 | 73.20 | 2.88 | 1.06 | 79.45 | 2.50 | 0.92 | 67.08 | 2.47 | 0.90 | 65.70 |
| IFI44L | 5.26 | 1.66 | 78.10 | 4.17 | 1.43 | 84.66 | 3.81 | 1.34 | 75.13 | 3.56 | 1.27 | 72.89 |
| IFI6 | 13.07 | 2.57 | 91.93 | 11.19 | 2.41 | 99.08 | 9.39 | 2.24 | 90.45 | 8.89 | 2.19 | 89.56 |
| IFIH1 | 1.11 | 0.10 | 35.45 | 0.92 | -0.09 | 40.49 | 0.66 | -0.42 | 28.14 | 0.70 | -0.36 | 28.28 |
| IFIT1 | 7.06 | 1.95 | 83.57 | 5.22 | 1.65 | 87.12 | 4.52 | 1.51 | 74.91 | 4.26 | 1.45 | 71.03 |
| IFIT2 | 1.38 | 0.32 | 32.85 | 1.06 | 0.06 | 35.89 | 1.19 | 0.17 | 34.43 | 1.08 | 0.08 | 30.48 |
| IFIT3 | 6.09 | 1.81 | 71.76 | 4.38 | 1.48 | 74.23 | 5.09 | 1.63 | 71.69 | 4.44 | 1.49 | 65.98 |
| IFIT5 | 0.86 | -0.15 | 31.70 | 0.79 | -0.24 | 38.04 | 0.69 | -0.38 | 30.45 | 0.67 | -0.39 | 29.71 |
| IFITM1 | 2.68 | 0.99 | 60.81 | 2.67 | 0.98 | 78.83 | 2.51 | 0.92 | 68.13 | 3.38 | 1.22 | 72.26 |
| IFITM2 | 13.73 | 2.62 | 92.51 | 15.07 | 2.71 | 99.69 | 14.51 | 2.67 | 95.34 | 14.96 | 2.71 | 95.51 |
| IFITM3 | 1.28 | 0.24 | 19.88 | 1.40 | 0.34 | 24.85 | 1.56 | 0.44 | 24.70 | 1.47 | 0.39 | 23.59 |
| IRF7 | 5.69 | 1.74 | 83.57 | 4.18 | 1.43 | 86.50 | 4.03 | 1.39 | 79.77 | 3.72 | 1.31 | 76.26 |
| ISG15 | 30.29 | 3.41 | 99.42 | 23.39 | 3.15 | 100.00 | 19.56 | 2.97 | 96.98 | 19.65 | 2.98 | 96.84 |
| ISG20 | 19.89 | 2.99 | 94.24 | 16.00 | 2.77 | 99.39 | 15.63 | 2.75 | 95.29 | 15.61 | 2.75 | 94.77 |
| LAG3 | 2.49 | 0.91 | 40.06 | 1.56 | 0.45 | 36.50 | 0.79 | -0.23 | 17.62 | 0.99 | -0.02 | 19.35 |
| LAMP3 | 0.85 | -0.17 | 26.80 | 0.42 | -0.86 | 21.17 | 0.46 | -0.78 | 20.90 | 0.43 | -0.84 | 19.44 |
| LAP3 | 2.92 | 1.07 | 66.57 | 2.39 | 0.87 | 74.85 | 2.29 | 0.83 | 65.09 | 2.23 | 0.80 | 63.22 |
| LGALS3 | 6.94 | 1.94 | 70.61 | 6.42 | 1.86 | 79.14 | 4.38 | 1.48 | 55.25 | 4.68 | 1.54 | 57.00 |
| LGALS3BP | 0.58 | -0.55 | 20.17 | 0.73 | -0.32 | 34.66 | 0.76 | -0.27 | 32.26 | 0.76 | -0.27 | 31.15 |

**Table 10. scRNA-seq identification of ISGs induced by IFNβ in mock- or HIV-infected cells** - *Page 2*

| | HIV-infected (pooled donor 1 & 2 data) | | | | | | | | | mock-infected (pooled donor 1 & 2 data) | | |
|---|---|---|---|---|---|---|---|---|---|---|---|---|
| | vRNAhi | | | vRNAlo | | | vRNA- | | | | | |
| **GENE** | avg.exp. | avg.exp. scaled | percent exp. | avg.exp. | avg.exp. scaled | percent exp. | avg.exp. | avg.exp. scaled | percent exp. | avg.exp. | avg.exp. scaled | percent exp. |
| LGALS9 | 2.38 | 0.87 | 55.62 | 2.20 | 0.79 | 71.17 | 2.19 | 0.78 | 63.71 | 2.13 | 0.76 | 62.75 |
| LY6E | 26.09 | 3.26 | 96.83 | 23.42 | 3.15 | 100.00 | 19.54 | 2.97 | 95.66 | 19.18 | 2.95 | 95.78 |
| MT2A | 22.03 | 3.09 | 91.07 | 17.89 | 2.88 | 95.71 | 18.13 | 2.90 | 94.73 | 18.24 | 2.90 | 93.77 |
| MX1 | 13.93 | 2.63 | 91.07 | 11.15 | 2.41 | 99.08 | 9.18 | 2.22 | 89.39 | 8.78 | 2.17 | 87.96 |
| MX2 | 6.45 | 1.86 | 81.56 | 5.77 | 1.75 | 89.88 | 4.78 | 1.56 | 78.95 | 4.51 | 1.51 | 77.09 |
| N4BP1 | 1.56 | 0.44 | 45.82 | 1.22 | 0.20 | 53.37 | 0.94 | -0.07 | 37.12 | 0.99 | -0.01 | 38.46 |
| NAPA | 1.73 | 0.55 | 52.45 | 1.75 | 0.56 | 67.18 | 1.58 | 0.46 | 54.70 | 1.45 | 0.37 | 51.96 |
| NMI | 2.58 | 0.95 | 61.96 | 2.27 | 0.82 | 72.70 | 2.13 | 0.76 | 62.86 | 2.08 | 0.73 | 61.18 |
| NT5C3A | 1.52 | 0.42 | 46.97 | 1.49 | 0.40 | 59.20 | 1.29 | 0.26 | 46.71 | 1.29 | 0.25 | 46.07 |
| NUB1 | 2.82 | 1.04 | 65.42 | 2.71 | 1.00 | 76.99 | 2.45 | 0.90 | 65.13 | 2.34 | 0.85 | 63.93 |
| OAS1 | 7.44 | 2.01 | 87.03 | 5.51 | 1.71 | 92.64 | 4.68 | 1.54 | 81.13 | 4.48 | 1.50 | 79.12 |
| OAS2 | 1.75 | 0.56 | 53.31 | 1.51 | 0.41 | 59.20 | 1.15 | 0.14 | 43.98 | 1.22 | 0.20 | 45.10 |
| OAS3 | 1.22 | 0.20 | 38.33 | 1.07 | 0.07 | 46.93 | 0.88 | -0.13 | 34.97 | 0.95 | -0.06 | 36.48 |
| OASL | 4.71 | 1.55 | 71.18 | 3.59 | 1.28 | 82.21 | 2.70 | 0.99 | 62.17 | 2.68 | 0.98 | 59.98 |
| ODF2L | 2.38 | 0.87 | 53.03 | 1.54 | 0.43 | 54.91 | 1.18 | 0.16 | 41.36 | 1.26 | 0.23 | 42.06 |
| PARP12 | 1.07 | 0.07 | 38.62 | 0.86 | -0.15 | 40.49 | 0.70 | -0.36 | 30.41 | 0.70 | -0.36 | 29.56 |
| PARP14 | 3.34 | 1.20 | 66.28 | 2.68 | 0.99 | 76.38 | 2.14 | 0.76 | 61.08 | 2.42 | 0.88 | 63.44 |
| PARP9 | 3.07 | 1.12 | 70.61 | 2.53 | 0.93 | 74.85 | 2.14 | 0.76 | 62.96 | 2.11 | 0.75 | 62.45 |
| PHF11 | 3.09 | 1.13 | 67.15 | 2.67 | 0.98 | 76.38 | 2.47 | 0.91 | 66.66 | 2.45 | 0.90 | 65.53 |
| PLSCR1 | 6.43 | 1.86 | 80.98 | 4.72 | 1.55 | 88.96 | 3.86 | 1.35 | 75.01 | 3.70 | 1.31 | 73.03 |
| PNPT1 | 1.10 | 0.10 | 33.43 | 0.86 | -0.15 | 41.10 | 0.73 | -0.31 | 30.22 | 0.82 | -0.20 | 32.01 |
| PPM1K | 1.97 | 0.68 | 51.59 | 1.53 | 0.43 | 58.90 | 1.36 | 0.31 | 46.38 | 1.45 | 0.37 | 48.26 |
| PSMB9 | 8.85 | 2.18 | 92.51 | 8.34 | 2.12 | 98.47 | 9.39 | 2.24 | 93.85 | 8.90 | 2.19 | 93.44 |
| RARRES3 | 4.70 | 1.55 | 79.54 | 5.02 | 1.61 | 88.34 | 5.62 | 1.73 | 84.69 | 5.23 | 1.65 | 83.09 |
| RBCK1 | 1.78 | 0.58 | 50.72 | 1.55 | 0.44 | 65.95 | 1.51 | 0.41 | 52.89 | 1.53 | 0.43 | 52.85 |
| RNF213 | 9.15 | 2.21 | 88.47 | 7.46 | 2.01 | 95.09 | 6.10 | 1.81 | 84.31 | 6.84 | 1.92 | 85.17 |
| RPL5 | 18.06 | 2.89 | 95.39 | 22.86 | 3.13 | 100.00 | 28.76 | 3.36 | 98.17 | 27.69 | 3.32 | 98.06 |
| RSAD2 | 2.08 | 0.73 | 48.41 | 1.77 | 0.57 | 60.43 | 1.46 | 0.38 | 48.70 | 1.47 | 0.39 | 47.92 |
| RTP4 | 1.50 | 0.41 | 50.14 | 1.28 | 0.25 | 53.37 | 1.12 | 0.11 | 43.03 | 1.14 | 0.13 | 42.54 |
| S100A4 | 25.26 | 3.23 | 93.95 | 23.67 | 3.16 | 97.55 | 22.66 | 3.12 | 95.06 | 24.35 | 3.19 | 95.08 |
| SAMD9 | 4.95 | 1.60 | 79.83 | 3.68 | 1.30 | 85.89 | 3.09 | 1.13 | 70.52 | 3.22 | 1.17 | 69.11 |
| SAMD9L | 4.65 | 1.54 | 78.96 | 3.63 | 1.29 | 84.36 | 3.02 | 1.10 | 70.53 | 3.21 | 1.16 | 71.14 |
| SAT1 | 4.62 | 1.53 | 78.39 | 3.88 | 1.36 | 82.52 | 3.37 | 1.22 | 71.34 | 3.50 | 1.25 | 72.38 |
| SELL | 3.35 | 1.21 | 61.67 | 2.79 | 1.03 | 62.58 | 2.99 | 1.09 | 61.11 | 2.71 | 1.00 | 57.89 |
| SLFN5 | 3.05 | 1.12 | 64.84 | 2.57 | 0.94 | 76.07 | 2.07 | 0.73 | 59.46 | 2.22 | 0.80 | 61.27 |
| SMCHD1 | 4.69 | 1.55 | 74.93 | 3.81 | 1.34 | 84.97 | 3.23 | 1.17 | 71.34 | 3.45 | 1.24 | 71.88 |
| SNX6 | 6.00 | 1.79 | 83.00 | 5.10 | 1.63 | 92.02 | 4.93 | 1.60 | 83.45 | 4.82 | 1.57 | 83.01 |
| SP100 | 6.37 | 1.85 | 84.73 | 5.51 | 1.71 | 95.71 | 4.86 | 1.58 | 83.94 | 4.92 | 1.59 | 83.66 |
| SP110 | 3.83 | 1.34 | 74.06 | 3.51 | 1.26 | 84.05 | 3.39 | 1.22 | 75.48 | 3.28 | 1.19 | 74.09 |
| SP140 | 1.31 | 0.27 | 41.21 | 0.94 | -0.06 | 42.64 | 0.95 | -0.05 | 35.99 | 1.00 | 0.00 | 37.41 |
| SPATS2L | 2.90 | 1.06 | 63.98 | 2.06 | 0.72 | 64.72 | 1.67 | 0.51 | 50.27 | 1.63 | 0.49 | 49.06 |
| STAT1 | 7.03 | 1.95 | 83.57 | 7.18 | 1.97 | 94.48 | 6.61 | 1.89 | 85.26 | 6.50 | 1.87 | 84.56 |
| STAT2 | 2.56 | 0.94 | 61.38 | 2.22 | 0.80 | 68.40 | 1.92 | 0.65 | 57.12 | 2.00 | 0.69 | 57.83 |
| SUB1 | 10.93 | 2.39 | 93.37 | 9.58 | 2.26 | 98.47 | 9.33 | 2.23 | 94.13 | 9.67 | 2.27 | 94.47 |
| TNFSF10 | 5.78 | 1.75 | 72.91 | 5.36 | 1.68 | 80.98 | 4.74 | 1.56 | 73.29 | 4.88 | 1.59 | 71.94 |
| TRANK1 | 0.73 | -0.31 | 23.63 | 0.48 | -0.72 | 24.54 | 0.50 | -0.70 | 22.69 | 0.54 | -0.62 | 23.93 |
| TREX1 | 1.09 | 0.09 | 35.73 | 0.94 | -0.06 | 38.96 | 0.79 | -0.23 | 33.08 | 0.80 | -0.23 | 32.45 |
| TRIM22 | 4.68 | 1.54 | 79.83 | 4.14 | 1.42 | 85.58 | 3.36 | 1.21 | 73.63 | 3.67 | 1.30 | 75.12 |
| TYMP | 2.10 | 0.74 | 54.47 | 2.27 | 0.82 | 71.47 | 2.13 | 0.76 | 59.08 | 2.25 | 0.81 | 60.46 |
| UBE2L6 | 7.51 | 2.02 | 86.74 | 6.49 | 1.87 | 96.93 | 5.97 | 1.79 | 88.47 | 5.59 | 1.72 | 86.95 |
| USP18 | 1.57 | 0.45 | 46.69 | 1.26 | 0.23 | 51.53 | 1.03 | 0.03 | 39.63 | 0.97 | -0.03 | 37.92 |
| VAMP5 | 3.34 | 1.21 | 68.88 | 3.09 | 1.13 | 80.06 | 2.95 | 1.08 | 69.15 | 2.97 | 1.09 | 69.01 |
| WARS | 1.29 | 0.25 | 41.21 | 1.17 | 0.16 | 47.85 | 1.37 | 0.31 | 46.16 | 1.31 | 0.27 | 44.69 |
| XAF1 | 3.98 | 1.38 | 72.33 | 3.07 | 1.12 | 81.60 | 2.44 | 0.89 | 65.59 | 2.51 | 0.92 | 66.30 |
| XRN1 | 2.54 | 0.93 | 59.37 | 2.21 | 0.79 | 68.71 | 2.12 | 0.75 | 60.54 | 2.26 | 0.82 | 61.40 |
| ZBP1 | 1.14 | 0.13 | 38.04 | 0.71 | -0.34 | 32.21 | 0.53 | -0.64 | 21.84 | 0.57 | -0.57 | 23.13 |

**Table 11. Fold change ISG expression in vRNA$^{hi}$, vRNA$^{lo}$, or vRNA$^{-}$ relative to mock-infected cells**

| | No treatment | | | IFNβ-treated | | |
|---|---|---|---|---|---|---|
| **GENE** | vRNAhi | vRNAlo | vRNA- | vRNAhi | vRNAlo | vRNA- |
| ADAR | 0.107 | 0.010 | 0.027 | 0.385 | 0.149 | -0.072 |
| ALOX5AP | -0.036 | 0.215 | -0.027 | 0.024 | 0.326 | -0.028 |
| APOL6 | 0.241 | 0.050 | 0.047 | 0.248 | 0.121 | -0.016 |
| BST2 | 0.102 | 0.296 | 0.212 | 0.096 | 0.170 | -0.030 |
| C19orf66 | 0.250 | 0.129 | 0.044 | 0.485 | 0.216 | 0.018 |
| C5orf56 | 0.060 | -0.029 | 0.054 | 0.370 | 0.007 | 0.029 |
| CARD16 | 0.195 | 0.152 | 0.042 | 0.408 | 0.245 | -0.007 |
| CASP1 | 0.095 | 0.136 | 0.062 | 0.348 | 0.229 | 0.078 |
| CD164 | 0.136 | 0.100 | 0.038 | 0.280 | 0.239 | -0.018 |
| CHMP5 | 0.001 | 0.146 | 0.111 | 0.183 | 0.112 | 0.076 |
| CHST12 | 0.135 | 0.190 | 0.048 | 0.492 | 0.209 | -0.022 |
| CLEC2D | 0.197 | 0.138 | -0.078 | 0.451 | 0.115 | -0.021 |
| CMPK2 | -0.023 | -0.026 | 0.095 | 0.405 | 0.299 | 0.078 |
| CNP | 0.105 | -0.013 | 0.027 | 0.132 | 0.029 | -0.002 |
| COX5A | -0.074 | 0.065 | 0.027 | 0.176 | 0.090 | 0.021 |
| CTSS | 0.165 | 0.104 | 0.089 | 0.343 | 0.248 | -0.013 |
| DDX58 | -0.038 | -0.061 | 0.049 | 0.265 | 0.086 | -0.023 |
| DDX60 | 0.027 | 0.043 | 0.110 | 0.177 | 0.021 | 0.008 |
| DDX60L | 0.048 | 0.143 | 0.078 | 0.306 | 0.170 | -0.052 |
| DRAP1 | 0.150 | 0.200 | 0.129 | 0.371 | 0.190 | 0.041 |
| DTX3L | -0.045 | -0.014 | 0.053 | 0.141 | 0.083 | -0.016 |
| DYNLT1 | 0.021 | 0.062 | 0.026 | 0.360 | 0.037 | -0.053 |
| EIF2AK2 | 0.045 | 0.147 | 0.211 | 0.473 | 0.191 | 0.027 |
| EPSTI1 | -0.054 | 0.053 | 0.308 | 0.336 | 0.249 | 0.102 |
| GBP1 | -0.321 | -0.232 | 0.166 | -0.154 | -0.121 | 0.089 |
| GIMAP4 | 0.146 | 0.133 | 0.024 | 0.166 | 0.111 | -0.043 |
| GIMAP7 | -0.034 | -0.078 | 0.045 | 0.193 | -0.005 | 0.023 |
| GNG5 | 0.126 | 0.070 | 0.058 | 0.233 | 0.019 | -0.029 |
| GPX4 | 0.224 | 0.161 | -0.037 | 0.177 | 0.156 | 0.042 |
| GZMB | 0.808 | 1.034 | 0.090 | 0.426 | 0.413 | -0.158 |
| H3F3B | -0.007 | 0.054 | 0.010 | 0.013 | -0.067 | -0.044 |
| HELZ2 | 0.051 | 0.036 | 0.019 | 0.140 | -0.026 | -0.033 |
| HERC5 | 0.251 | 0.265 | 0.166 | 0.616 | 0.288 | -0.072 |
| HERC6 | 0.024 | 0.047 | 0.049 | 0.232 | 0.102 | -0.009 |
| HLA-C | 0.091 | 0.172 | 0.111 | 0.190 | 0.179 | 0.021 |
| HLA-E | 0.271 | 0.150 | 0.069 | 0.377 | 0.309 | 0.082 |
| HM13 | -0.014 | 0.083 | 0.081 | 0.234 | 0.215 | 0.063 |
| HSH2D | 0.009 | 0.087 | 0.047 | 0.309 | 0.044 | 0.005 |
| IFI16 | -0.165 | 0.071 | 0.091 | 0.169 | 0.067 | -0.104 |
| IFI27 | 0.187 | 0.106 | 0.104 | -0.037 | 0.071 | 0.070 |
| IFI35 | -0.100 | 0.033 | 0.187 | 0.253 | 0.068 | -0.001 |
| IFI44 | 0.167 | 0.159 | 0.191 | 0.414 | 0.160 | 0.013 |
| IFI44L | -0.129 | 0.082 | 0.254 | 0.458 | 0.181 | 0.079 |
| IFI6 | 0.148 | 0.216 | 0.219 | 0.509 | 0.301 | 0.070 |
| IFIH1 | -0.080 | 0.048 | 0.065 | 0.309 | 0.171 | -0.035 |
| IFIT1 | -0.067 | 0.139 | 0.172 | 0.616 | 0.243 | 0.069 |
| IFIT2 | -0.077 | -0.067 | 0.065 | 0.194 | -0.012 | 0.072 |
| IFIT3 | -0.307 | -0.152 | 0.238 | 0.383 | -0.015 | 0.164 |
| IFIT5 | 0.059 | 0.037 | 0.045 | 0.152 | 0.095 | 0.011 |
| IFITM1 | -0.085 | 0.064 | 0.181 | -0.253 | -0.257 | -0.320 |
| IFITM2 | -0.349 | -0.088 | 0.012 | -0.116 | 0.009 | -0.042 |
| IFITM3 | -0.210 | -0.185 | 0.030 | -0.120 | -0.043 | 0.048 |
| IRF7 | 0.167 | 0.127 | 0.255 | 0.504 | 0.135 | 0.091 |
| ISG15 | 0.142 | 0.267 | 0.352 | 0.600 | 0.240 | -0.006 |
| ISG20 | -0.283 | -0.168 | 0.260 | 0.331 | 0.033 | 0.001 |
| LAG3 | 0.907 | 0.303 | -0.084 | 0.812 | 0.369 | -0.149 |
| LAMP3 | 0.032 | -0.014 | 0.052 | 0.369 | -0.008 | 0.030 |
| LAP3 | 0.080 | 0.046 | 0.113 | 0.276 | 0.069 | 0.026 |
| LGALS3 | 0.547 | 0.442 | -0.242 | 0.484 | 0.386 | -0.077 |
| LGALS3BP | -0.077 | -0.036 | 0.075 | -0.159 | -0.028 | -0.002 |
| LGALS9 | -0.134 | -0.040 | 0.160 | 0.112 | 0.031 | 0.027 |

| | No treatment | | | IFNβ-treated | | |
|---|---|---|---|---|---|---|
| **GENE** | vRNAhi | vRNAlo | vRNA- | vRNAhi | vRNAlo | vRNA- |
| LY6E | 0.154 | 0.221 | 0.219 | 0.425 | 0.275 | 0.026 |
| MT2A | -0.156 | -0.184 | 0.152 | 0.260 | -0.026 | -0.008 |
| MX1 | 0.253 | 0.279 | 0.345 | 0.610 | 0.313 | 0.057 |
| MX2 | 0.038 | 0.064 | 0.262 | 0.435 | 0.297 | 0.069 |
| N4BP1 | 0.195 | 0.142 | -0.017 | 0.366 | 0.159 | -0.037 |
| NAPA | 0.054 | 0.084 | 0.085 | 0.156 | 0.168 | 0.075 |
| NMI | -0.078 | -0.007 | 0.098 | 0.215 | 0.086 | 0.021 |
| NT5C3A | 0.070 | -0.040 | 0.043 | 0.139 | 0.123 | 0.003 |
| NUB1 | 0.096 | 0.074 | 0.086 | 0.192 | 0.153 | 0.045 |
| OAS1 | 0.232 | 0.197 | 0.234 | 0.623 | 0.249 | 0.051 |
| OAS2 | 0.059 | 0.006 | 0.095 | 0.309 | 0.176 | -0.042 |
| OAS3 | -0.039 | 0.027 | 0.049 | 0.192 | 0.087 | -0.051 |
| OASL | 0.168 | 0.183 | 0.151 | 0.634 | 0.319 | 0.009 |
| ODF2L | 0.247 | 0.111 | -0.007 | 0.578 | 0.166 | -0.055 |
| PARP12 | -0.064 | -0.022 | 0.028 | 0.287 | 0.133 | 0.003 |
| PARP14 | 0.174 | -0.018 | 0.001 | 0.344 | 0.109 | -0.120 |
| PARP9 | -0.092 | 0.070 | 0.077 | 0.387 | 0.184 | 0.014 |
| PHF11 | 0.089 | 0.084 | 0.134 | 0.245 | 0.089 | 0.010 |
| PLSCR1 | 0.332 | 0.210 | 0.250 | 0.661 | 0.283 | 0.047 |
| PNPT1 | -0.025 | 0.086 | 0.044 | 0.210 | 0.034 | -0.067 |
| PPM1K | 0.060 | 0.114 | 0.032 | 0.277 | 0.047 | -0.054 |
| PSMB9 | -0.187 | -0.015 | 0.171 | -0.006 | -0.084 | 0.071 |
| RARRES3 | -0.227 | -0.174 | 0.145 | -0.127 | -0.048 | 0.088 |
| RBCK1 | -0.153 | -0.004 | 0.065 | 0.134 | 0.009 | -0.012 |
| RNF213 | 0.484 | 0.265 | -0.039 | 0.373 | 0.110 | -0.143 |
| RPL5 | -0.531 | -0.288 | 0.020 | -0.590 | -0.266 | 0.053 |
| RSAD2 | -0.032 | 0.049 | 0.084 | 0.317 | 0.164 | -0.006 |
| RTP4 | -0.011 | 0.015 | 0.031 | 0.224 | 0.093 | -0.018 |
| S100A4 | 0.142 | 0.180 | -0.156 | 0.050 | -0.039 | -0.100 |
| SAMD9 | 0.311 | 0.215 | 0.086 | 0.498 | 0.150 | -0.043 |
| SAMD9L | 0.089 | 0.165 | 0.124 | 0.425 | 0.138 | -0.066 |
| SAT1 | -0.051 | 0.044 | 0.026 | 0.320 | 0.118 | -0.041 |
| SELL | 0.050 | -0.174 | 0.079 | 0.230 | 0.032 | 0.106 |
| SLFN5 | 0.314 | 0.246 | 0.032 | 0.332 | 0.149 | -0.069 |
| SMCHD1 | 0.193 | 0.039 | 0.005 | 0.356 | 0.113 | -0.070 |
| SNX6 | 0.168 | 0.121 | 0.080 | 0.265 | 0.066 | 0.027 |
| SP100 | -0.034 | 0.081 | 0.107 | 0.316 | 0.136 | -0.016 |
| SP110 | -0.129 | 0.026 | 0.101 | 0.174 | 0.076 | 0.036 |
| SP140 | -0.007 | 0.104 | 0.019 | 0.207 | -0.043 | -0.040 |
| SPATS2L | 0.177 | 0.244 | 0.088 | 0.570 | 0.223 | 0.023 |
| STAT1 | -0.349 | -0.220 | 0.184 | 0.097 | 0.125 | 0.021 |
| STAT2 | -0.035 | 0.012 | 0.079 | 0.248 | 0.100 | -0.042 |
| SUB1 | -0.048 | 0.034 | -0.019 | 0.161 | -0.012 | -0.046 |
| TNFSF10 | -0.080 | 0.099 | 0.063 | 0.206 | 0.113 | -0.034 |
| TRANK1 | 0.063 | 0.052 | 0.033 | 0.172 | -0.052 | -0.039 |
| TREX1 | -0.102 | 0.007 | 0.057 | 0.217 | 0.110 | -0.003 |
| TRIM22 | 0.206 | 0.010 | 0.072 | 0.282 | 0.137 | -0.099 |
| TYMP | -0.162 | 0.085 | 0.101 | -0.070 | 0.007 | -0.053 |
| UBE2L6 | -0.112 | 0.034 | 0.206 | 0.370 | 0.186 | 0.081 |
| USP18 | 0.011 | 0.056 | 0.093 | 0.382 | 0.197 | 0.047 |
| VAMP5 | 0.098 | 0.092 | 0.097 | 0.128 | 0.042 | -0.006 |
| WARS | -0.125 | -0.106 | 0.078 | -0.011 | -0.088 | 0.038 |
| XAF1 | -0.097 | 0.141 | 0.119 | 0.505 | 0.214 | -0.030 |
| XRN1 | 0.055 | 0.081 | 0.096 | 0.119 | -0.021 | -0.064 |
| ZBP1 | 0.120 | 0.154 | 0.025 | 0.451 | 0.129 | -0.037 |

# REFERENCES


Ahel, J., A. Lehner, A. Vogel, A. Schleiffer, A. Meinhart, D. Haselbach, and T. Clausen. 2020. 'Moyamoya disease factor RNF213 is a giant E3 ligase with a dynein-like core and a distinct ubiquitin-transfer mechanism', *Elife*, 9.

Alberti, M. O., J. J. Jones, R. Miglietta, H. Ding, R. K. Bakshi, T. G. Edmonds, J. C. Kappes, and C. Ochsenbauer. 2015. 'Optimized Replicating Renilla Luciferase Reporter HIV-1 Utilizing Novel Internal Ribosome Entry Site Elements for Native Nef Expression and Function', *AIDS Res Hum Retroviruses*, 31: 1278-96.

Albin, J. S., and R. S. Harris. 2010. 'Interactions of host APOBEC3 restriction factors with HIV-1 in vivo: implications for therapeutics', *Expert Rev Mol Med*, 12: e4.

Altfeld, M., and M. Gale, Jr. 2015. 'Innate immunity against HIV-1 infection', *Nat Immunol*, 16: 554-62.

Anders, S., P. T. Pyl, and W. Huber. 2015. 'HTSeq--a Python framework to work with high-throughput sequencing data', *Bioinformatics*, 31: 166-9.

Anderson, S. L., J. M. Carton, J. Lou, L. Xing, and B. Y. Rubin. 1999. 'Interferon-induced guanylate binding protein-1 (GBP-1) mediates an antiviral effect against vesicular stomatitis virus and encephalomyocarditis virus', *Virology*, 256: 8-14.

Andrews, L. P., A. E. Marciscano, C. G. Drake, and D. A. Vignali. 2017. 'LAG3 (CD223) as a cancer immunotherapy target', *Immunol Rev*, 276: 80-96.

Andrews, S. 2010. "FastQC:  A Quality Control Tool for High Throughput Sequence Data [Online]." In.

Archin, N. M., J. M. Sung, C. Garrido, N. Soriano-Sarabia, and D. M. Margolis. 2014. 'Eradicating HIV-1 infection: seeking to clear a persistent pathogen', *Nat Rev Microbiol*, 12: 750-64.

Archin, N. M., N. K. Vaidya, J. D. Kuruc, A. L. Liberty, A. Wiegand, M. F. Kearney, M. S. Cohen, J. M. Coffin, R. J. Bosch, C. L. Gay, J. J. Eron, D. M. Margolis, and A. S. Perelson. 2012. 'Immediate antiviral therapy appears to restrict resting CD4+ cell HIV-1 infection without accelerating the decay of latent infection', *Proc Natl Acad Sci U S A*, 109: 9523-8.

Ashokkumar, M., A. Sonawane, M. Sperk, S. P. Tripathy, U. Neogi, and L. E. Hanna. 2020. 'In vitro replicative fitness of early Transmitted founder HIV-1 variants and sensitivity to Interferon alpha', *Sci Rep*, 10: 2747.

Astronomo, R. D., S. Santra, L. Ballweber-Fleming, K. G. Westerberg, L. Mach, T. Hensley-McBain, L. Sutherland, B. Mildenberg, G. Morton, N. L. Yates, G. J. Mize, J. Pollara, F. Hladik, C. Ochsenbauer, T. N. Denny, R. Warrier, S. Rerks-Ngarm, P. Pitisuttithum, S. Nitayapan, J. Kaewkungwal, G. Ferrari, G. M. Shaw, S. M. Xia, H. X. Liao, D. C. Montefiori, G. D. Tomaras, B. F. Haynes, and J. M. McElrath. 2016. 'Neutralization Takes Precedence Over IgG or IgA

Isotype-related Functions in Mucosal HIV-1 Antibody-mediated Protection', *EBioMedicine*, 14: 97-111.

Barre-Sinoussi, F., J. C. Chermann, F. Rey, M. T. Nugeyre, S. Chamaret, J. Gruest, C. Dauguet, C. Axler-Blin, F. Vezinet-Brun, C. Rouzioux, W. Rozenbaum, and L. Montagnier. 1983. 'Isolation of a T-lymphotropic retrovirus from a patient at risk for acquired immune deficiency syndrome (AIDS)', *Science*, 220: 868-71.

Bashiri, K., N. Rezaei, M. Nasi, and A. Cossarizza. 2018. 'The role of latency reversal agents in the cure of HIV: A review of current data', *Immunol Lett*, 196: 135-39.

Benjamini, Yoav, and Yosef Hochberg. 1995. 'Controlling the False Discovery Rate: A Practical and Powerful Approach to Multiple Testing', *Journal of the Royal Statistical Society: Series B (Methodological)*, 57: 289-300.

Berg, R. K., J. Melchjorsen, J. Rintahaka, E. Diget, S. Soby, K. A. Horan, R. J. Gorelick, S. Matikainen, C. S. Larsen, L. Ostergaard, S. R. Paludan, and T. H. Mogensen. 2012. 'Genomic HIV RNA induces innate immune responses through RIG-I-dependent sensing of secondary-structured RNA', *Plos One*, 7: e29291.

Board, N. L., M. Moskovljevic, F. Wu, R. F. Siliciano, and J. D. Siliciano. 2021. 'Engaging innate immunity in HIV-1 cure strategies', *Nat Rev Immunol*.

Bosinger, S. E., Q. Li, S. N. Gordon, N. R. Klatt, L. Duan, L. Xu, N. Francella, A. Sidahmed, A. J. Smith, E. M. Cramer, M. Zeng, D. Masopust, J. V. Carlis, L. Ran, T. H. Vanderford, M. Paiardini, R. B. Isett, D. A. Baldwin, J. G. Else, S. I. Staprans, G. Silvestri, A. T. Haase, and D. J. Kelvin. 2009. 'Global genomic analysis reveals rapid control of a robust innate response in SIV-infected sooty mangabeys', *J Clin Invest*, 119: 3556-72.

Bosinger, S. E., and N. S. Utay. 2015. 'Type I interferon: understanding its role in HIV pathogenesis and therapy', *Curr HIV/AIDS Rep*, 12: 41-53.

Bosque, A., and V. Planelles. 2009. 'Induction of HIV-1 latency and reactivation in primary memory CD4+ T cells', *Blood*, 113: 58-65.

Bradley, T., G. Ferrari, B. F. Haynes, D. M. Margolis, and E. P. Browne. 2018. 'Single-Cell Analysis of Quiescent HIV Infection Reveals Host Transcriptional Profiles that Regulate Proviral Latency', *Cell Rep*, 25: 107-17 e3.

Bui. 2017. *PLoS Pathog*.

Butler, A., P. Hoffman, P. Smibert, E. Papalexi, and R. Satija. 2018. 'Integrating single-cell transcriptomic data across different conditions, technologies, and species', *Nat Biotechnol*, 36: 411-20.

Buzon, M. J., H. Sun, C. Li, A. Shaw, K. Seiss, Z. Ouyang, E. Martin-Gayo, J. Leng, T. J. Henrich, J. Z. Li, F. Pereyra, R. Zurakowski, B. D. Walker, E. S. Rosenberg, X. G. Yu, and M. Lichterfeld. 2014. 'HIV-1 persistence in CD4+ T cells with stem cell-like properties', *Nat Med*, 20: 139-42.

Calvanese, V., L. Chavez, T. Laurent, S. Ding, and E. Verdin. 2013. 'Dual-color HIV reporters trace a population of latently infected cells and enable their purification', *Virology*, 446: 283-92.

Cameron, P. U., S. Saleh, G. Sallmann, A. Solomon, F. Wightman, V. A. Evans, G. Boucher, E. K. Haddad, R. P. Sekaly, A. N. Harman, J. L. Anderson, K. L. Jones, J. Mak, A. L. Cunningham, A. Jaworowski, and S. R. Lewin. 2010. 'Establishment of HIV-1 latency in resting CD4+ T cells depends on chemokine-induced changes in the actin cytoskeleton', *Proc Natl Acad Sci U S A*, 107: 16934-9.

Cavrois, M., T. Banerjee, G. Mukherjee, N. Raman, R. Hussien, B. A. Rodriguez, J. Vasquez, M. H. Spitzer, N. H. Lazarus, J. J. Jones, C. Ochsenbauer, J. M. McCune, E. C. Butcher, A. M. Arvin, N. Sen, W. C. Greene, and N. R. Roan. 2017. 'Mass Cytometric Analysis of HIV Entry, Replication, and Remodeling in Tissue CD4+ T Cells', *Cell Rep*, 20: 984-98.

Ceccarelli, G., M. Giovanetti, C. Sagnelli, A. Ciccozzi, G. d'Ettorre, S. Angeletti, A. Borsetti, and M. Ciccozzi. 2021. 'Human Immunodeficiency Virus Type 2: The Neglected Threat', *Pathogens*, 10.

Cheng, L., J. Ma, J. Li, D. Li, G. Li, F. Li, Q. Zhang, H. Yu, F. Yasui, C. Ye, L. C. Tsao, Z. Hu, L. Su, and L. Zhang. 2017. 'Blocking type I interferon signaling enhances T cell recovery and reduces HIV-1 reservoirs', *J Clin Invest*, 127: 269-79.

Cheng, L., H. Yu, G. Li, F. Li, J. Ma, J. Li, L. Chi, L. Zhang, and L. Su. 2017. 'Type I interferons suppress viral replication but contribute to T cell depletion and dysfunction during chronic HIV-1 infection', *JCI Insight*, 2.

Chun, T. W., D. Finzi, J. Margolick, K. Chadwick, D. Schwartz, and R. F. Siliciano. 1995. 'In vivo fate of HIV-1-infected T cells: quantitative analysis of the transition to stable latency', *Nat Med*, 1: 1284-90.

Chun, T. W., L. Stuyver, S. B. Mizell, L. A. Ehler, J. A. Mican, M. Baseler, A. L. Lloyd, M. A. Nowak, and A. S. Fauci. 1997. 'Presence of an inducible HIV-1 latent reservoir during highly active antiretroviral therapy', *Proc Natl Acad Sci U S A*, 94: 13193-7.

Cohn, L. B., I. T. da Silva, R. Valieris, A. S. Huang, J. C. C. Lorenzi, Y. Z. Cohen, J. A. Pai, A. L. Butler, M. Caskey, M. Jankovic, and M. C. Nussenzweig. 2018. 'Clonal CD4(+) T cells in the HIV-1 latent reservoir display a distinct gene profile upon reactivation', *Nat Med*, 24: 604-09.

Cohn, L. B., I. T. Silva, T. Y. Oliveira, R. A. Rosales, E. H. Parrish, G. H. Learn, B. H. Hahn, J. L. Czartoski, M. J. McElrath, C. Lehmann, F. Klein, M. Caskey, B. D. Walker, J. D. Siliciano, R. F. Siliciano, M. Jankovic, and M. C. Nussenzweig. 2015. 'HIV-1 integration landscape during latent and active infection', *Cell*, 160: 420-32.

Dahabieh, M. S., M. Ooms, V. Simon, and I. Sadowski. 2013. 'A doubly fluorescent HIV-1 reporter shows that the majority of integrated HIV-1 is latent shortly after infection', *J Virol*, 87: 4716-27.

Dalgleish, A. G., P. C. Beverley, P. R. Clapham, D. H. Crawford, M. F. Greaves, and R. A. Weiss. 1984. 'The CD4 (T4) antigen is an essential component of the receptor for the AIDS retrovirus', *Nature*, 312: 763-7.

Diamond, M. S., and M. Farzan. 2013. 'The broad-spectrum antiviral functions of IFIT and IFITM proteins', *Nat Rev Immunol*, 13: 46-57.

Dobin, A., C. A. Davis, F. Schlesinger, J. Drenkow, C. Zaleski, S. Jha, P. Batut, M. Chaisson, and T. R. Gingeras. 2013. 'STAR: ultrafast universal RNA-seq aligner', *Bioinformatics*, 29: 15-21.

Doehle, B. P., K. Chang, A. Rustagi, J. McNevin, M. J. McElrath, and M. Gale, Jr. 2012. 'Vpu mediates depletion of interferon regulatory factor 3 during HIV infection by a lysosome-dependent mechanism', *J Virol*, 86: 8367-74.

Doehle, B. P., F. Hladik, J. P. McNevin, M. J. McElrath, and M. Gale, Jr. 2009. 'Human immunodeficiency virus type 1 mediates global disruption of innate antiviral signaling and immune defenses within infected cells', *J Virol*, 83: 10395-405.

Dong, B., Q. Zhou, J. Zhao, A. Zhou, R. N. Harty, S. Bose, A. Banerjee, R. Slee, J. Guenther, B. R. Williams, T. Wiedmer, P. J. Sims, and R. H. Silverman. 2004. 'Phospholipid scramblase 1 potentiates the antiviral activity of interferon', *J Virol*, 78: 8983-93.

Doyle, T., C. Goujon, and M. H. Malim. 2015. 'HIV-1 and interferons: who's interfering with whom?', *Nat Rev Microbiol*, 13: 403-13.

Dube, M., B. B. Roy, P. Guiot-Guillain, J. Binette, J. Mercier, A. Chiasson, and E. A. Cohen. 2010. 'Antagonism of tetherin restriction of HIV-1 release by Vpu involves binding and sequestration of the restriction factor in a perinuclear compartment', *PLoS Pathog*, 6: e1000856.

El Kharroubi, A., G. Piras, R. Zensen, and M. A. Martin. 1998. 'Transcriptional activation of the integrated chromatin-associated human immunodeficiency virus type 1 promoter', *Mol Cell Biol*, 18: 2535-44.

Finak, G., A. McDavid, M. Yajima, J. Deng, V. Gersuk, A. K. Shalek, C. K. Slichter, H. W. Miller, M. J. McElrath, M. Prlic, P. S. Linsley, and R. Gottardo. 2015. 'MAST: a flexible statistical framework for assessing transcriptional changes and characterizing heterogeneity in single-cell RNA sequencing data', *Genome Biol*, 16: 278.

Finzi, D., M. Hermankova, T. Pierson, L. M. Carruth, C. Buck, R. E. Chaisson, T. C. Quinn, K. Chadwick, J. Margolick, R. Brookmeyer, J. Gallant, M. Markowitz, D. D. Ho, D. D. Richman, and R. F. Siliciano. 1997. 'Identification of a reservoir for HIV-1 in patients on highly active antiretroviral therapy', *Science*, 278: 1295-300.

Fitzgerald, K. A. 2011. 'The interferon inducible gene: Viperin', *J Interferon Cytokine Res*, 31: 131-5.

Folks, T., S. Benn, A. Rabson, T. Theodore, M. D. Hoggan, M. Martin, M. Lightfoote, and K. Sell. 1985. 'Characterization of a continuous T-cell line susceptible to the cytopathic effects of the acquired immunodeficiency syndrome (AIDS)-associated retrovirus', *Proc Natl Acad Sci U S A*, 82: 4539-43.

Folks, T. M., K. A. Clouse, J. Justement, A. Rabson, E. Duh, J. H. Kehrl, and A. S. Fauci. 1989. 'Tumor necrosis factor alpha induces expression of human immunodeficiency virus in a chronically infected T-cell clone', *Proc Natl Acad Sci U S A*, 86: 2365-8.

Fromentin, R., W. Bakeman, M. B. Lawani, G. Khoury, W. Hartogensis, S. DaFonseca, M. Killian, L. Epling, R. Hoh, E. Sinclair, F. M. Hecht, P. Bacchetti, S. G. Deeks, S. R. Lewin, R. P. Sekaly, and N. Chomont. 2016. 'CD4+ T Cells Expressing PD-1, TIGIT and LAG-3 Contribute to HIV Persistence during ART', *PLoS Pathog*, 12: e1005761.

Gao, D., J. Wu, Y. T. Wu, F. Du, C. Aroh, N. Yan, L. Sun, and Z. J. Chen. 2013. 'Cyclic GMP-AMP synthase is an innate immune sensor of HIV and other retroviruses', *Science*, 341: 903-6.

Garcia-Vidal, E., M. Castellvi, M. Pujantell, R. Badia, A. Jou, L. Gomez, T. Puig, B. Clotet, E. Ballana, E. Riveira-Munoz, and J. A. Este. 2017. 'Evaluation of the Innate Immune Modulator Acitretin as a Strategy To Clear the HIV Reservoir', *Antimicrob Agents Chemother*, 61.

Gornalusse, Germán Gustavo, Lucia N. Vojtech, Claire N. Levy, Sean M. Hughes, Yeseul Kim, Rogelio Valdez, Urvashi Pandey, Christina Ochsenbauer, Rena Astronomo, Julie McElrath, and Florian Hladik. 2021. 'Buprenorphine Increases HIV-1 Infection In Vitro but Does Not Reactivate HIV-1 from Latency', *Viruses*, 13.

Gottlieb, M. S., R. Schroff, H. M. Schanker, J. D. Weisman, P. T. Fan, R. A. Wolf, and A. Saxon. 1981. 'Pneumocystis carinii pneumonia and mucosal candidiasis in previously healthy homosexual men: evidence of a new acquired cellular immunodeficiency', *N Engl J Med*, 305: 1425-31.

Goudarzi, K. M., and M. S. Lindstrom. 2016. 'Role of ribosomal protein mutations in tumor development (Review)', *Int J Oncol*, 48: 1313-24.

Goujon, C., O. Moncorge, H. Bauby, T. Doyle, C. C. Ward, T. Schaller, S. Hue, W. S. Barclay, R. Schulz, and M. H. Malim. 2013. 'Human MX2 is an interferon-induced post-entry inhibitor of HIV-1 infection', *Nature*, 502: 559-62.

Green, R., R. C. Ireton, and M. Gale, Jr. 2018. 'Interferon-stimulated genes: new platforms and computational approaches', *Mamm Genome*, 29: 593-602.

Hahn, B. H., G. M. Shaw, S. K. Arya, M. Popovic, R. C. Gallo, and F. Wong-Staal. 1984. 'Molecular cloning and characterization of the HTLV-III virus associated with AIDS', *Nature*, 312: 166-9.

Hahn, B. H., G. M. Shaw, K. M. De Cock, and P. M. Sharp. 2000. 'AIDS as a zoonosis: scientific and public health implications', *Science*, 287: 607-14.

Han, Y., M. Wind-Rotolo, H. C. Yang, J. D. Siliciano, and R. F. Siliciano. 2007. 'Experimental approaches to the study of HIV-1 latency', *Nat Rev Microbiol*, 5: 95-106.

Hardy, G. A., S. Sieg, B. Rodriguez, D. Anthony, R. Asaad, W. Jiang, J. Mudd, T. Schacker, N. T. Funderburg, H. A. Pilch-Cooper, R. Debernardo, R. L. Rabin, M. M. Lederman, and C. V. Harding. 2013. 'Interferon-alpha is the primary plasma type-I IFN in HIV-1 infection and correlates with immune activation and disease markers', *Plos One*, 8: e56527.

Harrison, A. R., and G. W. Moseley. 2020. 'The Dynamic Interface of Viruses with STATs', *J Virol*, 94.

Ho, Y. C., L. Shan, N. N. Hosmane, J. Wang, S. B. Laskey, D. I. Rosenbloom, J. Lai, J. N. Blankson, J. D. Siliciano, and R. F. Siliciano. 2013. 'Replication-competent noninduced proviruses in the latent reservoir increase barrier to HIV-1 cure', *Cell*, 155: 540-51.

Horner, S. M., and M. Gale, Jr. 2013. 'Regulation of hepatic innate immunity by hepatitis C virus', *Nat Med*, 19: 879-88.

Huang, C. T., C. J. Workman, D. Flies, X. Pan, A. L. Marson, G. Zhou, E. L. Hipkiss, S. Ravi, J. Kowalski, H. I. Levitsky, J. D. Powell, D. M. Pardoll, C. G. Drake, and D. A. Vignali. 2004. 'Role of LAG-3 in regulatory T cells', *Immunity*, 21: 503-13.

Hutter, G., D. Nowak, M. Mossner, S. Ganepola, A. Mussig, K. Allers, T. Schneider, J. Hofmann, C. Kucherer, O. Blau, I. W. Blau, W. K. Hofmann, and E. Thiel. 2009. 'Long-term control of HIV by CCR5 Delta32/Delta32 stem-cell transplantation', *N Engl J Med*, 360: 692-8.

Itsui, Y., N. Sakamoto, S. Kakinuma, M. Nakagawa, Y. Sekine-Osajima, M. Tasaka-Fujita, Y. Nishimura-Sakurai, G. Suda, Y. Karakama, K. Mishima, M. Yamamoto, T. Watanabe, M. Ueyama, Y. Funaoka, S. Azuma, and M. Watanabe. 2009. 'Antiviral effects of the interferon-induced protein guanylate binding protein 1 and its interaction with the hepatitis C virus NS5B protein', *Hepatology*, 50: 1727-37.

Iyer, S. S., F. Bibollet-Ruche, S. Sherrill-Mix, G. H. Learn, L. Plenderleith, A. G. Smith, H. J. Barbian, R. M. Russell, M. V. Gondim, C. Y. Bahari, C. M. Shaw, Y. Li, T. Decker, B. F. Haynes, G. M. Shaw, P. M. Sharp, P. Borrow, and B. H. Hahn. 2017. 'Resistance to type 1 interferons is a major determinant of HIV-1 transmission fitness', *Proc Natl Acad Sci U S A*, 114: E590-E99.

Jacquelin, B., V. Mayau, B. Targat, A. S. Liovat, D. Kunkel, and G. Petitjean. 2009. 'Nonpathogenic SIV infection of African green monkeys induces a strong but rapidly controlled type I IFN response', *J Clin Invest*, 119: 3544-55.

Jakobsen, M. R., R. O. Bak, A. Andersen, R. K. Berg, S. B. Jensen, J. Tengchuan, A. Laustsen, K. Hansen, L. Ostergaard, K. A. Fitzgerald, T. S. Xiao, J. G. Mikkelsen, T. H. Mogensen, and S. R. Paludan. 2013. 'IFI16 senses DNA forms of the lentiviral replication cycle and controls HIV-1 replication', *Proc Natl Acad Sci U S A*, 110: E4571-80.

Jensen, S., and A. R. Thomsen. 2012. 'Sensing of RNA viruses: a review of innate immune receptors involved in recognizing RNA virus invasion', *J Virol*, 86: 2900-10.

Jordan, A., D. Bisgrove, and E. Verdin. 2003. 'HIV reproducibly establishes a latent infection after acute infection of T cells in vitro', *EMBO J*, 22: 1868-77.

Kane, M., S. S. Yadav, J. Bitzegeio, S. B. Kutluay, T. Zang, S. J. Wilson, J. W. Schoggins, C. M. Rice, M. Yamashita, T. Hatziioannou, and P. D. Bieniasz. 2013. 'MX2 is an interferon-induced inhibitor of HIV-1 infection', *Nature*, 502: 563-6.

Kell, A., M. Stoddard, H. Li, J. Marcotrigiano, G. M. Shaw, and M. Gale, Jr. 2015. 'Pathogen-Associated Molecular Pattern Recognition of Hepatitis C Virus Transmitted/Founder Variants by RIG-I Is Dependent on U-Core Length', *J Virol*, 89: 11056-68.

Khanal, S., M. Schank, M. El Gazzar, J. P. Moorman, and Z. Q. Yao. 2021. 'HIV-1 Latency and Viral Reservoirs: Existing Reversal Approaches and Potential Technologies, Targets, and Pathways Involved in HIV Latency Studies', *Cells*, 10.

Khoury, G., G. Darcis, M. Y. Lee, S. Bouchat, B. Van Driessche, D. F. J. Purcell, and C. Van Lint. 2018. 'The Molecular Biology of HIV Latency', *Adv Exp Med Biol*, 1075: 187-212.

Kile, B. T., and W. S. Alexander. 2001. 'The suppressors of cytokine signalling (SOCS)', *Cell Mol Life Sci*, 58: 1627-35.

Kim, Y. J., E. T. Kim, Y. E. Kim, M. K. Lee, K. M. Kwon, K. I. Kim, T. Stamminger, and J. H. Ahn. 2016. 'Consecutive Inhibition of ISG15 Expression and ISGylation by Cytomegalovirus Regulators', *PLoS Pathog*, 12: e1005850.

Kleinman, C. L., M. Doria, E. Orecchini, E. Giuliani, S. Galardi, N. De Jay, and A. Michienzi. 2014. 'HIV-1 infection causes a down-regulation of genes involved in ribosome biogenesis', *Plos One*, 9: e113908.

Kramer, A., J. Green, J. Pollard, Jr., and S. Tugendreich. 2014. 'Causal analysis approaches in Ingenuity Pathway Analysis', *Bioinformatics*, 30: 523-30.

Krapp, C., D. Hotter, A. Gawanbacht, P. J. McLaren, S. F. Kluge, C. M. Sturzel, K. Mack, E. Reith, S. Engelhart, A. Ciuffi, V. Hornung, D. Sauter, A. Telenti, and F. Kirchhoff. 2016. 'Guanylate Binding Protein (GBP) 5 Is an Interferon-Inducible Inhibitor of HIV-1 Infectivity', *Cell Host Microbe*, 19: 504-14.

Kumar, A., M. Commane, T. W. Flickinger, C. M. Horvath, and G. R. Stark. 1997. 'Defective TNF-alpha-induced apoptosis in STAT1-null cells due to low constitutive levels of caspases', *Science*, 278: 1630-2.

Langfelder, P., and S. Horvath. 2008. 'WGCNA: an R package for weighted correlation network analysis', *BMC Bioinformatics*, 9: 559.

Langfelder, P., B. Zhang, and S. Horvath. 2008. 'Defining clusters from a hierarchical cluster tree: the Dynamic Tree Cut package for R', *Bioinformatics*, 24: 719-20.

Langmead, B., and S. L. Salzberg. 2012. 'Fast gapped-read alignment with Bowtie 2', *Nat Methods*, 9: 357-9.

Lassen, K. G., A. M. Hebbeler, D. Bhattacharyya, M. A. Lobritz, and W. C. Greene. 2012. 'A flexible model of HIV-1 latency permitting evaluation of many primary CD4 T-cell reservoirs', *Plos One*, 7: e30176.

Lau, D. T., A. Negash, J. Chen, N. Crochet, M. Sinha, Y. Zhang, J. Guedj, S. Holder, T. Saito, S. M. Lemon, B. A. Luxon, A. S. Perelson, and M. Gale, Jr. 2013. 'Innate immune tolerance and the role of kupffer cells in differential responses to interferon therapy among patients with HCV genotype 1 infection', *Gastroenterology*, 144: 402-13 e12.

Law, C. W., Y. Chen, W. Shi, and G. K. Smyth. 2014. 'voom: Precision weights unlock linear model analysis tools for RNA-seq read counts', *Genome Biol*, 15: R29.

Lee. 2014. *JCI*.

Levy, C. N., S. M. Hughes, P. Roychoudhury, D. B. Reeves, C. Amstuz, H. Zhu, M. L. Huang, Y. Wei, M. E. Bull, N. A. J. Cassidy, J. McClure, L. M. Frenkel, M. Stone, S. Bakkour, E. R. Wonderlich, M. P. Busch, S. G. Deeks, J. T. Schiffer, R. W. Coombs, D. A. Lehman, K. R. Jerome, and F. Hladik. 2021. 'A highly multiplexed droplet digital PCR assay to measure the intact HIV-1 proviral reservoir', *Cell Rep Med*, 2: 100243.

Li, P., P. Kaiser, H. W. Lampiris, P. Kim, S. A. Yukl, D. V. Havlir, W. C. Greene, and J. K. Wong. 2016. 'Stimulating the RIG-I pathway to kill cells in the latent HIV reservoir following viral reactivation', *Nat Med*, 22: 807-11.

Liao, Y., J. Wang, E. J. Jaehnig, Z. Shi, and B. Zhang. 2019. 'WebGestalt 2019: gene set analysis toolkit with revamped UIs and APIs', *Nucleic Acids Research*, 47: W199-W205.

Liberatore, R. A., and P. D. Bieniasz. 2011. 'Tetherin is a key effector of the antiretroviral activity of type I interferon in vitro and in vivo', *Proc Natl Acad Sci U S A*, 108: 18097-101.

Ling, X. B., H. W. Wei, J. Wang, Y. Q. Kong, Y. Y. Wu, J. L. Guo, T. F. Li, and J. K. Li. 2016. 'Mammalian Metallothionein-2A and Oxidative Stress', *Int J Mol Sci*, 17.

Liu, Z., Q. Pan, S. Ding, J. Qian, F. Xu, J. Zhou, S. Cen, F. Guo, and C. Liang. 2013. 'The interferon-inducible MxB protein inhibits HIV-1 infection', *Cell Host Microbe*, 14: 398-410.

Lu, J., Q. Pan, L. Rong, W. He, S. L. Liu, and C. Liang. 2011. 'The IFITM proteins inhibit HIV-1 infection', *J Virol*, 85: 2126-37.

Marsili, G., A. Borsetti, M. Sgarbanti, A. L. Remoli, B. Ridolfi, E. Stellacci, B. Ensoli, and A. Battistini. 2003. 'On the role of interferon regulatory factors in HIV-1 replication', *Ann N Y Acad Sci*, 1010: 29-42.

Martin, Marcel. 2011. 'Cutadapt removes adapter sequences from high-throughput sequencing reads', *EMBnet.journal*, 17.

Meas, H. Z., M. Haug, M. S. Beckwith, C. Louet, L. Ryan, Z. Hu, J. Landskron, S. A. Nordbo, K. Tasken, H. Yin, J. K. Damas, and T. H. Flo. 2020. 'Sensing of HIV-1 by TLR8 activates human T cells and reverses latency', *Nat Commun*, 11: 147.

Nasr, N., A. A. Alshehri, T. K. Wright, M. Shahid, B. M. Heiner, A. N. Harman, R. A. Botting, K. J. Helbig, M. R. Beard, K. Suzuki, A. D. Kelleher, P. Hertzog, and A. L. Cunningham. 2017. 'Mechanism of Interferon-Stimulated Gene Induction in HIV-1-Infected Macrophages', *J Virol*, 91.

Nchioua, R., M. Bosso, D. Kmiec, and F. Kirchhoff. 2020. 'Cellular Factors Targeting HIV-1 Transcription and Viral RNA Transcripts', *Viruses*, 12.

Nittayananta, W., R. Tao, L. Jiang, Y. Peng, and Y. Huang. 2016. 'Oral innate immunity in HIV infection in HAART era', *J Oral Pathol Med*, 45: 3-8.

Okamoto, M., A. Hidaka, M. Toyama, and M. Baba. 2019. 'Galectin-3 is involved in HIV-1 expression through NF-kappaB activation and associated with Tat in latently infected cells', *Virus Res*, 260: 86-93.

Okumura, A., T. Alce, B. Lubyova, H. Ezelle, K. Strebel, and P. M. Pitha. 2008. 'HIV-1 accessory proteins VPR and Vif modulate antiviral response by targeting IRF-3 for degradation', *Virology*, 373: 85-97.

Okumura, A., G. Lu, I. Pitha-Rowe, and P. M. Pitha. 2006. 'Innate antiviral response targets HIV-1 release by the induction of ubiquitin-like protein ISG15', *Proc Natl Acad Sci U S A*, 103: 1440-5.

Pan, W., X. Zuo, T. Feng, X. Shi, and J. Dai. 2012. 'Guanylate-binding protein 1 participates in cellular antiviral response to dengue virus', *Virol J*, 9: 292.

Pardons, M., A. E. Baxter, M. Massanella, A. Pagliuzza, R. Fromentin, C. Dufour, L. Leyre, J. P. Routy, D. E. Kaufmann, and N. Chomont. 2019. 'Single-cell characterization and quantification of translation-competent viral reservoirs in treated and untreated HIV infection', *PLoS Pathog*, 15: e1007619.

Park, S. Y., A. A. Waheed, Z. R. Zhang, E. O. Freed, and J. S. Bonifacino. 2014. 'HIV-1 Vpu accessory protein induces caspase-mediated cleavage of IRF3 transcription factor', *J Biol Chem*, 289: 35102-10.

Pitha, P. M. 2011. 'Innate antiviral response: role in HIV-1 infection', *Viruses*, 3: 1179-203.

Pliner, H. A., J. Shendure, and C. Trapnell. 2019. 'Supervised classification enables rapid annotation of cell atlases', *Nat Methods*, 16: 983-86.

Prévost, J., J. Richard, H. Medjahed, A. Alexander, J. Jones, J. C. Kappes, C. Ochsenbauer, and A. Finzi. 2018. 'Incomplete Downregulation of CD4 Expression Affects HIV-1 Env Conformation and Antibody-Dependent Cellular Cytotoxicity Responses', *J Virol*, 92.

Raftery, N., and N. J. Stevenson. 2017. 'Advances in anti-viral immune defence: revealing the importance of the IFN JAK/STAT pathway', *Cell Mol Life Sci*, 74: 2525-35.

Ranganath, N., T. S. Sandstrom, S. Fadel, S. C. Cote, and J. B. Angel. 2016. 'Type I interferon responses are impaired in latently HIV infected cells', *Retrovirology*, 13: 66.

Remoli, A. L., G. Marsili, E. Perrotti, E. Gallerani, R. Ilari, F. Nappi, A. Cafaro, B. Ensoli, R. Gavioli, and A. Battistini. 2006. 'Intracellular HIV-1 Tat protein represses constitutive LMP2 transcription increasing proteasome activity by interfering with the binding of IRF-1 to STAT1', *Biochem J*, 396: 371-80.

Ringeard, M., V. Marchand, E. Decroly, Y. Motorin, and Y. Bennasser. 2019. 'FTSJ3 is an RNA 2'-O-methyltransferase recruited by HIV to avoid innate immune sensing', *Nature*, 565: 500-04.

Ritchie, M. E., B. Phipson, D. Wu, Y. Hu, C. W. Law, W. Shi, and G. K. Smyth. 2015. 'limma powers differential expression analyses for RNA-sequencing and microarray studies', *Nucleic Acids Research*, 43: e47.

Rotger, M., J. Dalmau, A. Rauch, P. McLaren, S. E. Bosinger, R. Martinez, N. G. Sandler, A. Roque, J. Liebner, M. Battegay, E. Bernasconi, P. Descombes, I. Erkizia, J. Fellay, B. Hirschel, J. M. Miro, E. Palou, M. Hoffmann, M. Massanella, J. Blanco, M. Woods, H. F. Gunthard, P. de Bakker, D. C. Douek, G. Silvestri, J. Martinez-Picado, and A. Telenti. 2011. 'Comparative transcriptomics of extreme phenotypes of human HIV-1 infection and SIV infection in sooty mangabey and rhesus macaque', *J Clin Invest*, 121: 2391-400.

Rustagi, A., B. P. Doehle, M. J. McElrath, and M. Gale, Jr. 2013. 'Two new monoclonal antibodies for biochemical and flow cytometric analyses of human interferon regulatory factor-3 activation, turnover, and depletion', *Methods*, 59: 225-32.

Saito, T., D. M. Owen, F. Jiang, J. Marcotrigiano, and M. Gale, Jr. 2008. 'Innate immunity induced by composition-dependent RIG-I recognition of hepatitis C virus RNA', *Nature*, 454: 523-7.

Saleh, S., A. Solomon, F. Wightman, M. Xhilaga, P. U. Cameron, and S. R. Lewin. 2007. 'CCR7 ligands CCL19 and CCL21 increase permissiveness of resting memory CD4+ T cells to HIV-1 infection: a novel model of HIV-1 latency', *Blood*, 110: 4161-4.

Sandler, N. G., S. E. Bosinger, J. D. Estes, R. T. Zhu, G. K. Tharp, E. Boritz, D. Levin, S. Wijeyesinghe, K. N. Makamdop, G. Q. del Prete, B. J. Hill, J. K. Timmer, E. Reiss, G. Yarden, S. Darko, E. Contijoch, J. P. Todd, G. Silvestri, M. Nason, R. B. Norgren, Jr., B. F. Keele, S. Rao, J. A. Langer, J. D. Lifson, G. Schreiber, and D. C. Douek. 2014. 'Type I interferon responses in rhesus macaques prevent SIV infection and slow disease progression', *Nature*, 511: 601-5.

Schlaepfer, E., A. Audige, H. Joller, and R. F. Speck. 2006. 'TLR7/8 triggering exerts opposing effects in acute versus latent HIV infection', *J Immunol*, 176: 2888-95.

Schoggins, J. W., and C. M. Rice. 2011. 'Interferon-stimulated genes and their antiviral effector functions', *Curr Opin Virol*, 1: 519-25.

Shan, L., K. Deng, H. Gao, S. Xing, A. A. Capoferri, C. M. Durand, S. A. Rabi, G. M. Laird, M. Kim, N. N. Hosmane, H. C. Yang, H. Zhang, J. B. Margolick, L. Li, W. Cai, R. Ke, R. A. Flavell, J. D. Siliciano, and R. F. Siliciano. 2017. 'Transcriptional Reprogramming during Effector-to-Memory Transition Renders CD4(+) T Cells Permissive for Latent HIV-1 Infection', *Immunity*, 47: 766-75 e3.

Shaulian, E., and M. Karin. 2002. 'AP-1 as a regulator of cell life and death', *Nat Cell Biol*, 4: E131-6.

Sheehy, A. M., N. C. Gaddis, and M. H. Malim. 2003. 'The antiretroviral enzyme APOBEC3G is degraded by the proteasome in response to HIV-1 Vif', *Nat Med*, 9: 1404-7.

Siliciano, R. F., and W. C. Greene. 2011. 'HIV latency', *Cold Spring Harb Perspect Med*, 1: a007096.

Simonetti. 2015. 'Clonally expanded CD4+ T cells can produce infectious HIV-1 in vivo', *PNAS*.

Sivro, A., R. C. Su, F. A. Plummer, and T. B. Ball. 2013. 'HIV and interferon regulatory factor 1: a story of manipulation and control', *AIDS Res Hum Retroviruses*, 29: 1428-33.

Solis, M., P. Nakhaei, M. Jalalirad, J. Lacoste, R. Douville, M. Arguello, T. Zhao, M. Laughrea, M. A. Wainberg, and J. Hiscott. 2011. 'RIG-I-mediated antiviral signaling is inhibited in HIV-1 infection by a protease-mediated sequestration of RIG-I', *J Virol*, 85: 1224-36.

Song, M. M., and K. Shuai. 1998. 'The suppressor of cytokine signaling (SOCS) 1 and SOCS3 but not SOCS2 proteins inhibit interferon-mediated antiviral and antiproliferative activities', *J Biol Chem*, 273: 35056-62.

Stark, G. R., and J. E. Darnell, Jr. 2012. 'The JAK-STAT pathway at twenty', *Immunity*, 36: 503-14.

Stunnenberg, M., T. B. H. Geijtenbeek, and S. I. Gringhuis. 2018. 'DDX3 in HIV-1 infection and sensing: A paradox', *Cytokine Growth Factor Rev*, 40: 32-39.

Tanaka, T., B. M. Warner, T. Odani, Y. Ji, Y. Q. Mo, H. Nakamura, S. I. Jang, H. Yin, D. G. Michael, N. Hirata, F. Suizu, S. Ishigaki, F. R. Oliveira, A. C. F. Motta, A. Ribeiro-Silva, E. M. Rocha, T. Atsumi, M. Noguchi, and J. A. Chiorini. 2020. 'LAMP3 induces apoptosis and autoantigen release in Sjogren's syndrome patients', *Sci Rep*, 10: 15169.

Taube, R., and M. Peterlin. 2013. 'Lost in transcription: molecular mechanisms that control HIV latency', *Viruses*, 5: 902-27.

Trapnell, C., D. Cacchiarelli, J. Grimsby, P. Pokharel, S. Li, M. Morse, N. J. Lennon, K. J. Livak, T. S. Mikkelsen, and J. L. Rinn. 2014. 'The dynamics and regulators of cell fate decisions are revealed by pseudotemporal ordering of single cells', *Nat Biotechnol*, 32: 381-86.

UNAIDS. 2021. "Global HIV & AIDS statistics — Fact sheet." In.: Joint United Nations Programme on HIV/AIDS (UNAIDS).

Van der Sluis, R. M., J. M. Zerbato, J. W. Rhodes, R. D. Pascoe, A. Solomon, N. A. Kumar, A. I. Dantanarayana, S. Tennakoon, J. Dufloo, J. McMahon, J. J. Chang, V. A. Evans, P. J. Hertzog, M. R. Jakobsen, A. N. Harman, S. R. Lewin, and P. U. Cameron. 2020. 'Diverse effects of interferon alpha on the establishment and reversal of HIV latency', *PLoS Pathog*, 16: e1008151.

Van Lint, C., S. Bouchat, and A. Marcello. 2013. 'HIV-1 transcription and latency: an update', *Retrovirology*, 10: 67.

Vanhamel, Jef, Anne Bruggemans, and Zeger Debyser. 2019. 'Establishment of HIV latent reservoirs: what do we really know?', *Journal of virus eradication*, 5: 3-9.

Ventura, J. D., J. Beloor, E. Allen, T. Zhang, K. A. Haugh, P. D. Uchil, C. Ochsenbauer, C. Kieffer, P. Kumar, T. J. Hope, and W. Mothes. 2019. 'Longitudinal bioluminescent imaging of HIV-1 infection during antiretroviral therapy and treatment interruption in humanized mice', *PLoS Pathog*, 15: e1008161.

Wain-Hobson, Simon, Pierre Sonigo, Olivier Danos, Stewart Cole, and Marc Alizon. 1985. 'Nucleotide sequence of the AIDS virus, LAV', *Cell*, 40: 9-17.

Whitney, James B. 2009. 'Rapid seeding of the viral reservoir prior to SIV viraemia in rhesus monkeys', *Nature*.

Wickham, Hadley. 2011. 'ggplot2', *Wiley Interdisciplinary Reviews: Computational Statistics*, 3: 180-85.

Wong, J. K., and S. A. Yukl. 2016. 'Tissue reservoirs of HIV', *Curr Opin HIV AIDS*, 11: 362-70.

Yan, N., A. D. Regalado-Magdos, B. Stiggelbout, M. A. Lee-Kirsch, and J. Lieberman. 2010. 'The cytosolic exonuclease TREX1 inhibits the innate immune response to human immunodeficiency virus type 1', *Nat Immunol*, 11: 1005-13.

Yang, H., F. Ito, A. D. Wolfe, S. Li, N. Mohammadzadeh, R. P. Love, M. Yan, B. Zirkle, A. Gaba, L. Chelico, and X. S. Chen. 2020. 'Understanding the structural basis of HIV-1 restriction by the full length double-domain APOBEC3G', *Nat Commun*, 11: 632.

Yin, X., S. Langer, Z. Zhang, K. M. Herbert, S. Yoh, R. Konig, and S. K. Chanda. 2020. 'Sensor Sensibility-HIV-1 and the Innate Immune Response', *Cells*, 9.

Yu, J., M. Li, J. Wilkins, S. Ding, T. H. Swartz, A. M. Esposito, Y. M. Zheng, E. O. Freed, C. Liang, B. K. Chen, and S. L. Liu. 2015. 'IFITM Proteins Restrict HIV-1 Infection by Antagonizing the Envelope Glycoprotein', *Cell Rep*, 13: 145-56.

Zhen, A., V. Rezek, C. Youn, B. Lam, N. Chang, J. Rick, M. Carrillo, H. Martin, S. Kasparian, P. Syed, N. Rice, D. G. Brooks, and S. G. Kitchen. 2017. 'Targeting type I interferon-mediated activation restores immune function in chronic HIV infection', *J Clin Invest*, 127: 260-68.

Zheng, G. X., J. M. Terry, P. Belgrader, P. Ryvkin, Z. W. Bent, R. Wilson, S. B. Ziraldo, T. D. Wheeler, G. P. McDermott, J. Zhu, M. T. Gregory, J. Shuga, L. Montesclaros, J. G. Underwood, D. A. Masquelier, S. Y. Nishimura, M. Schnall-Levin, P. W. Wyatt, C. M. Hindson, R. Bharadwaj, A. Wong, K. D. Ness, L. W. Beppu, H. J. Deeg, C. McFarland, K. R. Loeb, W. J. Valente, N. G. Ericson, E. A. Stevens, J. P. Radich, T. S. Mikkelsen, B. J. Hindson, and J. H. Bielas. 2017. 'Massively parallel digital transcriptional profiling of single cells', *Nat Commun*, 8: 14049.